Developing physical models to understand the growth of plants in reduced gravity environments for applications in life-support systems

Lucie Poulet

UNIVERSITÉ CLERMONT-AUVERGNE

ÉCOLE DOCTORALE SCIENCES POUR L'INGÉNIEUR

THÈSE

présentée par

Lucie POULET

pour obtenir le grade de

DOCTEUR D'UNIVERSITÉ

Spécialité : GÉNIE DES PROCÉDÉS

DEVELOPPEMENT DE MODÉLES PHYSIQUES POUR COMPRENDRE LA CROISSANCE DES PLANTES EN ENVIRONNEMENT DE GRAVITÉ RÉDUITE POUR DES APPLICATIONS DANS LES SYSTÉMES SUPPORT-VIE

Soutenue publiquement le 11 juillet 2018 devant le jury :

Présidente :	
Valérie LEGUE	Professeure des Universités - Université Clermont-Auvergne
Rapporteurs :	
Giovanna ARONNE	Professeure des Universités - Université de Naples Federico II
Jack LEGRAND	Professeur des Universités - Université de Nantes
Examinateurs :	
Gioia D. MASSA	Scientifique Senior au NASA Kennedy Space Center
Christophe LASSEUR	Coordinateur R&D Support-Vie - Manager projet MELiSSA à l'ESA
François SPIERO	Manager de la stratégie au CNES
Membre invité :	
Christian TAMPONNET	Chargé de Mission auprès du Directeur scientifique à l'ISRN
Directeurs :	
Claude-Gilles DUSSAP	Professeur des Universités - Université Clermont-Auvergne
Jean-Pierre FONTAINE	Professeur des Universités - Université Clermont-Auvergne

UNIVERSITÉ CLERMONT-AUVERGNE

DOCTORAL SCHOOL OF ENGINEERING SCIENCES

THESIS

presented by

Lucie POULET

to obtain the degree of

DOCTOR OF PHILOSOPHY

Specialty : PROCESS ENGINEERING

DEVELOPING PHYSICAL MODELS TO UNDERSTAND THE GROWTH OF PLANTS IN REDUCED GRAVITY ENVIRONMENTS FOR APPLICATIONS IN LIFE-SUPPORT SYSTEMS

Publicly defended on 11th July 2018 in front of the jury :

President :	
Valérie LEGUE	Professor - Université Clermont-Auvergne
Reviewers :	
Giovanna ARONNE	Professor - Université de Naples Federico II
Jack LEGRAND	Professor - Université de Nantes
Examinors :	
Gioia D. MASSA	NASA Senior Scientist at Kennedy Space Center
Christophe LASSEUR	ESA Life-Support R&D Coordinator - MELiSSA project manager
François SPIERO	CNES Strategy Manager
Invited member :	
Christian TAMPONNET	Mission Manager for the Scientific Director at ISRN
Supervisors :	
Claude-Gilles DUSSAP	Professor - Université Clermont-Auvergne
Jean-Pierre FONTAINE	Professor - Université Clermont-Auvergne

Acknowledgements

Firstly, I would like to express my sincere thankfulness to my advisors Prof. Claude-Gilles Dussap and Prof. Jean-Pierre Fontaine for their efficient guidance during my Ph.D, as well as for the autonomy they allowed me to have in the choices I made regarding this project and the side projects I was able to pursue. A special thank you for supporting me, both on the proposal writing and financially, on the parabolic flight experiments, which were not scheduled at the beginning of my PhD and induced a 6-month delay. Besides my advisors, I would like to thank my thesis reviewers, Prof. Giovanna Aronne and Prof. Jack Legrand, for their insightful comments and encouragements, but also for the hard questions which incented me to widen my research from various perspectives.

I would like also to thank the rest of my thesis committee for accepting to participate in my defense, and critically read and question my thesis; especially Dr. Gioia Massa, who attended my defense from the Kennedy Space Center (Florida) and who gave me the will to pursue a career as a researcher, 8 years ago; François Spiero, who represented CNES during my defense, which enabled me to pursue my PhD by financing half of it; Prof. Valérie Legué, who accepted to be the president of my committee during the defense and for the fruitful discussions we have had regarding the parabolic flight experiment; Dr. Christian Tamponnet, who spontaneously offered to attend my defense; Dr. Christophe Lasseur, for making me discover the MELiSSA project 8 years ago, for his insightful comments on the manuscript and for providing the frame of this PhD.

I also thank Christel Paillé, Prof. Danny Geelen, and Lorenzo Bucchieri, who were members of my first-year PhD monitoring committee and with whom I had fruitful discussions on several aspects of my work. I'd like also to acknowledge the whole MELiSSA community for their insights during the MELiSSA yearly meetings.

Je remercie en particulier le CNES et le CNRS qui ont financé ces travaux de recherche pendant 3 ans. Mention particulière à Dr. Guillemette Gauquelin-Koch, ma référente CNES, qui m'a laissé une autonomie totale sur ce projet : je la remercie pour sa confiance.

Merci à Antoine qui a accepté de rejoindre l'équipe Space Farmers en 2016 et qui a géré la majeure partie de l'analyse de données et de la logistique des campagnes de vols paraboliques. Merci d'avoir assuré la partie fous-rires et poney pendant ces années. Thank you Helia for initiating the project together in July 2015 and not giving up at our first rejection, and for dealing with all the IR camera application development. Thank you Vasiliki for joining the team in 2016 and for your constant support to the project. Un énorme merci à Benjamin qui a pris sur son temps de rédaction pendant une froide après-midi de décembre pour m'aider à écrire un code dans Visual Studio.

Merci enfin à tous ceux qui ont cru à cette manip depuis le début et qui nous ont aidés à la monter et à faire les réglages des capteurs : merci énormément David de l'avoir montée et de nous avoir conseillés sur les choix techniques ; merci beaucoup Christelle, Pascal, Brigitte, Christophe et André (de l'INRA) pour vos conseils, prêts de matériel, formation et présence. Je remercie aussi chaleureusement Dr. Jérôme Ngao, Dr. Marc Saudreau et Dr. François Bizet pour leur collaboration sur ce projet et pour les discussions intéressantes sur ce thème. Merci à Béatrice, Françoise et Dominique pour la gestion administrative de cette manip. Merci également à Pascal Laffont qui a sponténement offert de nous imprimer en 3D des cadres spécifiquement conçus pour tenir fils en nylon et hygromètres. Merci à Jalil Ouazzani pour sa formation au logiciel Phoenics et son énorme soutien sur la conception de modèles CFD. Merci à toute l'équipe de Novespace, en particulier Thomas et Frédéric, pour leur soutien et leurs remarques constructives et, bien sûr, un gros merci à Fred pour son accueil chaleureux et sa bonne humeur, y compris le matin de bonne heure les jours de vol. Merci à Vincent Meens du CNES, qui nous a sélectionnés pour notre première campagne via le programme CNES Paraboles et nous a permis d'accéder au vol parabolique en assurant un super soutien logistique. Merci à l'ESA de nous avoir fait confiance sur deux campagnes en nous sélectionnant via le programme ESA CORA.

Je tiens à remercier vivement mon laboratoire, l'axe GePEB de l'Institut Pascal, pour son accueil chaleureux et pour m'avoir intégrée à la vie du labo. Je remercie tout particulièrement le groupe des doctorants, qui a rendu ces 3 ans et demi joyeux et agréables, même les soirées tardives et les weekends passés au bureau, et dont beaucoup sont devenus des amis : Nelly, Azin, Ghiles, Vincent, Alex, Vanessa, Paolo, Bhawna, Caro, Maarouf, Victor, Sanaa, Benoît, Clément, Amaury, Amélie. Et les non doctorants Véronique, Nico et Pompom.

Un gros merci à l'équipe Retour à l'Ecole, Antoine, Benjamin, Mathilde, Pauline, Thibault, Juliette, Vanessa, Amandine et Geoffrey ! Vous êtes géniaux et ce projet était une des plus belles expériences de ma thèse.

Je voudrais remercier mes amis de la radio, du Puy de la Recherche et de Doct'Auvergne, qui ont égayé mes soirées à coup de réunions tardives, émissions déjantées et Doct'Au Verre : Alice, Arthur, Ludivine, Jeanne, Olivier, Clément, Fred, et en particulier mon amie et colocataire Barbara pour son soutien moral sans faille ces derniers mois, les fous rires, le 100km de l'OXFAM et ses petits plats.

Merci à mes amis qui ont été compréhensifs sur mon manque de temps ces dernières années mais qui m'ont soutenue malgré tout, notamment Marylin, Gaëlle, Chloé, Rosa et Emmanuelle. Thank you Nikos, Inês, Mika, and Fredrik for your regular cheering and keeping in touch despite the distance. Florence, merci d'avoir été présente si souvent, merci pour tes conseils et pour nos discussions out of this world ! Et merci à toutes celles et ceux qui ont égayé ces années de thèse à l'escalade et à la danse et que je ne peux pas tous citer ici.

Merci également à toutes celles et ceux qui m'ont fait confiance pour donner des conférences de médiation scientifique, que ce soit dans des établissements scolaires, dans des cafés ou à l'opéra de Clermont. Je ne peux pas citer tout le monde ici, mais je tiens à remercier particulièrement Lionel et Dominique pour leur accompagnement sur le TEDx Clermont qui m'a permis de parler de mes recherches et m'a appris à formuler un « take

home message ».

Je remercie bien sûr ma famille, qui m'a soutenue et supportée tout au long de ma thèse mais qui m'a surtout permis d'arriver jusque-là et qui s'est déplacée massivement le jour de ma soutenance. Maman, Papa : merci d'avoir pris le temps de répondre une à une aux questions de la petite fille curieuse que j'étais et de m'avoir soutenue dans mes choix. Elise, merci d'être venue à la soutenance alors que tu étais enceinte de 7 mois et que tu as passé ta première nuit loin de Jacques. Adèle, merci d'avoir fait le déplacement depuis le Canada !

Last but not least : Stef je te remercie du fond du cœur pour ton soutien sans faille sur ces derniers mois de thèse, de m'avoir supportée, de m'avoir écoutée discuter des parties entières de ce manuscrit, pour tes conseils, de m'avoir forcée à aller prendre l'air pendant des weekends que j'avais passés à rédiger, pour l'organisation parfaite du jour de ma soutenance et surtout d'être toujours là quoiqu'il advienne.

Contents

List of Figures i
List of Tables vi
List of Symbols vii
Abstract in French xiii

Introduction **1**

1 Literature review and context **7**
1.1 Crewed deep space missions: context and challenges 7
1.2 Bioregenerative LSS : Definition and history 10
1.3 The MELiSSA project 18
1.3.1 MELiSSA Loop Overview 18
1.3.2 Development phases 19
1.3.3 The Higher Plant Compartment 21
1.4 The MELiSSA strategy 22
1.5 Extended abstract of the review article 24
1.6 Review article 25
1.7 Chapter's outcomes 38

2 Gas Exchanges Model in Reduced Gravity Environment **41**
2.1 Introduction 41
2.2 Including gravity in a holistic plant growth model: first assessment of the theoretical influence of reduced gravity on gas exchanges and plant growth 43
2.3 Towards the assessment of reduced gravity influences on the boundary layer thickness and introduction of the energy balance 63
2.4 Detailed energy model 72

2.4.1 Energy coming from incident light: photons energy 72
2.4.2 Radiation energy 73
2.4.3 Convection energy 74
2.4.4 Transpiration energy 77
2.4.5 Energy balance at steady state 79
2.5 Detailed model of the boundary layer 85
2.5.1 Assessment of the previous model 85
2.5.2 Leaf geometry 93
2.5.3 Modeling the boundary layer 94
2.6 Conclusions and model improvements 99
2.7 Chapter's outcomes 100

3 Development of a mechanistic model accounting for gravity influence and coupled mass, heat, and radiative transfers 103
3.1 Introduction 103
3.2 Stoichiometric module 105
3.2.1 Dry mass synthesis 105
3.2.2 Photosynthetic yield 107
3.2.3 Fresh mass synthesis 108
3.2.4 Total Water consumption 108
3.3 Morphology module 109
3.4 Heat and Mass transfer at a solid surface boundary 110
3.4.1 The stagnant boundary layer model 111
3.4.2 The laminar boundary layer model 112
3.4.3 The Chilton Colburn analogy 114
3.4.4 The penetration theory model 115
3.4.5 The surface renewal model 116
3.4.6 Influence of free convection 118
3.4.7 Overview of the influences of different types of convection 121
3.5 The kinetic model for higher plant growth 123
3.6 The new MELiSSA plant growth model - Summary 125
3.6.1 The morphological module 125
3.6.2 Free convection, conductance, and boundary layer 125

3.6.3 The physical and biochemical modules . . . 127
3.6.4 The energy balance module . . . 129
3.6.5 The transient state balance . . . 130
3.7 Sensitivity analysis . . . 131
3.7.1 Transient mode: two minutes . . . 134
3.7.2 Steady-state mode: one hour . . . 141
3.8 Conclusion . . . 148
3.9 Chapter's outcomes . . . 149

4 Model validation **151**
4.1 Introduction . . . 151
4.2 Materials and Methods . . . 154
4.2.1 Parabolic Flight . . . 154
4.2.2 Experimental set-up . . . 155
4.2.3 Spinach plants and agar gel . . . 157
4.2.4 Sensors . . . 159
4.2.5 LED lighting system, light spectrum and patterns . . . 160
4.2.6 Thermal cameras and Android phones . . . 162
4.2.7 IR images analysis . . . 162
4.2.8 Statistical analysis . . . 163
4.2.9 Post flight biological analyses . . . 164
4.3 Computational Fluid Dynamics study . . . 165
4.3.1 Evaluation of the fan flow rate . . . 165
4.3.2 Work hypotheses . . . 165
4.3.3 Simulation results . . . 168
4.4 Preliminary results . . . 172
4.4.1 Results of the statistical analysis . . . 172
4.4.2 Results of the dynamical analysis . . . 176
4.4.3 Conclusion . . . 189
4.5 Lessons learned and new set-up . . . 190
4.5.1 Anemometers . . . 190
4.5.2 Lighting system . . . 190
4.5.3 Thermocouples . . . 192

4.5.4 New procedures . . . 193
4.5.5 New application for cameras . . . 193
4.5.6 IRGA tests . . . 193
4.6 Conclusion . . . 194
4.7 Chapter's outcomes . . . 195

5 Sap transport and plant morphology 197
5.1 Introduction . . . 197
5.2 Sap transport: mechanisms and existing models . . . 198
5.2.1 Xylem transport . . . 198
5.2.2 Phloem transport . . . 202
5.2.3 Modeling sap transport . . . 204
5.3 Functional-structural models: linking sap transport and plant morphology 208
5.3.1 Towards the inclusion of phloem/xylem interactions within functional-structural models . . . 209
5.3.2 Towards an object-oriented modeling approach . . . 210
5.3.3 Consequences for our model . . . 211
5.3.4 Next steps . . . 214
5.4 Leaf senescence . . . 215
5.4.1 Mechanisms of leaf senescence . . . 215
5.4.2 Including leaf senescence in our model . . . 216
5.5 Chapter's outcomes . . . 216

Conclusion 219

Bibliography 223

A Matlab Code 241
A.1 Main: Sensitivity Study . . . 241
A.2 Main: Parabolic Flight . . . 249
A.3 Function Fluxes . . . 257
A.4 Function BL . . . 260

B Murashige and Skoog Medium Recipe 263

C Retour à l'Ecole: An outreach project for primary school children - Conference Article at the 68th IAC 267

List of Figures

1.1 Simplified roadmap illustrating NASA's Journey to Mars. Source: NASA. . 9

1.2 This chart is a reproduction from (Eckart 1996), representing the mass of a LSS as a function of the mission duration for different technologies. Red dots are breakeven points. 12

1.3 Diagram showing the MELiSSA loop as a lake ecosystem. Credits: MELiSSA. 18

1.4 Diagram of the MELiSSA loop and its five compartments. Credits: MELiSSA. 19

2.1 Total radiated heat flux for Tb = 300 K (dashes) and Tb = 293 K (line) . 74

2.2 Convection heat flux with no forced convection at 2g (straight line), 1g (long dashes), 0.38g (dashes and dots), 0.16g (small dashes), and 0g (dots). 76

2.3 Convection heat flux with a forced convection velocity of 0.5 m/s at 2g (straight line), 1g (long dashes), 0.38g (dashes and dots), 0.16g (small dashes), and 0g (dots). 76

2.4 Convection heat flux with a forced convection velocity of 1 m/s at 2g (straight line), 1g (long dashes), 0.38g (dashes and dots), 0.16g (small dashes), and 0g (dots). 77

2.5 Transpiration heat flux with no forced convection at 2g (straight line), 1g (long dashes), 0.38g (dashes and dots), 0.16g (small dashes), and 0g (dots). 79

2.6 Transpiration heat flux with a forced convection velocity of 0.5 m/s at 2g (straight line), 1g (long dashes), 0.38g (dashes and dots), 0.16g (small dashes), and 0g (dots). 80

2.7 Transpiration heat flux with a forced convection velocity of 1 m/s at 2g (straight line), 1g (long dashes), 0.38g (dashes and dots), 0.16g (small dashes), and 0g (dots). 80

2.8 Leaf surface temperature as a function of gravity for different values of forced convection velocity: 0 m/s (line), 0.5 m/s (dashes), and 1 m/s (dots). 83

2.9 Schematic of heat and mass transfer in the boundary layer 86
2.10 Schematic of the leaf surface with the free and forced convection vectors and the resulting vector V_{tot} for four different cases. 92
2.11 Schematic of the difference in CO_2 concentration at the leaf surface 99

3.1 Leaf surface temperature, boundary layer thickness, free convection velocity and CO_2 and H_2O partial pressures evolution over 2 minutes for different forced convection velocity values. 135
3.2 Leaf surface temperature, boundary layer thickness, free convection velocity and CO_2 and H_2O partial pressures evolution over 2 minutes for different gravity levels. 137
3.3 Leaf surface temperature, boundary layer thickness, free convection velocity and CO_2 and H_2O partial pressures evolution over 2 minutes for different light values. 138
3.4 Leaf surface temperature, boundary layer thickness, free convection velocity and CO_2 and H_2O partial pressures evolution over 2 minutes for different leaf inclination values. 139
3.5 Leaf surface temperature, boundary layer thickness, free convection velocity and CO_2 and H_2O partial pressures evolution over 2 minutes for different transpiration ratios. 141
3.6 Leaf surface temperature, boundary layer thickness, free convection velocity and CO_2 and H_2O partial pressures evolution over one hour for different forced convection velocity values. 143
3.7 Leaf surface temperature, boundary layer thickness, free convection velocity and CO_2 and H_2O partial pressures evolution over one hour for different gravity levels. 144
3.8 Leaf surface temperature, boundary layer thickness, free convection velocity and CO_2 and H_2O partial pressures evolution over one hour for different light values. 145
3.9 Leaf surface temperature, boundary layer thickness, free convection velocity and CO_2 and H_2O partial pressures evolution over one hour for different leaf inclination values. 146

3.10 Leaf surface temperature, boundary layer thickness, free convection velocity and CO_2 and H_2O partial pressures evolution over one hour for different transpiration ratios. 148

4.1 Whole flight gravity profile with the 31 parabolas. 154
4.2 Gravitational acceleration during the second parabola. 155
4.3 Experimental set-up with lights on. Enclosure from EJM Plastic with fans on the side and LED lighting system on top of the lid. 155
4.4 Inside the enclosure: Spinach plants under 3D printed frames equipped with hygrometer holders and nylon thread to hold the leaves horizontally. On both sides, the perforated plates are shown. 156
4.5 Inside the rack: the enclosure is wrapped in ropes and fixed on a aluminum plate. 157
4.6 Experimental rack in the A310 ZEROG plane. The whole experimental set-up is inside, except for the phones and the laptop computer. 157
4.7 Agar-grown 6-week old spinach plants. On the lid the filter enables gas exchanges and blocks potential contamination. 158
4.8 LED lighting system seen through the polycarbonate lid. 161
4.9 Probability Density Function of the LED lighting system used in October 2017. 161
4.10 3D model of the enclosure - Front View. 166
4.11 3D model of the enclosure - Side View. 166
4.12 Diagram showing the position of the different leaves in the enclosure. . . . 167
4.13 3D model of the enclosure with the mesh used for the computations. 167
4.14 Velocity profile into the enclosure at the lower air flow rate (in m/s) - Front View. 169
4.15 Velocity profile into the enclosure at the lower air flow rate (in m/s) - Side View. 170
4.16 Velocity profile into the enclosure at the lower air flow rate (m/s) - Top View. 170
4.17 Velocity profile in the enclosure at the higher air flow rate - Front View. . . 171
4.18 Velocity profile in the enclosure at the higher air flow rate - Side View. . . 172
4.19 Velocity profile in the enclosure at the higher air flow rate - Top View. . . 172

4.20 IR image collected with the FLIR ONE cameras showing the baseline, the transpiring leaf and the non-transpiring leaf for plant 1. 174
4.21 Results of the LME test for each phone computed in R. 175
4.22 Temperature evolution over 25 seconds in 0g without ventilation, model simulation and experimental results for the 4 plants. Average on all usable parabolas (see Table 4.7). 179
4.23 Temperature evolution over 25 seconds in 0g with the lower ventilation level (plant 1: 0.0225 m/s; plant 2: 0.00198 m/s; plant 3: 0.0789 m/s; plant 4: 0.00624 m/s), model simulation and experimental results for the 4 plants. Average on all usable parabolas (see Table 4.7). 180
4.24 Temperature evolution over 25 seconds in 0g with the higher ventilation setting (plant 1: 0.0243 m/s; plant 2: 0.00586 m/s; plant 3: 0.0786 m/s; plant 4: 0.00433 m/s), model simulation and experimental results for the 4 plants. Average on all usable parabolas (see Table 4.7). 181
4.25 Temperature evolution over 25 seconds in 2g before the 0g phase, without ventilation, model simulation and experimental results for the 4 plants. Average on all usable parabolas (see Table 4.7). 183
4.26 Temperature evolution over 25 seconds in 2g after the 0g phase, without ventilation, model simulation and experimental results for the 4 plants. Average on all usable parabolas (see Table 4.7). 184
4.27 Temperature evolution over an average parabola of 65 seconds, without ventilation, model simulation and experimental results for the 4 plants. Average on all usable parabolas (see Table 4.7). 185
4.28 Temperature evolution over 22 seconds in 2g before the 0g phase, with the lower ventilation setting (plant 1: 0.0225 m/s; plant 2: 0.00198 m/s; plant 3: 0.0789 m/s; plant 4: 0.00624 m/s), model simulation and experimental results for the 4 plants. Average on all usable parabolas (see Table 4.7). . . 186
4.29 Temperature evolution over 20 seconds in 2g after the 0g phase, with the lower ventilation setting (plant 1: 0.0225 m/s; plant 2: 0.00198 m/s; plant 3: 0.0789 m/s; plant 4: 0.00624 m/s), model simulation and experimental results for the 4 plants. Average on all usable parabolas (see Table 4.7). . . 187

4.30 Temperature evolution over 22 seconds in 2g before the 0g phase, with the higher ventilation setting (plant 1: 0.0243 m/s; plant 2: 0.00586 m/s; plant 3: 0.0786 m/s; plant 4: 0.00433 m/s), model simulation and experimental results for the 4 plants. Average on all usable parabolas (see Table 4.7). . . 188
4.31 Temperature evolution over 20 seconds in 2g after the 0g phase, with the higher ventilation setting (plant 1: 0.0243 m/s; plant 2: 0.00586 m/s; plant 3: 0.0786 m/s; plant 4: 0.00433 m/s), model simulation and experimental results for the 4 plants. Average on all usable parabolas (see Table 4.7). . . 189
4.32 New lighting system installed on the enclosure - Side View 191
4.33 New lighting system installed on the enclosure - Top View 191
4.34 New LED module back (left) and front (right) 191
4.35 Probability Density Function of the new LED lighting system 192

5.1 Diagram of cavitation mechanism in the xylem. 199
5.2 Diagram of sugar translocation in the phloem. 203
5.3 Simplified scheme of sap ascent and resources allocation in plants. 206

List of Tables

1.1 Relative supply mass according to the level of closure of the LSS. Reproduction from Eckart 1996. 13

1.2 MELiSSA's five compartments functions (Lasseur et al. 2011). 20

2.1 Values of T_{leaf} for different values of forced convection and gravity when $T_b = 300$ K. 81

2.2 Values of T_{leaf} for different values of forced convection and gravity when $T_b = 293$ K. 81

2.3 Gradients $|\Delta T_{leaf}|$ depending on gravity levels for values of forced convection of 0 and 1 m/s when $T_b = 300$ K. 82

2.4 Gradients $|\Delta T_{leaf}|$ depending on gravity levels for values of forced convection of 0 and 1 m/s when $T_b = 293$ K. 82

2.5 Dimensionless numbers associated with mass transport and heat transfer . 86

2.6 Values of $F'(\theta)$ computed for two different numerical methods. 90

3.1 Correlations with dimensionless numbers for heat and mass transfer in forced and free convection. 121

3.2 Correlations of the Nüsselt number for upper and lower faces of hot and cold horizontal plates. 123

3.3 Tested parameters in the sensitivity study. 132

3.4 Parameters used for the sensitivity study. 132

4.1 Average total velocity measured by the anemometers during the flight. . . . 159

4.2 Average temperatures and relative humidity during the flight of 31 parabolas. 162

4.3 Dimensionless numbers in the enclosure during the parabolic flight. 168

4.4 Simulation results of the air velocity at the leaves surfaces for the lower air flow rate. 169

4.5 Simulation results of the air velocity at the leaves surfaces for the higher air flow rate. 173
4.6 Parameters used for the parabolic flight simulations. 177
4.7 Usable parabolas for each plant, gravity level, and ventilation level. 178
4.8 Air velocity at the leaves surfaces used as the forced convection velocity parameter (in m/s). 180

List of Symbols

Air properties

$[CO_2]$ Air CO_2 Concentration, ppm

λ Latent Heat of Vaporization, J.mol^{-1}

ν Air Kinematic Viscosity, m^2.s^{-1}

ρ_{mol} Molar Water Vapour Density, mol.m^{-3}

Cp_w Molar Heat Capacity at P, J.mol^{-1}.K^{-1}

D_c Diffusion Coefficient of CO_2, m^2.s^{-1}

D_o Diffusion Coefficient of O_2, m^2.s^{-1}

D_w Diffusion Coefficient of water vapour, m^2.s^{-1}

k_t Air Conduction Coefficient, W.m^{-1}.K^{-1}

M_{CO_2} CO_2 Molar Mass, kg.mol^{-1}

M_{H_2O} H_2O Molar Mass, kg.mol^{-1}

M_{N_2} N_2 Molar Mass, kg.mol^{-1}

M_{O_2} O_2 Molar Mass, kg.mol^{-1}

P Total Pressure, Pa

$P^0(T)$ Water Vapor Saturating Pressure at T, Pa

p_{CO_2} CO_2 Partial Pressure, Pa

p_{H_2O} H_2O Partial Pressure, Pa

p_{N_2} N_2 Partial Pressure, Pa

p_{O_2} O_2 Partial Pressure, Pa

RH Relative Humidity, %

T Temperature, K

Physical Module

δ Boundary Layer Thickness, m

μ Nutrient Solution Dynamic Viscosity, Pa.s

Ψ_{ext} Nutrient Solution Water Potential, Pa

Ψ_{int} Leaf Water Potential, Pa

θ Leaf Inclination, rad

ε Vegetation Emissivity

H Standard Plant Chamber length, m

I Light Intensity, µmol.m^2.s^{-1}

v_{forced} Forced Convection Velocity, m.s^{-1}

v_{free} Free Convection Velocity, m.s^{-1}

Morphological Module

a_s Stomatal Cross-Sectional area, m^2

d_s Stomatal Density, m^{-2}

k_1 Ratio Leaf Area / Fresh Biomass, m^2.g^{-1}

k_2 Ratio Stem Length / Fresh Biomass, m.g^{-1}

k_3 Ratio Number Sap Vessels / Fresh Biomass, g^{-1}

l_s Stomatal Pore Depth, m

R_{vessel} Sap vessel Radius, m

Biochemical Module

ω_X Dry Matter Content in Plant, $g_X.g^{-1}{}_{FX}$

$BCmol$ C-molar mass, $g.mol_C^{-1}$

$Y_{C_{photon}}$ Quantum Yield, $mol_C.mol_\mu^{-1}$

Physics Constants

σ Boltzmann Constant, $W.m^{-2}.K^{-4}$

c Light Speed, $m.s^{-1}$

g Gravitational Constant, $m.s^{-2}$

h Planck Constant, J.s

N_A Avogadro Number, mol^{-1}

R Ideal Gas Constant, $J.mol^{-1}.K^{-1}$

Subscripts

0 Initial

b Bulk Air

FX Fresh Mass

$leaf$ Leaf Surface

X Dry Mass

Abstract in French

L'exploration du système solaire sur le long terme va nécessiter la croissance de plantes et d'autres organismes biologiques, capables d'assurer les fonctions de production d'oxygène et de nourriture, ainsi que la revitalisation de l'atmosphère et le recyclage de l'eau, afin d'assurer une autonomie aux équipages. En effet, on change de paradigme par rapport à la station spatiale internationale, les distances étant beaucoup plus importantes, ce qui limite les possibilités de ravitaillement. Actuellement sur la station spatiale internationale, seulement une partie de l'eau et de l'air est recyclée, le reste des consommables est acheminé par vaisseaux cargo régulièrement, qui sont ensuite utilisés pour stocker les déchets et brûlent dans l'atmosphère terrestre à leur retour. Le seul moyen de produire de la nourriture en autonomie est d'utiliser des organismes vivants tels des plantes et des algues, qui permettent aussi d'assurer les fonctions de revitalisation de l'air et de recyclage de l'eau : on parle alors de système support-vie biorégénératif. Cela implique une intégration de toutes les fonctions : absorption de CO_2, production d'oxygène, recyclage d'eau et des déchets et production de nourriture. Pour pouvoir contrôler et prédire les différents processus biologiques impliqués, il est nécessaire d'avoir une approche modulaire par compartiments avec des spécifications précises et des modèles de connaissance, ce qui diffère des écosystèmes naturels qui évoluent vers un état stationnaire de manière spontanée.

Cette approche intégrée et contrôlée est celle du système support-vie biorégénératif de l'Agence Spatiale Européenne (ESA) MELiSSA (Micro Ecological Life-Support System Alternative), qui permettra aux équipages d'être autonomes en termes de production de nourriture, revitalisation de l'air et de recyclage d'eau, tout en fermant les cycles de l'eau, de l'oxygène, de l'azote et du carbone, pendant les missions longue durée. Pour prédire la croissance des plantes dans ces conditions non-standard, il est crucial de développer des modèles mécanistes de croissance, permettant des études multi-échelles de différents phénomènes, ainsi que d'acquérir une meilleure compréhension de tous les processus impliqués dans le développement des plantes en environnements de gravité réduite et d'identifier les données manquantes. C'est l'objet de cette thèse : développer un modèle mécaniste pour comprendre la croissance des plantes en environnement de gravité réduite, en particulier les échanges gazeux au niveau de la surface foliaire.

Le premier chapitre donne le contexte de l'étude, en rappelant l'histoire des systèmes support-vie biorégénératifs et en donnant une description détaillée du projet MELiSSA et de son approche mécaniste. Un article de revue publié dans Botany Letters en 2016 résume les effets connus de l'impesanteur sur la croissance des plantes, au niveau cellulaire, des tissus et de la plante dans son ensemble et dresse un inventaire des technologies existantes et challenges restants pour la culture de plantes dans l'espace.

Le deuxième chapitre est dédié à la présentation d'un modèle préliminaire d'échanges gazeux en gravité réduite, au travers de deux articles, l'un présenté au 47^{th} International Conference on Environment System, détaillant les étapes de l'introduction de la gravité en tant que paramètre du modèle, et le deuxième, accepté publié dans le numéro 18, issue 9 du journal Astrobiology, précisant la modélisation des échanges gazeux avec l'addition d'un bilan énergétique.

Le troisième chapitre détaille le nouveau modèle MELiSSA de croissance de plantes, en détaillant pour chaque module les équations utilisées dans la version initiale du modèle MELiSSA. Différentes approches sont expliquées et discutées pour la modélisation de la couche limite de surface foliaire et un résumé de toutes les équations est donné. Une étude de sensibilité à différents paramètres en fin de chapitre permet d'identifier les principales tendances et influences.

Le quatrième chapitre présente l'expérimentation en vol parabolique qui a été conçue et implémentée pour la validation du modèle. Le design expérimental et les méthodes de caractérisation sont détaillés ; une analyse de mécanique des fluides numérique a permis de caractériser le comportement des fluides et les vitesses d'air dans l'enceinte expérimentale. Les résultats d'une étude statistique sont donnés et la validation du modèle est discutée pour les différentes phases de vol pour différents niveaux de ventilation. Une évolution du dispositif expérimental qui vient d'être testé en vol (avril 2018) est proposé en fin de chapitre.

Le cinquième et dernier chapitre présente une ouverture sur le transport de sève et la morphologie et leurs modèles physiques existants. Ces thèmes n'ont pas été abordés trop en détails pendant ce projet, mais leur prise en compte est toutefois cruciale avant de développer un modèle de croissance végétale précis et représentent les prochaines étapes de ce travail de modélisation.

Premier chapitre

L'étude des systèmes support-vie a commencé pendant les années 1950 et s'est poursuivie jusqu'à nos jours. Chaque agence spatiale du monde (Russie, USA, Japon, Chine, Europe) a ses propres spécificités quant à leur étude, se concentrant sur les algues ou sur les plantes, avec inclusion d'humain ou d'animaux. Le projet majeur en Europe est le projet MELiSSA, commencé en 1989. Divisé en 5 compartiments : le liquéfacteur, le photohétérotrophique anxygénique, le nitrifiant, le photoautotrophique pour les plantes et les algues et le compartiment de l'équipage. L'accent est mis ici sur le compartiment des plantes supérieures. Leur modélisation est plus complexe que celle des algues, puisqu'il faut prendre en compte leur morphologie, ainsi que leurs différentes phases de croissance. Les plantes peuvent pousser dans l'espace et ont poussé en orbite terrestre depuis les années 50. En revanche, les environnements de gravité réduite entrainent des modifications sur le comportement et le développement des plantes, dues à des effets directs ou indirects. Les effets directs comprennent l'action de la force de pesanteur sur la direction de croissance des racines, le gravitropisme, qui est supprimé en impesanteur. L'expression génétique et le développement des graines sont aussi modifiés en conditions d'impesanteur. Les effets indirects incluent les changements dans les plantes dus à des modifications physiques des conditions environnementales, comme la forte réduction de la convection naturelle, entrainant des échanges gazeux sous-optimaux au niveau des feuilles, ou la domination des forces de capillarité, entrainant des films d'eau accrochés aux racines pouvant provoquer leur asphyxie. En particulier, les échanges gazeux à la surface de la feuille étant altérés en gravité réduite, cela pourrait ralentir la croissance des plantes dans l'espace.

Deuxième chapitre

Pour obtenir une croissance de plante similaire à celle sur Terre (gravité terrestre), il est nécessaire de fournir aux plantes une ventilation adéquate. Pour limiter les dépenses énergétiques, il convient donc de déterminer la vitesse de convection forcée minimale pour assurer une photosynthèse optimale.

Dans un premier temps, le modèle développé par P. Hézard en 2012 est décrit ; il se base sur un bilan de masse sur une feuille unique. Les paramètres morphologiques tels que la surface foliaire totale, la longueur de tige et le nombre de vaisseaux sont propor-

tionnels à la biomasse. La production de biomasse dépend des taux d'échange en CO_2, d'absorption d'eau, de transpiration de vapeur d'eau et d'absorption de lumière. Et ces taux d'échanges dépendent des paramètres morphologiques. L'apport majeur du modèle développé est d'insérer la gravité comme paramètre de modélisation. Un premier article de conférence présenté au 47^{th} International Conference on Environmental Systems (ICES) en juillet 2017 a permis d'établir que la conductance de la feuille à la vapeur d'eau est une combinaison des conductances stomatique et de couche limite et que la vitesse de convection naturelle peut être exprimée en fonction des gradients de gravité et de température. Les premières simulations montrent que les taux de transpiration, d'échange en CO_2 et de production de biomasse sont plus faibles en 0g. En revanche, avec de la ventilation, les taux de production de biomasse en impesanteur et en gravité terrestre sont similaires. Un article accepté par le journal Astrobiology en janvier 2018 pour une publication en septembre 2018 discute des effets de gravité réduite sur la conductance foliaire, l'épaisseur de couche limite et les échanges gazeux. Il est mis en évidence qu'il existe une vitesse de convection forcée seuil, en dessous de laquelle l'épaisseur de couche limite et les taux d'échanges gazeux ne dépendent que des niveaux de gravité et au-dessus de laquelle ils dépendent de la valeur de l'intensité de convection forcée (représentée par sa vitesse). Pour être plus complet, le modèle doit coupler le modèle existant de bilan de masse à un bilan d'énergie, ce qui fait apparaître la température de surface comme nouvelle variable du modèle. Le bilan d'énergie de la feuille comporte l'énergie de radiation lumineuse, un bilan radiatif de l'énergie de radiation, l'énergie résultant des échanges convectifs, ainsi que l'énergie liée à la transpiration. L'énergie liée aux réactions métaboliques est négligée. Ce bilan énergétique montre que la température de surface foliaire est moins dépendante des niveaux de gravité pour des vitesses de convection forcée plus importantes.

Finalement, les hypothèses qui ont permis l'ajout de la gravité comme un paramètre du modèle et à la définition de la couche limite sont discutées et des suggestions pour affiner le modèle sont données. L'inclusion de la gravité dans les modèles d'échanges gazeux demande des descriptions précises des transferts de masse et de chaleur dans la couche limite. La convection naturelle ne résulte pas seulement des gradients de température mais provient aussi des différences de densité gazeuses dues à la photosynthèse. L'orientation de la feuille joue un rôle important dans les échanges et doit être également prise en compte.

Troisième chapitre

Ce chapitre donne le développement complet du modèle : stœchiométrie, cinétique, morphologie. L'équation utilisée pour le module stœchiométrique fait l'hypothèse que la biomasse peut être représentée par un sucre complexe avec des atomes de carbone, d'hydrogène et d'oxygène. Les coefficients stœchiométriques utilisés découlent des études de P. Hézard et S. Sasidharan (2012). La biomasse fraiche est composée de 9% de masse sèche et 91% d'eau ; la transpiration est environ 10 fois plus élevée en masse que la masse fraiche. Pour obtenir un modèle dynamique, cette stœchiométrie doit être liée à un modèle cinétique, qui donne la limitation des différents flux de matière. Comme dans le modèle initial développé par P. Hézard (2012), les paramètres morphologiques (surface foliaire, longueur de tiges, nombre de vaisseaux) sont proportionnels à la biomasse produite.

L'épaisseur de couche limite est définie avec un modèle de renouvellement de surface et non plus comme un paramètre d'entrée empirique, après une revue critique de différents modèles de couche limite. Le modèle de renouvellement de surface développé par Dankwerts est celui qui donne les meilleures estimations des coefficients de transfert. Ainsi, l'expression de la vitesse de convection naturelle est calculée de manière explicite et dépend de la gravité et des gradients de densité de gaz.

Le couplage des bilans de masse et d'énergie introduit des variations de la température de surface qui dépendent du temps.

Une étude de sensibilité montre que pour des fortes valeurs de convection forcée, l'épaisseur de couche limite diminue plus rapidement au cours du temps ; pour des faibles valeurs de convection forcée, la température de surface foliaire augmente plus. L'épaisseur de couche limite est beaucoup plus grande pour les cas de 0g et présente des variations temporelles quasi nulles. Logiquement, les taux d'absorption de CO_2 sont réduits avec cette augmentation de l'épaisseur de couche limite. L'augmentation de l'illumination entraine bien sûr une augmentation de la température foliaire, mais aussi une augmentation de la convection naturelle et donc une diminution de l'épaisseur de couche limite. L'étude a aussi révélé une forte sensibilité à l'inclinaison de la feuille. Le taux de transpiration, quant à lui a un effet non linéaire sur tous les paramètres.

Ce nouveau modèle de transfert est mécaniste et permet de prédire les échanges localement, au lieu de travailler en valeurs moyennées comme ce qui est fait d'habitude.

Quatrième chapitre

Ce chapitre est dédié à la validation du modèle. La température de surface peut être mesurée à l'aide de caméras infra-rouges (IR) et nous avons dessiné, assemblé et mis en place un montage expérimental permettant de réaliser ces mesures en vol parabolique. Le vol parabolique est composé de 31 paraboles, chacune comportant une phase de 20 secondes à 0g précédée et suivie d'une phase de 20 secondes à 2g. Quatre plants d'épinard sont contenus dans une enceinte éclairée par des LEDs et avec des ventilateurs permettant de faire varier la ventilation au sein de l'enceinte. Le système d'acquisition d'images infra-rouges a été conçu avec du matériel destiné aux particuliers et non à la recherche, disponible en magasin à des coûts bien en deçà des caméras IR classiques, tout en conservant une précision suffisante. Les paramètres biologiques et morphologiques sont estimés avec des études destructives post vol, permettant de mesurer la surface foliaire, la masse sèche, la masse fraîche, la longueur de racine et le nombre de stomates.

Les vitesses d'air près de la surface des feuilles peuvent être estimées avec une bonne précision grâce une étude de CFD sur le logiciel Phoenics et corrélées avec les mesures faites par les anémomètres dans l'enceinte.

L'étude statistique a révélé que les tendances observées dans les variations de température sont en accord avec les résultats de la littérature. Les tendances d'évolution de la température de surface sont les mêmes expérimentalement et sur les simulations modèles dans le cas sans ventilation, en 0g et en 2g. Ainsi, à partir d'une mesure locale (la température de surface foliaire), nous sommes en mesure de déduire des tendances réalistes sur des phénomènes globaux. L'étude des régimes transitoires avec des constantes de temps courtes (20s) nous permet de comprendre l'évolution des transferts gazeux locaux. Mais avec de la ventilation dans l'enceinte, les prédictions du modèle ne sont plus en accord avec les données expérimentales pour la température de surface. Cela peut s'expliquer par une surestimation de l'influence de la convection forcée dans le modèle, ou une estimation trop approximative des températures de surface.

Ces résultats seront confirmés par 6 vols paraboliques supplémentaires et mériteraient d'être extrapolés pour des interprétations physiologiques. Le chapitre se termine sur les améliorations apportées au système expérimental. De nouveaux anémomètres permettent des mesures sur une gamme plus précise et le système d'éclairement permet d'apporter 20

fois plus de photons, ce qui correspond aux besoins physiologiques des plantes. En outre, les thermocouples sont remplacés par des pt100, matériel plus adapté à nos conditions expérimentales. Enfin, le milieu de culture est remplacé par de la laine de roche, pour éviter les contaminations de l'agar. Un complément d'expérience consisterait à évaluer les échanges en CO_2 et vapeur d'eau des épinards à l'aide d'un analyseur de gaz infra-rouge et à coupler ces mesures à de l'imagerie infra-rouge pour obtenir les températures de surface.

Cinquième chapitre

Le transport de sève dans le xylème est assuré par la transpiration et la pression au niveau des racines, de manière passive suivant la théorie de cohésion-tension. Des phénomènes de cavitation peuvent se produire, qui peuvent endommager la plante sévèrement.
Le transport de sève par le phloème est assuré par un gradient de pression osmotique, qui vient de l'activité photosynthétique des feuilles (sources) et de la fonction de stockage de certains organes (puits). Le transport de sève tant dans le phloème que dans le xylème est modélisé avec une analogie à la loi d'Ohm. La relation entre le gradient de pression et le flux dans le xylème et le phloème est donné par la loi de Darcy.
L'évolution de la morphologie de la plante peut être liée au transport de sève en utilisant des modèles orientés objet, basés sur le modèle C-TRAM. En revanche ces modèles sont adaptés à des gravité terrestres et la répartition des ressources carbonées et le transport de sève doivent être étudiés en gravité réduite. A terme, le modèle d'échanges gazeux présenté ici devra être intégré dans un modèle fonctionnel-structurel liant morphologie et transport de sève, pour arriver à un modèle mécaniste complet de la croissance des plantes en environnement de gravité réduite.
Enfin, la sénescence des feuilles est étudiée, puisque ce phénomène devra être intégré au modèle. Ce phénomène est dû à une baisse de l'activité photosynthétique, provenant soit d'un niveau de sucre trop important, signe que la feuille a atteint sa taille maximale, soit d'un manque d'illumination. La valeur seuil de niveaux de sucre dans la feuille devra être déterminée expérimentalement.

Les plantes sont nécessaires au futur de l'exploration habitée du système solaire, puisqu'elles sont le seul moyen d'aboutir à une autonomie en termes de production de nourriture. Ainsi il est nécessaire de comprendre leur fonctionnement en détail dans des conditions envi-

ronnementales non standards, en particulier dans des environnements de gravité réduite. En particulier, les échanges gazeux sont perturbés en gravité réduite, en raison des mouvements de convection naturelle réduits. Le développement de modèles mécanistes de croissance permet de réaliser des études multi-échelles des phénomènes. L'inclusion de la gravité dans ce type de modèle implique une description précise des transferts de masse et d'énergie dans la couche limite se développant à la surface des feuilles et de coupler le bilan de masse avec le bilan énergétique. Le nouveau modèle présenté dans ce document s'appuie sur le modèle bilan de masse précédemment développé dans le cadre du projet MELiSSA, est mécaniste et utilise un modèle de renouvellement de surface pour décrire la couche limite. Une expérience en vol parabolique a permis de valider une partie du modèle grâce à des mesures infra-rouges de la température foliaire pour des niveaux de gravité et de ventilation variables. Le transport de sève, la croissance racinaire et la sénescence des feuilles doivent être étudiés en conditions de gravité réduite. Cela permettrait de lier notre modèle d'échanges gazeux à la morphologie des plantes et aux allocations de ressources dans une plante.

Introduction

The deep solar system exploration by humankind will mark the 21st century and push scientific and technological limits always further. The prime reason for human missions is exploration and the need of going always further and expanding into the solar system. The second reason is science: even though robots, probes, and rovers have already surveyed all planets in the solar system, some more precisely than others, and can provide a tremendous amount of data, human eye and expertise is irreplaceable. A robot, or at least robots as we can build them at the moment, will only analyze what they are told to analyze and not question results obtained or take initiative to test and survey unplanned samples. Additionally, surface robots on Mars, for example, are operated remotely and can thus only travel a few kilometers per day: Curiosity rover has been on Mars for almost 6 years and has travelled 19 km, while Apollo 17 astronauts travelled 36 km during their 75-hour stay on the Moon! Finally, a third reason for sending humans into the solar system is technological development and tests, since engineers are forced to find innovative solutions to develop technology that can sustain the harsh environment of space, while performing under very strict energy and mass constraints. The necessity to develop engineered technological solutions corresponding to autonomous, closed, and sustainable systems capable of human life-support functions forces to work with the recycling of elements and circular notions, limiting the buffer stocks, the burdens and the ultimate waste.

In this context, the Micro-Ecological Life-Support System Alternative (MELiSSA) project of the European Space Agency (ESA) envisions to sustain humans in space, using very few resources and energy, thanks to a closed loop system based on biological processes. Three stages of human wastes bacterial degradation allow the provision of nutrients (e.g nitrogen) and minerals to higher plants and micro-algae Spirulina, which use the carbon dioxide exhaled by the crew to produce food, oxygen, and water. This requires a very

thorough understanding of all biological phenomena, but also of growth mechanisms of plants, micro-algae, and bacteria, as well as the interactions between all sub-systems. On a systemic approach, MELiSSA must be considered as an integrated sum of interconnected unit operations, including biological compartments. On one hand, all unit operations in charge of the elementary functions constitutive of the entire loop must be understood and described up to a thorough translation in mathematical models. On the other hand, the systemic approach of complex, highly branched systems with feedback loops is performed. This necessitates to study waste degradation, water recycling, atmosphere revitalization, and food production systems with the same degree of accuracy and the same language and concepts, before the integration of knowledge based control models, organized in several hierarchical levels including a decision system interface with a human environment.

Contrarily to the Earth biosphere, which was produced by evolution and stochastic control, in a human-made small closed ecosystem the diversity and size are not sufficient for stochastic mechanisms to operate successfully. A deterministic control system is therefore a prerequisite for its sustainable existence. This includes at the prime level, the triptych: measurements by reliable sensors, scheme of control, and regulation. Consequently, mechanistic and knowledge models are developed to enable a multi-scale study and identify knowledge gaps, in parallel with tests performed in the ground demonstrator MELiSSA Pilot Plant in Barcelona, as well as tests in the International Space Station (ISS) of, for example, the miniature photobioreactor ARTEMiSS. The mathematical and deterministic modeling and simulation of the different interacting parts of the system constitute the brain-level of this artificial ecosystem. The intelligence of the system is therefore based on the adequacy of the model to represent each unit operation and their interrelations in a suitable degree of accuracy and an adequate validity range of the models to implement a hierarchical strategy of control. Ultimately, the goal is to be able to predict the behaviour of the biological processes used, for a wide range of environmental parameters, and develop predictive tools that can be used to prepare the first human missions that will require a bioregenerative life-support system (LSS). This project has already numerous Earth applications, since the research performed in its frame leads to innovative technological answers to sustainability and circular economy challenges.

Experiments on plant growth in space have shown that low gravity has direct effects on roots growth, since they follow the gravity direction to grow; and it also has an

indirect effect on photosynthesis, since the lower natural convection in reduced gravity environments leads to sub-optimal gas exchanges at the leaf surface. It was observed that in weightlessness, the leaf surface temperature raises, because of impaired gas exchanges. This can be solved by the addition of ventilation, but in large-scale food production modules, ensuring a homogeneous ventilation everywhere is utopian and it is also necessary to quantify how much ventilation is needed, in order not to waste energy. To be able to accurately predict plant behaviour in low gravity settings and thus anticipate what humans during future missions might face in case of a ventilation or lighting system failure for example, the development of a mechanistic model of plant growth in reduced gravity environment is necessary. The first version of the MELiSSA plant growth model is a holistic plant mass balance, validated on long-term lettuce growth in 1g. The new version presented in this document focuses on gas exchanges at the leaf surface, with a detailed characterization of mechanisms in the boundary layer, a fine-tuned description of the leaf conductance and of the free convection velocity. It also couples the previously developed mass balance to an energy balance, hence adding a new variable to the model, the leaf surface temperature.

An experiment in a parabolic flight was proposed to validate the new model, which was selected for three parabolic flight campaigns, one by the Centre National d'Etudes Spatiales (CNES), and two by ESA. It has already flown in 4 flights and only the first one, performed in October 2017, is detailed here. The experiment was made in collaboration with two universities, Clermont Auvergne and Bremen, and two laboratories, the Institut Pascal and the INRA-PIAF (Physique et Physiologie Integrative de l'Arbre en environement Fluctuant) in Clermont-Ferrand, with the collaborators from Bremen working at the Parallel Computing for Embedded Sensor Systems and the Human-Centred Cognitive Assistance Lab.

This document reviews in a first chapter the context of the study and the history of bioregenerative LSS and provides a detailed description of the MELiSSA project, especially its strategy of mechanistic model development and the higher plant compartment. Then a review article published in Botany Letters in 2016 summarizes the currently known effects of weightlessness on plant growth, on the cellular, organ, and whole plant scale, and inventories the existing technologies and remaining challenges for plant cultivation in space, in terms of watering systems, lighting systems, and controlled environment. An

emphasis is set on the importance of mechanistic modeling to gain understanding about plant growth and a review of parameters that need to be included in the model is included.
The second chapter is dedicated to presenting a preliminary model of gas exchanges in reduced gravity environment, through two articles, one presented at the 47^{th} International Conference on Environment System, detailing the steps of adding gravity as a parameter of the model, and the other published in the Astrobiology journal (Vol. 18, issue 9), going further into gas exchanges modeling and the addition of the energy balance at steady state. The energy balance is then further detailed and discussed, with the time-dependent energy balance equation linking leaf surface temperature and mass balance. Lastly the hypotheses, which led to the addition of gravity and the definition of the boundary layer are discussed and suggestions for fine-tuning the model are made.
The third chapter details the new MELiSSA plant growth model, refining in each module the equations used in the initial version of the MELiSSA plant growth module. Different modelling approaches of the boundary layer are explained and discussed and a summary of all equations used in the model is given. A sensitivity study to different parameters of the model ends this chapter and enables to identify main trends and influences. These results are not published yet.
The fourth chapter presents the parabolic flight experiment that was designed for model validation. The experimental design as well as the materials and methods used for testing this experiment are detailed; a computational fluid dynamics study was performed to characterize fluids behaviour and air velocity in the experimental enclosure and the results are presented here. The results of a statistical analysis on the data collected are given and the model validation is discussed for the different phases of flight, as well as different ventilation settings. These results are not published yet. The chapter ends with the lessons learned for a new experimental design, that flew in April 2018.
The fifth and last chapter provides an opening on sap transport and plant morphology and the ways of modeling these mechanisms. These topics were not investigated into much details during this project, but they are nevertheless crucial for an accurate plant growth model development and represent the next steps of this modeling work. Hence this chapter gives a state of the art of what had been done so far and what remains to be done to link gas exchanges, plant morphology, and sap ascent.

Chapter 1

Literature review and context

1.1 Crewed deep space missions: context and challenges

The twenty first century will be the century of the first human missions to Mars, as well as the beginning of human exploration of the deep solar system. Multiple scenarios exist but all converge towards a first crewed mission to Mars in the late 2030s or early 2040s (International Space Exploration Coordination Group 2013; ESA 2015; NASA 2015a; NASA 2015b).

The International Space Station has been a very valuable laboratory since its commissioning in 2011 enabling cutting-edge research in physics, medicine or biology, and enabling the tests of advanced technologies for deep space exploration. Initially scheduled to last until 2020, its life has been extended until 2024 and after its retirement a cislunar space station is foreseen by the ISS contributing agencies (NASA, Roskosmos, ESA, JAXA) and a space station in Low Earth Orbit (LEO) is planned by the China National Space Administration (CNSA). Additionally ESA is preparing the grounds for a "Moon Village", which is a concept aiming at creating momentum for international collaborations on developing technologies for lunar exploration. It could also well take the shape of a permanent scientific base on the Moon, like what is done in Antarctica, through an ESA – CNSA collaboration (Dunne 2017; ESA Human Spaceflight 2017; Qiu 2017). Many precursor robotic missions aiming at studying lunar landing, use of lunar resources or Earth/Moon communications are currently being developed at ESA. New propulsion and transportation technologies, such as the NASA Space Launch System (SLS) will enable crewed missions to go beyond LEO. As a reminder, the last human mission which left the

Earth vicinity was Apollo 17 in 1972. Many robotic missions for Mars exploration are currently in operation or being developed worldwide. The NASA Curiosity rover has been exploring and analyzing the Martian surface since August 2012; the Trace Gas Orbiter of the ESA-Roscosmos Exomars 2016 mission has been orbiting Mars since October 2016; and many surface robotic missions are in preparation worldwide: Insight in 2018 (NASA), Mars 2020 (NASA), Exomars 2020 (ESA, Roscosmos) (International Space Exploration Coordination Group 2013; ESA 2015; NASA 2015c). These missions aim at studying the Martian environment, such as seismography, atmosphere and surface composition, as well as preparing an international Mars sample return mission. They also pave the way for human exploration of Mars and the solar system (see Figure 1.1).
The main reasons for human and robotic deep space exploration are exploration, science, and technology.

- Exploration: it is intrinsic to human nature to venture always further and push back its own limitations and humankind is not bound to stay in the cradle of Earth forever but rather to become a multi-planetary species.

- Science: discoveries and knowledge that will be associated with long-duration crewed missions in space will be invaluable in many disciplines including but not limited to fundamental physics and chemistry, medicine, and human physiology and psychology. As it was proven on the ISS, space offers conditions that enable tests and experiments that are not feasible in Earth conditions. Longer journey will include deep space conditions, and new challenges such as radiations.

- Technology: space environment and planetary surfaces are extreme environments that require the development of very specific equipment. Most of the time technology development for space exploration leads to spin-offs that are directly applicable on Earth. Velcro tape is an example: it was developed to facilitate astronauts' work on the International Space Station.

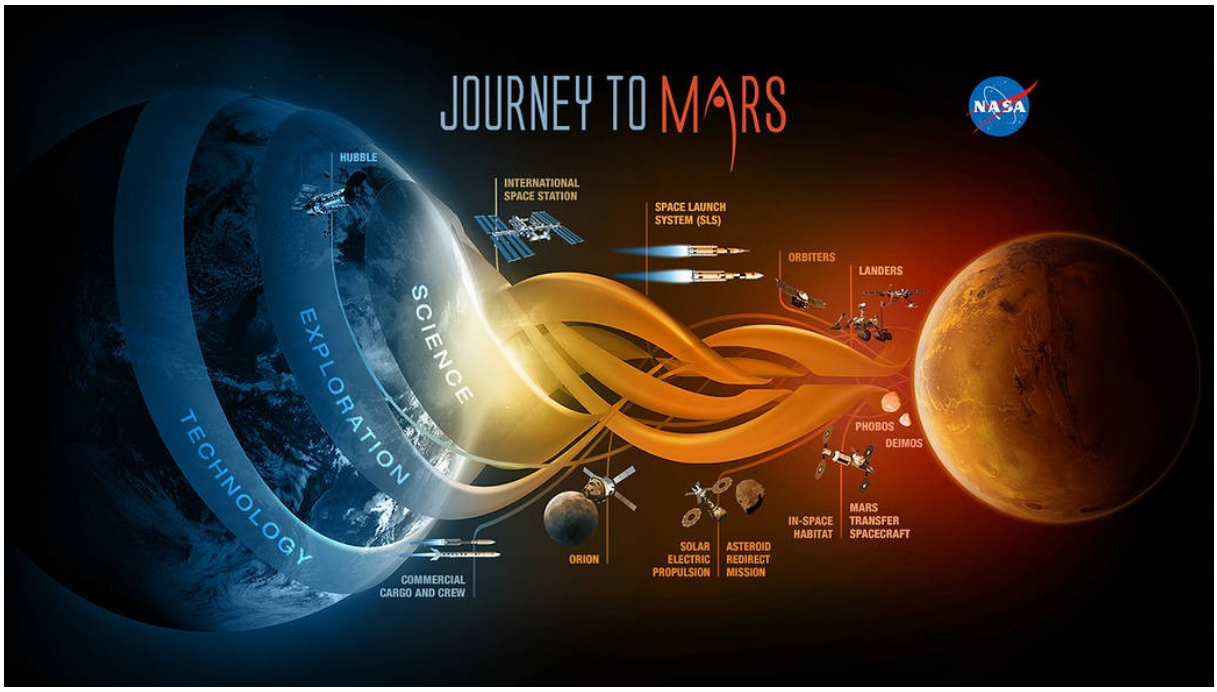

Figure 1.1: Simplified roadmap illustrating NASA's Journey to Mars. Source: NASA.

Classical scenarios for a mission to Mars are 1000-day missions, including 6 to 8 months of travel one way and about 500 days on the surface. With a crew of 6 people (respectively 4 people), such a mission requires a minimum of 30 tons (respectively 20 tons) of consumables including oxygen, food, as well as drinking water and water for basic hygiene, which would require multiple SLS launches. Indeed current NASA scenarios include a crew of 4 and estimate the need of more than 20 launches, among them at least one crewed mission to Phobos, one of the two moons of Mars, in order to assemble and deliver all needed equipment of a first mission to the surface of Mars (Goodliff et al. 2016).

SpaceX founder and CEO Elon Musk revealed his plans of permanent settlement on Mars using his very ambitious Big Falcon Rocket (BFR), which is currently under development (SpaceX 2016). This launcher could bring 150 tons in LEO and would be reusable, which should bring costs down. Transfer vehicles in LEO would bring passengers to Mars, land vertically, and travel back to Earth to bring more passengers. However landing large masses on the Martian surface still remains a challenge, the largest mass landed on the red planet so far being the Curiosity rover, whose mass is 1 ton.

The option of resupplying consumables from Earth, like it is currently done on the ISS, could be an option. However the shortest travel time from the Earth to Mars (around 180 days) and most fuel-efficient is when the planets are in conjunction, providing a launch window every two years. Costs are also prohibitive since sending a kilogram to LEO is

$4653 with the SpaceX Falcon 9, and estimated to be around $1400 with the SpaceX Falcon Heavy and $10000 on average with NASA Space Launch Systems (Bryce Space & Technology for The FAA's Office of Commercial Space Transportation 2018); sending one kilogram to Geostationary Transfer Orbit (GTO) with Falcon 9 and Falcon Heavy costs respectively $12620 and $3370 (Bryce Space & Technology for The FAA's Office of Commercial Space Transportation 2018). Resupplying crews on Mars is thus not a viable option and they will have to produce their own consumables (food, oxygen, and water). The solution is thus to recycle consumables that will have been brought along and use in situ resources. On the ISS 93% of water is recovered from urine and air condensate (Carter et al. 2017), and 42% of oxygen is recovered from CO_2 using a Sabatier reactor and water electrolysis (Anderson 2017; Carter et al. 2017). Studies show that Martian atmosphere CO_2 could be recovered to produce water, oxygen, and methane (for propulsion purposes) with similar techniques (England 2001; Muscatello 2011); water could be extracted from Martian regolith (Wiens et al. 2001; Zubrin 2011). However these physicochemical regenerative systems do not include food production; this can only be achieved by including biological processes, like plants and algae cultivation, in the life-support systems. In addition, seeds can be kept viable for many years and can be produced in space, which is not the case of packaged food currently used on the ISS. NASA and ESA, as well as the International Space Exploration Coordination Group (ISECG), have included the development of high reliability life-support systems and closed-loops as priorities in their roadmaps for successfully carrying out these long-duration crewed missions (International Space Exploration Coordination Group 2013; ESA 2015; NASA 2015b).

1.2 Bioregenerative LSS : Definition and history

Life-support systems (LSS) main functions are to maintain humans alive during space missions by providing oxygen, water, and food, as well as environmental control, crew safety, and waste treatment (Mitchell 1994; Eckart 1996; Anderson et al. 2015). Non-regenerative functions include compensating system leakage and system monitoring; regenerative LSS functions include the provision of water, oxygen, and food and they can function in open, semi-closed or closed loop, depending on the level of recycling achieved and on the amount of external inputs added into the system. In open-loop systems, all consumables come

from stored resources, which are either sent all at once at the beginning of the mission or regularly resupplied during the mission. Although these systems are the most used since the beginning of human spaceflight because they are simple and reliable, they also require a mass of consumables that is proportional to mission duration and crew size, making it not sustainable for long-duration crewed missions (Eckart 1996). Semi-closed and closed-loop systems include recycling of all or part of the elements in order to revitalize the air and water, produce food, and treat wastes, hence limiting the mass of external inputs (Eckart 1996). These external inputs can be based on stored consumables or on in-situ resources; in the latter case the semi-closed system is more sustainable, since it is autonomous from the Earth.

Semi-closed or closed-loop LSS, also called regenerable LSS can be based on sole physicochemical technologies, on sole biological processes or on both, which is referred to as a hybrid LSS (Eckart 1996; Tikhomirov et al. 2007; Zabel, Schubert, and Tajmar 2013). Physicochemical regenerable LSS have extensively been used for spaceflight and are currently used on the ISS (Anderson 2017; Carter et al. 2017). In order to close the loop, food production using biological processes (plants, algae) is necessary (Ewert et al. 2002; Drayer and Howard 2014; Fu et al. 2016). The term bioregenerative LSS is then employed when referred to systems that are based on biological processes, such as plant, algae, and micro-organisms to regenerate these consumables, functioning as artificial ecosystems. These systems compared to physicochemical-based systems are less compact, have a slower response time, and also require a lot of energy.

Realistically a LSS adapted for long-duration missions will be a combination of physicochemical and biological processes, because of the necessity to have function redundancy based on different technologies, which is more robust in case of failure (Zabel, Schubert, and Tajmar 2013). Tikhomirov et al. (2007) investigated different combinations of hybrid LSS, using algae and/or higher plants for water and oxygen production, as well as partial food production, and physicochemical processes for waste degradation (Tikhomirov et al. 2007). The closure of the system is only partial and they discuss, among others, the sizing of different hybrid LSS based on the percentage of vegetarian food production and the need of adding extra minerals into the system to meet algae and higher plants daily requirements. In their study algae and plants are redundant for air revitalization but a physicochemical air recycling system as back-up for redundancy purposes is missing.

LSS functions must be achieved with the highest percentage of closure, while respecting safety standards, and minimizing wastes and consumables mass, as well as energy for recycling. In particular there is a trade-off between the mass of the LSS and the mission duration. Like Eckart and Wieland highlighted it in the 1990s, the longer the mission, the heavier the LSS (see Figure 1.2) and this mass varies according to the type of technologies chosen for the LSS (Wieland 1994; Eckart 1996). For very short duration missions, the non regenerative LSS is the lighter; then using physicochemical technologies for regeneration is more interesting and there is a breakeven point when the mission is so long that the lowest mass is achieved with a durable system such as a bioregenerative LSS, with a maximum closure. This comes from the fact that the higher the closure of the LSS, the lower the consumables mass to bring along with the crew (see Table 1.1). In order to precisely define these breakeven points, the different mission scenarios and assumptions must be established and the technologies used must have a high Technology Readiness Level (TRL).

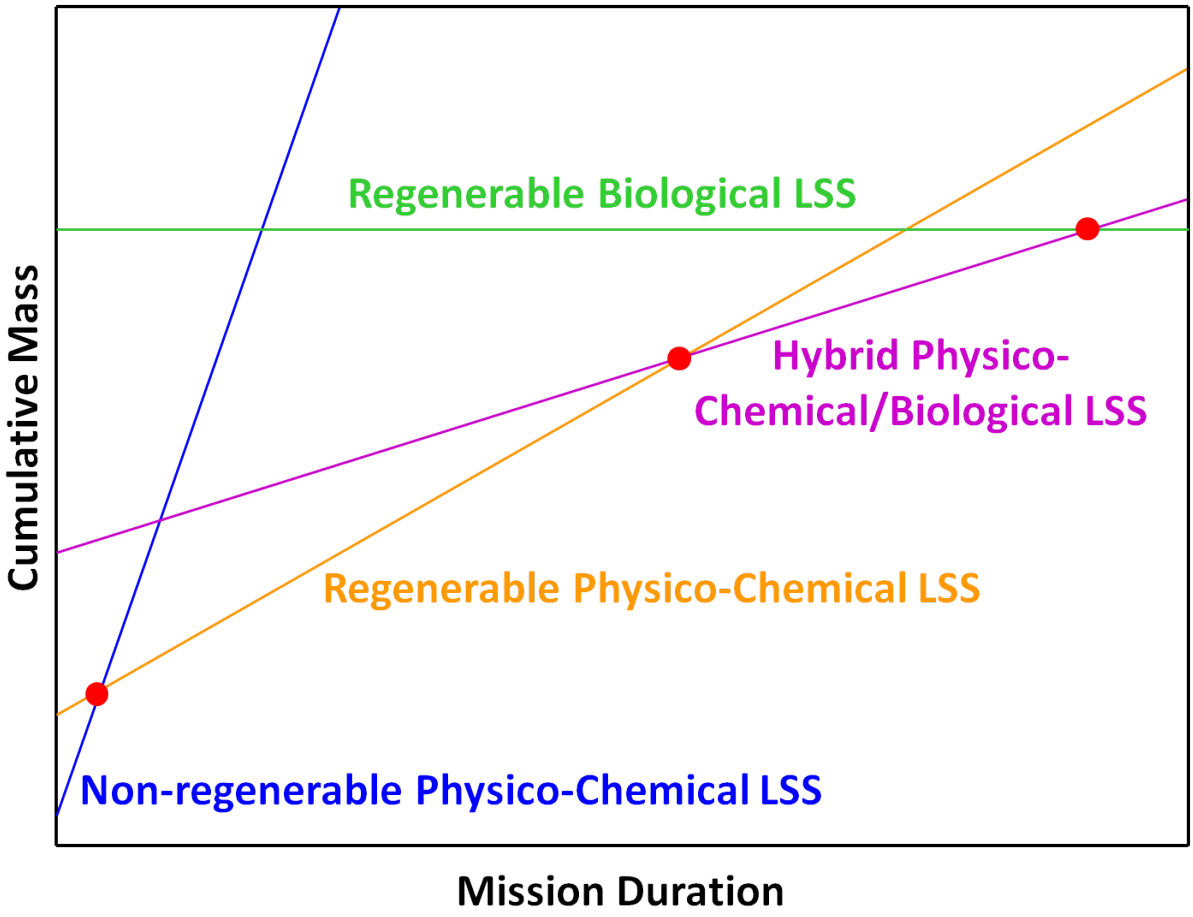

Figure 1.2: This chart is a reproduction from (Eckart 1996), representing the mass of a LSS as a function of the mission duration for different technologies. Red dots are breakeven points.

Table 1.1: Relative supply mass according to the level of closure of the LSS. Reproduction from Eckart 1996.

Step	**Method**	**Relative Supply Mass**
0	Open Loop	100%
1	Waste water recycling	45%
2	Regenerative carbon dioxide-absorption	30%
3	Oxygen recycling from carbon dioxide	20%
4	Food production from recycled wastes	10%
5	Elimination of leakage	5%

For an open loop, the mass of the system itself is low but all consumables need to be brought from Earth, so the relative supply mass is 100%; introducing water recycling technologies cuts this relative supply mass to more than half; complete air revitalization leaves it to 20%, i.e. a relative supply mass reduction of more than half compared to sole water recycling; this is the level currently reached on the ISS. When food is produced using wastes recycling, this mass is again cut in half, bringing it down to only 10%. But the initial system mass is much heavier than an open loop, since more buffers, reactors, or spare parts are needed.
Briefly, humans have basic needs that need to be met each day (in average values) (Anderson et al. 2015):

- 800 g of O_2
- 3.2 kg of water
- 600 g of dry matter (food)

To these needs, we can add 15 L per days and per person of hygiene water (shower, cleaning, etc.). And each day humans reject:

- 900 g of CO_2
- 3.6 kg of water
- 100 g of dry matter

Hence, the LSS must be able to produce sufficient quantities of consumables, while being able to absorb all human wastes. Certain nutritional values also need to be met, with a precise composition in carbohydrates, proteins, and lipids.

Optimizing technologies for a space LSS thus means optimizing mass reduction, but also achieving accurate predictive and control systems, since the behavior of biological processes needs to be anticipated in order to deliver the appropriate quantities and quality of substances for human survival.

Russia and former USSR

Research in the topics of bioregenerative LSS has begun in the early 1950s, with Jack Myers on algal systems on the American side and scientists Henry Lisovsky and Iosef Gitelson on the soviet side (Gitelson and Lisovsky 2008; R. M. Wheeler 2011). In former USSR, tests on gas exchanges between the algae chlorella and humans were performed in the early 1960s in Krasnoyarsk, Siberia and the first regenerative LSS was a semi-closed system called BIOS 1, created in 1965 and tested until 1968 (Gitelson et al. 1989; Gitelson and Lisovsky 2008; Salisbury, Gitelson, and Lisovsky 1997; Salisbury and Bugbee 1988). BIOS 1 focused on air regeneration: one human was sealed in a 12m3 chamber, whose atmosphere was recycled using an 18-Liter algal cultivator containing Chlorella Vulgaris. BIOS 2 followed in 1968 with the inclusion of higher plants (mainly wheat, but also carrots, cucumber and dill) and performed water recycling in addition to air regeneration. Then came BIOS 3 in 1972 and tested until 1985, which included food production on top of water recycling and air regeneration. But BIOS 3 was not a fully closed regenerative LSS, only a semi-closed, because urine and feces were not recycled but stored and the vegetarian diet from plant and algae was supplemented by dried meat. Ten closure experiments with humans were performed and the longest mission lasted for 180 days with a crew of three. Unfortunately, even on this longest mission, they did not manage to stabilize the microbial population within the system. In addition, BIOS had other problems that were not solved at the end of the testing like air leaking and the buildup of toxic oxides (Gitelson et al. 1989; Gitelson and Lisovsky 2008; Salisbury, Gitelson, and Lisovsky 1997).

Research in the field of bioregenerative LSS has continued in Russia and is still ongoing, especially on the use of higher plants within these systems and their cultivation strategies (Tikhomirov 1996), as well as on mass cycling within a LSS combining biological and physicochemical processes (Tikhomirov et al. 2003a; Tikhomirov et al. 2003b; Tikhomirov et al. 2007; Tikhomirov et al. 2012). The efficiency of the closed loop using different tech-

nologies and processes is also in their focus (Tikhomirov et al. 2007; Tikhomirov et al. 2012).

USA

Between 1991 and 1994, in Arizona, the private enterprise Biosphere 2, initiated by the joint venture Space Biosphere Ventures, primarily funded by Ed Bass's Decisions investment, aimed at demonstrating the feasibility of self-sufficiency in terms of food, with total recycling of human and animal wastes, complete water regeneration, and air regeneration with minimal air leakage, while maintaining safe levels of trace gases within the 200 m^3 atmosphere. Two crews of seven to eight people stayed 2 years and 6 months within the site. Although the first crew managed to produce enough food to survive, major problems with O_2 and CO_2 levels forced them to open the system (Marino 1999).

Except for some tests in 1961 investigating gas exchanges between monkey and Chlorella algae and small closed ecological systems with micro-organisms at University of Hawaii in 1967 (Eckart 1996), bioregenerative LSS research restarted in the USA in the late 1970s and really in 1980 when NASA launched its Controlled Ecological Life Support Systems (CELSS), involving a network of university researchers. The goal was to investigate food production and processing, nutrition, ecology of closed systems, and waste processing (Salisbury and Bugbee 1988; Kliss and MacElroy 1990; MacElroy, Kliss, and Straight 1992; R. M. Wheeler 2011; R. M. Wheeler 2017). In the late 1980s the Biomass Production Chamber, a large (20 m^2 of arable area), atmospherically closed chamber at Kennedy Space Center was created. The goal was to demonstrate food production, water recycling, and atmospheric control, as well as testing the effects of a tightly closed atmosphere on plant growth (Salisbury and Bugbee 1988; R. M. Wheeler 2011; R. M. Wheeler 2017). Between 1995 and 1997 within the Lunar-Mars Life Support Test Project (LMLSTP) at NASA Johnson Space Center four tests were performed on a bioregenerative LSS with human crews from one to four people and mission length from 15 to 91 days, with 5% of the caloric intake of the crew of four coming from the plant cultivation chamber. The goal of the project was to test an integrated closed-loop system that could recycle water, process wastes and revitalize the atmosphere, investigating physicochemical and biological techniques, but also study human factors, crew training, psychology, and physiology (Lane,

Sauer, and Feeback 2002). More recently in the USA, a Lunar Greenhouse prototype was developed at University of Arizona and is still being tested and upgraded (Sadler et al. 2009; Sadler et al. 2011; Giacomelli et al. 2012; Furfaro et al. 2017). This system does not include a human crew but aims at investigating plant growth in controlled environment, water and waste recycling, as well as air revitalization. The NASA group at Kennedy Space Center has been investigating plant growth in microgravity with the Veggie plant growth system since 2013 (Massa 2016a; Massa 2016b). Veggie is more of a hardware demonstration than a system to perform science experiments on plant growth (Massa, Romeyn, and Fritsche 2017). So the Advanced Plant Habitat was developed and will soon be tested in microgravity (Massa et al. 2016).

Japan

In 1990, the Institute for Environmental Sciences (IES) was established in Japan and four years later, the construction of the Closed Ecology Experiment Facilities (CEEF) began (Ashida and Nitta 1995), including a habitat module, a plant module and an animal habitation module, with the aim of performing tests on bioregenerative LSS (Tako et al. 2008). The CEEF was finished in 2001 and week-long experiments started in 2005, lasting from one to four weeks involving two crew members and two goats (Tako et al. 2008). In the first tests 82% of the crew's food originated from the plant cultivation module and the goat's milk and the air was fully revitalized (Tako et al. 2007). Later the water loop was added, and in 2007 a waste processing system was integrated into the CEEF (Tako et al. 2010). This facility is not intended primarily at studying human space exploration, but at studying and understanding ecosystems in prevision of a potential nuclear catastrophe.

China

In the years 2000, experiments on bioregenerative LSS started in China (Ai et al. 2008; Chunxiao and Hong 2008; Guo et al. 2008). The gas loop was among the first tests and consisted of volunteers breathing in a tube connected to a photo-bioreactor containing the algae Chlorella; then human subjects breathed oxygen produced by lettuces and Chlorella and finally silkworms were introduced (Tong et al. 2011). The facility Lunar PALACE 1 (PALACE is the acronym for Permanent Astrobase Life-support Artificial Closed Ecosystem) at the Beihang University in Beijing enables large-scale bioregenerative LSS exper-

iments involving humans, with one crew module and two cultivation modules, covering 160 m^2 for a total volume of 500 m^3. The first experiment of this kind took place in 2014 and lasted 105 days with three human test subjects (Dong et al. 2016; Xie et al. 2017). The second experiment started in July 2017 and is still ongoing: it lasted for 200 days and two crews of four were locked inside (Beihang University 2017).

Europe

In Europe, fundamental research on plant physiology, ecophysiology, and controlled environment agriculture was investigated at the Atomic Energy and Alternative Energies Commission (CEA) center of Cadarache in France in the 1960s as a precursor research to regenerative LSS.

Then in the 80s new bioregenerative LSS research projects were born: in 1987 the Micro-Ecological Life-Support System Alternative (MELiSSA) project, which is detailed in the next paragraph, was born (Mergeay et al. 1988) and in 1986 in Germany, the Closed Equilibrated Biological Aquatic System (C.E.B.A.S.) was developed by the Ruhr-University of Bochum (RUB) (Bluem 1992). It consisted of a closed aquatic ecosystem containing fish, water snails, bacteria, and water plants and flew three times aboard the Space Shuttle and on the Chinese Spacecraft SHENZHOU-II (Bluem et al. 2000; Wang et al. 2004). It targeted the influence of space conditions on these organisms and on an ecosystem as a whole. Between 1998 and 2013, the German projects Aquacells and Omegahab, followers of the C.E.B.A.S. flew aboard Russian satellites with fish and the algae Euglena (Häder et al. 2006; Hilbig and Lebert 2010). The algae Euglena is also studied within the DLR project Eu:CROPIS scheduled for launch in 2018 aboard the Falcon 9 rocket, which will analyze urea breakdown into nitrate in an ecosystem including the Euglena and tomatoes (Hauslage, Lebert, and Müller 2014). Taking over the C.E.B.A.S. research, the OHB project MOduLES started investigating an algae photo-bioreactor with Chlamydomonas in parabolic flights (Hilbig, Anken, and Grimm 2010). Another bioregenerative LSS concept is the joined European-American project (University of Rome (Italy), University of Turku, (Finland), DLR Institute of Planetary Research, and NASA Ames Research Center) CyBLiSS (Cyanobacterium-Based Life-Support System), investigating how cyanobacteria could provide food, oxygen and fuel to the crew, as well as

process Martian resources in order to support the growth of higher plants (Verseux et al. 2016). Other research groups in Europe focus on specific parts of regenerative LSS, like for instance, the growth of higher plants in controlled environment (EDEN group of DLR in Bremen, Germany and the CAB project led by TASI in Italy) (Lobascio et al. 2008; Zabel et al. 2016; Zabel et al. 2017).

1.3 The MELiSSA project

1.3.1 MELiSSA Loop Overview

The leading bioregenerative LSS project in Europe for more than 27 years is the Micro-Ecological Life-Support System Alternative (MELiSSA) (Mergeay et al. 1988; Lasseur et al. 2011). This project is led by ESA and gathers 14 official partners, from Europe and Canada, bonded with a Memorandum of Understanding and involves more than 40 organizations from 13 different countries (Belgium, Canada, France, Germany, Ireland, Italy, Norway, Romania, Russia, Spain, Switzerland, The Netherlands, and Great Britain).

Figure 1.3: Diagram showing the MELiSSA loop as a lake ecosystem. Credits: MELiSSA.

MELiSSA is a closed-loop LSS inspired by a lake ecosystem (see Figure 1.3), based on micro-organisms, micro-algae, and plants, and using light as a source of energy and the metabolism of plants and algae to recover food, air, and water (Hendrickx et al. 2006). Micro-organisms degrade organic wastes of the crew and transform them into simple elements that can be fed to algae and plants, which combine them to the CO2 expired by the crew to produce breathable oxygen, food, and pure water. The five compartments of the bioregenerative LSS MELiSSA recreate the five degradation steps in a lake (see Figure 1.4 and Table 1.2).

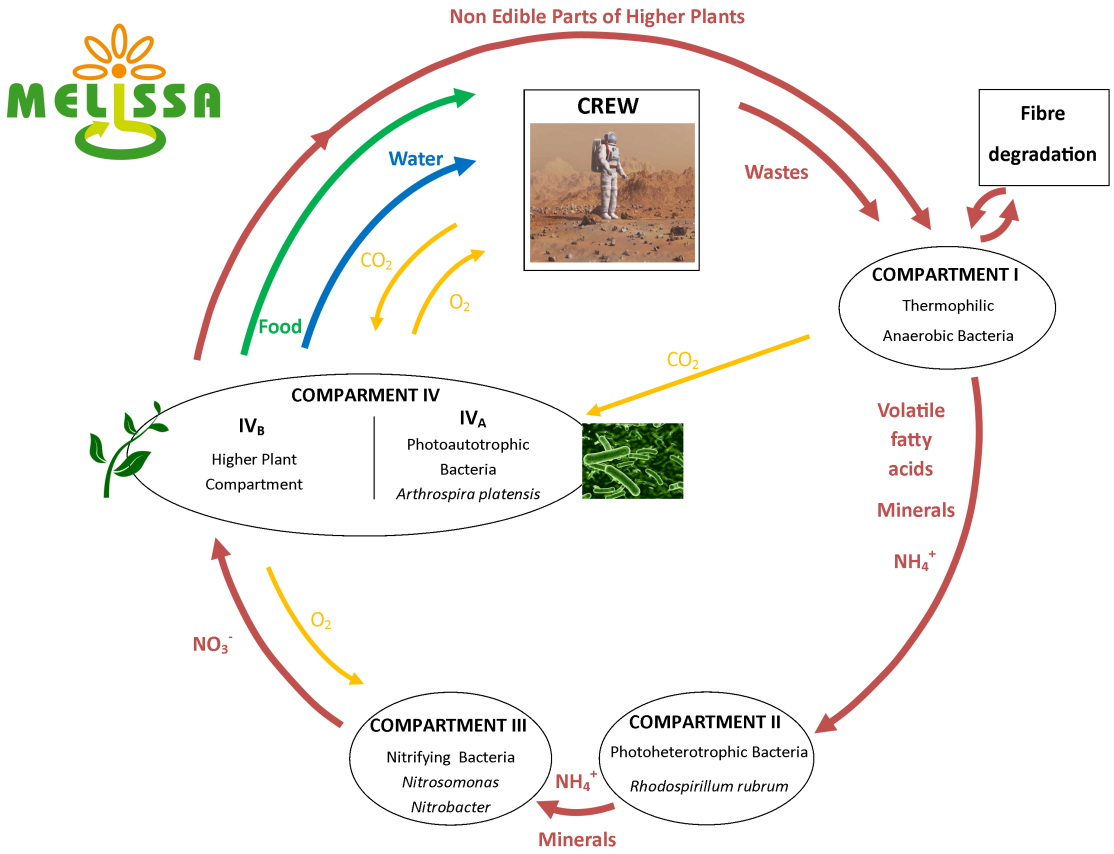

Figure 1.4: Diagram of the MELiSSA loop and its five compartments. Credits: MELiSSA.

1.3.2 Development phases

MELiSSA follows five development phases which run in parallel. Phases 1 to 3 focus on the development and test of each compartment, as well as their integration, while phase 4 focuses on terrestrial applications, and phase 5 on public outreach.

Table 1.2: MELiSSA's five compartments functions (Lasseur et al. 2011).

#	**Name**	**Organism**	**Input**	**Output**	**Action**
CI	Liquefying compartment	Thermophilic anoxygenic bacteria	Non-edible part of plants from CIV, food waste, feces, paper, non-edible microbial biomass	NH4+, CO_2, VFA, minerals	Degrading and Solubilizing organic wastes • Proteolysis: 70% • Fiber degradation: 44%
CII	Photoheterotrophic anoxygenic compartment	Photoheterotrophic bacteria	NH_4^+, CO_2, VFA, minerals from CI	NH_4^+, minerals	Transforming organic carbon into inorganic carbon
CIII	Nitrifying compartment	Nitrifying bacteria	NH_4^+ and minerals from CI; urine from CV; O_2 from CIVa	NO_3^-	Transforming different sources of nitrogen into nitrates
CIVa	Photoautotrophic compartment: algae	Cyanobacteria Arthrospira Platensis	NO_3^- from CIII and CO_2 from CV and CI	O_2 and food	Regenerating the atmosphere and producing protein-based food: the blue-green alga is edible and has a high protein content
CIVb	Photoautotrophic compartment: higher plants	Edible plants: two types of wheat, potato, soybean, rice, beet root, and lettuce	NO_3^- from CIII and CO_2 from CV and CI	O_2, food, and water	Regenerating the atmosphere and water and providing food diversity
CV	Crew compartment	Humans	O_2, food, and water from CIV	CO_2, organic wastes, urine, and sweat	Consumers

The basic research and development of each compartment is done in phase 1, including characterization (Poughon, Dussap, and Gros 1999; Cogne, Gros, and Dussap 2003; Clauwaert et al. 2015; Cruvellier et al. 2016), stoichiometry (Dussap, Cornet, and Gros 1993; Cornet, Dussap, and Gros 1998), mathematical models (Poughon, Dussap, and Gros 1997; Pérez et al. 2005; Holmberg, Paille, and Lasseur 2013), and control strategy (Poughon, Dussap, and Gros 1999; Cornet, Dussap, and Leclercq 2001). Each compartment is assessed by a chemical engineering concept and approach, described with a mass balance that experimental data from batch and continuous cultures can validate, as well as kinetics describing it dynamically (Gros et al. 2003). Mechanistic models of each compartment and of the loop as a whole are developed, in order to reuse previous work in various settings and conditions (see part 1.4) (Hézard et al. 2010; Sasidharan et al. 2010). Preliminary flight experiments are performed in phase 2 in order to gain knowledge on the behaviors of some biological processes in space environment. These experiments are

simple and small and are used to validate mathematical models, or a hypothesis on a behavior, and to validate the technology used. Especially the adaptation of bacteria to spaceflight environment has been investigated many times: MESSAGE (Microbial Experiment in Space Station About Gene Expression) 1 and 2 respectively flew in 2002 and 2003, and BASE flew in 2006 and 2009. In 2015 the experiment BISTRO on the ISS investigated micro-organisms bioprocess recovery after spaceflight and the experiment DEMES tested crew perception of snacks based on MELiSSA-produced products. The experiment ArtEMISS is scheduled for flight in 2017 and will study the growth kinetics of Spirulina when exposed to space environment.

Phase 3 encompasses space and ground demonstration. The MELiSSA loop is first tested on the ground with the ground demonstrator MELiSSA Pilot Plant located at the Universitat Autonoma de Barcelona (Gòdia et al. 2004), where the progressive integration of all compartments is done step by step (Gòdia et al. 2004; Poughon et al. 2009). Each compartment liquid, gas, and solid phases are separately linked together until full integration is achieved (Cabello et al. 2001). Currently compartments CIII, CIVa, and CV have been successfully integrated together, with the crew compartment hosting rats but the ultimate goal is to have a MELiSSA loop demonstrator functioning with humans.

MELiSSA has other goals like enabling the innovative solutions created within MELiSSA to benefit Earth applications (phase 4) and inform and create awareness about space exploration (phase 5). A spin-off company was thus created to manage this technology transfer: IPStar BV. Communication about the MELiSSA project ranges from actions targeting experts to the general public and school students. Numerous educational activities have been performed in the frame of MELiSSA; hundreds of posters and scientific presentations and articles, as well as scientific reports; but also hundreds of magazine, newspaper, web articles, and many TV and radio participations and exhibitions.

1.3.3 The Higher Plant Compartment

The focus of this thesis is set on MELiSSA's higher plant compartment. A prototype of the higher plant chamber is located at the MELiSSA Pilot Plant in the Universidad Autonoma de Barcelona (Gòdia et al. 2004). Plants are grown using the nutrient-film technique under high-pressure sodium lamps. The atmospheric system is separated from the lamps using a glass plate, to limit the heat load inside the plant chamber. Candidate

crops of the MELiSSA project include durum and bread wheat, rice, potato, soybean, lettuce, and beet root. However tests conducted in the HPC at the MPP are exclusively done with lettuce as this a very good model crop (short growth cycle, easy to grow from seeds, much data collected on many cultivars).

Compartment IVb has been the centre of many studies lately within the MELiSSA Food Characterization phases 1 and 2, and more specifically with the HySSE (HYdropoonic SubSystems Engineering) and AtSSE (ATmospheric SubSystems Engineering) projects. University Clermont Auvergne was a partner of the AtSSE project for the modeling part and the following paragraphs are inspired from the TN 117.1 written for the AtSSE project (Poulet, Fontaine, and Dussap 2016).

The aim of HySSE was to design the root zone system of a plant cultivation unit, combining biological and engineering approaches. Indeed one focus was to study the ecosystem of the root zone and the interactions between plant roots and micro-organisms and the other focus was to find hardware solutions for an advanced plant cultivation unit.

The aim of AtSSE was to design the atmospheric (shoot zone) system of a plant cultivation unit, enabling precise scientific measurements on gas exchanges and photosynthesis rates by measuring:

- Air temperature
- Total and partial pressures of the main gases (water (VPD), oxygen, carbon dioxide)
- Light intensity and spectral composition
- Photoperiod
- Hydroponic solution temperature
- Nutrient solution pH and Electrical Conductivity (EC)

This should enable the validation of plant growth models developed at University Clermont Auvergne.

1.4 The MELiSSA strategy

MELiSSA aims at recycling the atmosphere and water, managing wastes, and producing food, based on biological processes, with the highest percentage of closure, while respect-

ing safety standards. Hence the efficiency and compatibility of these processes must be demonstrated and their model and control must be established. Modeling the MELiSSA loop goes through different stages:

- Knowledge and mechanistic models to understand basic underlying mechanisms of biological processes of all-subsystems of the loop
- Calibration of knowledge models thanks to experimental data, enabling predictive tools
- Control model of the closed loop system

Developing a mechanistic model of the loop requires characterizing mass and energy balances and to establish accurate stoichiometry and limiting rates (Dussap, Cornet, and Gros 1993; Gros et al. 2003; Poughon et al. 2009). Ultimately the mechanistic model will need to be robust and predict processes at nominal points and degraded modes. It is built in such a way that it can predict and extrapolate the behavior of biological processes for a wide range of parameters. This is one of the most crucial requirements for life support systems control. Indeed sustaining humans requires having a very accurate control of the processes involved in their survival. A mechanistic model implies a thorough understanding of all mechanisms involved and can thus predict the behaviour of the different processes and of the loop in case of failure, especially the implications in terms of oxygen, water and food production. A complete modelling of the MELiSSA loop will include a dynamic model (Poughon 1998), taking kinetics and limitations into account, as well as time constants of each compartment. This was already done on the micro-algae compartment (CIVa) using Matlab/Simulink (Poughon 1994; Cornet et al. 1995; Poughon 2005), which is the best described and understood compartment of the loop. A dynamic model describing the gas phase of the coupled CIVa and crew compartment was also achieved (Poughon 2007) and enabled to identify challenges in using Matlab/Simulink to model closed systems.

The three microbial compartments of the MELiSSA loop (CI, CII, and CIII) have also already been modelled in a mechanistic way (Poughon, Dussap, and Gros 1999; Pérez et al. 2005; Poughon 2005), predicting their growth in terms of outputs (for example oxygen, nitrate, CO_2) depending on environmental conditions and mass and energy inputs in the reactor functioning continuously.

The modelling effort is now set on the higher plant compartment (CIVb) (Ordoñez et al. 2004) and specifically plant growth mechanistic models (Sasidharan et al. 2010; Hézard et al. 2010; Hézard 2012). Typical agronomy models for plant growth are empirical or set to work for a given range of environmental data, since they are intended for agricultural decision support (Hézard 2012), e.g. predicting the yield of a certain crop under certain environmental conditions (Lopez et al. 2010; Ordoñez et al. 2004), or for fundamental plant biology knowledge models, e.g. understanding the phenomenon of gravitropism (Bastien, Douady, and Moulia 2015) or sap ascent (Da Silva et al. 2011) ; they are very good predictive tools but do not provide a better understanding of plant growth mechanisms. The objectives of a mechanistic model are to characterize plant growth mechanisms and composition under a wide range of environmental parameters. Eventually this will serve as a predictive tool for optimization and control of MELiSSA Higher Plant Chamber.
The difference in size between microorganisms and plants changes the modelling strategy, since the type of culture is different. Microorganisms can be modelled as a community, as the individual behaviour of one individual does not change the overall behaviour. On the contrary, plants are complex organisms, with many different organs and growth phases, requiring different environmental conditions. The model cannot infer a homogeneous compartment but must differentiate time and space. Hence plant morphology and environmental conditions at the organ scale, as well as plant development and growth history must be included (Hézard et al. 2010). The model is thus more complex, with several layers of description, including gas exchanges at the leaf surface, water and solutes absorption in the roots and transport through the stem, as well as light interception. Plants are thus first modelled as individuals, at a local scale, and then this model can be integrated on a canopy as a whole.

1.5 Extended abstract of the review article

The study of higher plant growth in space started in the 1950s both on the Russian and the American sides. The first experiments were intended to assess whether plants could grow outside Earth and to determine what differences there were between spaceflight-grown and Earth-grown plants. As plant-growth hardware started to adapt to spaceflight, more opportunities for plant experiments in space became available. Direct microgravity

effects started being differentiated from confinement effects and Earth orbit started to become a laboratory where plants could be grown without the influence of Earth gravity. Experiments have shown that, with adapted ventilation, plant growth in space is similar to plant growth on Earth in 1g. Indeed the lack of free convection in weightlessness results in stagnant air leading to the accumulation of volatile organic compounds and creating thick boundary layers around plant's leaves, which reduce gas exchanges associated with photosynthesis, and leading to suboptimal plant growth. Some morphological traits are modified in reduced gravity environments: roots do not grow in a preferred direction and gravitropism does not occur in weightlessness. However only small-scale experiments on plant growth, like LADA on the Russian side or Veggie on the American side, were performed in Earth orbit, which provided insufficient data on crop yield for reduced gravity environments.

Challenges remain to grow plants in space, in terms of nutrient delivery, lighting, and ventilation, but also on the choice of plant species and traits to favour. Additionally, significant effort must be made on mechanistic modelling of plant growth to reach a more thorough understanding of the intricate and combined physical, biochemical, and morphological phenomena involved, which is necessary to accurately control and predict plant growth in life-support systems. This is a necessary requirement for life-support systems since this will condition human survival outside of Earth. The system behaviour must be predicted for a wide range of parameters since space conditions can be very different than Earth conditions and in case of failure of one equipment, losing all biological systems is not acceptable. Instead the prediction of a failure impact on oxygen, water and food production should be made possible thanks to mechanistic modelling.

This review intends to list the main spaceflight effects to take into account for plant growth in space, as well as to give an overview of the current state of plant-growth hardware while stressing out the challenges associated with their development.

1.6 Review article

This part was published in Botany Letters in July 2016.

Botany Letters

ISSN: 2381-8107 (Print) 2381-8115 (Online) Journal homepage: http://www.tandfonline.com/loi/tabg21

Plant's response to space environment: a comprehensive review including mechanistic modelling for future space gardeners

L. Poulet, J.-P. Fontaine & C.-G. Dussap

To cite this article: L. Poulet, J.-P. Fontaine & C.-G. Dussap (2016): Plant's response to space environment: a comprehensive review including mechanistic modelling for future space gardeners, Botany Letters, DOI: 10.1080/23818107.2016.1194228

To link to this article: http://dx.doi.org/10.1080/23818107.2016.1194228

Published online: 07 Jul 2016.

BOTANY LETTERS, 2016
http://dx.doi.org/10.1080/23818107.2016.1194228

Taylor & Francis
Taylor & Francis Group

Plant's response to space environment: a comprehensive review including mechanistic modelling for future space gardeners

L. Poulet[a,b], J.-P. Fontaine[a,c] and C.-G. Dussap[a,c]

[a]Institut Pascal, Université Clermont Auvergne, Clermont-Ferrand, France; [b]CNRS, UMR 6602, IP, Aubière, France; [c]Institut Pascal, Université Clermont Auvergne, Université Blaise Pascal, Clermont-Ferrand, France

ABSTRACT

The study of higher plant growth in space started in the 1950s both on the Russian and the American sides. The first experiments were intended to assess whether plants could grow outside Earth and to determine what differences there were between spaceflight-grown and Earth-grown plants. As plant-growth hardware started to adapt to spaceflight, more opportunities for plant experiments in space became available. Direct microgravity effects started being differentiated from confinement effects and Earth orbit started to become a laboratory where plants could be grown without the influence of Earth gravity. Experiments have shown that, with adapted ventilation, plant growth in space is similar to plant growth on Earth in 1 g, except for some morphological traits. However, only small-scale experiments on plant growth were performed in Earth orbit, which provided insufficient data on crop yield for reduced gravity environments. Challenges remain to grow plants in space, in terms of nutrient delivery, lighting and ventilation, but also on the choice of plant species and traits to favour. Additionally, significant effort must be made on mechanistic modelling of plant growth to reach a more thorough understanding of the intricate and combined physical, biochemical, and morphological phenomena involved, which is necessary to accurately control and predict plant growth in life-support systems. This review intends to list the main spaceflight effects to take into account for plant growth in space, as well as to give an overview of the current state of plant-growth hardware while stressing the challenges associated with their development.

ARTICLE HISTORY
Received 17 February 2016
Accepted 14 May 2016

KEYWORDS
Environmental control and life-support system; mechanistic modelling; microgravity; plants; space

Introduction

Growing plants in space requires a deep understanding of plant growth mechanisms (Hezard et al. 2010) and proficient know-how in controlled-environment agriculture (Steinberg, Ming and Henninger 2002; Kiss et al. 2014). For many decades, healthy plants have grown on spacecraft environments; Porterfield et al. (2003) gave an extensive review of the evolution of plant growth experiments in space and associate hardware in the years 1960–2000. However, long-term effects of the space environment on plant growth and reproduction are not yet well known and understood, and could impact the role of plants as food source in bioregenerative life-support systems (Wolff et al. 2014). Indeed plants will play a critical role in the survival of human beings outside Earth for long-durational missions within the Solar System.

Environmental control and life-support systems

Survival of astronauts in space is ensured by Life-Support Systems (LSS), which have the functions of recycling water and revitalization of the atmosphere. On the International Space Station (ISS) the current standard are physicochemical LSS: oxygen is produced using water electrolysis in the Oxygen Generation Assembly and a Sabatier reactor uses the metabolically generated CO_2 and the by-product of water electrolysis H_2 to produce water (Bagdigian and Cloud 2005; Burkey et al. 2010); urine is recycled into potable water in the Urine Processor Assembly and water vapour is also recovered from the cabin air to be used as potable water (Carter 2010). Although these LSS are easier to set up and to control than bioregenerative LSS, they are unable to provide the astronauts with food. Only biological processes have the ability to grow fresh food. Bioregenerative LSS are based on living organisms (micro-organisms, algae, plants, fish, etc.) and therefore require very precise control to be efficient and reliable.

Research on bioregenerative LSS has been ongoing since the early 1950s (Salisbury, Gitelson and Lisovsky 1997; Wheeler 2010). BIOS 1 to 3 were the first bioregenerative LSS tested in the former USSR from 1965 to 1985, which included alga *Chlorella vulgaris*, plants and human subjects (Gitelson et al. 1989). The longest mission lasted for 180 days (half a year), consisting of

CONTACT L. Poulet Lucie.Poulet@etudiant.univ-bpclermont.fr

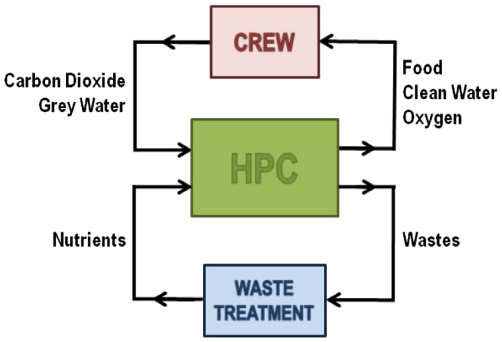

Figure 1. Diagram showing the different mass fluxes between the higher plant chamber (HPC) and the crew and waste treatment unit of a regenerative life-support system (not including crew organic waste treatment in this figure).

three crewmates, performing air regeneration, water recycling and provision of vegetarian food (including wheat, chufa, beet, carrots), supplemented by dried meat, although urine and faeces were not recycled but simply stored (Gitelson and Lisovsky 2008). The BIOS systems demonstrated that, even on the longest test (6 months), the microbial population within the system could not be stabilized; there were also problems with system leakage and the building up of toxic oxides in the system atmosphere due to the incineration of inedible parts of the plants (Rygalov, Kovrov and Denisov 1997). In the 1980s, the NASA Controlled Ecological Life Support Systems program investigated food production and processing, nutrition, ecology of closed systems, and waste processing (Wheeler 2010). In the late 1980s, scale-up tests of the fundamental findings from the university laboratories were performed in the Biomass Production Chamber at the Kennedy Space Center. With an arable area of 20 m^2, this large, atmospherically closed chamber was used to demonstrate food production, water recycling and atmospheric control, as well as testing the effects of a tightly closed atmosphere on plant growth. Tests performed in the Biomass Production Chamber provided baseline values for different candidate plant species, in terms of productivity, gas exchanges, evapotranspiration and mineral nutrition, which could be used in bioregenerative LSS calculations, as well as lessons learned for future similar studies (e.g. the necessity to emphasize the use of dwarf plants in space or the criticality to control volatile organic compounds to a low level in confined environments, since they negatively affect whole-plant growth and therefore also harvesting index) (Wheeler et al. 1996).

On the European side, the leading project for the last 26 years on regenerative life-support research has been the Micro-Ecological Life-Support System Alternative (MELiSSA) project led by the European Space Agency (ESA). Inspired by a lake ecosystem, the concept of MELiSSA is a closed loop organized in five compartments: three of which are based on micro-organisms degrading and transforming the organic wastes of the crew into elements that are used, together with carbon dioxide from the crew and organic wastes of the mission, to feed the fourth compartment – which is based on higher plants and algae, that in return provides food, oxygen and water to the fifth compartment, which is the crew (Gòdia et al. 2002; Lasseur et al. 2010). One challenge of the project is to avoid contamination between the different compartments, while ensuring a mass and energy balance of the loop. It was shown that about 90% of the water absorbed by plant roots is transpired, so entering the gas loop, and 10% is used for biomass creation in plants (Hezard et al. 2012). When plants only provide 20% of the astronauts' diet, water recycling is achieved (Eckart 1994). Atmosphere can be recycled and all breathable oxygen provided when 50% of the astronauts' diet is covered by plants (Eckart 1994). The average respiratory quotient of one human being is in the range of 0.8–0.9 (Poughon 1997), so the objective is to recycle 1.1 to 1.3 mol of oxygen per mol of carbon dioxide, which is achieved by all candidate crops of the MELiSSA project (e.g. wheat, rice, soybean, potato, lettuce) (Poughon 1997). The average harvest index of these crops is 50%, meaning that half of the biomass produced in the MELiSSA loop is edible and goes to the crew compartment, whereas the other half is inedible waste needing to be recycled (see Figure 1, where the mass fluxes to and from a higher-plant chamber are represented, including the crew compartment and a partial waste treatment). To have a reliable system, it is necessary to accurately predict behaviour of biological processes and control their activity at a compartment level and at a loop level. This is achievable by understanding the mechanisms, which govern such biological processes (see Figure 2).

The MELiSSA approach is therefore to develop mechanistic models of the entire loop and in parallel to build and test lab-scale prototypes of each compartment. All three microbial compartments and the algae compartment are effectively modelled mechanistically (Cornet, Dussap and Gros 1998; Cogne, Gros and Dussap 2003; Ordoñez et al. 2004), while modelling efforts on the higher plant compartment are currently ongoing (Hezard et al. 2010, 2012). The main difference with existing agronomy models is that plants in bioregenerative LSS will grow in a confined environment, so slight variations in environmental parameters can strongly affect the whole system, because there are no buffer effects of the atmosphere, oceans or soil. Therefore it is critical to understand plant growth mechanisms, as well as variations of the physical environmental surrounding plants, using platforms, such as the ISS in Low Earth Orbit, which offers microgravity environments.

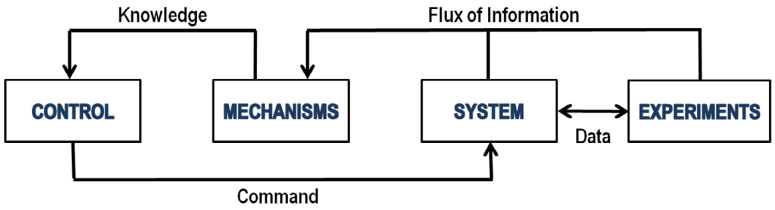

Figure 2. Diagram showing the links between a system, the experiments conducted on it, its mechanisms, and a control loop, which are the principles of mechanistic modelling. Information about the system enables us to understand mechanisms about this system, which provides knowledge on how to control it.

Understanding mechanisms of plant growth and development

The goal of many fundamental plant growth experiments in Earth orbit since the 1960s (Porterfield et al. 2003) has been to study plant growth and development, from germination to reproduction mechanisms, tropisms and circumnutation, as well as biochemistry and molecular biology (Paul et al. 2013). Experimenting in Earth orbit (space stations such as Mir or the ISS, Space Shuttle, or satellites), in parabolic flights, in sounding rockets, or even on clinostats, enables us to investigate certain growth mechanisms outside the influence of gravity. Phototropism and gravitropism have therefore been extensively studied in orbit and there has been a significant effort made to separate the overlapping effects of light and gravity on plant growth (Vandenbrink et al. 2014).

It was shown that the gaseous environment was very important for plant growth and development in space. It was initially thought that microgravity led to smaller plants and that their reproduction was impaired (Musgrave et al. 2005; Paul et al. 2013) but as plant growth hardware for space improved, these artefacts disappeared and it was shown that plants can grow normally in microgravity provided that the plants grow in a well-ventilated area (Monje, Stutte and Chapman 2005). A major result in space biology was the demonstration of a seed-to-seed growth of *Arabidopsis thaliana* on orbit during STS-68 mission, which showed no difference with ground controls (Kuang, Xiao and Musgrave 1996; Paul et al. 2013).

After reviewing the different effects of spaceflight on plant growth, which are critical for food production in space, this paper intends to provide an overview of state of the art plant-growth technologies developed for Earth orbit and planetary surfaces, while highlighting the remaining challenges of space agriculture.

Effects of spaceflight on plant growth

In early spaceflight experiments on plant growth and development, many observed effects that were attributed to microgravity were actually due to indirect spaceflight effects (Paul et al. 2013), such as confinement – leading to build-up of volatile organic compounds, such as ethylene – and lack of convection – resulting in super-elevated CO_2 levels in the spacecraft and locally at plant-leaf surfaces (Monje et al. 2003). Elevated radiation levels also have negative, not yet fully known, effects on plant growth and development. On-orbit plant experiments can therefore be confounded by these spacecraft-specific artefacts (Musgrave 2002).

With the development of improved hardware for microgravity experiments minimizing indirect spaceflight effects, results on plant growth in space became more reliable and on-orbit plant growth appeared less chaotic than what was initially thought (Paul et al. 2013). It also seems that microgravity response is species- and cultivar-dependent, making it hard to find general patterns of plant growth and development in microgravity (Paul et al. 2013). The effects of microgravity on plant growth and development have been thoroughly reviewed in recent years (Wolverton and Kiss 2009; De Micco et al. 2014; Paradiso et al. 2014; Wolff et al. 2014; Kittang Jost, Hoson and Iversen 2015; Vandenbrink and Kiss 2016) and hence this review focuses on the aspects that are critical for plant cultivation in space. Radiation and magnetic field are also known to affect plant growth. As reviewed in Arena et al. (2014), plants can sustain radiation doses one hundred times higher than mammals can and low radiation doses might lead to positive outcomes such as increase in growth and photosynthesis. Their effects are thoroughly reviewed in De Micco et al. (2011) and Wolff et al. (2014) but will not be discussed herein.

Cellular and biochemical scale

Secondary metabolism

Although it was shown that, provided with adequate ventilation in space, plant development is similar to that on Earth (Monje, Stutte and Chapman 2005), secondary metabolism is affected by altered hypo- and hyper-gravity as reviewed by Tuominen, Levine and Musgrave (2009) and major changes in storage reserves were observed in the spaceflight environment, with seeds produced on orbit having different composition and developmental stages than seeds grown not only on Earth (Musgrave et al. 2005), but also on clinostats (Brown, Piastuch and Knott 1994). These changes in starch storage and metabolite production could impact

the vigour and nutritional content of seeds produced in space plants (Musgrave, Kuang and Matthews 1997) and might affect the flavour of plants produced in space (Musgrave et al. 2005), which could become a problem on long-duration space missions where crews would rely on plant-based diets. De Micco and colleagues in 2006 and 2008 found that the amount and repartition of starch and other metabolites were different in soy seedlings grown on clinostat and on the ISS than in their 1 g control plants (De Micco, Aronne and De Pascale 2006; De Micco and Aronne 2008). The seed-to-seed cycle of on-orbit grown plants, especially seedling development and establishment, as well as gametogenesis and pollination, were thoroughly reviewed by De Micco et al. in 2014. They concluded that these responses to altered gravity conditions could be interpreted as stress-induced morphogenic responses (De Micco et al. 2014).

Cell growth and proliferation

Cell growth and proliferation are two related processes that are coupled in 1 g but they seem to be decoupled in microgravity, which could have an impact on plant growth and development and hence on food production in reduced gravity environments (Medina et al. 2015). Manzano et al. in 2009 found that cell proliferation was enhanced, whereas cell growth was decreased in microgravity; they hypothesized that this decoupling was due to acceleration in cell division caused by a shorter G2 phase, leading to the formation of more cells with shorter sizes (Manzano et al. 2009). This result was confirmed in 2010 by Medina et al., who found that meristematic cell proliferation was enhanced while meristematic cell growth was reduced in microgravity (Medina et al. 2010). This was reviewed by Herranz and Medina in 2014, who hypothesized that changes in cell growth and proliferation in non-specialized cells in microgravity could be a result of gravity resistance mechanisms (Herranz and Medina 2014).

Gene expression

Recent progress in gene expression studies (e.g. microarray technology) has enabled the identification of changes in gene expression in microgravity, as reported in a review by Wolverton and Kiss (2009). Important results about gene expression in microgravity are (i) the overexpression of heat-shock-related genes, although plants were not exposed to elevated temperatures (Paul et al. 2005); (ii) the differential expression (down-regulation and up-regulation) of some genes in fern spores between 1 g and microgravity (Salmi and Roux 2008); (iii) the down-regulation of genes essential for normal root hair development (Known et al. 2015); (iv) a significant increase of proteins related to stress responses, defence and metabolism and a significant decrease of proteins related to auxin metabolism and trafficking (Mazars et al. 2014; Zhang et al. 2015). Herranz and Medina (2014) hypothesized that microgravity is perceived by the plant transcriptome as a novel stressful environment and that the genome lacks adequate genes to respond accordingly; hence the observation of up- and down-regulation of certain genes in microgravity (Herranz and Medina 2014). Understanding mechanisms of gene expression in microgravity will enable the selection of plants that adapt the best to reduced-gravity environments and to genetically engineer plants that are adapted for spaceflight and planetary surfaces food production.

Indirect effects at the organ scale

Although the activity of photosystems and the expression of some proteins involved in photosynthesis can be affected by spaceflight (Giardi et al. 2013), photosynthesis rate does not seem to be affected by microgravity (Monje, Stutte and Chapman 2005; Wolverton and Kiss 2009). Changes observed at the organ scale are mostly indirect consequences of the lack of gravity, altering fluids behaviour (no buoyancy-driven convection) and dominating forces (surface tension is prevalent in microgravity). The influence of spaceflight environment and the interaction between gas exchange, photosynthesis, and plant nutrition were thoroughly reviewed by Wolff et al. (2014), so a brief overview is given herein, highlighting how it could impact the growth of plants in space in future long-duration missions.

Domination of surface-tension forces

In microgravity, water creates thicker boundary layers around plant roots, which become oxygen deficient because of the roots' respiration, leading to root hypoxia (Porterfield et al. 1997; Monje et al. 2003). Therefore it was often observed in the early on-orbit plant experiments that the plants showed hypoxia-like ultra-structural changes due to oxygen limitation (Slocum, Gaynor and Galston 1984; Monje et al. 2003). Hence it became necessary to develop microgravity-specific watering systems enabling water and nutrient delivery and roots aeration.

Lack of convection

The fact that there is almost no natural convection in microgravity has direct consequences on plant growth. Indeed without adequate ventilation, thicker mass boundary layers form around plant leaves, increasing the transport resistance by diffusion, which in turns reduces gas exchange at the leaf surface and around the roots, inducing a depletion of certain gases (e.g. O_2, CO_2) in these layers because of the plant's activity such as respiration or photosynthesis, which can cause hypoxia (Porterfield 2002). This leads to a decrease in photosynthesis rates as reported during a parabolic flight experiment on sweet potato and barley leaves (Kitaya et al. 2001). As a result, leaf transpiration is decreased, causing an increase in leaf temperature. Kitaya et al. reported a mean increase of 1°C on leaf temperature

during a 20-second microgravity phase of a parabola (Kitaya et al. 2003a). A later parabolic flight experiment confirmed that the lack of natural convection in microgravity slowed down water vapour transfer, which decreased transpiration rate of plant leaves by 46% when gravity levels decreased from 1 g to 10^{-2} g, and increased the rate by 32% when gravity levels increased from 1 g to 2 g (Hirai and Kitaya 2009).

The lack of convection also leads to accumulation of gases and volatile organic compounds, resulting sometimes in very high ethylene concentrations, which is detrimental to plant growth (Musgrave 2002; Monje et al. 2003). High ethylene concentrations (i.e. 100–1000 parts per billion) can inhibit root and hypocotyl growth because ethylene is phytotoxic and disrupts or induces a variety of metabolic pathways (Levinskikh et al. 2000). Therefore, adequate ventilation is mandatory for regular plant development in microgravity and to ensure vital functions such as germination and plant reproduction (Monje et al. 2003; Monje, Stutte and Chapman 2005). Studying the gaseous environment surrounding plants and including it in the modelling effort of plant growth is crucial for optimal food production in space.

Morphological changes

Many flight experiments demonstrated that plants develop normally in microgravity (Ferl et al. 2002), i.e. the overall plant architecture is not altered by the lack of gravity, as long as adequate ventilation is provided. However, the pattern of root growth is more random than what is observed in ground controls, especially lateral roots tend to develop much more in microgravity instead of having a large primary root (Ferl et al. 2002) and V. Legué (personal communication, April 2015).

Plants tropisms have been extensively studied in orbit. For example, it was shown that *Arabidopsis thaliana* seedlings had a greater phototropic response to blue light in microgravity than in Earth gravity (Millar et al. 2010). Studies of plant roots in weightlessness have revealed much about the metabolic pathways of gravitropism and how plants grow according to the direction of the gravity vector, as well as about the mechanism of graviresistance, which is sensitive to the magnitude of this gravity vector (Wolverton and Kiss 2009; Herranz and Medina 2014). It was also shown that roots keep their skewing and waving pattern in microgravity (Paul, Amalfitano and Ferl 2012) although this was thought to be an effect of gravity. This experiment also showed that with a directional light, roots of plants grown in orbit are strongly negatively phototropic and grow in the opposite direction to the shoot, as is observed in 1 g on Earth (Paul, Amalfitano and Ferl 2012).

Understanding the different tropism mechanisms in plants and how they influence plant growth and development will enable us to use plants more efficiently for food production in future long-duration missions.

Existing solutions and remaining challenges for growing plants in space

The first seeds in space flew aboard the soviet Sputnik 4 in 1960 and the first plant growth system flew aboard the US Biosatellite II in 1967 with four pepper plants (Porterfield et al. 2003). Plant growth hardware which has flown in space until now had a weight in the order of a few kilograms and a power consumption in the order of the tens of watts (Porterfield et al. 2003). Plant-related experiments were intended to demonstrate the capability of plants to grow in a spacecraft environment and to study plant growth mechanisms, but they were not aimed at large-scale food production.

Watering and nutrient-delivery systems

An efficient and viable watering and nutrient-delivery system (NDS) in microgravity needs to provide water, nutrients and adequate aeration, as well as support plant growth from seed to harvest, while respecting operational and safety constraints of a spacecraft, especially triple nutrient solution containment (Stutte et al. 2011). Therefore substrate-based NDS have been used in microgravity instead of aeroponic or hydroponic systems (Monje et al. 2003). Moreover it was shown that moisture distribution in microgravity substrate-based NDS is similar to that of a hydroponic system in 1 g (Monje et al. 2003). A small-grained soil enables good water distribution in the root zone but prevents good soil aeration and a large grain soil enables proper aeration but voids between grains tend to be filled by air, not only water, which leads to poor root hydration (Casado 2006). A trade-off on particle size is therefore necessary and grain sizes used in microgravity-based NDS have ranged from < 0.5 mm to > 5 mm, the most commonly used being zeoponic particles with size 0.5–1 mm and arcillite with sizes 1–2 mm (Monje et al. 2003).

In addition, a nutrient-rich solid substrate or slow-release fertilizer is preferred to a nutrient solution, because it limits crew time spent on mixing fresh nutrient solution or making sure the solution is recirculated (Monje et al. 2003).

The lack of buoyancy-driven convection in microgravity prevents an efficient nutrient delivery and aeration of the roots. Due to capillary forces, water in microgravity tends to accumulate around water supply tubes, preventing it from reaching the roots uniformally and making nutrient delivery difficult (Dreschel and Sager 1989; Casado 2006). Early plant growth hardware, such as the soviet Oasis series, suffered from poor water distribution and lack of aeration in the roots (Porterfield et al. 2003). Later, systems such as the American Astroculture or the Russian Svet, used porous tubes within nutrient-charged zeolite granules to deliver water and nutrient to the plants by capillarity (Porterfield, Wright and Bausch 1984; Morrow et al.

Table 1. Significant examples of microgravity plant growth hardware – nutrients and water-delivery system and lighting system characteristics (Ivanova et al. 1997; Porterfield, et al. 2003; Casado 2006; Stutte, et al. 2011).

Name	Oasis 1, 1M, 1AM, 1A (Roskosmos)	Plant Growth Unit (Lockheed and NASA ARC)	SVET SG, 2SG, GEMS (USU and UBMP)	Astroculture & Advanced Astroculture (WCSAR)	LADA (USU and IBMP)	Veggie (NASA KSC)
Growth medium and nutrient delivery	Ion-exchange resin (plant nutrients and roots support)	Saturated foam or agar	Zeolite-based ion exchange matrix	Nutrient-rich zeolite granules	Granulated clay with slow-release fertilizer	Arcilite with controlled-release fertilizer
Water delivery	Manual pump	Wicking technique	Porous polyethylene tubes	Porous stainless steel tubes	Porous polyethylene tubes	Syringe – manual
Lights	Fluorescent	Fluorescent	Fluorescent	LEDs (Red + Blue)	Fluorescent then LEDs	LEDs (Red + Blue + Green)
Location	Salyut 1, 4, 6, 7	STS	MIR	STS, MIR, ISS	ISS	ISS

1994). Nowadays most microgravity NDS use porous tubes or drip irrigation for water delivery (Monje et al. 2003). Control and monitoring of moisture distribution in the growth media have also enabled better growth of plants in microgravity (Monje et al. 2003). The most recent plant cultivation system onboard the ISS, Veggie, is composed of pouches with rooting media and controlled-release fertilizer; water is delivered to the pouches using a syringe (Stutte et al. 2011), see Table 1.

Watering systems for planetary and moon surfaces can take advantage of the reduced gravity and be similar to terrestrial NDS and hence hydroponic (especially nutrient-film technique) and aeroponic systems can be used. For these systems to be efficient in plant growth, the use of real-time ion-specific sensors will be necessary, to monitor and control individual ions in the nutrient solution (Bamsey et al. 2012). Indeed plant nutrient uptake is not constant and depends on the crop species and cultivar, the growth phase, and the environment. Such systems have not yet been tested in space but are being developed (Bamsey, Berinstain and Dixon 2012).

Lighting

In the early years of plant growth in Earth orbit, lighting was provided by fluorescent lamps (Table 1). For example, on the Russian plant growth hardware Oasis 1, which flew on Salyut 1, fluorescent lamps supplied 50 to 68 μmol/m^2/s to *Brassica capitata*, *Linum usitatissimum*, and *Allium porrum* plants (Porterfield et al. 2003). Today, the American Veggie system uses Light-Emitting Diodes (LED) to illuminate plants on the ISS (Stutte et al. 2011). In 2006, Massa et al. performed an extensive review of plant growth lighting in space and concluded that LED lights were the future of plant growth lighting in space (Massa et al 2006). Indeed LEDs are small, light, have a long lifetime, and a cool emitting surface, and are solid-state light sources, which makes them ideal candidates for plant lighting in space (Bourget 2008). Plant productivity is directly related to light intensity, and in order to reduce the planted surface, significant amounts of energy are required (Wheeler et al. 2003; Casado 2006). A recent study showed that using LED lights instead of traditional High Pressure Sodium or fluorescent lamps can reduce power use per unit of growing area up to one order of magnitude and that the coupled use of targeted close-canopy lighting and spectral optimization with LED lights could significantly reduce energy costs for plant lighting in space and on Earth (Poulet et al. 2014a). Furthermore past studies have shown that red and blue wavelengths are best absorbed by plants (McCree 1971/1972) and so could mitigate the need for high-intensity lighting. Blue light is less efficient than red light from a photosynthetic point of view but it is very important for plant photomorphogenesis, like stem elongation and leaf expansion (Hoenecke, Bula and Tibbitts 1992; Dougher and Bugbee 2001).

Saving energy could also be achieved by taking advantage of sunlight on the surface of the planets and the moons. Sun collection systems composed of parabolic mirrors collecting sunlight and optic fibres transmitting this to a greenhouse module could be used in addition to LED lamps (Nakamura et al. 2009; Nakamura, Monje and Bugbee 2013). A joint study by the German Space Centre (DLR) and the ESA MELiSSA group showed that it was preferable to use such a hybrid lighting system in a Moon greenhouse module (Poulet et al. 2013; Eriksson, Doule and Poulet 2014).

Ventilation and controlled environment

On the ISS, ethylene concentrations are maintained below 50 ppb, but even such low concentrations have been shown to impact crop yields significantly (Monje et al. 2003). The European Modular Cultivation System is equipped with a precise atmospheric control system that removes ethylene from the experiment and controls temperature, humidity and air composition (ESA 2013), enabling small-scale and short-term fundamental plant physiology studies. Bigger-scale systems like Lada or Veggie, which are prototypes of food production systems, use cabin-air, which does not enable the collection of accurate data on gas exchange. There is a remaining gap in the know-how and knowledge of large-scale food production systems in microgravity and reduced gravity environments. This is because only small-scale plant growth systems have been taken into orbit.

Table 2. Parameters that need to be measured to mechanistically model plant growth in reduced gravity environments.

Parameter to observe	Type of measurement	Measurement technique
Water vapour released by the leaf	Water vapour concentration in the mass boundary layer	Infra-red gas analyser (IRGA), thermography, hygrometer
Water absorbed by the roots	Water content evolution in a solid substrate or water level evolution in a hydroponic root zone	Growing technique dependent
Stored water in the plant	Water content in plant tissue (leaf, stem)	Destructive sampling – wet and dry mass measurement
CO_2 absorption at the leaf level	CO_2 concentration evolution in the mass boundary layer	Infra-red gas analyser (IRGA)
CO_2 released by the roots	CO_2 concentration evolution in the root zone	O_2 probe
O_2 absorbed by the roots	O_2 concentration evolution in the root zone	CO_2 probe

Note: It is assumed that the root zone is hermetically sealed from the atmosphere compartment so that water does not evaporate from the root zone to the atmosphere compartment.

Confined space

Available room in a spacecraft or in a planetary module is much reduced. Therefore it is critical to select plants and cultivars with high yields but reduced size (De Micco et al. 2012). Utah State University has been doing research on dwarf plants for many decades and has developed and tested seeds of dwarf wheat, dwarf cherry tomato, dwarf rice, dwarf pepper, dwarf soybean and dwarf pea, which have successfully grown on orbit and in analogue planetary habitats (Salisbury 1997; Poulet et al. 2014b). In addition, research is currently on-going on controlled-environment cultivation of dwarf plum trees at Kennedy Space Center (Graham et al. 2015). A solution for future long-duration space missions could be to genetically engineer plants and create cultivars that are specifically adapted for confined space and spaceflight environment.

Parameters that need to be observed

A key point for managing growth of plants in space for food production is being able to predict plant yield and accurately control plant growth and development in a spacecraft environment. This can only be achieved with a thorough understanding of the intricate combination of the biochemical, physical and morphological phenomena that govern plant growth in weightlessness. Such knowledge can be ensured with the development of specific experiments and mechanistic and knowledge models of plant growth in reduced gravity environments, which could be validated with the observation and local measurement of a certain set of parameters (see Table 2). Hence such an approach would lead to accurate mass and energy balances of the plant (Hezard 2012). Water transfer within a plant has proven to be critical for understanding plant growth mechanisms and this needs an accurate evaluation of water absorption at the root level and water transpiration at the leaf surface. The estimation of water content within plant tissue can be achieved by measuring wet and dry masses in destructive sampling. Carbon cycle and carbon balance within a plant are also critical, as this is directly linked to biomass production (Wheeler 2003). Carbon fixation through photosynthesis and carbon release through respiration, therefore need to be accurately measured. Carbon dioxide and water vapour release at the leaf surface are linked to the aerodynamic profile of the surrounding air and of the mass boundary layer around the leaf (Kitaya et al. 2003b). In order to predict gas exchanges at the leaf surface, it is critical to accurately characterize and describe the aerodynamic profile of the air surrounding the leaf.

Conclusion

So far, plant experiments in space have focused on the feasibility of plant growth and/or on the study of specific fundamental mechanisms of plant growth and development, and only a few experiments have accurately locally measured inputs and outputs within a plant.

Effects of spaceflight on plant growth are not yet fully understood but it seems that it causes no major obstacle to plant growth in space, as long as adequate ventilation, lighting, and temperature and humidity control are provided. However, large-scale tests for food production in reduced gravity are still lacking. Research and technological tests on optimal nutrient-delivery systems for microgravity or partial gravity are still on-going; lighting for plant growth in space has progressed tremendously since the 1980s but the energetic burden generated by electrical lighting remains a limit for large-scale plant production; much work remains to be done on plant gas-exchange in reduced gravity environments, especially when it comes to larger growth chambers; the limited amount of room in a spacecraft drives the choice of plant species towards small crops, with a high harvest index, and cultivar selection for food production in space currently is on-going; finally growth mechanisms under space factors need to be fully understood to accurately predict the behaviour of biological processes and have a reliable LSS based on higher plants. Therefore developing mechanistic models of plant growth subjected to space environment (e.g. reduced gravity, high radiations, changing magnetic field, and low pressure) is crucial, as it helps us to understand underlying mechanisms and identify knowledge gaps in plant growth and development.

Acknowledgements

The authors would like to thank the Centre National d'Etudes Spatiales (CNES) and Centre National de Recherche Scientifique (CNRS) who supported this work.

Disclosure statement

No potential conflict of interest was reported by the authors.

Notes on contributors

Lucie Poulet worked for 2 years at the German Aerospace Center Institut of Space Systems (prior to starting her PhD at University Blaise Pascal) where she acquired experience in managing European Space Agency (ESA) projects, as well as participating in and leading concurrent engineering studies. Her experience in the 4-month simulated Mars mission HI-SEAS mission and at Purdue University during her Master's degree in aerospace engineering has led her to acquire competence in designing plant-related experiments and identifying flaws in hardware for plant growth in controlled environments. Focusing on developing physical models of higher plant growth in reduced gravity environment led her to review how plants grow in space and how microgravity influences their growth and development, as well as what are the remaining challenges on this topic. *Contribution:* Lucie Poulet's work at the University Blaise Pascal is focused on developing physical models of higher plant growth in reduced gravity environment. This work led her to review how plants grow in space and how microgravity influences their growth and development, as well as what are the remaining challenges on this topic.

J.-P. Fontaine has focused on the modelling of complex multi-physics phenomena: non-linear, coupled processes, multi-scale, hydrodynamic convective instabilities, rotating flows, interfacial phenomena (moving boundaries, thermocapillary flows), phase changes (evaporation/condensation, solidification), reduced gravity environments, experiments/modelling interface and industrial/engineering-related problems. He has worked on the implementation of numerical methods (finite elements, finite volumes, finite differences) related to transport phenomena: fluid, heat, species, ions, light. He also has experience in the characterization of thermophysical properties of materials. He is currently concentrating on a precise characterization of the heterogeneous transfer occurring at interfaces during condensation phases and at the modelling of the influence of gravity on higher plant growth, particularly in reduced gravity. *Contribution:* as one of L. Poulet's PhD supervisor, offering necessary directions and insights to assist in her research, as well as revisions on this paper.

C.-G. Dussap has been much involved in the analysis of the relationships that exist between the physiological responses of microorganisms and the bioreactor environment. This includes insightful investigation in metabolic engineering (metabolic fluxes distribution, control and regulation of metabolism) and thorough analysis of bioreactor performances regarding the mass, heat, light-energy transfer and mixing properties of reactors. He has strong experience in mathematical modelling of biological kinetics, thermodynamic equilibrium properties of aqueous solutions and of reactor characteristics. He has a track record of experience in the design and the mathematical modelling of the MELiSSA (Micro-Ecological Life Support System Alternative) ecosystem developed by the ESA for long-duration space missions. He has been involved as UBP representative in the ESA Memorandum of Understanding concerning MELiSSA system since its start in 1993. His main domain of expertise covers all the process engineering aspects of MELiSSA, especially the bioreactor design, modelling, scale-up and control. This includes for his research team the management of the experimental assays and of the studies, which are performed for ESA in various European centres Ghent, Barcelona, Clermont-Ferrand, Guelph...etc.). He is the author of more than 150 international publications. *Contribution:* as one of L. Poulet's PhD supervisor, offering necessary directions and insights to assist in her research, as well as revisions on this paper.

References

Arena, C., V. De Micco, E. Macaeva, and R. Quintens. 2014. "Space radiation effects on plant and mammalian cells." *Acta Astronautica* 104: 419–431.

Bagdigian, R. M., and D. Cloud. 2005. "Status of the International Space Station Regenerative ECLSS Water Recovery and Oxygen Generation Systems." *Society of Automotive Engineers, Inc.* 2005-01-2779 (2005).

Bamsey, M., A. Berinstain, and M. Dixon. 2012. "Development of a potassium-selective optode for hydroponic nutrient solution monitoring." *Analytica Chimica Acta* 737: 72–82.

Bamsey, M., T. Graham, C. Thompson, A. Berinstain, A. Scott, and M. Dixxon. 2012. "Ion-Specific Nutrient Management in Closed Systems: The Necessity for Ion-Selective Sensors in Terrestrial and Space-Based Agriculture and Water Management Systems." *Sensors (Basel)* 12 (10): 13349–13392.

Bourget, C. M. 2008. "An introduction to light emitting diodes." *HortScience* 43 (7): 1944–1946.

Brown, C. S., W. C. Piastuch, and W. M. Knott. 1994. "Soybean cotyledon starch metabolism is sensitive to altered gravity conditions." *Advances in Space Research* 14 (8): 107–110.

Burkey, R. C., S. T. Green, S. P. Siebenaler, and J. C. Buckingham. 2010. "From CO_2 to H2O." *Technology Today, Summer* 2010: 6–9.

Carter, D. L. 2010. *Status of the Regenerative ECLSS Water Recovery System*. Marshall Space Flight Center: NASA.

Casado, J. 2006. "Cultivating the Future – Growing food in space." *Spaceflight*, May 2006: 180–189.

Cogne, G., J.-B. Gros, and C.-G. Dussap. 2003. "Identification of a metabolic network structure representative of Arthrospira (Spirulina) platensis metabolism." *Biotechnology and Bioengineering* 84 (6): 667–676.

Cornet, J.-F., C. G. Dussap, and J.-B. Gros. 1998. "Kinetics and energetics of photosynthetic micro-organisms in photobioreactors: application to Spirulina growth." *Advances in Biochemical Engineering/Biotechnolog* 59: 153–224.

De Micco, V., G. Aronne, and S. De Pascale. 2006. "Effect of simulated microgravity on seedling development and vascular differentiation of soy." *Acta Astronautica* 58: 139–148.

De Micco, V., and G. Aronne. 2008. "Biometric anatomy of seedlings developed onboard of Foton-M2 in an automatic system supporting growth." *Acta Astronautica* 62: 505–513.

De Micco, V., C. Arena, D. Pignalosa, and M. Durante. 2011. "Effects of sparsely and densely ionizing radiation on plants." *Radiation and Environmental Biophysics* 50: 1–19.

De Micco, V., R. Buonomo, R. Paradiso, S. De Pascale, and S. Aronne. 2012. "Soybean cultivar selection for Bioregenerative Life Support Systems (BLSS) – Theoretical selection." *Advances in Space Research* 49 (10): 1415–1421.

De Micco, V., S. De Pascale, R. Paradiso, and G. Aronne. 2014. "Microgravity effects on different stages of higher plant life cycle and completion of the seed-to-seed cycle." *Plant Biology* 16 (1): 31–38.

Dougher, T. A. O., and B. Bugbee. 2001. "Differences in the response of wheat, soybean and lettuce to reduced blue radiation." *Photochemistry and Photobiology* 73 (2): 199–207.

Dreschel, T. W., and J. C. Sager. 1989. "Control of water and nutrients using a porous tube: a method for growing plants in space." *Horticultural Science* 24 (6): 944–947.

Eckart, P. 1994. *Life Support and Biospheric*. Munich: Herbert Utz publishers.

Eriksson, K., O. Doule, and L. Poulet. 2014. "Architectural Concepts For A Lunar Greenhouse Within The Melissaframework." *65th International Astronautical Congress*. Toronto, Canada, 2014.

ESA. 2013. "European Modular Cultivation System (EMCS)." ESA-HSO-COU-013, 2013.

Ferl, R., R. Wheeler, H. G. Levine, and A. L. Paul. 2002. "Plants in space." *Current Opinions in Plant Biology* 5 (3): 528–563.

Giardi, M. T., G. Rea, M. D. Lambreva, A. Antonacci, S. Pastorelli, I. Bertalan, U. Johanningmeier, and A. K. Mattoo. 2013. "Mutations of Photosystem II D1 protein that empower efficient phenotypes of *Chlamydomonas reinhardtii* under extreme environment in space." *PLOS One 8*, no. 5 (2013).

Gitelson, I. I., I. A. Terskov, B. G. Kovrov, G. M. Lisovsky, Y. N. Okladnikov, F. Y. Sid'ko, I. N. Trubachev, et al. 1989. "Long-term experiments on man's stay in biological life-support system." *Advances in Space Research* 9 (8): 6–71.

Gitelson, I. I., and G. M. Lisovsky. 2008. "Creation of Closed Ecological Life Support Systems: Results, Critical Problems and Potentials." *Journal of Siberian Federal University Biology* 1: 19–39.

Gòdia, F., J. Albiol, J. L. Montesinos, J. Pérez, N. Creus, F. Cabello, X. Mengual, A. Montras, and C. Lasseur. 2002. "MELiSSA: a loop of interconnected bioreactors to develop life support in Space." *Journal of Biotechnology* 99 (3): 319–330.

Graham, T., R. Scorza, R. M. Wheeler, C. Dardick, B. Smith, A. Dixit, D. Raines, et al. 2015. "Over expression of FT1 in plum (Prunus domestica) results in phenotypes compatible with spaceflight: A new candidate crop for bioregenerative life-support systems." *Gravitational and Space Research* 3 (1): 39–50.

Herranz, R., and F. J. Medina. 2014. "Cell proliferation and plant development under novel altered gravity environments." *Plant Biology* 16 (1): 23–30.

Hezard, P. 2012. Higher Plant Growth Modelling for Life Support Systems: Global Model Design and Simulation of Mass and Energy Transfers at the Plant Level. PhD Thesis, Clermont Ferrand: Doctoral school of Life Sciences, Health, Agronomy, Environment – Université Blaise Pascal, Université d'Auvergne, 2012.

Hezard, P., L. S. Sasidharan, C. Creuly, and C.-G. Dussap. 2010. "Higher plant modeling for bioregenerative life support applications: General structure of modeling." *Proceedings of the 40th International Conference on Environmental Systems*. Barcelona, Spain, 2010.

Hezard, P., S. Sasidharan, C.-G. Dussap, C. Creuly, and L. Poughon. 2012. "Predicting and controlling higher plant growth following mass and energy balances approach: a review and new model design." *Functional Plant Biology*, 2012

Hirai, H., and Y. Kitaya. 2009. "Effects of Gravity on Transpiration of Plant Leaves." *Interdisciplinary Transport Phenomena: Annals of the New York Academy of Science* 1161: 166–172.

Hoenecke, M. E., R. J. Bula, and T. W. Tibbitts. 1992. "Importance of blue photon levels for lettuce seedlings grown under red light-emitting diodes." *HortScience* 27 (5): 427–430.

Ivanova, T., S. Sapunova, P. Kostov, and I. Dandolov. 1997. *First Successful Space Seed-to-Seed Plant Growth Experiment in the SVET-2 Space Greenhouse in 1997*. Sofia, Bulgaria: Space Research Institute, Bulgarian Academy of Sciences.

Kiss, J. Z., G. Aanes, M. Schiefloe, L. H. F. Coelho, K. D. L. Millar, and R. E. Edelmann. 2014. "Changes in operational procedures to improve spaceflight experiments in plant biology in the European Modular Cultivation System." *Advances In Space Research* 53 (5): 818–827.

Kitaya, Y., M. Kawai, J. Tsuruyama, H. Takahashi, A. Tani, E. Goto, T. Saito, and M. Kiyota. 2001. "The effect of gravity on surface temperature and net photosynthetic rate of plant leaves." *Advances in Space Research* 28 (4): 659–664.

Kitaya, Y., M. Kawai, J. Tsuruyama, H. Takahashi, A. Tani, E. Goto, T. Saito, and M. Kiyota. 2003a. "The effect of gravity on surface temperatures of plant leaves." *Plant, Cell And Environment* 26: 497–503.

Kitaya, Y., J. Tsuruyama, T. Shibuya, M. Yoshida, and M. Kiyota. 2003b. "Effects of air current speed on gas exchange in plant leaves and plant canopies." *Advances in Space Research* 31 (1): 177–182.

Kittang Jost, A.-I., T. Hoson, and T.-H. Iversen. 2015. "The Utilization of Plant Facilities on the ISS the composition, growth, and development of plant cell walls under microgravity conditions." *Plants* 5: 44–62.

Known, T., J. A. Sparks, J. N. Nakashima, S. N. Allen, Y. Tang, and E. B. Blancaflor. 2015. "Transcriptional response of Arabidopsis seedlings during spaceflight reveals peroxidase and cell wall remodeling genes associated with root hair development." *American Journal of Botany* 102 (1): 21–35.

Kuang, A., Y. Xiao, and M. E. Musgrave. 1996. "Cytochemical localization of reserves during seed development in arabidopsis thaliana under spaceflight conditions." *Annals Of Botany* 78: 343–351.

Lasseur, C., J. Brunet, H. De Weever, M. Dixon, C.-G. Dussap, F. Godia, N. Leys, M. Mergeay, and D. Van Der Straeten. 2010. "MELiSSA: The European Project Of Closed Life Support System." *Gravitational and Space Biology* 23 (2): 3–12.

Levinskikh, M. A., V. N. Sychev, T. A. Derendyaeva, O. B. Signalova, F. B. Salisbury, W. F. Campbell, G. E. Bingham, D. L. Bubenheim, and G. Jahns. 2000. "Analysis of the spaceflight effects on growth and development of Super Dwarf wheat grown on the Space Station Mir." *Journal of Plant Physiology* 156 (4): 522–529.

Manzano, A. I., I. Matia, F. Gonzalez-Camacho, E. Carnero-Diaz, J. J. W. A. Van Loon, C. Dijkstra, O. Larkin, et al. 2009. "Germination of *Arabidopsis* seed in Space and in simulated microgravity: alterations in root cell growth and proliferation." *Microgravity Science and Technology* 21: 293–297.

Massa, G. D., J. C. Emmerich, R. C. Morrow, C. M. Bourget, and C. A. Mitchell. 2006. "Plant-growth lighting for space life support: a review." *Gravitational and Space Biology* 19 (2): 19–30.

Mazars, C., C. Briere, S. Grat, C. Pichereaux, M. Rossignol, V. Pereda-Loth, B. Eche, et al. 2014. "Microgravity induces changes in microsome-associated proteins of Arabidopsis seedlings grown on board the International Space Station." *PLoS ONE* 9 (3).

McCree, K. J. 1971–1972. "The action spectrum, absorptance and quantum yield of photosynthesis in crop plants." *Agric. Meteorol.* 9 (1971-1972): 191–216.

Medina, J., A. I. Manzano, R. Herranz, C. Dijkstra, O. Larkin, R. Hill, E. Carnero-Díaz, et al. 2010. "Effects of real or simulated microgravity on plant cell growth and proliferation." 38th COSPAR Scientific Assembly. Bremen, Germany, 2010. 12.

Medina, F. J., R. Herranz, C. Arena, G. Aronne, and V. De Micco. 2015. "Chapter 24: Growing plants under generated extra-terrestrial environments: effects of altered gravity and radiation." In *Generation and Applications of Extra-Terrestrial Environments on Earth*, edited by D. A. Beysens and J. J. W. A. Van Loon, 239–254. Aalborg, Denmark: River Publishers.

Millar, K. D., P. Kumar, M. J. Correll, J. L. Mullen, R. P. Hangarter, R. E. Edelmann, and J. Z. Kiss. 2010. "A novel phototropic response to red light is revealed in microgravity." *New Phytologist* 186 (3): 648–656.

Monje, O., G. Stutte, and D. Chapman. 2005. "Microgravity does not alter plant stand gas exchange of wheat at moderate light levels and saturating CO_2 concentration." *Planta* 222 (2): 336–345.

Monje, O., G. W. Stutte, G. D. Goins, D. M. Porterfield, and G. E. Bingham. 2003. "Farming in space: environmental and biophysical concerns." *Advances in Space Research* 31 (1): 151–167.

Morrow, R. C., R. J. Bula, T. W. Tibbitts, and W. R. Dinauer. 1994. "The astroculture tm flight experiment series, validating technologies for growing plants in space." *Advances in Space Research* 14 (11): 29–37.

Musgrave, M. E. 2002. "Seeds in Space." *Seed Science Research* 12 (1): 1–16.

Musgrave, M. E., A. Kuang, and S. W. Matthews. 1997. "Plant reproduction during spaceflight: importance of the gaseous environment." *Planta* 203: 177–184.

Musgrave, M. E., A. Kuang, L. K. Tuominen, L. H. Levine, and R. C. Morrow. 2005. "Seed storage reserves and glucosinolates in Brassica rapa L. grown on the International Space Station." *Journal of the American Society for Horticultural Science* 130 (6): 848–856.

Nakamura, T., A. D. Van Pelt, N. C. Yorio, A. E. Drysdale, R. M. Wheeler, and J. C. Sager. 2009. "Transmission and distribution of photosynthetically active radiation (PAR) from solar and electric light sources." *Habitation* 12: 103–117.

Nakamura, T., O. Monje, and B. Bugbee. 2013. "Solar Food Production and Life Support in Sapce Exploration." *AIAA SPACE 2013 Conference and Exposition*. San Diego, 2013.

Ordoñez, L., C. Lasseur, L. Poughon, and G. Waters. 2004. "MELiSSA Higher Plants Compartment modeling using EcoSim Pro." *SAE International* 2004-01-2351 (2004).

Paradiso, R., V. De Micco, R. Buonomo, G. Aronne, G. Barbieri, and S. De Pascale. 2014. "Soilless cultivation of soybean for Bioregenerative Life Support Systems (BLSSs): a literature review and the experience of the MELiSSA Project - Food characterization Phase I." *Plant Biology* 16: 69–78.

Paul, A. L., C. L. Amalfitano, and R. J. Ferl. 2012. "Plant growth strategies are remodeled by spaceflight." *Plant Biology* 2012: 12–232.

Paul, A. L., M. P. Popp, W. B. Gurley, C. Guy, K. L. Norwood, and R. J. Ferl. 2005. "Arabidopsis gene expression patterns are altered during spaceflight." *Advances in Space Research* 36 (7): 1175–1181.

Paul, A. L., R. M. Wheeler, H. G. Levine, and R. J. Ferl. 2013. "Fundamental plant biology enabled by the Space Shuttle." *American Journal of Botany* 100 (1): 226–234.

Porterfield, D. M. 2002. "The biophysical limitations in physiological transport and exchange in plants grown in microgravity." *Journal of Plant Growth Regulation* 21 (2): 177–190.

Porterfield, D. M., B. D. Wright, and W. C Bausch. 1984. "A Plant Growth System for Orbital Plant Experiments." *Amer. Soc. Agric. Eng.* New Orleans, LA, 1984. Paper # 84-2524.

Porterfield, D. M., S. W. Matthews, C. J. Daugherty, and M. E. Musgrave. 1997. "Spaceflight exposure effects on transcription, activity, andlocalization of alcohol dehydrogenase in the roots of *Arabidopsis thaliana*." *Plant Physiology* 113 (3): 685–693.

Porterfield, D. M., G. S. Neichitailo, A. L. Mashinski, and M. E. Musgrave. 2003. "Spaceflight hardware for conducting plant growth experiments in space: the early years 1960–2000." *Advances in Space Research* 31 (1): 183–193.

Poughon, L. 2007. Dynamic Modelling of a Coupled MELiSSA Crew – Compartment C4a with Matlab/Simulink. MELiSSA Technical Note 83.2, ESA/ESTEC CONTRACT, 2007.

Poughon, L. 1997. Including of a Higher Plants Chamber in the MELiSSA loop Description of a HPC for MELiSSA loop steady state simulations. MELiSSA Technical Note 32.3, ESA/ESTEC CONTRACT, 1997.

Poulet, L., D. Schubert, C. Zeidler, P. Zabel, V. Maiwald, E. David, and C. Paillé. 2013. "Greenhouse Modules and Regenerative Life-Support Systems for Space."*AIAA SPACE 2013 Conference and Exposition*.San Diego, CA, 2013.

Poulet, L., G. D. Massa, R. C. Morrow, C. M. Bourget, R. M. Wheeler, and C. A. Mitchell. 2014a. "Significant reduction in energy for plant-growth lighting in space using targeted lighting and spectral manipulation." *Life Sciences in Space Research* 2: 43–53.

Poulet, L., G. D. Massa, R. M. Wheeler, T. Gill, C. Steele, R. C. Morrow, T. M. Swarmer, K. Binsted, and J. Hunter. 2014b. "Demonstration Test of Electrical Lighting Systems For Plant Growth in HI-SEAS Analog Mars Habitat ." *65th International Astronautical Congress*. Toronto, 2014.

Rygalov, V., B. G. Kovrov, and G. S. Denisov. 1997. "Interaction of physical-chemical and biological regeneration processes in ecological life support systems." *Advances in Space Research* 20 (10): 1995–2000.

Salisbury, F. B. 1997. "Growing Super-Dwarf wheat in Space Station Mir." *Life Support Biosphere Science* 4 (3–4): 155–166.

Salisbury, F. B., J. I. Gitelson, and G. M. Lisovsky. 1997. "Bios-3: Siberian Experiments in Bioregenerative Life Support." *BioScience* 47 (9): 575–585.

Salmi, M. L., and S. J. Roux. 2008. "Gene expression changes induced by space flight in single-cells of the fern *Ceratopteris richardii*." *Planta* 229 (1).

Slocum, R. D., J. J. Gaynor, and A. W. Galston. 1984. "Cytological and ultrastructural studies on root tissues." *Annals of Botany* 54 (3): 65–76.

Steinberg, S. L., D. W. Ming, and D. Henninger. 2002. *Plant production systems for microgravity: critical issues in water, air, and solute transport through unsaturated porous media*. Washington, DC: NASA.

Stutte, G. W., G. Newsham, R. M. Morrow, and R. M. Wheeler. 2011. "Operational Evaluation of VEGGIE Food Production System in the Habitat Demonstration Unit." Reston, VA: American Institute of Aeronautics and Astronautics (AIAA), 2011.

Tuominen, L. K., L. H. Levine, and M. E. Musgrave. 2009. "Plant secondary metabolism in altered gravity." *Methods in Molecular Biology* 547: 373–386.
Vandenbrink, J. P., J. Z. Kiss, R. Herranz, and F. J. Medina. 2014. "Light and gravity signals synergize in modulating plant." *Frontiers in Plant Science* 5 (563).
Vandenbrink, J. P., and J. Z. Kiss. 2016. "Space, the final frontier: a critical review of recent experiments performed in microgravity." *Plant Science* 243: 115–119.
Wheeler, R. M. 2003. "Carbon balance in bioregenerative life support systems: some effects of system closure, waste management, and crop harvest index." *Advances in Space Research* 31 (1): 169–175.
Wheeler, R. M. 2010. "Plants For Human Life Support In Space: From Myers To Mars." *Gravitational and Space Biology* 23 (2): 25–35.
Wheeler, R. M., J. C. Sager, R. P. Prince, W. M. Knott, C. L. Mackowiak, G. W. Stutte, N. C. Yorio, L. M. Ruffe, et al. 2003. *Crop Production for Advanced Life Support Systems - Observations From the Kennedy Space Center Breadboard Project*. Technical Report, Kennedy Space Center: NASA.
Wheeler, R. M., C. L. Mackowiak, G. W. Stutte, J. C. Sager, N. C. Yorio, L. M. Ruffe, R. E. Fortson, T. T. W. Dreschel, W. M. Knott, and K. A. Corey. 1996. "NASA's Biomass Production Chamber: a testbed for bioregenerative life support studies." *Advances in Space Research* 18 (4–5): 215–224.
Wolff, S. A., L. H. Coelho, I. Karoliussen, and A. I. Kittang Jost. 2014. "Effects of the extraterrestrial environment on plants: recommendations for future space experiments for the MELiSSA Higher Plant Compartment." *Life* 4 (2): 189–204.
Wolverton, C., and J. Z. Kiss. 2009. "An Update on Plant Space Biology." *Gravitational and Space Biology* 22 (2): 13–20.
Zhang, Y., L. Wang, J. Xie, and H. Q. Zheng. 2015. "Differential protein expression profiling of *Arabidopsis thaliana* callus under microgravity on board the Chinese SZ-8 spacecraft." *Planta* 241: 475–488.

1.7 Chapter's outcomes

- Long-term human space exploration will necessitate the growth of plants and other biological organisms.
- Plants can grow in space and have grown in Earth orbit since the 1950s. However low gravity environments lead to modifications in plants behaviour and development, through direct and indirect effects.
- Article published in Botany Letters in 2016: to predict plant growth in these non-standard conditions, it is crucial to develop mechanistic models of plant growth, enabling multi-scale study of different phenomena, as well as gaining understanding on all processes involved in plant development in low gravity environment and identifying knowledge gaps.

Chapter 2

Gas Exchanges Model in Reduced Gravity Environment

2.1 Introduction

Indirect effects of weightlessness, and low gravity environments in general, on plant growth are consequences of altered fluid behavior, such as the lack of or the little free convection, and changes in dominating forces, such as surface tension prevailing in microgravity, as detailed in chapter 1. In the first case, gas exchanges are reduced leading to poorer photosynthesis and accumulation of Volatile Organic Compounds (VOCs) such as ethylene, leading to a suboptimal plant growth; in the second case, roots suffer from hypoxia because the thickness of the liquid phase boundary layer around the roots is significantly increased under the action of surface tension forces and the disappearance of buoyancy forces.

In this chapter the focus is set on the altered behavior of fluids and its consequences on gas exchanges at the leaf surface. Experiments in parabolic flights have shown that the net photosynthetic rate can be reduced by 13% in 20s of weightlessness compared to the one in Earth gravity, because of suboptimal gas exchanges at the leaf surface; and it was 7% higher in 2g than in 1g, since natural convection is more significant in larger gravity environments (Kitaya et al. 2001). In the long run, this decrease in photosynthesis rate is likely to impair plant growth. Experiments on the ISS have shown that adequate forced convection enables to eliminate suboptimal gas exchanges at the leaf surface and grow plants in similar conditions than in 1g (Monje, G. Stutte, and Chapman 2005). To our

knowledge no mechanistic study was performed to define this "adequate ventilation" and plant growth experiments on the ISS only used empirical estimates to set this ventilation. So how can the adequate ventilation be determined? Is-it species specific? In a context of spaceflight, an effort is set on saving energy, so forced convection using fans needs to be as energy-efficient as possible, i.e. small enough not to waste energy and large enough to enable optimal photosynthesis. It is thus crucial to determine the threshold value of forced convection where plants have adequate gas exchanges. But it is also important to determine what happens to gas exchanges in sub-optimal ventilation. How are the biomass and oxygen productions affected by low gravity (i.e. low natural convection) environments? Indeed, in bioregenerative LSS the survival of humans depends on photosynthetic organisms, such as plants and micro-algae, so their behaviors need to be anticipated for a wide range of environmental parameters.

Building on the already existing holistic MELiSSA plant growth model developed by Hézard (2012), which is based on a mass balance, we added gravity as a parameter of the gas exchanges model. This is detailed in section 2 of this chapter, along with a review of the original plant growth model, which includes the paper that was presented at the 47^{th} International Conference on Environment Systems. It gives preliminary results on CO_2 uptake, water evaporation, and biomass production for different gravity and ventilation levels.

Further details of gas exchanges modeling hypotheses and the implications of low gravity on leaf conductance, boundary layer thickness, and gas exchanges are given in section 3, which is a paper that was published in the Astrobiology journal (Vol. 18, issue 9). An overview of the energy balance at steady state and its link with the original holistic plant growth model is given, leading to an expression of the leaf temperature, that is not an entry parameter of the model anymore, but a variable.

In section 4, the detailed energy balance is presented, with a complete discussion on the definition of each term of the balance, and the validity at steady state. The leaf surface temperature is computed for different gravity and ventilation levels. Finally, the equation linking mass and energy balance and giving the leaf surface temperature in time-dependent state is detailed.

Section 5 comes back to the mechanistic model of mass and heat transfer based on the

boundary layer theory with a special emphasis on the introduction of gravity in the boundary layer theory, which is not usual in classical developments. Improvement of the model is suggested to reach a more accurate and realistic model. The emphasis is set on the definitions of free and forced convection regimes, on the transition from laminar to turbulent in the boundary layer, and on the leaf geometry itself.

2.2 Including gravity in a holistic plant growth model: first assessment of the theoretical influence of reduced gravity on gas exchanges and plant growth

This part is an article that was published in the proceedings of the 47^{th} International Conference on Environmental Systems in July 2017. This paper was inspired from a technical note written for the MELiSSA AtSSE (Atmospheric SubSystems Engineering) project.

 ICES-2017-143

Modelling higher plants gas exchange in reduced gravity environment

Lucie Poulet[1], Claude-Gilles Dussap[2] and Jean-Pierrre Fontaine[3]
CNRS, UMR 6602, IP, F-63178 Aubière, France
Université Clermont Auvergne, Institut Pascal, BP 10448, F-63000 Clermont-Ferrand, France

Long-duration human space missions and the establishment of permanent off-Earth bases (e.g. on the Moon or Mars) is one of the main focuses of today's space exploration. This poses many severe challenges at the life-support level, which needs to recycle atmosphere, water and waste for crew survival. The European Space Agency (ESA) project Micro-Ecological Life Support System Alternative (MELiSSA) can ensure these functions. It is a closed-loop bio-regenerative life-support system functioning with microorganisms and higher plants and providing a circular cycling of mass, including O_2 production, CO_2 capture, water recycling and food production. The growth and development of higher plants are strongly influenced by environmental conditions (e.g. gravity, pressure, temperature, relative humidity, partial pressure of O_2 or CO_2) so bio-regenerative life support systems require a high level of control and management. The goal is to develop a mechanistic physical model of plant growth to predict the effects of microgravity or of a reduced gravity environment (like on Mars or on the Moon) on plant growth at its morphological, physicochemical and biochemical levels. Current existing plant growth models are developed for agronomy and are therefore not adapted for modeling plant growth for applications in life-support systems, which require being able to extrapolate plants behavior for a wide range of environmental conditions. The first mechanistic plant growth model developed in the framework of the MELiSSA project has attempted to address these limitations. Based on this work, a preliminary structure of the model was defined. In this presentation, the addition of gravity as a parameter is addressed, taking into account the altered gas exchanges due to the low or lack of free convection in reduced gravity environments. The influences of forced and free convection are studied according to the levels of gravity and the interdependence of low gravity and ventilation are addressed.

I. Introduction

A. Life-Suport Systems and higher plants in space

ASTRONAUTS going to Mars or further into the solar system will need food, water, and oxygen for the whole length of the mission - about 1000 days for a typical scenario of a mission to Mars[1]. Since sending all consumables from Earth or ressupplying are not viable options[2–4], sustainable solutions are key to succeed in future human space exploration. On the International Space Station (ISS), partial recycling is already a standard step for water and oxygen using physicochemical technologies[5,6]. However, these technologies cannot provide food to the astronauts; this can only be achieved with biological processes, i.e. by the use of microbial bioconversions and higher plants cultivation[7,8]. Future regenerative life-support systems (LSS) will likely be a combination of

[1] PhD Student in Bio- and Physical Process Engineering, Chemical Engineering, Engineering Thermodynamics And Biosystems Department, Institut Pascal, Campus Universitaire des Cézeaux 4 Avenue Blaise Pascal Batiment Physique 3 TSA60026 CS 60026 63178 Aubière Cedex.
[2] Professor and Department Head, Chemical Engineering, Engineering Thermodynamics And Biosystems Department, Institut Pascal, Campus Universitaire des Cézeaux 4 Avenue Blaise Pascal Batiment Physique 3 TSA60026 CS 60026 63178 Aubière Cedex.
[3] Professor and Responsible of Polytech Physics Engineering Department, Chemical Engineering, Engineering Thermodynamics And Biosystems Department, Institut Pascal, Campus Universitaire des Cézeaux 4 Avenue Blaise Pascal Batiment Physique 3 TSA60026 CS 60026 63178 Aubière Cedex.

physicochemical technologies and biological processes to ensure matter and water recycling and oxygen and food production[9].

B. Principles of mechanistic modelling and goal of our study

In order to have efficient and reliable LSS and reduce the risk of system failure when humans embark on long trips into the solar system, it is crucial to be able to predict the behaviour of any recycling system whatever it is a combination of biological processes[10]. The European Space Agency (ESA) project Micro-Ecological Life-Support System Alternative (MELiSSA) is a closed-loop LSS inspired by a lake ecosystem and based on microorganisms and higher plants and aimed at sustaining humans on long-duration space travels[11]. The approach of this project is to develop a mechanistic model of the whole loop in order to achieve a deep understanding of underlying mechanisms and acquire a good knowledge about systems control. The three microbial compartments and the algae compartment of the MELiSSA loop are effectively modelled mechanistically[12,13], while modelling efforts on the higher plants compartment are currently on-going[14–16]. The ground basis of such model was laid by Hézard in 2012 for Earth gravity conditions[16]. The aim of a mechanistic model of plant growth is to get a thorough multi-scale description of elementary mechanisms of plant growth accounting both for physical or biochemical phenomena, including transport phenomena and metabolic regulations. An integration synthesis then enables to go back to whole-system variables. Figure 1 gives an overview of the definition of mechanistic models in comparison to empirical models, when applied to a higher plant system. The ultimate goal of the plant growth model described hereafter is to remove empirical equations and parameters from the model to achieve a mechanistic description of each process. The first iterations of the mechanistic model will be less accurate on, for example, yield predictions than commonly used empirical models, but when all processes are described mechanistically, it will be well adapted for prediction and control of a plant chamber in a closed-loop LSS for a wide range of parameters, since each growth mechanism will be fully understood.

Typically in agronomy the two main types of models used are the process-based models (e.g. CERES, ORYZA, STICS), mainly used for predicting yield of a given crop in a given field with a given range of environmental conditions, and the functional-structural models (e.g. GREENLAB, L-PEACH), based on a geometrical description of plant morphology[16]. In both cases, some processes are described empirically, mainly because of accuracy of predictions, since these models are meant to be used for assisting agricultural production, and not for plant growth mechanism understanding. However plants in bioregenerative LSS will grow in confined environments and uncanny conditions. Thus it must be understood how slight variations in environmental parameters in space conditions can affect the whole plant system, since there are no buffer effects of the atmosphere, oceans or soil and genetic regulations that may regulate the effects of space environmental variations. Therefore it is critical to take into account the influence of non-terrestrial gravity conditions on elementary plant growth mechanisms, as well as for the variations of the physical environmental surrounding the plants.

Globally the gravity may have influence at three levels:

- Orientation of growth of the roots i.e. gravitropism;
- Fluid migration between root, stems and leaves;
- Gas exchange and influence on photosynthesis rate.

This work is concerned by the last item, knowing that various models of plant gas exchange in Earth gravity have been developed in recent years but to our knowledge no model accounts for changes in gravity levels. The goal of this study is to investigate and propose a preliminary model of plant gas exchanges with gravity as a parameter.

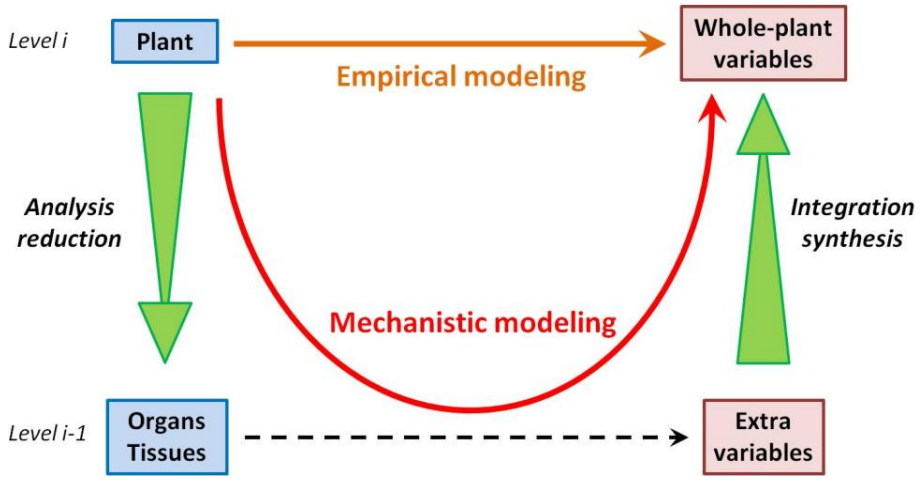

Figure 1. Mechanistic modeling vs. empirical modeling.[17]

C. Plants gas exchanges and the influence of the environment

Gas exchanges in plants occur during photosynthesis, respiration and transpiration. When plants receive light, typically during the day, they photosynthesize: they absorb CO_2 and release O_2 and water vapour. Without light, typically during night time, they respire: they absorb O_2 and release CO_2. In BLSS, gas exchanges in plants ensure air revitalization via O_2 production and water recycling via transpiration. Indeed non-limiting irrigation methods such as hydroponics or nutrient-film technique are envisioned for plant irrigation in BLSS. Food production also relies on proper gas exchanges since higher plants growth depends on photosynthesis, which is a coupled phenomenon between photon capture, water evaporation and CO_2 and O_2 counter-diffusion.

CO_2 and water vapour transfer is made by diffusion between the leaf and the boundary layer through the stomata[18] (Figure 2). When plants are under high water stress, they reduce stomatal conductance to reduce risks of damaging the leaves and the plant[19]. Stomatal conductance corresponds to the rate of CO_2 entering or water vapour exiting the leaf through the stomata, as opposed to the stomatal resistance. It depends on stomatal density, stomatal aperture, and stomatal size.

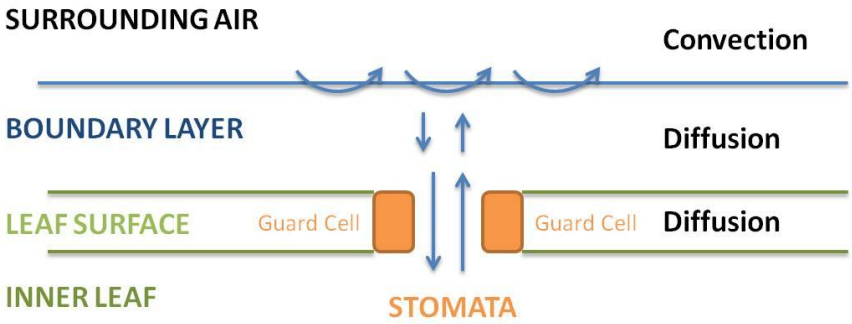

Figure 2. Mechanisms of gas exchange between the leaf and the surrounding air through diffusion and convection.

Furthermore, exchange between the boundary layer and the surrounding air is ensured by convection (Figure 2) and the gas transfer between the leaf surface and the gas are dependent on the convective system of the outside air. A mechanistic model consists in considering that the gas transfer resistance is represented by the diffusion of the species (CO_2, O_2 and vapour water) in a boundary layer at the leaf surface, the thickness of which is characteristic of bulk gas turbulence. Kitaya et al. showed that when ventilation is increased from 0.01 to 1 m/s in a chamber containing sweet potato plant, the leaf boundary layer resistance decreased (at 0.2 m/s it was one third of the leaf boundary layer resistance at 0.01 m/s), inducing an increase in transpiration and photosynthesis rate, though the

latter was almost constant between 0.5 and 1 m/s[20]. The environmental conditions at the leaf surface can indeed be considered like a micro-climate in the boundary layer of the leaf, with high gradients in temperature, CO_2 concentrations and water vapour[21]. In addition ventilation was shown to have a direct effect on the relative humidity in the surrounding of the leaf surface and an increase in relative humidity was observed 5 mm from the underside of leaves during day-time when crop transpiration reached its maximum[21]. Kitaya et al. also showed that the net photosynthesis rate of a plant canopy can be doubled, by increasing the air velocity from 0.1 m/s to 1 m/s above a tomato leaflet canopy[20], and from 0.01 m/s to 0.8 m/s above a rice plant canopy[22]. The air current speed inside a tomato leaflet canopy indeed decreased to 30% of the air velocity above the canopy[20]. This led them to conclude that the boundary layer of a whole canopy was greater than the boundary layer on a single leaf. They also concluded that the minimum air current velocity to improve gas exchanges was 1 m/s above a plant canopy and 0.2 m/s around the leaves[20]. These results were confirmed under an elevated CO_2 level[23].
As a confirmation of the diffusive character of CO_2 through the boundary layer between the gas and the leaf surface, it was been demonstrated that elevated CO_2 is known to promote photosynthesis of C3 and C4 plants[24] and is associated with an increase in biomass production, when it is coupled to high photosynthetic rates[25,26], otherwise super-elevated CO_2 levels are known for triggering stomata closure, resulting in a decrease in photosynthetic rate[24,27]. However Wheeler et al. showed that super-elevated CO_2 levels (10000 ppm) can increase stomatal conductance during dark periods, with a consequence of increasing water use, i.e. transpiration, which could be used for throttling up or down water purification[25].

D. Plants gas exchanges in reduced gravity environments

The effects of microgravity on plant growth have been extensively reviewed[10,28–32]. From the above, it is clearly demonstrated that the thickness of the gas boundary layer and of CO_2 partial pressure gradient between the bulk air and the leaf surface directly acts on photosynthetic activity. As the thickness of the boundary layer depends on bulk agitation, the question is therefore to understand how this could be altered by reduced gravity. One of the indirect effects of a weightless environment is the resulting altered gas exchanges. Early plant growth experiments on the ISS[33]and experiments in parabolic flights[34–36] have shown that poor ventilation or lack of ventilation in spaceflight induces stagnant air boundary layers with decreased conductance around the leaves due to the lack of free convection in microgravity, decreasing heat and gas transfer at the leaf surface[37,38]. In 2001 and 2003 Kitaya et al. studied leaf temperature in weightlessness during a parabolic flight campaign[34,35] and in 2009 Hirai et al. investigated leaf transpiration in weightlessness[36]. They found that leaf temperature increased by 1°C and that gas exchanges were reduced with decreased gravity levels without providing adequate ventilation to the plants.
This deficiency in optimal gas exchange is directly linked to photosynthetic activity (CO_2 uptake and O_2 release) and also to water evapotranspiration that in turns regulates leaf temperature. In turn, the entire cascade of metabolic events and finally, overall plant growth may be affected.
Later experiments on the MIR space station and on the ISS showed that plant gas exchange processes in microgravity, including transpiration and photosynthesis, are similar to that in Earth gravity, when adequate ventilation is provided[39,40] at moderate light levels[41].
All these observations show that there is at the boundary layer level a mixed effect between natural convection (mostly driven by density gradients and dependent on gravity) and forced convection in the bulk. The objective is here to investigate how these microscopic effects ineract on the overall plant growth.

II. MELiSSA Plant growth model description

A. Current MELiSSA plant model – mass balance

The model as defined by Hézard is divided into four modules; three are related to the plant itself: morphological, physical and biochemical, and the fourth one links the environment surrounding the plants to the plant modules. Figure 3 gives an overview of this model structure and Table 1 gathers the model parameters.

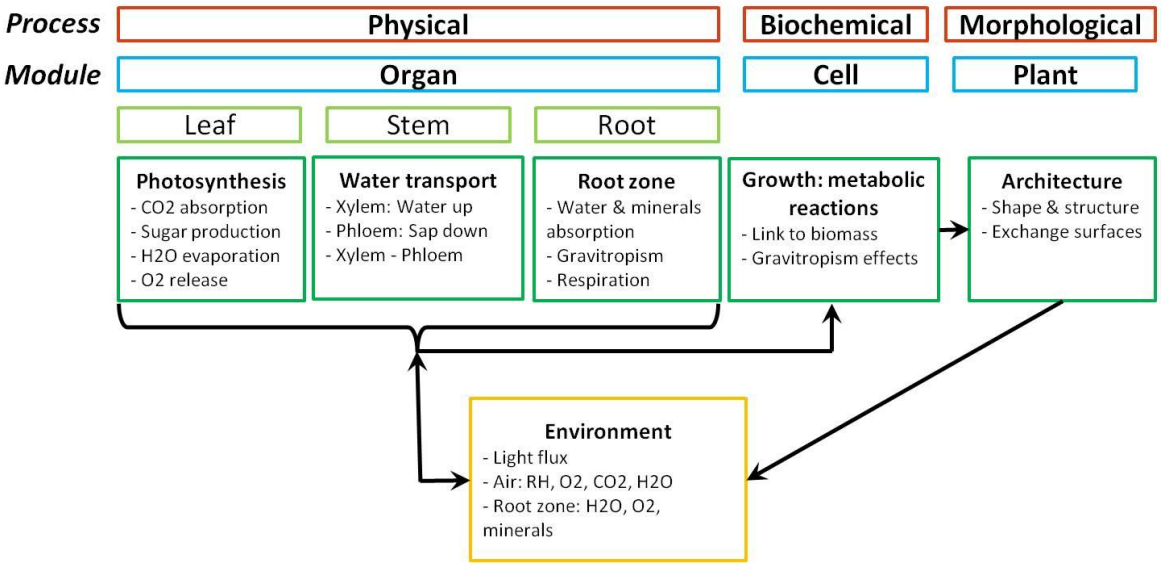

Figure 3. Diagram illustrating the model structure.

As a first approach, the approximation of a single leaf is made, represented by a total leaf area parameter (LA), a total stem length (L_{stem}), and an average number of vessels (N_{vessel}). All of these parameters are proportional to the biomass fresh mass produced. The morphological module is still described with empirical equations and morphological laws are based on empirical coefficients for mature lettuce crops k_1, k_2, k_3:

$$\begin{aligned} LA &= k_1 \,.\, Biomass \\ L_{stem} &= k_2 \,.\, Biomass \\ N_{vessel} &= k_3 \,.\, Biomass \end{aligned} \quad (1)$$

with k_1 the ratio the canopy surface to the biomass, equal to 0.0012 m²/g, k_2 the ratio of the stem length to the biomass, equal to 4.9 10^{-4} m/g, and k_3 the ratio of the number of sap vessels to the biomass, equal to 0.0979 g^{-1} [16]. These values k_1, k_2, k_3 are average for any lettuce crop and were estimated from experiment and available literature. The single-leaf approach is justified by the fact that upper leaves contribute to most of the gas exchanges in a plant, since they are directly under solar radiation and absorb more of it[42].

Equations in the physical module give the maximum fluxes for light interception, CO_2 uptake, water vapour release via transpiration, as well as water absorption through the roots. All parameters used in the parameters below are detailed in Table 1. The three equations describing the process of photosynthesis at the leaf level depend on the leaf area:

- The intercepted light flux is derived from the Beer-Lambert law and depends on the light extinction coefficient k, the incident light flux I_0, and the leaf area index LAI[16]:

$$I = I_0(1 - e^{(-k.LAI)}) \quad (2)$$

with $LAI = LA \,.\, Dens$.

- CO_2 uptake is calculated with Fick's first law of diffusion, the driving force being the gradient of CO_2 concentration between the leaf (Ci) and the outside air (Ca). It depends on the leaf area LA, the CO_2 diffusion coefficient Dc, and the mass boundary layer thickness δ which surrounds the leaf[16]:

$$U_{CO2} = \frac{D_c(C_a - C_i)}{\delta_{mass}} . LA \quad (3)$$

- The driving force for H_2O transpiration is the water gradient between the leaf and the outside air (1-RH), and depends on a conductance parameter G, the saturating vapour pressure $P^0_{(T)}$, the gas constant R, the temperature for water vapour transfer T, and the leaf area LA[16]:

$$R_{H2O} = G\ \frac{P^0_{(T)}}{RT}(1 - RH)LA \tag{4}$$

The water absorption equation is derived from the Hagen-Poiseuille formula. The driving force for H_2O absorption is the water potential gradient between the roots (Ψ_i) and the nutrient solution in the root zone (Ψ_s). It depends on the resistance to water flow given by the radius of the sap vessel R_{vessel}, the xylem sap dynamic viscosity μ_{xylem}, and the stem length L_{stem}, multiplied by the sap vessel number N_{vessel}. M is the water molar mass M and ρ the water density[16]:

$$U_{H2O} = N_{vessel}\ \frac{\rho.(\psi_s - \psi_i).\pi.R^4_{vessel}}{M.8.\mu_{xylem}.L_{stem}} \tag{5}$$

These four fluxes are limited by the metabolic reactions, reflecting the biochemical processes. The following four equations are evaluated to determine the limiting factor and constitute a stoechiometric test.
The quantum yield QY links the available incident light flux I to the CO_2 uptake by photosynthesis U_{CO2} with the following equation[16]:

$$\frac{I}{Dens} = \frac{U_{CO2}}{QY} \tag{6}$$

The oxygen availability is not considered to be a limiting factor, thus the respiration rate R_{CO2} is not included in the physical module. Instead, a fixed parameter Resp links the respiration rate to the total carbon uptake U_{CO2}, which is valid for both day and night behaviours[16]:

$$R_{CO2} = Resp.U_{CO2} \tag{7}$$

Water lost by transpiration R_{H2O} is a fixed percentage of total water uptake U_{H2O}, which is illustrated with the fixed parameter Tr. The remaining water is the one accumulated in the plant, constituting the biomass[16]:

$$R_{H2O} = Tr.U_{H2O} \tag{8}$$

This accumulated water (difference between water uptake U_{H2O} and transpiration rate R_{H2O}) is relatively evaluated to the carbon content in biomass (difference between photosynthesis rate U_{CO2} and respiration rate R_{CO2}) using the following equation[16]:

$$\frac{(U_{CO2} - R_{CO2}).BC_{mol}}{DM} = \frac{(U_{H2O} - R_{H2O}).18}{1 - DM} \tag{9}$$

The ratio between carbon content and water content in biomass depends on the dry matter content DM and the biomass C-molar mass BC_{mol}.

Then the following metabolic equation enables the evaluation of instantaneous biomass production[16]:

$$J_{Biomass} = BC_{mol}.U_{CO2} + 18.(U_{H2O} - R_{H2O}) \tag{10}$$

The integration of this equation on a time period gives the total biomass produced over this period[16]:

$$Biomass = \int_{t=0}^{t} J_{Biomass}.dt \tag{11}$$

Table 1. Model parameters for the MELiSSA plant growth model [16]

Parameter	Description
I	Intercepted light flux
I_0	Incident light flux
k	Light extinction coefficient
LAI	Leaf area index
U_{CO2}	CO_2 uptake rate
Dc	CO_2 Diffusion coefficient
Ca	CO_2 concentration in the outside air
Ci	CO_2 concentration in the leaf
δmass	Mass boundary layer thickness
LA	Leaf area
R_{H2O}	H_2O transpiration rate
G	Leaf conductance
T	Temperature for water vapour transfer
$P^0(T)$	Saturating vapour pressure at T
R	Gas constant
T	Temperature for water vapour transfer T
RH	Relative humidity
U_{H2O}	H_2O uptake rate
N_{vessel}	Sap vessel number
ρ	Water density
ψ_s	Water potential gradient in the nutrient solution
ψ_i	Water potential gradient in the roots
R_{vessel}	Radius of the sap vessel
M	Water molar mass
L_{stem}	Stem length
μ_{xylem}	Xylem sap dynamic viscosity
Dens	Planting density
QY	Quantum yield
R_{CO2}	Respiration rate
Resp	Respiration/Photosynthesis ratio
Tr	Transpired/Absorbed water ratio
DM	Dry Matter content per water content in biomass
BC_{mol}	Biomass C-molar mass
$J_{Biomass}$	Biomass production rate
Biomass	Biomass accumulation

B. Gas exchanges modelling

The most common models used for gas exchanges are stomatal optimality, detailed mechanistic or empirical model. The first one expresses the stomatal conductance to CO_2 regulated by the plant to have maximum C assimilation over a defined time step, according to water availability[19]. Empirical models are models that are adapted for agronomy or ecology applications or to predict yields for given environmental parameters and plant species.

In the MELiSSA plant growth model presented above, gas exchanges are expressed via the CO_2 uptake and water vapour release:

$$U_{CO2} = \frac{D_c(C_a - C_i)}{\delta_{mass}} . LA \quad (3)$$

$$R_{H2O} = G \ \frac{P^0_{(T)}}{RT}(1 - RH)LA \quad (4)$$

Like other current mechanistic models of plant gas exchanges, it is adapted for plant growth on Earth and do not include gravity as a parameter. In order to study gas exchanges and plant growth in reduced gravity environment, we modified this model and expressed the transpiration and CO_2 uptake rate as functions of gravity.

1. Conductance

The water vapour conductance G is a combination of the stomatal and the boundary layer conductance (Figure 4). Since 95% of gas exchanges occur through stomatal pores[43], we neglect cuticle conductance in front of stomatal conductance. We also neglect mesophyll conductance for CO_2 diffusion. Thus the conductance is a combination of stomatal and boundary layer conductance for water and CO_2. Given the expression we have for the CO_2 uptake rate (U_{CO2}), the conductance is implicitly expressed with the product of the diffusion coefficient D_c with the difference between the outside and inside CO_2 concentration (C_a-C_i) divided by the thickness of the boundary layer δ_{mass}.

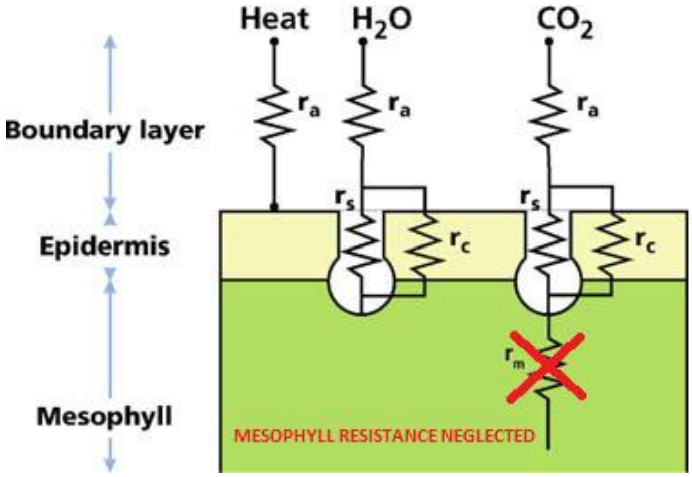

Figure 4. Diagram representing the different resistances to gas diffusion from the atmosphere to the leaf.[44]

New parameters used in this section are gathered in Table 2.

Table 2. Parameters for gas modelling.

Parameter	Description
g_w^s	Stomatal conductance
g_w^{BL}	Boundary layer conductance
Dw	diffusion coefficient of water vapour
$\rho_{mol,w}$	molar water vapour density
l	length of the diffusive pathway
l_s	depth of the stomatal pore
a_s	stomatal cross-sectional area
d_s	stomatal density
v	Total air velocity
η	air kinematic viscosity
L	characteristic length of a leaf
g	Acceleration of gravity
β	Thermal expansion coefficient
h	Characteristic length of the plant chamber
Tair	Temperature of the surrounding air
Tleaf	Temperature of the leaf

For the transpiration rate RH_2O, the total conductance G is found with the expression:

$$\frac{1}{G} = \frac{1}{g_w^s} + \frac{1}{g_w^{BL}}$$

Leading to:

$$G = \frac{g_w^{BL} g_w^s}{g_w^s + g_w^{BL}} \tag{12}$$

with g_w^s the stomatal conductance for water vapour and g_w^{BL} the boundary layer conductance for water vapour.

The stomatal conductance is species-dependent and is expressed as:

$$g_w^s = \frac{D_w \rho_{mol,w}}{l} \tag{13}$$

where D_w is the diffusion coefficient of the water vapour, $\rho_{mol,w}$ is the molar water vapour density, and l is the length of the diffusive pathway. It can be expressed as a function of the stomata geometry, the depth of the stomatal pore l_s, the stomatal cross-sectional area a_s, and the stomatal density d_s:

$$l = \frac{l_s}{d_s a_s} \tag{14}$$

The stomatal density depends on the plant species but also on environmental factors such as light, relative humidity, water availability, and atmospheric CO_2 concentration, and thus it can vary between individuals of a same species[45]. Stomatal density in *Sorghum* ranges between 107 and 177 mm^{-2} [46], whereas in most tree species in the Amazonian forest it is between 271 and 543 mm^{-2} [45], and in *Proteaceae* it ranges between 44 and 521 mm^{-2} [47]. There is an inverse relationship between size and density of stomata on a given plant and in sun leaves stomatal density is higher than on shaded leaves[45]. It was also shown to be positively correlated with minor veins density on *Proteaceae* [47]. A typical stomatal size for *Sorghum* is 7.69 – 19 µm, leading to a cross-sectional area of 46.4 to 283.5 µm², similar to that found on Amazionan trees (7.5 – 22.5 µm)[45], but smaller than those of *Proteaceae* (20.5 – 67.7 µm)[47]. Stomatal depth in *Sorghum* ranges between 10.6 and 11.7 µm[46]. The values taken for our simulations are given in Table 3.

Replacing equation 14 into equation 13, the new expression for the stomatal conductance is:

$$g_w^s = \frac{d_s a_s D_w \rho_{mol,w}}{l_s} \tag{15}$$

The boundary layer conductance depends on the convective regime of the air surrounding the leaf and is expressed with the following expression:

$$g_w^{BL} = \frac{D_w \rho_{mol,w}}{\delta_{mass}} \tag{16}$$

where δ_{mass} is the mass boundary layer thickness.
Combining equations 12, 15 and 16, we get the following expression for the total conductance for water vapour through the leaf:

$$G = \frac{D_w \rho_{mol,w} d_s a_s}{\delta_{mass} d_s a_s + l_s} \tag{17}$$

With this expression, the leaf conductance to water vapour, which was a constant of the previous model, is now dependent on the boundary layer thickness. It also depends on the stomatal geometry and thus on the plant species that is being studied.

Using the values of the parameters given in Table 3 and a typical boundary layer thickness of 8 mm[16,21], we find the length of the diffusive pathway for a lettuce crop equal to $4.62.10^{-4}$ $m.pores^{-1}$, a stomatal conductance for water vapour of g_w^s= 2.54 $mol.m^{-2}.s^{-1}$, a boundary layer conductance for water vapour equal to g_w^{BL}=0.15 $mol.m^{-2}.s^{-1}$, and

thus we find G = 139 mmol.m^{-2}.s^{-1}. The values for stomatal conductance are higher than values from the literature, since Holmberg et al. (2013) estimated a stomatal conductance ranging from 200 to 800 mmol.m^{-2}.s^{-1} for MELiSSA crops using values from Nobel et al. (2009)[18,48], and Smith et al. (2004) observed stomatal conductances in the range 460-660 mmol.m^{-2}.s^{-1} for *Tradescantia virginiana* crops[49]. Holmberg et al. (2013) calculated a total conductance ranging from 63 to 1121 mmol.m^{-2}.s^{-1}, so our total calculated conductance G is in agreement with values from the literature.

2. Boundary layer

We consider a laminar flow with a speed *v* circulating above our single leaf. The boundary layer is defined as the distance from the leaf surface where the concentration of a given compound is less than 99% of the ambient air value. It is expressed with the following expression[50]:

$$\delta_{mass} = 4.6\sqrt{\frac{L\eta}{v}} \tag{18}$$

where η the air kinematic viscosity and L is the characteristic length of a leaf. Here L is expressed as the diameter of our single leaf:

$$L = 2\sqrt{\frac{LA}{\pi}} \tag{19}$$

3. Convection

The air velocity results from free and forced convection. Air velocity from forced convection is a constant in our model and depends on the environment in which the plants are grown:

$$v = v_{free} + v_{forced} \tag{20}$$

Free convection depends on the temperature gradient between the surrounding air (Tair) and the leaf (Tleaf), and on the gravity levels and can be calculated using the following equation:

$$v_{free} = \sqrt{g\beta h(T_{air} - T_{leaf})} \tag{21}$$

where g is the acceleration of gravity, β the thermal expansion coefficient, and h the characteristic length of the plant chamber.

4. Transpiration rate as a function of gravity

Equation 21 enables a link between the gravity levels and the transpiration rate. Combining equations 4, 17, 18 and 21, we obtain the following expression for the transpiration rate:

$$R_{H_2O} = \frac{D_w \rho_{mol,w} \mathrm{d_s a_s}}{4.6\sqrt{\frac{L\mu}{\sqrt{g\beta h(T_{air} - T_{leaf}) + v_{forced}}}}\,\mathrm{d_s a_s} + \mathrm{l_s}} \frac{P^0_{(T)}}{RT}(1 - RH)LA \tag{22}$$

This expression is a function of the gravity levels and can be used to study gas exchanges and plant growth in reduced gravity environments in a mechanistic way. L is no longer a constant deduced empirically from the literature but is a variable of the model, depending on the leaf area, which itself is a function of the produced biomass. Moreover with the species-specific values of l_s, a_s, and d_s, this expression of the transpiration rate can be used for species-specific studies.

5. CO_2 uptake as a function of gravity

Combining equations 3, 18, and 21, we obtain the following expression for the CO_2 uptake rate:

$$U_{CO_2} = \frac{D_c(C_a - C_i)}{4.6} \sqrt{\frac{\sqrt{g\beta h(T_{air} - T_{leaf}) + v_{forced}}}{L\mu}} . LA \quad (23)$$

Gas exchanges in the model are now expressed according to the gravity levels in the environment surrounding the plants.

III. Simulations results and discussion

Simulations using this model were made using Matlab R2016b (9.1) version 13.5. Plants were grown for 50 days with a 14-hour photoperiod. The values of the different parameters used for the simulations are given on Table 3. Species-specific parameters are taken for a lettuce crop and taken from the literature.

Table 3. Parameters values used for simulations. All values are taken from Hézard et al. (2012) unless otherwise indicated.

Parameter	Value	Unit
I_0	1.44	$mol.m^{-2}.h^{-1}$
k	0.66	dimensionless
Dc	$6.12.10^{-2}$	$m^2.h^{-1}$
Ca	$4.087.10^{-3}$ (1000 ppm)	$mol.m^{-3}$
Ci	$1.23.10^{-3}$ (300 ppm)	$mol.m^{-3}$
ψ_s	-120	Pa
ψ_i	-1800	Pa
R_{vessel}	$4.8.10^{-5}$	m
RH_{air}	70	%
RH_{leaf}	100	%
M	18.01	$g.mol^{-1}$
μ_{xylem}	$2.778.10^{-7}$	Pa.h
Dens	24	number of plants.m^{-2}
QY	0.054	$mol_C.mol_{photon}^{-1}$
Resp	0.27	$mol_{respired}. mol_{absorbed}^{-1}$
Tr	0.41	dimensionless
DM	0.07	$g_{dry}.g_{fresh}^{-1}$
BC_{mol}	30.5	$g.mol_C^{-1}$
D_w	0.0000282	$m^2.s^{-1}$
$\rho_{mol,w}$	41.58	$mol.m^{-3}$
l_s	11.10^{-6} [18,46]	m
a_s	170.10^{-12} [18,46]	m^2
d_s	$1.4.10^{8}$ [18,46]	pores.m^{-2}
η	0.000018	$m^2.s^{-1}$
β	0.003412969	K^{-1}
h	1	M
Tair	293	K
Tleaf	296	K
Photoperiod	14	h
Initial Biomass	28	g

We looked at the dependence on the gravity parameter, for a given forced convection value for CO_2 uptake and transpiration, as well as biomass production; and the dependence on the forced convection, for a given gravity value.

A. Gravity dependence

1. Transpiration rate and CO_2 uptake

The forced convection air velocity was fixed to 1m/s. The transpiration rate (mol/h) and CO_2 uptake rate (mol/h) were computed for microgravity (10^{-5} m/s²), Martian gravity (3.711 m/s²) and Earth gravity (9.807 m/s²) (Figure 5 and Figure 6). The overall trend and orders of magnitude were similar for all three conditions, for both the transpiration rate and the CO_2 uptake rate. However the final transpiration rate on Earth gravity was higher than on Mars or in microgravity, 0.0146 mol/h, against 0.0132 mol/h and 0.0110 mol/h respectively. The final CO_2 uptake was also higher in Earth gravity conditions (1.28 10^{-3} mol/h) than on Mars (1.16 10^{-3} mol/h) and in microgravity (0.967 10^{-3} mol/h).

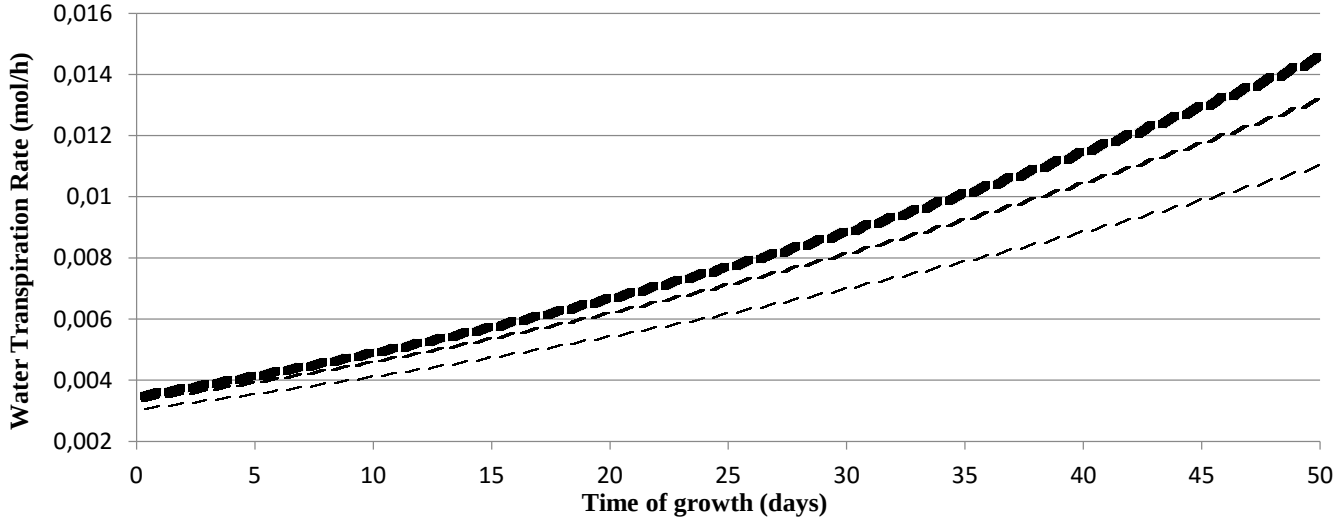

Figure 5. Water transpiration rate for microgravity (thin hyphened line), Mars gravity (medium thickness hyphened line), and Earth gravity (thick hyphened line) over 50 days of growth on a lettuce crop.

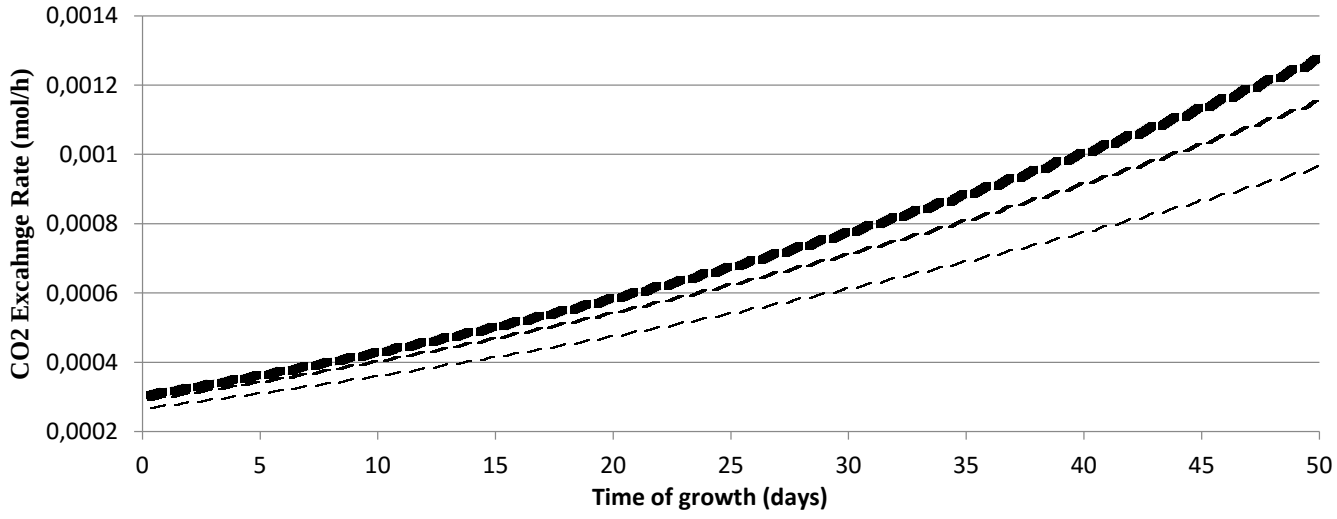

Figure 6. CO_2 uptake rate for microgravity (thin hyphened line), Mars gravity (medium thickness hyphened line), and Earth gravity (thick hyphened line) over 50 days of growth on a lettuce crop.

2. Biomass

The biomass production (in g) over the 50 days of growth was computed with the same growth conditions (forced convection air velocity fixed to 1m/s) and depends on the gas exchanges, namely CO_2 uptake rate and transpiration. As a result, the biomass produced in Earth gravity conditions is 21% higher than in microgravity and 7% only in Martian conditions (Figure 7). And biomass produced in Martian gravity conditions was 13% higher than in microgravity.

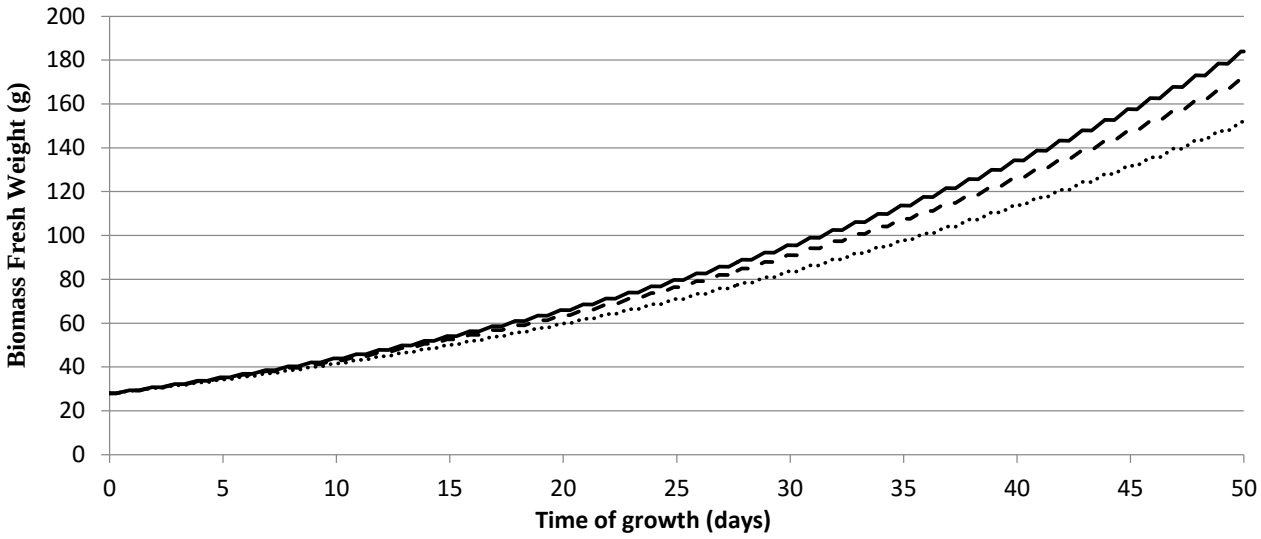

Figure 7. Biomass accumulation for microgravity (dotted line), Mars gravity (hyphened line), and Earth gravity (continuous line) over 50 days of growth on a lettuce crop.

These simulations show a non negligible effect of the gravity parameter on gas exchanges, which have a direct incidence on biomass production. It is in accordance to experiments performed in the past on parabolic flights and on the MIR space station and on the ISS[35,36,40].

The importance of forced convection is highlighted here. Although there was an airspeed of 1m/s in each case, it was not enough to counter the indirect effects of low gravity resulting in lower free convection speeds. Consequently for future plant growth in space, forced convection will need to be adapted carefully in order to obtain optimal gas exchanges and biomass production.

B. Ventilation dependence

In this section, only computations of biomass production are shown. For each gravity level: microgravity (Figure 8), Mars (Figure 9), Earth (Figure 10), three forced convection speeds are applied: 0 m/s, 0.5 m/s, and 1 m/s.

1. Microgravity

The biomass produced in microgravity with 0.5 m/s is 34% lower than with a forced convection of 1 m/s. When forced convection is removed, plants do not grow: 1.1 g only produced over 50 days. This is in accordance to what was observed in the past on plant growth in low Earth orbit[33].

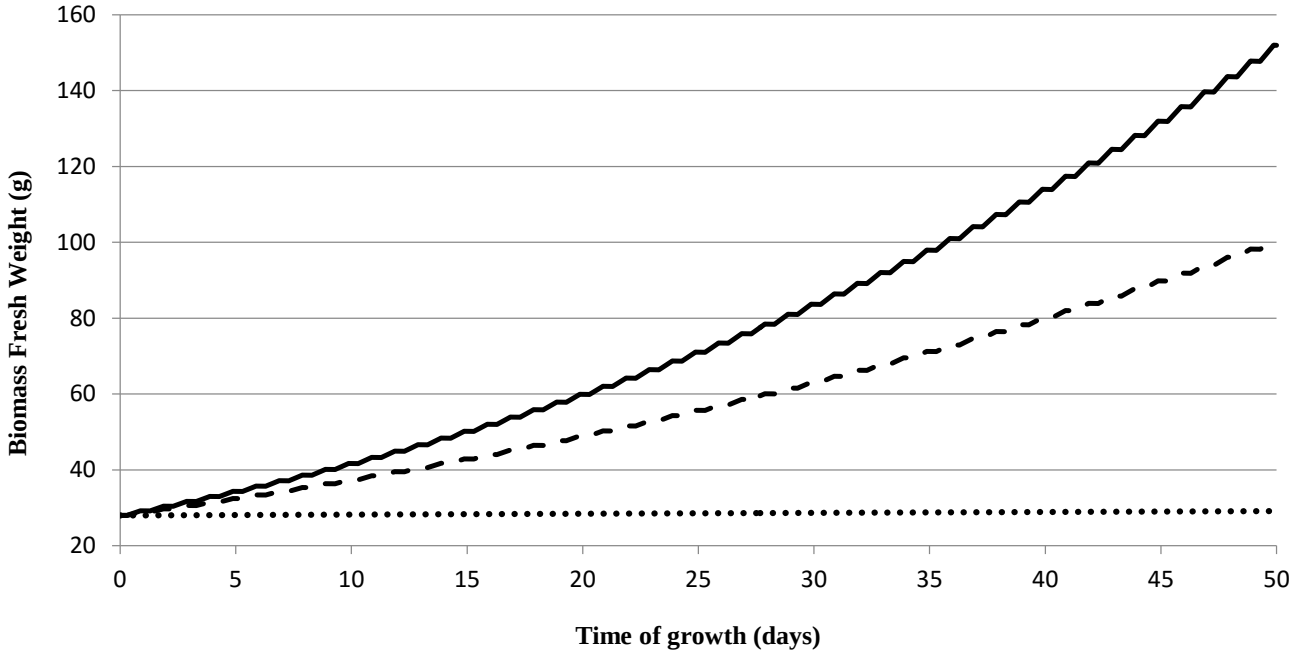

Figure 8. Biomass accumulation in microgravity with a forced convection air velocity of 0 m/s (dotted line), 0.5 m/s (hyphened line), and 1 m/s (continuous line) over 50 days of growth on a lettuce crop.

2. Mars gravity

In Martian gravity, the effects of no forced gravity are less inhibitor than for microgravity, but biomass produced with no forced convection is 46% lower than with 0.5 m/s and 62% lower than with 1 m/s.

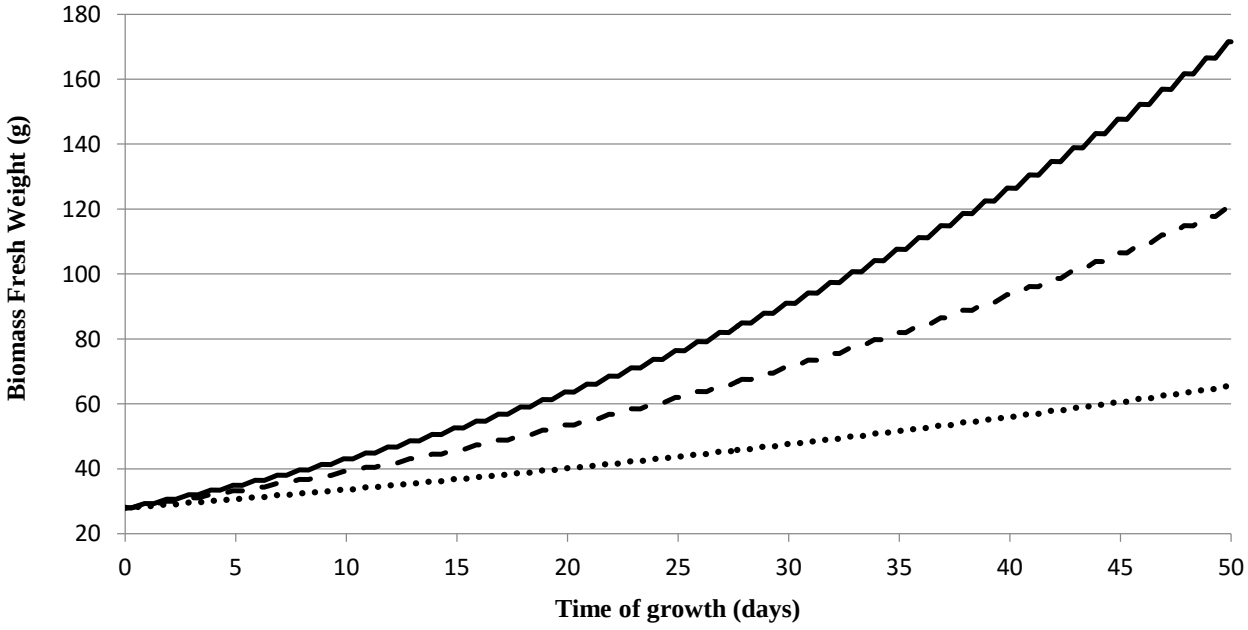

Figure 9. Biomass accumulation in Martian gravity level with a forced convection air velocity of 0 m/s (dotted line), 0.5 m/s (hyphened line), and 1 m/s (continuous line) over 50 days of growth on a lettuce crop.

3. Earth gravity

These computations show the importance of a well ventilated growth chamber even on Earth. Indeed biomass produced with no forced convection is 40% lower than with 0.5 m/s and 56% lower than with 1 m/s.

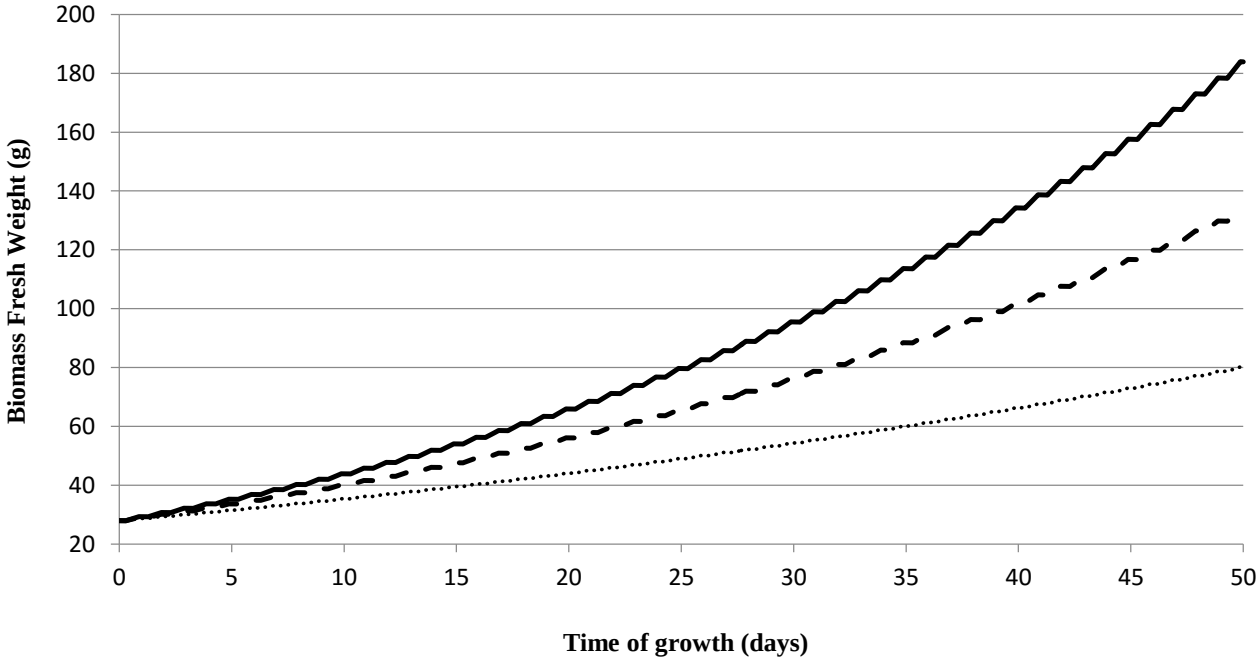

Figure 10. Biomass accumulation in Earth gravity level with a forced convection air velocity of 0 m/s (dotted line), 0.5 m/s (hyphened line), and 1 m/s (continuous line) over 50 days of growth on a lettuce crop.

In our example in part II.B.1, with the values used for the simulations, the stomatal conductance was 2.54 $mol.m^{-2}.s^{-1}$, while the boundary layer conductance was 0.15 $mol.m^{-2}.s^{-1}$, suggesting that plant gas exchanges are driven mostly by the stomata. Indeed the control of transpiration in plants is usually attributed to stomata[18] but our simulations show that the boundary layer and control of the convective regime surrounding the leaves also play a significant role in plant gas exchanges. In microgravity (no free convection) without forced convection, the boundary layer becomes so thick that gas cannot diffuse through it and plants did not grow; this proves that stomatal conductance solely is not enough. Gas exchanges at the leaf surface are the results of intricate coupled diffusion and convection mechanisms that need to be investigated further to fully understand plant growth in reduced gravity environments.

IV. Conclusion and future work

Gas exchanges play a crucial role in plant growth and their dependency on gravity levels and forced ventilation have been studied experimentally in the past in parabolic flights and in Earth orbit. Building on the bases of the already existing MELiSSA plant growth model, we have added a more detailed description of the gas exchanges at the leaf level, with gravity as a varying parameter of the model. This has enabled us to study more in details the underlying mechanisms of gas exchanges and look at the influences of gravity and ventilation on the transpiration and CO_2 uptake, and ultimately biomass production. The results shown and discussed above are mostly intended for studying the dependency on forced convection and gravity levels, not for accurate predictions of plant growth in reduced gravity environment. They show that an adequate ventilation of the plant chamber is more important than the indirect effect of reduced gravity on free convection. Indeed our results indicate that without forced convection plants do not grow very well, whatever the level of gravity. When adequate convection is provided, as expected from past experiments, plants in reduced gravity environment grow as well as plants on Earth in 1g.

An experiment in a parabolic flight planned for late 2017 will enable to gather enough data on plant gas exchanges to validate the model in microgravity. This will in return enable us to fine-tune the model and acquire more accurate simulations for better quantification of gas exchanges and biomass production. This will have implications on the

planning of future crewed space missions where plants will be used as food source and enable oxygen and water recycling for supporting humans.
Future versions of the model will include an accurate growth limitation in time and a coupling with the energy balance. Ultimately the morphological module presented above will also be described using a mechanistic approach and not only relying on empirical parameters.

Acknowledgments

The authors would like to thank the Centre National d'Etudes Spatiales (CNES) and the Centre National de Recherche Scientifique (CNRS).

References

1. Drysdale, A. *et al.* Advanced Life Support Requirements, Assumptions and Reference Missions. (2002). Available at: http://papers.sae.org/2002-01-2480/. (Accessed: 27th February 2017)
2. Futron Corporation. Space Transportation Costs: Trends in Price Per Pound to Orbit ... *yumpu.com* (2002). Available at: https://www.yumpu.com/en/document/view/36996100/space-transportation-costs-trends-in-price-per-pound-to-orbit-. (Accessed: 27th February 2017)
3. Drysdale, A. E., Rutkze, C. J., Albright, L. D. & LaDue, R. L. The minimal cost of life in space. *Adv. Space Res.* **34,** 1502–1508 (2004).
4. Wheeler, R. M. Plants For Human Life Support In Space: From Myers To Mars. *Gravitational Space Res.* **23,** (2011).
5. Burkey, R., Green, S., Siebenaler, S. & Buckingham, C. From CO2 to H2O. *Technol. Today* (2010).
6. Bagdigian, R. & Cloud, D. Status of the International Space Station Regenerative ECLSS Water Recovery and Oxygen Generation Systems. *ResearchGate* doi:http://dx.doi.org/10.4271/2005-01-2779
7. Wheeler, R. Horticulture For Mars. *Acta Hortic.* **642,** 201–215 (2004).
8. Sadler, P. D. *et al.* Bio-regenerative life support systems for space surface applications. in (2011).
9. Zabel, P., Schubert, D. & Tajmar, M. in *43rd International Conference on Environmental Systems* (American Institute of Aeronautics and Astronautics, 2013). doi:10.2514/6.2013-3333
10. Poulet, L., Fontaine, J.-P. & Dussap, C.-G. Plant's response to space environment: a comprehensive review including mechanistic modelling for future space gardeners. *Bot. Lett.* **163,** 337–347 (2016).
11. Lasseur, C. *et al.* MELiSSA: THE EUROPEAN PROJECT OF CLOSED LIFE SUPPORT SYSTEM. *Gravitational Space Res.* **23,** (2011).
12. Cornet, J.-F., Dussap, C. G. & Gros, J.-B. in *Bioprocess and Algae Reactor Technology, Apoptosis* 153–224 (Springer Berlin Heidelberg, 1998). doi:10.1007/BFb0102299

13. Cogne, G., Gros, J.-B. & Dussap, C.-G. Identification of a metabolic network structure representative of Arthrospira (spirulina) platensis metabolism. *Biotechnol. Bioeng.* **84,** 667–676 (2003).
14. Sasidharan, S., Hezard, P., Poughon, L. & Dussap, C. G. in *40th International Conference on Environmental Systems* (American Institute of Aeronautics and Astronautics, 2010). doi:10.2514/6.2010-6192
15. Hézard, P., Sasidharan, S., Cruely, C. & Dussap, C.-G. in *40th International Conference on Environmental Systems* (American Institute of Aeronautics and Astronautics, 2010). doi:10.2514/6.2010-6079
16. Hézard, P. Higher Plant Growth Modelling for Life Support Systems: Global Model Design and Simulation of Mass and Energy Transfers at the Plant Level. (Doctoral school of Life Sciences, Health, Agronomy, Environment. Université Blaise Pascal, Université d'Auvergne, 2012).
17. Thornley, J. H. M. & Johnson, I. R. *Plant and crop modelling: a mathematical approach to plant and crop physiology*. (Clarendon Press, 1990).
18. Holmberg, M., Paille, C. & Lasseur, C. Preliminary Modelling of Mass Flux at the Surface of Plant Leaves within the MELiSSA Higher Plant Compartments. *Upps. Univ. ESA* (2013).
19. Manzoni, S. *et al.* Optimizing stomatal conductance for maximum carbon gain under water stress: a meta-analysis across plant functional types and climates. *Funct. Ecol.* **25,** 456–467 (2011).
20. Kitaya, Y., Tsuruyama, J., Shibuya, T., Yoshida, M. & Kiyota, M. Effects of air current speed on gas exchange in plant leaves and plant canopies. *Adv. Space Res.* **31,** 177–182 (2003).
21. Boulard, T. *et al.* Tomato leaf boundary layer climate: implications for microbiological whitefly control in greenhouses. *Agric. For. Meteorol.* **110,** 159–176 (2002).
22. Kitaya, Y., Tsuruyama, J., Kawai, M., Shibuya, T. & Kiyota, M. in *Transplant Production in the 21st Century* (eds. Kubota, C. & Chun, C.) 83–90 (Springer Netherlands, 2000). doi:10.1007/978-94-015-9371-7_13
23. Kitaya, Y., Shibuya, T., Yoshida, M. & Kiyota, M. Effects of air velocity on photosynthesis of plant canopies under elevated CO2 levels in a plant culture system. *Adv. Space Res.* **34,** 1466–1469 (2004).
24. Wang, M. *et al.* Effects of different elevated CO2 concentrations on chlorophyll contents, gas exchange, water use efficiency, and PSII activity on C3 and C4 cereal crops in a closed artificial ecosystem. *Photosynth Res* (2015). doi:http://dx.doi.org/10.1007/s11120-015-0134-9
25. Wheeler, R. M., Mackowiak, C. L., Yorio, N. C. & Sager, J. C. Effects of CO2 on Stomatal Conductance: Do Stomata Open at Very High CO2 Concentrations? *Ann. Bot.* **83,** 243–251 (1999).

26. Ainsworth, E. A. & Rogers, A. The response of photosynthesis and stomatal conductance to rising [CO2]: mechanisms and environmental interactions. *Plant Cell Environ.* **30,** 258–270 (2007).
27. Nelson, J. A. & Bugbee, B. Analysis of Environmental Effects on Leaf Temperature under Sunlight, High Pressure Sodium and Light Emitting Diodes. *PLOS ONE* **10,** e0138930 (2015).
28. Wolverton, C. & Kiss, J. Z. An Update on Plant Space Biology. *Gravitational Space Res.* **22,** (2011).
29. De Micco, V., De Pascale, S., Paradiso, R. & Aronne, G. Microgravity effects on different stages of higher plant life cycle and completion of the seed-to-seed cycle. *Plant Biol. Stuttg. Ger.* **16 Suppl 1,** 31–38 (2014).
30. Wolff, S. A., Coelho, L. H., Karoliussen, I. & Jost, A.-I. K. Effects of the Extraterrestrial Environment on Plants: Recommendations for Future Space Experiments for the MELiSSA Higher Plant Compartment. *Life Open Access J.* **4,** 189–204 (2014).
31. Jost, A.-I. K., Hoson, T. & Iversen, T.-H. The Utilization of Plant Facilities on the International Space Station—The Composition, Growth, and Development of Plant Cell Walls under Microgravity Conditions. *Plants* **4,** 44–62 (2015).
32. Vandenbrink, J. P. & Kiss, J. Z. Space, the final frontier: A critical review of recent experiments performed in microgravity. *Plant Sci.* **243,** 115–119 (2016).
33. Porterfield, D. M., Neichitailo, G. S., Mashinski, A. L. & Musgrave, M. E. Spaceflight hardware for conducting plant growth experiments in space: The early years 1960–2000. *Adv. Space Res.* **31,** 183–193 (2003).
34. Kitaya, Y. *et al.* The effect of gravity on surface temperature and net photosynthetic rate of plant leaves. *Adv. Space Res.* **28,** 659–664 (2001).
35. Kitaya, Y. *et al.* The effect of gravity on surface temperatures of plant leaves. *Plant Cell Environ.* **26,** 497–503 (2003).
36. Hirai, H. & Kitaya, Y. Effects of Gravity on Transpiration of Plant Leaves. *Ann. N. Y. Acad. Sci.* **1161,** 166–172 (2009).
37. Jones, M. B. in *Photosynthesis and Production in a Changing Environment* (eds. Hall, D. O., Scurlock, J. M. O., Bolhàr-Nordenkampf, H. R., Leegood, R. C. & Long, S. P.) 47–64 (Springer Netherlands, 1993). doi:10.1007/978-94-011-1566-7_4
38. Yabuki, K. & Harazono, Y. Studies on the Effects of Wind Speed on Photosynthesis. *J. Agric. Meteorol.* **34,** 87–94 (1978).

39. Monje, O. *et al.* Canopy photosynthesis and transpiration in micro-gravity: Gas exchange measurements aboard Mir. *Adv. Space Res.* **26,** 303–306 (2000).
40. Monje, O., Stutte, G. & Chapman, D. Microgravity does not alter plant stand gas exchange of wheat at moderate light levels and saturating CO2 concentration. *Planta* **222,** 336–345 (2005).
41. Stutte, G. W., Monje, O., Goins, G. D. & Tripathy, B. C. Microgravity effects on thylakoid, single leaf, and whole canopy photosynthesis of dwarf wheat. *Planta* **223,** 46 (2005).
42. Kichah, A., Bournet, P.-E., Migeon, C. & Boulard, T. Measurement and CFD simulation of microclimate characteristics and transpiration of an Impatiens pot plant crop in a greenhouse. *Biosyst. Eng.* **112,** 22–34 (2012).
43. Lawson, T. & Blatt, M. R. Stomatal Size, Speed, and Responsiveness Impact on Photosynthesis and Water Use Efficiency. *Plant Physiol.* **164,** 1556–1570 (2014).
44. Lambers, H., Chapin, F. S. & Pons, T. L. *Plant Physiological Ecology*. (Springer, 2008).
45. Camargo, M. A. B. & Marenco, R. A. Density, size and distribution of stomata in 35 rainforest tree species in Central Amazonia. *Acta Amaz.* **41,** 205–212 (2011).
46. Muchow, R. C. & Sinclair, T. R. Epidermal conductance, stomatal density and stomatal size among genotypes of Sorghum bicolor (L.) Moench. *Plant Cell Environ.* **12,** 425–431 (1989).
47. Brodribb, T. J., Jordan, G. J. & Carpenter, R. J. Unified changes in cell size permit coordinated leaf evolution. *New Phytol.* **199,** 559–570 (2013).
48. Nobel, P. S. in *Physicochemical and Environmental Plant Physiology (Fourth Edition)* 364–437 (Academic Press, 2009). doi:10.1016/B978-0-12-374143-1.00008-9
49. Smith, W. K. *Photosynthetic Adaptation - Chloroplast to Landscape*. (Springer, 2004).
50. Vesala, T. On the Concept of Leaf Boundary Layer Resistance for Forced Convection. *J. Theor. Biol.* **194,** 91–100 (1998).

2.3 Towards the assessment of reduced gravity influences on the boundary layer thickness and introduction of the energy balance

This part is a paper accepted in January 2018 and published in Astrobiology, Volume 18 Issue 9 (September 2018).

ASTROBIOLOGY
Volume 18, Number 9, 2018

DOI: 10.1089/ast.2017.1804

Rapid Communications

A Physical Modeling Approach for Higher Plant Growth in Reduced Gravity Environments

Lucie Poulet, Jean-Pierre Fontaine, and Claude-Gilles Dussap

Abstract

Including plants in bioregenerative life-support systems enables simultaneous food production and water and air recycling, while closing cycles for water, oxygen, nitrogen, and carbon. To understand and predict higher plant behavior for a wide range of environmental conditions, including reduced gravity levels, a mechanistic physical model is being developed. The emphasis is set on the influence of gravity levels and forced convection on higher plant leaf gas exchanges, which are altered by reduction of free convection in lower gravity environments, such as microgravity or martian and lunar gravities. This study highlights the significance of understanding leaf boundary layer limitations and ultimately will lead to complete mechanistic modeling of mass and energy balances on plant growth in reduced gravity environments. Key Words: Bioregenerative life-support systems—Mechanistic modeling of gas exchanges—Low gravity—Higher plants—Energy fluxes—Artificial ecosystem. Astrobiology 18, 1093–1100.

1. Introduction

A CLOSED-LOOP life-support system (LSS) comprises several functions: atmosphere regeneration, waste treatment, and water recycling (Mitchell, 1994; Eckart, 1996; Anderson *et al.*, 2015). In the domain of space exploration, one major constraint is the payload mass and resupply costs for long-term exploration or permanent habitation LSSs (Anderson *et al.*, 2015). To improve the closure of a human LSS, and because physicochemical technologies alone are not sufficient, it becomes necessary to include biological compartments, at least at the food production level, such as a photoautotrophic compartment, including higher plants and microalgae (Ewert *et al.*, 2002; Drayer and Howard, 2014; Fu *et al.*, 2016), for *in situ* food production (Wheeler, 2004, 2011, 2017; Furfaro *et al.*, 2016), complementary to water recycling, O_2 production, and CO_2 removal. By definition, the bioregenerative LSS is a loop system so that all functions are strongly intertwined and interact with each other (Wheeler, 2003; Clauwaert *et al.*, 2015; Dong *et al.*, 2017), and since there is no buffer effect in space, slight variations in environmental parameters can dramatically affect the whole loop. To use bioregenerative LSSs to sustain human beings off Earth, a complete understanding of the dynamical functioning of the system is required. This can be achieved with a mechanistic modeling approach based on basic principles of element conservation, chemical and biological kinetics, and a thorough understanding of the coupling phenomena between physical and biochemical determinants.

In particular, the influence of space environmental conditions, such as reduced gravity, on plant growth mechanisms needs to be addressed. Major effects of impaired gravity on plant growth occur on the orientation of roots, on migration of sap within the stem, and on gas exchanges at the leaf surface (Poulet *et al.*, 2016).

Indeed, a lower gravity level also means lower free convection velocities (Kitaya *et al.*, 2001, 2003a; Hirai and Kitaya, 2009), leading to increased boundary layers of stagnant air forming around plant leaves, thus reducing gas exchanges at the leaf surface and photosynthesis (Kitaya *et al.*, 2000, 2003b, 2004; Boulard *et al.*, 2002; Kitaya, 2016). Long-duration tests on the International Space Station have shown that with adequate ventilation, photosynthesis rates are similar to those on Earth (Monje *et al.*, 2000, 2005), but to be able to predict plant behavior for a wide range of parameters, suboptimal cases must be studied. Indeed, in case of failure of one system, the model should predict, for example, how this will impact oxygen and food production or how much time the crew has left before losing parts of or the whole crop production.

The frame of this work is the Micro-Ecological Life-Support System Alternative (MELiSSA) project of the European Space Agency (ESA), a closed-loop artificial ecosystem that is inspired from a lake ecosystem comprising five compartments (Hendrickx *et al.*, 2006; Lasseur *et al.*, 2011) and for which modeling efforts of the higher plant compartment are still ongoing (Hézard, 2012; Poulet *et al.*, 2016, 2017). The initial plant growth model was based on

Université Clermont Auvergne, Institut Pascal, UMR 6602, Clermont-Ferrand, France.

mass balance aspects while addressing limitations of current, existing agronomy models (Hézard *et al.*, 2010).

In this article, emphasis is set on the influence of gravity levels such as microgravity and Earth, Mars, and lunar gravities, as well as the influence of free and forced convection on the leaf boundary layer thickness, higher plant gas exchanges, and biomass production. The link between gas exchanges and the plant energy balance is also discussed.

2. Materials and Methods

2.1. Overall structure of the higher plant growth model

The higher plant growth model encompasses four modules corresponding to four study levels (Fig. 1): the environmental module accounts for variations of process parameters at the surrounding environmental scale; the morphological module includes structural changes at the plant scale; the physical module represents the rate-limiting processes impacting biomass growth at the organ scale; and the biochemical module accounts for metabolic growth equations at the cell scale, including stoichiometric constraints (Hézard, 2012).

This model is built so that it can be adapted to virtually any plant species by entering adequate species-dependent parameters. In a first approach, the higher plant is considered as a circular single leaf, with the leaf area, stem length, and number of vessels within the leaf increasing proportionally with biomass increase. The proportionality coefficients used to compute these morphological traits are species dependent and can be assessed experimentally for the studied species. The leaf area or stem growth will thus differ according to the studied species. These morphological traits are used within physical equations to compute the maximum fluxes for water uptake and transpiration, as well as CO_2 uptake and light interception. To assess the influence of different gravity levels on the physical module, the behavior of gas exchanges must be investigated. The application here is a study of transfer rates at a leaf level, the leaf being considered as a solid horizontal plate, with the surface increasing proportionally with the biomass increase.

The light interception follows the Beer–Lambert law, while the CO_2 uptake and the water transpiration are diffusion equations following Fick's law (Fig. 2), and the water uptake equation is the Poiseuille law. The metabolic description coupled to the kinetic uptake rate of CO_2 derived from the light energy transfer model provides the calculation of metabolic fluxes for lit periods and of instantaneous biomass production rates. These metabolic fluxes are computed using the quantum yield, which is species dependent, especially depending on if the plant is a C3 or a C4 (Ehleringer and Björkman, 1977).

Integration along time, accounting for lit and dark periods, leads to biomass production over a given period of time.

2.2. Gas exchanges at the leaf surface

Gas exchanges at the leaf surface between the plant and the atmosphere depend on two diffusion phenomena, one through the leaf's stomata and one through the boundary layer, and on the convection regime around the plant (Lambers *et al.*, 2008; Poulet *et al.*, 2017). The gas exchange equations follow Fick's law of diffusion, with an exchange coefficient and a concentration gradient driving the exchange (Fig. 2).

In the case of CO_2 uptake, the gradient driving the exchange is the difference between the external CO_2 concentration (Ca in Fig. 2) and internal leaf CO_2 concentration (Ci in Fig. 2) (Hézard, 2012). The exchange coefficient ($k_{CO2}(\delta_{mass})$ in Fig. 2) is the ratio between the diffusion coefficient for CO_2 D_c and the thickness of the boundary layer δ_{mass}:

$$k_{CO_2} = \frac{D_c}{\delta_{mass}}.$$

For water transpiration, the water partial pressure gradient driving the exchange is the difference between the surface

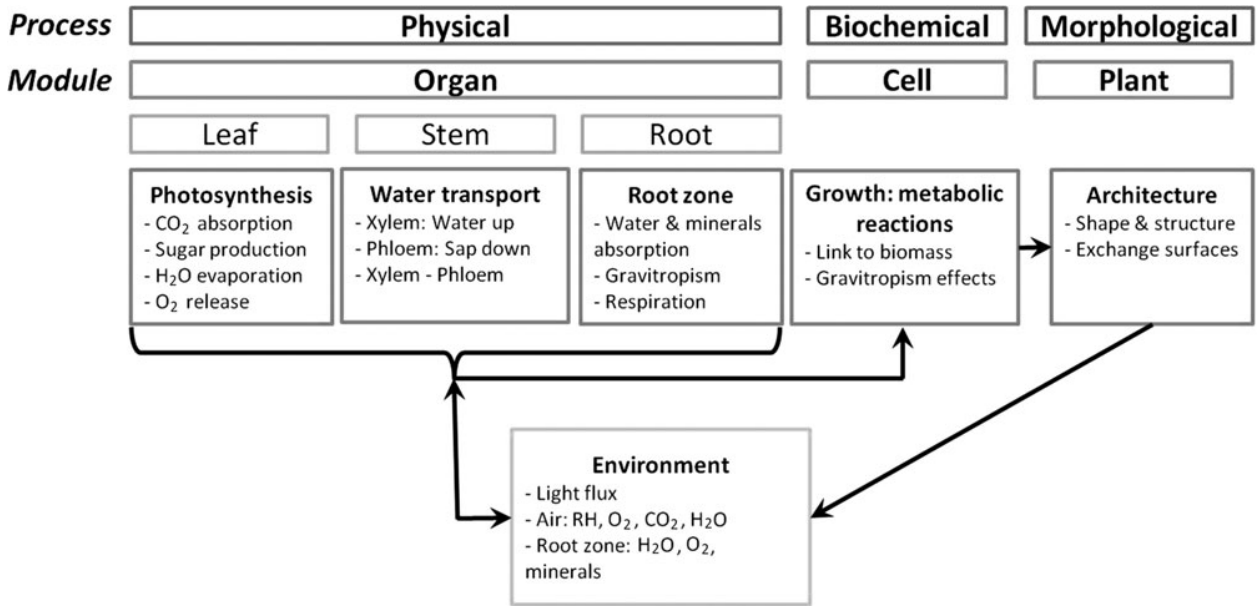

FIG. 1. Diagram illustrating the model structure with four main modules: physical, biochemical, morphological, and environmental modules.

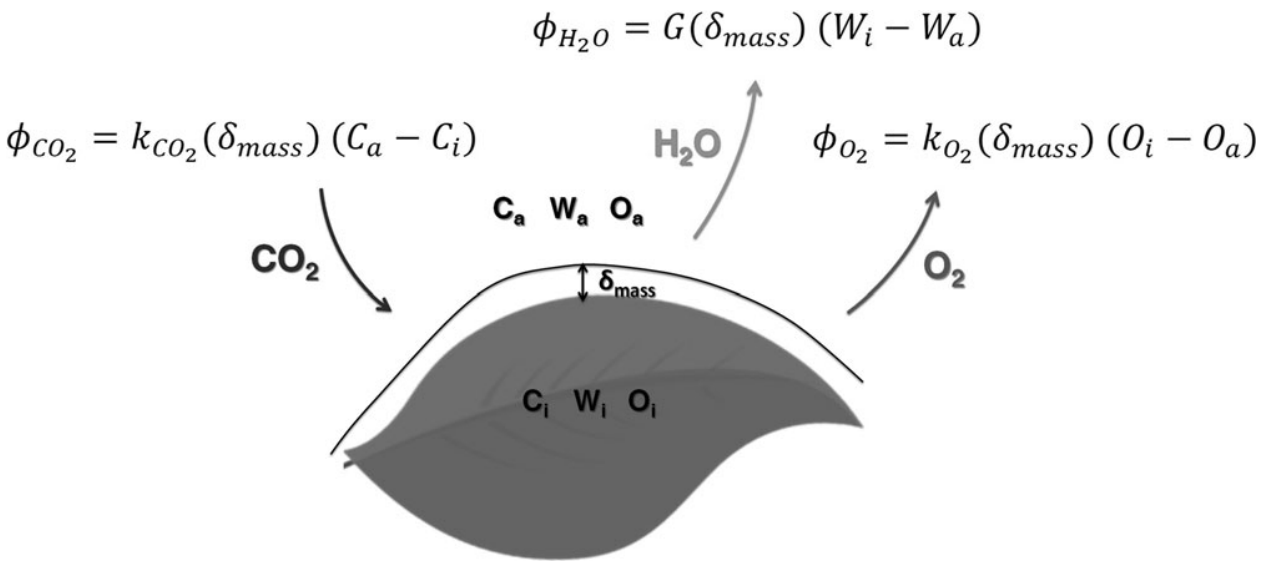

FIG. 2. Schematic view of gas exchanges at the leaf surface. φ_{CO_2} is the CO_2 uptake rate, φ_{H_2O} is the water vapor release (transpiration) rate, and φ_{O_2} the O_2 production rate; $k_{CO_2}(\delta_{mass})$ and $k_{O_2}(\delta_{mass})$ are exchange coefficients for, respectively, CO_2 uptake and O_2 release; C_a, W_a, and O_a are, respectively, the external CO_2, water vapor, and O_2 concentrations and C_i, W_i, and O_i are, respectively, the leaf internal CO_2, water vapor, and O_2 concentrations.

water partial pressure that is considered as saturated at the surface temperature and the atmosphere bulk water partial pressure. In other words, this corresponds to a difference in relative humidity between the inside and the outside of the leaf. The exchange coefficient ($G(\delta_{mass})$ in Fig. 2) is the leaf conductance, which is a function of the thickness of the mass boundary layer surrounding the leaf.

2.3. Leaf conductance

The total leaf conductance describes the diffusion capacity through the leaf. It is also defined as the inverse of the leaf's resistance to diffusion processes. It is a combination of the two conductances associated with the two diffusion processes occurring at the leaf surface: stomatal conductance and boundary layer conductance. The boundary layer conductance for water is a function of the diffusion coefficient for water vapor D_w, molar water vapor density $\rho_{mol,w}$, and thickness of the boundary layer δ_{mass} (Lambers *et al.*, 2008):

$$g_w^{BL} = \frac{D_w \rho_{mol,w}}{\delta_{mass}}.$$

Stomatal conductance is a function of parameters that are plant and species dependent, so it differs from one plant species to another and enables the gas exchange model to be adapted for a specific plant species:

$$g_w^s = \frac{d_s a_s D_w \rho_{mol,w}}{l_s},$$

where d_s is the stomatal density on a leaf, a_s is the average cross-sectional area of a stomata, and l_s the average depth of a stomatal pore.

Total conductance is found by adding the mass transfer resistances in series, such as $\frac{1}{G} = \frac{1}{g_w^s} + \frac{1}{g_w^{BL}}$.

Thus,

$$G = \frac{D_w \rho_{mol,w} d_s a_s}{\delta_{mass} d_s a_s + l_s}.$$

2.4. Influence of gravity

To include gravity as a parameter of the model, three assumptions need to be stated:

1. The airflow above the leaf is laminar. This implies a static model of the boundary layer (Vesala, 1998). Its thickness, which is the distance from the leaf surface where the concentration of a given compound is <99% of the ambient air value, is thus expressed as a function of the velocity of flow above the leaf v, air kinematic viscosity ν, and characteristic length of the leaf L, with the following equation:

$$\delta_{mass} = 4.6\sqrt{\frac{L\nu}{v}}$$

L accounts for the size of the leaf. It is defined as the radius of a round leaf, whose surface is the leaf area, increasing with biomass production.

2. The airflow velocity is a combination of a free convection velocity and a forced convection velocity. Free and forced convection velocities are three-dimensional vectors. The assumption is that they are both in the same direction, parallel to the leaf surface. Thus, the expression for the airflow velocity module is the sum of the norms of vectors for free and forced convections:

$$v = v_{free} + v_{forced}$$

In this model, v_{forced} is fixed and depends on the type of ventilation chosen for the plant chamber. This is a process parameter.

3. The free convection velocity is then expressed using the dimensionless number of Richardson, expressing the ratio of buoyancy forces over inertial forces: $Ri = Gr/Re^2$, where Gr is the Grashof number and Re the Reynolds number. When these forces are of the same order of magnitude, the Richardson number is equal to unity and the free convection velocity is expressed as

$$v_{free} = \sqrt{g\beta H\left(T_{air} - T_{leaf}\right)},$$

where g is the acceleration of gravity, β the thermal expansion coefficient, H the characteristic length of the plant chamber, T_{air} the temperature of air in the growth chamber, and T_{leaf} the leaf surface temperature.

With these three assumptions, the thickness of the boundary layer and the total leaf conductance are expressed as functions of acceleration of gravity:

$$\delta_{mass} = 4.6\sqrt{\frac{L\nu}{\sqrt{g\beta H\left(T_{air} - T_{leaf}\right)} + v_{forced}}}$$

$$G = \frac{D_w \rho_{mol,w} d_s a_s}{4.6\sqrt{\frac{L\nu}{\sqrt{g\beta H\left(T_{air} - T_{leaf}\right)} + v_{forced}}}\, d_s a_s + l_s}$$

Hence, gravity is now included as a parameter in gas exchange equations, which led to study CO_2 uptake and water transpiration as functions of different gravity levels.

2.5. Link with energy balance

The energy balance of a leaf depends on the energy received and the energy emitted or used by the plant (Raschke, 1960; Jones and Rotenberg, 2001; Lambers *et al.*, 2008; Schymanski *et al.*, 2013). Energy received encompasses energy from direct incident light (photons) and energy from the surrounding radiative environment. Energy emitted by the plant is radiation energy and latent energy produced at the surface level by evaporation of liquid water from transpiration, as well as energy exchanges by convection. The metabolic energy used by the plant for photosynthesis and other metabolic reactions is usually neglected. Energy received from solar radiation, called shortwave radiation, is the main energy input and needs to be dissipated for the leaf to not burn. If not, a leaf could reach 100°C in <1 min (Lambers *et al.*, 2008).

All objects above 0K radiate energy in the form of longwave infrared radiation, including plants and objects surrounding the plants, including the sky, following the Stefan–Boltzmann equation, with ε being emissivity and σ the Stefan–Boltzmann constant (Siegel and Howell, 1992; Beek *et al.*, 1999):

$$E_{LW} = \varepsilon\sigma T^4$$

Hence, the total radiation energy for plants is $E_{LW} = \sigma\left(\varepsilon_{leaf}\, T_{leaf}^4 - \varepsilon_b T_b^4\right)$ with T_{leaf} being the leaf surface temperature, ε_{leaf} the leaf emissivity, ε_b the surrounding emissivity, and T_b the bulk air temperature.

The energy associated with convective transport is driven by the temperature gradient between the air and the leaf and depends on the boundary layer forming around the leaf (Lambers *et al.*, 2008):

$$E_{conv} = \frac{k_t}{\delta_{mass}}\left(T_b - T_{leaf}\right)$$

For gases, it is often admitted that the heat boundary layer thickness is equal to the mass boundary layer thickness, detailed here above. Indeed, the ratio between mass and heat boundary layer thickness is equal to $Le^{1/3}$ where Le is the Lewis number, which is equal to unity in the case of gases (Beek *et al.*, 1999).

The energy associated with transpiration is equal to the transpiration flux ϕ_{H_2O} multiplied by the molar latent heat of vaporization λ_{mol} (Schymanski *et al.*, 2013):

$$E_{transpi} = \lambda_{mol}\phi_{H_2O}$$

This gives an energy balance in steady state, linking mass fluxes (ϕ_{H_2O}), leaf temperature T_{leaf}, and energy coming from the external environment:

$$E_{photons} + E_{LW} + E_{transpi} + E_{conv} = I_0 N_A hc + \sigma\left(\varepsilon_{leaf}\, T_{leaf}^4 - \varepsilon_b T_b^4\right) + \lambda_{mol}\phi_{H_2O} + \frac{k_t}{\delta_{mass}}\left(T_b - T_{leaf}\right) = 0$$

with I_0 being the incident light flux, N_A the Avogadro number, h the Planck constant, and c the speed of light.

This enables to have the leaf temperature as a variable of the model and not anymore as a fixed parameter. In a first step, the balance is considered for a steady-state regime and the dynamic balance will be considered at a later stage. In the following simulations, the energy balance and mass balances are not coupled. This paragraph is an overview of the next steps to follow for model development.

3. Results

The computations below were performed by using parameters listed in Table 1. For simulation of biomass growth, the photoperiod was 14 h and the initial fresh biomass weight was 28 g.

3.1. Thickness of the boundary layer versus gravity and forced convection

The thickness of the boundary layer was computed for values of g varying from $0.000001\,m\cdot s^{-2}$ (microgravity) to $9.807\,m\cdot s^{-2}$ (Earth's gravity) and for five different forced convection velocities, from 0 to $1\,m\cdot s^{-1}$. The results are reported in Figure 3.

The higher the value of g and of forced convection, the lower the boundary layer. In lunar gravity ($1.625\,m\cdot s^{-2}$) with no forced convection, the boundary layer is 50%

TABLE 1. PARAMETERS USED FOR COMPUTATIONS AND SIMULATIONS

Parameter	*Description*	*Value*	*Unit*
I_0	Incident light flux	400	$\mu mol \cdot m^{-2} \cdot s^{-1}$
k	Light extinction coefficient	0.66	Dimensionless
D_c	CO_2 diffusion coefficient	$1.7 \cdot 10^{-5}$	$m^2 \cdot s^{-1}$
C_a	CO_2 concentration in the outside air	$4.087 \cdot 10^{-2}$ (1000 ppm)	$mol \cdot m^{-3}$
C_i	CO_2 concentration in the leaf	$1.23 \cdot 10^{-2}$ (300 ppm)	$mol \cdot m^{-3}$
D_w	Diffusion coefficient of water vapor	$2.82 \cdot 10^{-5}$	$m^2 \cdot s^{-1}$
$\rho_{mol, w}$	Molar water vapor density	41.58	$mol \cdot m^{-3}$
l_s	Depth of the stomatal pore	$11 \cdot 10^{-6}$	M
a_s	Stomatal cross-sectional area	$1.70 \cdot 10^{-10}$	m^2
d_s	Stomatal density	$1.4 \cdot 10^{8}$	$pores \cdot m^{-2}$
ν	Air kinematic viscosity	$1.9 \cdot 10^{-5}$	$m^2 \cdot s^{-1}$
β	Thermal expansion coefficient	$3.33 \cdot 10^{-3}$	K^{-1}
H	Characteristic length of the plant chamber	1	m
T_b	Temperature of the surrounding air	293	K
T_{leaf}	Temperature of the leaf	296	K
$P^0(T_b)$	Water vapor saturating pressure at T_b	2303.35	Pa
$P^0(T_{leaf})$	Water vapor saturating pressure at T_{leaf}	2768.56	Pa
L	Characteristic length of a leaf	0.05	m
R	Gas constant	8314	$J \cdot mol^{-1} \cdot K^{-1}$

Muchow and Sinclair (1989), Hézard (2012), and Holmberg *et al.* (2013).

thicker than in Earth gravity conditions and 20% thicker than in martian gravity ($3.711\ m \cdot s^{-2}$). It is interesting to note that in Earth's gravity, the boundary layer is twice as thick with no forced convection compared with a forced convection of $1\ m \cdot s^{-1}$, while it is 10 times thicker in microgravity.

3.2. Mass exchange rates versus gravity and forced convection

The previous boundary layer model is now used for assessing rates of mass exchanges between the gas bulk and the leaf surface. The water transpiration and CO_2 uptake rates per surface of leaf area were computed for values of g varying from $0.000001\ m \cdot s^{-2}$ (microgravity) to $9.807\ m \cdot s^{-2}$ (Earth's gravity) and for five different forced convection velocities, from 0 to $1\ m \cdot s^{-1}$.

As expected, the transpiration and CO_2 uptake rates are higher for higher forced convection velocities and higher gravity levels. Both CO_2 uptake and transpiration rates in Earth gravity conditions are twice as high for a forced convection of $1\ m \cdot s^{-1}$ compared with no forced convection; they are, respectively, 2.5 and 2.3 times higher in martian

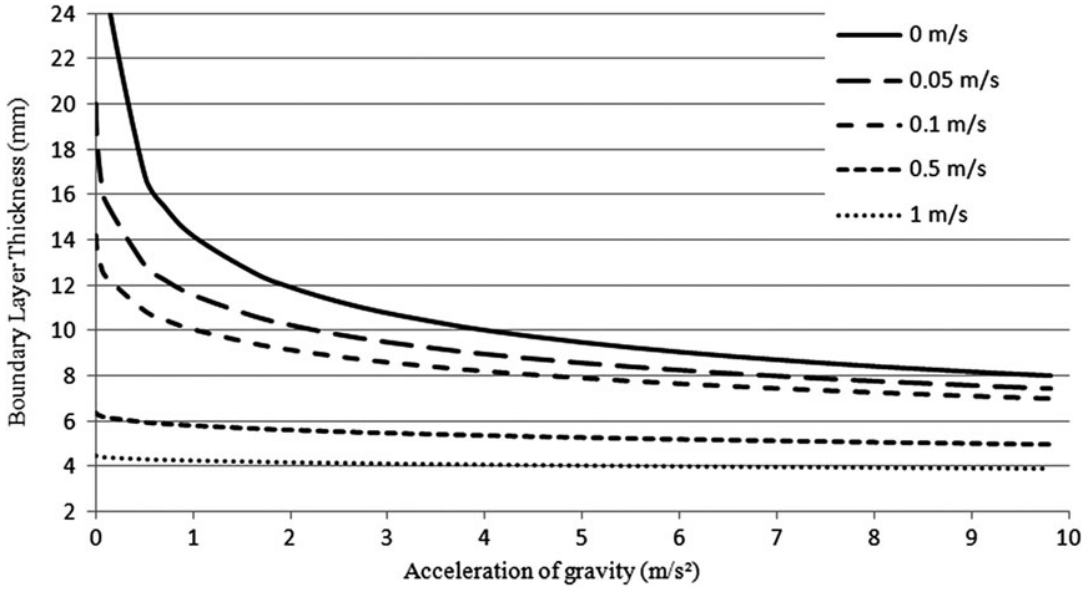

FIG. 3. Variations of boundary layer thickness according to the acceleration of gravity between 0.000001 and $9.807\ m \cdot s^{-2}$ for five different forced convection velocities: $0\ m \cdot s^{-1}$ (plain); $0.05\ m \cdot s^{-1}$ (long dashes); $0.1\ m \cdot s^{-1}$ (dashes); $0.5\ m \cdot s^{-1}$ (small dashes); and $1\ m \cdot s^{-1}$ (dots).

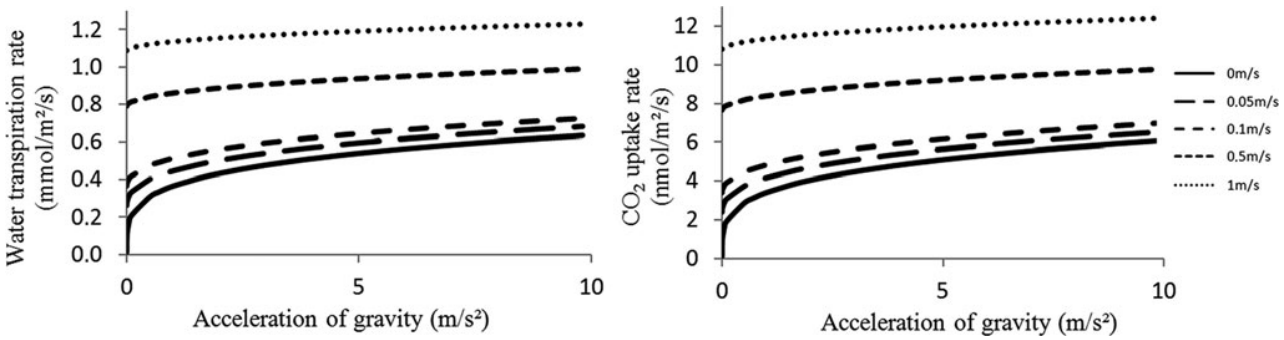

FIG. 4. Variations of the water transpiration rate (left) and the CO_2 uptake rate (right) according to acceleration of gravity between 0.000001 and 9.807 $m \cdot s^{-2}$ for five different forced convection velocities: 0 $m \cdot s^{-1}$ (plain); 0.05 $m \cdot s^{-1}$ (long dashes); 0.1 $m \cdot s^{-1}$ (dashes); 0.5 $m \cdot s^{-1}$ (small dashes); and 1 $m \cdot s^{-1}$ (dots).

gravity and both almost three times higher in lunar gravity (Fig. 4).

3.3. Biomass production versus gravity and forced convection

By using equations of the model described in the work of Hézard (2012) and Poulet *et al.* (2017), the biomass fresh weight of a lettuce crop was computed over a growth period of 50 days and under 400 $\mu mol \cdot m^{-2} \cdot s^{-1}$ of incident light for three different gravity levels (microgravity, martian, and Earth) and three forced convection velocities (Fig. 5). It is to be underlined that in Earth's gravity after 50 days, biomass production is three times as much with a forced convection of 1 $m \cdot s^{-1}$ compared with no forced convection and 50% higher with a forced convection of 0.5 $m \cdot s^{-1}$.

With no forced convection, biomass production is 25% higher in Earth gravity conditions than in martian gravity conditions and it is a little >1 g in microgravity. With a forced convection of 0.5 $m \cdot s^{-1}$, biomass production is over 20% higher in martian gravity conditions than in microgravity and 40% higher in Earth gravity conditions.

4. Discussion

4.1. Boundary layer thickness

The thickness of the boundary layer is more sensitive to gravity for lower values of forced convection. Indeed, with the parameters of the model, the value of free convection velocity varies between 0.001 $m \cdot s^{-1}$ in microgravity and 0.31 $m \cdot s^{-1}$ in Earth's gravity. Hence, for values of forced convection >0.3 $m \cdot s^{-1}$, the forced convection term prevails over the free convection term. This highlights the existence of a threshold value for forced convection velocity, under which boundary layer thickness depends on gravity levels and above which it mainly depends on forced convection.

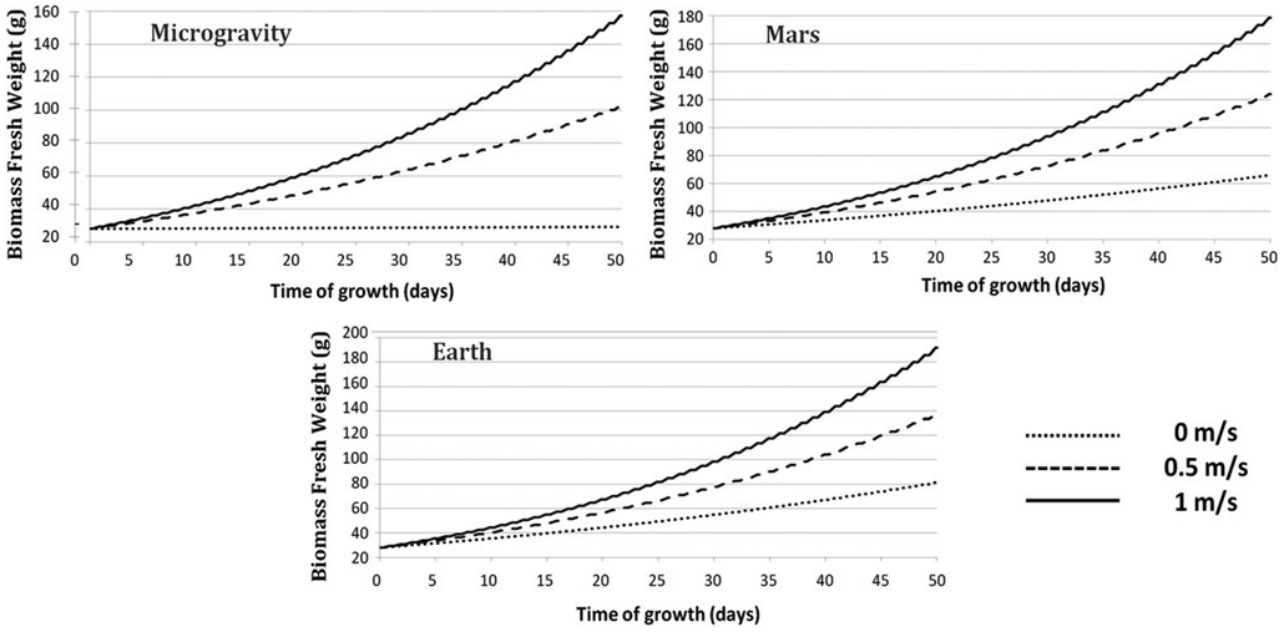

FIG. 5. Biomass fresh weight accumulation over time in microgravity (top left), in martian gravity (top right), and in Earth's gravity (bottom) for three different forced convection velocities: 0 $m \cdot s^{-1}$ (dotted line); 0.5 $m \cdot s^{-1}$ (dashed line); and 1 $m \cdot s^{-1}$ (plain line).

This threshold value gives the range of the mixed convection domain where free and forced convection effects are of the same order of magnitude: Ri ~ 1.

This boundary layer model is valid for a single leaf with a circular shape, exchanging gas only from the upper side of the leaf. The results for a whole plant will be slightly different since the shape of the plant is more complex, inducing aerodynamic interference between leaves such as eddy shedding and flow channeling (Schuepp, 1993), and since air velocity on the top and bottom of the plant is different. When this model is extrapolated to a whole canopy, the significant boundary layer will be that of the canopy, which is characterized with a shelter factor (Schuepp, 1993) and is more complex than a simple addition of the boundary layers of each individual plant.

4.2. Gas exchanges and biomass production

As noticed in the case of the boundary layer thickness, the gas exchange rates are more sensitive to the influence of gravity for lower forced convection velocities, and there is a threshold value under which water transpiration and CO_2 uptake depend on gravity levels and above which they depend on the forced convection velocity value. It would be interesting to simulate gas exchanges for a whole plant and then for a whole canopy to investigate if this threshold value holds at a larger scale. If it does, it means that in future greenhouse modules for food production, it will be crucial to ensure an adequate ventilation level around each plant to ensure optimum gas exchanges everywhere.

The results on biomass production underline the fact that it will be different on other celestial bodies, during planetary travels, and in the Earth's orbit than on Earth's surface; it also shows that adjusting the ventilation to an adequate level can lead to biomass production levels similar to those achieved in Earth gravity conditions. It is thus necessary to study the intricate relationship between forced convection, gravity levels, and biomass production to predict how much food can be produced during long-duration space missions.

Conclusion

This study highlights the importance of understanding interactions of gravity and convection on the leaf boundary layer to reliably predict biomass production, water recycling, and air revitalization in space conditions. The next step will include an energy balance and focus on variations of leaf temperature with gravity and convection. These results will be validated by experimental data with a parabolic flight experiment and ultimately it will lead to a thorough and accurate mechanistic model of plant growth in reduced gravity environments, including mass and energy balances.

Acknowledgments

The authors thank the Centre National d'Etudes Spatiales (CNES) and the Centre National de la Recherche Scientifique (CNRS) for financially supporting this work, the Institut Pascal for providing their facilities, and the ESA MELiSSA project for the support, as well as Dr. Jérôme Ngao and Dr. Marc Saudreau from the Institut National de Recherche Agronomique (INRA) for their fruitful discussions.

Author Disclosure Statement

No competing financial interests exist.

References

Anderson, M.S., Ewert, M.K., Keener, J.F., and Wagner, S.A. (2015) *Life Support Baseline Values and Assumptions Document*, NASA/TP-2015–218570. NASA Johnson Space Center, Houston, TX.

Beek, W.J., Muttzall, K.M.K., and van Heuven, J.W. (1999) *Transport Phenomena*, 2nd ed. Wiley, Chichester and New York.

Boulard, T., Mermier, M., Fargues, J., Smits, N., Rougier, M., and Roy, J.C. (2002) Tomato leaf boundary layer climate: implications for microbiological whitefly control in greenhouses. *Agric For Meteorol* 110:159–176.

Clauwaert, P., Ilgrande, C., Christiaens, M., Lindeboom, R., Luther, A., Muys, M., Alloul, A., Dussap, C.-G., Godia, F., Sas, B., Boon, N., Rabaey, K., Leys, N., Geelen, D., and Vlaeminck, S. (2015) The nitrogen cycle in life support systems. In: *COSPAR, 2nd Symposium, Abstracts*. Presented at the 2nd COSPAR symposium: Water and life in the universe.

Dong, C., Fu, Y., Xie, B., Wang, M., and Liu, H. (2017) Element cycling and energy flux responses in ecosystem simulations conducted at the Chinese Lunar Palace-1. *Astrobiology* 17:78–86.

Drayer, G.E. and Howard, A.M. (2014) Modeling and simulation of an aquatic habitat for bioregenerative life support research. *Acta Astronaut* 93:138–147.

Eckart, P. (1996) *Spaceflight Life Support and Biospherics*. Microcosm Press, Netherlands.

Ehleringer, J. and Björkman, O. (1977) Quantum yields for CO_2 uptake in C3 and C4 plants: dependence on temperature, CO_2, and O_2 concentration. *Plant Physiol* 59:86–90.

Ewert, M.K., Drysdale, A.E., Levri, J.A., Duffield, B.E., Hanford, A.J., Lange, K.E., and Stafford, K.W. (2002) *Advanced Life Support Requirements, Assumptions and Reference Missions* (SAE Technical Paper No. 2002-01-2480). SAE Technical Paper, Warrendale, PA.

Fu, Y., Li, L., Xie, B., Dong, C., Wang, M., Jia, B., Shao, L., Dong, Y., Deng, S., Liu, Hui, Liu, G., Liu, B., Hu, D., and Liu, Hong. (2016) How to establish a bioregenerative life support system for long-term crewed missions to the Moon or Mars. *Astrobiology* 16:925–936.

Furfaro, R., Sadler, P., and Giacomelli, G. (2016) Mars-lunar greenhouse (M-LGH) prototype for bioregenerative life support systems in future planetary outposts. In *Proceedings of the International Astronautical Congress, IAC*.

Hendrickx, L., De Wever, H., Hermans, V., Mastroleo, F., Morin, N., Wilmotte, A., Janssen, P., and Mergeay, M. (2006) Microbial ecology of the closed artificial ecosystem MELiSSA (Micro-Ecological Life Support System Alternative): reinventing and compartmentalizing the Earth's food and oxygen regeneration system for long-haul space exploration missions. *Res Microbiol* 157:77–86.

Hézard, P. (2012) Higher Plant Growth Modelling for Life Support Systems: Global Model Design and Simulation of Mass and Energy Transfers at the Plant Level. PhD thesis, Doctoral School of Life Sciences, Health, Agronomy, Environment. Université Blaise Pascal, Université d'Auvergne, Clermont-Ferrand.

Hézard, P., Sasidharan, S., Cruely, C., and Dussap, C.-G. (2010) Higher plants modeling for bioregenerative life support ap-

plications: general structure of modeling. In *40th International Conference on Environmental Systems (ICES)*. American Institute of Aeronautics and Astronautics.
Hirai, H. and Kitaya, Y. (2009) Effects of gravity on transpiration of plant leaves. *Ann N Y Acad Sci* 1161:166–172.
Holmberg, M., Paille, C., and Lasseur, C. (2013) Preliminary modelling of mass flux at the surface of plant leaves within the MELiSSA higher plant compartments. Master's thesis, Uppsala University, ESA.
Jones, H.G. and Rotenberg, E. (2001) Energy, radiation and temperature regulation in plants. *eLS*. doi:10.1002/9780470015902.a0003199.pub2.
Kitaya, Y. (2016) Air current around single leaves and plant canopies and its effect on transpiration, photosynthesis, and plant organ temperatures. In *LED Lighting for Urban Agriculture*, edited by T. Kozai, K. Fujiwara, and E.S. Runkle, Springer, Singapore, pp 177–187.
Kitaya, Y., Tsuruyama, J., Kawai, M., Shibuya, T., and Kiyota, M. (2000) Effects of air current on transpiration and net photosynthetic rates of plants in a closed plant production system. In *Transplant Production in the 21st Century*, edited by C. Kubota and C. Chun, Springer, Netherlands, pp 83–90.
Kitaya, Y., Kawai, M., Tsuruyama, J., Takahashi, H., Tani, A., Goto, E., Saito, T., and Kiyota, M. (2001) The effect of gravity on surface temperature and net photosynthetic rate of plant leaves. *Adv Space Res* 28:659–664.
Kitaya, Y., Kawai, M., Tsuruyama, J., Takahashi, H., Tani, A., Goto, E., Saito, T., and Kiyota, M. (2003a) The effect of gravity on surface temperatures of plant leaves. *Plant Cell Environ* 26:497–503.
Kitaya, Y., Tsuruyama, J., Shibuya, T., Yoshida, M., and Kiyota, M. (2003b) Effects of air current speed on gas exchange in plant leaves and plant canopies. *Adv Space Res* 31:177–182.
Kitaya, Y., Shibuya, T., Yoshida, M., and Kiyota, M. (2004) Effects of air velocity on photosynthesis of plant canopies under elevated CO_2 levels in a plant culture system. *Adv Space Res* 34:1466–1469.
Lambers, H., Chapin, F.S., and Pons, T.L. (2008) *Plant Physiological Ecology*, 2nd ed. Springer, New York.
Lasseur, C., Brunet, J., de Weever, H., Dixon, M., Dussap, G., Godia, F., Leys, N., Mergeay, M., and Van Der Straeten, D. (2011) MELiSSA: the European project of closed life support system. *Grav Space Res* 23:3–12.
Mitchell, C.A. (1994) Bioregenerative life-support systems. *Am J Clin Nutr* 60:820S–824S.
Monje, O., Bingham, G.E., Carman, J.G., Campbell, W.F., Salisbury, F.B., Eames, B.K., Sytchev, V., Levinskikh, M.A., and Podolsky, I. (2000) Canopy photosynthesis and transpiration in micro-gravity: gas exchange measurements aboard Mir. *Adv Space Res* 26:303–306.
Monje, O., Stutte, G., and Chapman, D. (2005) Microgravity does not alter plant stand gas exchange of wheat at moderate light levels and saturating CO_2 concentration. *Planta* 222: 336–345.
Muchow, R.C. and Sinclair, T.R. (1989) Epidermal conductance, stomatal density and stomatal size among genotypes of *Sorghum bicolor* (L.) Moench. *Plant Cell Environ* 12:425–431.
Poulet, L., Fontaine, J.-P., and Dussap, C.-G. (2016) Plant's response to space environment: a comprehensive review including mechanistic modelling for future space gardeners. *Bot Lett* 163:337–347.
Poulet, L., Dussap, C.-G., and Fontaine, J.-P. (2017) Modelling higher plants gas exchange in reduced gravity environment. Presented at the 47th International Conference on Environmental Systems (ICES). July 16–20, 2017. Charleston, SC.
Raschke, K. (1960) Heat transfer between the plant and the environment. *Annu Rev Plant Physiol* 11:111–126.
Schuepp, P.H. (1993) Tansley review no. 59 leaf boundary layers. *New Phytol* 125:477–507.
Schymanski, S.J., Or, D., and Zwieniecki, M. (2013) Stomatal control and leaf thermal and hydraulic capacitances under rapid environmental fluctuations. *PLoS One* 8:e54231.
Siegel, R. and Howell, J.R. (1992) *Thermal Radiation and Heat Transfer*, 3rd ed. Hemisphere, New York, 1992.
Vesala, T. (1998) On the concept of leaf boundary layer resistance for forced convection. *J Theor Biol* 194:91–100.
Wheeler, R.M. (2003) Carbon balance in bioregenerative life support systems: some effects of system closure, waste management, and crop harvest index. *Adv Space Res* 31:169–175.
Wheeler, R.M. (2004) Horticulture for Mars. *Acta Hortic* 642: 201–215.
Wheeler, R.M. (2011) Plants for human life support in space: from Myers to Mars. *Grav Space Res* 23:25–35.
Wheeler, R.M. (2017) Agriculture for space: people and places paving the way. *Open Agriculture* 2:14–32.

Address correspondence to:
Lucie Poulet
Université Clermont Auvergne
Institut Pascal UMR 6602
BP 10448, F-63000
Clermont-Ferrand, France

E-mail: lucie.poulet@uca.fr

Submitted 7 December 2017
Accepted 28 January 2018

Abbreviations Used

ESA = European Space Agency
LSS = life-support system
MELiSSA = Micro-Ecological Life-Support System Alternative

2.4 Detailed energy model

Section 2.3 (Astrobiology paper) gives an overview of the energy balance of a leaf at steady state:

$$E_{photons} - E_{ray} - E_{conv} - E_{transpi} = 0 \tag{2.1}$$

$E_{photons}$ is the radiant energy coming from the incident light, E_{ray} is the long wave radiant energy associated to energy radiated by the leaf (black body), which was named E_LW in the Astrobiology article, E_{conv} the heat exchanged through convection, and $E_{transpi}$ the heat exchanged through transpiration of the leaf. In this section, each term of the previous steady state energy balance equation is detailed, discussed, and computed with the parameters detailed in section 2.3. The steady state is discussed and the link with the mass balance is established, which requires a time-dependent equation on the leaf temperature.

2.4.1 Energy coming from incident light: photons energy

The energy of one photon of wavelength λ is given by the Planck-Einstein relationship:

$$E_{singlephoton} = \frac{h\,c}{\lambda} \tag{2.2}$$

h is the Planck constant and c the speed of light. As detailed in the MELiSSA plant growth model, the incident light is modeled as a first approximation with the equation:

$$I = I_0\,(1 - e^{-k\,LAI}) \tag{2.3}$$

The previous equation is derived from the Beer-Lambert law and depends on the dimensionless light extinction coefficient k, the incident light flux I_0 in µmol/m^2/s, and the leaf area index LAI. This law is valid for monochromatic light, normal to the surface, and a purely absorbing surface (with no diffusion of light), like it is the case for plant leaves.

The number of photons contained in this incident light per surface area and unit if time is equal to $I\,N_A$ with N_A the Avogadro number. So, the heat flux of photons contained

in the incident light for a given wavelength is:

$$\phi_{photons} = I\, N_A\, \frac{hc}{\lambda} = I_0\,(1 - e^{-k\,LAI})\, LA\, N_A \frac{hc}{\lambda} \tag{2.4}$$

Since the incident light is composed of many different wavelengths (n for example), it can also be written:

$$I = \sum_{i=1}^{n} \alpha_i\, I_i \tag{2.5}$$

α_i is the fraction of the wavelength λ_i and I_i is the corresponding intensity.
Consequently, the heat flux of this incident light (W.m^{-2}) is:

$$\phi_{photons} = I_0\,(1 - e^{-k\,LAI})\, N_A\, h\, c \sum_{i=1}^{n} \frac{\alpha_i}{\lambda_i} \tag{2.6}$$

And the corresponding heat per time unit (W) is:

$$E_{photons} = I_0\,(1 - e^{-k\,LAI})\, N_A\, h\, c \sum_{i=1}^{n} \frac{\alpha_i}{\lambda_i}\, LA \tag{2.7}$$

LA is the leaf area.
Using the parameters of part 2.3 (Astrobiology paper), a leaf area of 0.1 m^2, and the following light composition (n=3): 85% of 650 nm (red), 10% of 470 nm (blue), 5% of 530 nm (green) (Kim et al., 2004; Poulet et al., 2014), with N_A = 6.02 10^{23} mol^{-1}, h = 6.63 10^{-34} J.s, and c = 3 10^8 m.s^{-1}, the heat from incident light per unit of time is:

$$\phi_{photons} = 61.4 \text{ W.m}^{-2} \text{ and } E_{photons} = 6.14 \text{ W}.$$

2.4.2 Radiation energy

The total radiated energy is the sum of the energy received from the radiating environment and the energy emitted by the leaf. As detailed in section 2.3, the Stefan-Boltzmann equation gives the following relationship for the heat flux of long waves (W.m^{-2}):

$$\Phi_{ray} = \sigma\,(\varepsilon_{leaf}\, T_{leaf}^4 - \varepsilon_b\, T_b^4) \tag{2.8}$$

ε_{leaf} and ε_b are the emissivity of the leaf and of the environment respectively and since the vegetation emissivity varies from 0.95 to 0.99 (Jones and Rotenberg 2001, Chen 2015)

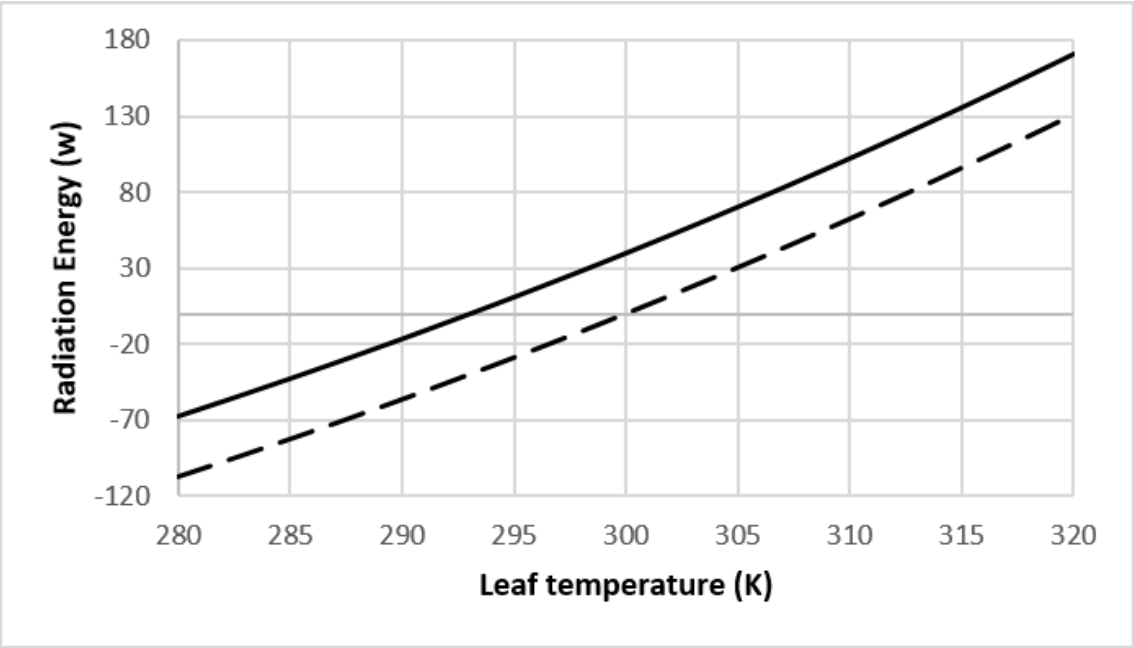

Figure 2.1: Total radiated heat flux for Tb = 300 K (dashes) and Tb = 293 K (line)

and the surrounding environment is a plants' canopy, we have: $\varepsilon_{leaf} = \varepsilon_b = \varepsilon = 0.97$. $\sigma = 5.67.10^{-8}$ W.m^{-2}.K^{-4} is the Stefan Boltzmann constant. Thus:

$$\Phi_{ray} = \varepsilon\, \sigma (T_{leaf}^4 - T_b^4) \tag{2.9}$$

The corresponding heat per time unit (W) is:

$$E_{ray} = \Phi_{ray}\, LA \tag{2.10}$$

Using two different bulk temperatures T_b equal to 293 K and 300 K, the total radiated energy can be plotted for a leaf surface temperature varying from 280 to 320 K (Figure 2.1). The total radiated energy is higher for lower external air temperatures.

2.4.3 Convection energy

As detailed in section 2.3, the convective heat flux between the leaf surface and the bulk (W.m^{-2}) can be represented by a heat transfer resistance:

$$\phi_{conv} = \frac{k_t}{\delta_X} (T_{leaf} - T_b) \tag{2.11}$$

k_t is the heat conduction coefficient and δ_X is the boundary layer thickness defined in

section 2 and 3 and then called δ_{mass}. The main assumption of this model involves a unique boundary layer thickness δ_X that characterizes the boundary layer thickness for mass and heat transfer. In itself, δ_X expression is derived from momentum transfer balance in the boundary layer, accounting for the gravity influence. Using the current assumptions formulated in sections 2.3 and 2.2, δ_X is defined as follows. These assumptions are detailed and discussed in section 2.5:

$$\delta_X = 4.64 \sqrt{\frac{L\,\nu}{\sqrt{g\,\beta\,H\,(T_b - T_{leaf})} + v_{forced}}} \tag{2.12}$$

g is the acceleration of gravity, β is the thermal expansion coefficient, H is the characteristic length of the plant chamber, T_b is the temperature of the air in the growth chamber, T_{leaf} is the leaf surface temperature, and v_{forced} is the forced convection velocity.

The corresponding heat per time unit (W), where the leaf is supposed to be isothermal, is:

$$E_{conv} = \phi_{conv}\,LA. \tag{2.13}$$

Using a bulk temperature of 300 K, the convection heat flux is plotted for a surface temperature varying from 280 to 320 K, a forced convection velocity of 0 m/s, 0.5 m/s, and 1 m/s, and for 5 different gravity values: 2g, 1g, 0.38g (Mars), 0.16g (Moon), and 0g (Figure 2.2, Figure 2.3, Figure 2.4). When $T_{leaf} < T_b$ (resp. $T_{leaf} > T_b$), the leaf receives (resp. gives) convection heat from the surroundings, so the term "$-E_{conv}$" in the energy equation is positive (resp. negative), and the heat flux associated with the heat exchanges through convection, ϕ_{conv}, is negative (resp. positive). Hence on the graphs below, we observe an inflexion point at $T_{leaf} = T_b = 300$ K. However, this inflexion in the curve decreases with the increase of the forced convection velocity and at 1 m/s, the convection heat flux is almost a straight line, increasing quasi linearly with the leaf surface temperature for all values of g (Figure 2.4). This demonstrates the lower impact of g on heat exchange at high forced convection velocities. On the contrary, at 0 m/s, the impact of gravity on heat exchange is very significant and the convection heat flux varies between -1.22 W and 1.22 W at 0g (Figure 2.2). For lower values of the forced convection velocity, unsurprisingly, the convection heat flux values are lower than for higher values of the forced convection velocity. Convection heat flux for given values of g is also higher at higher forced convection velocities.

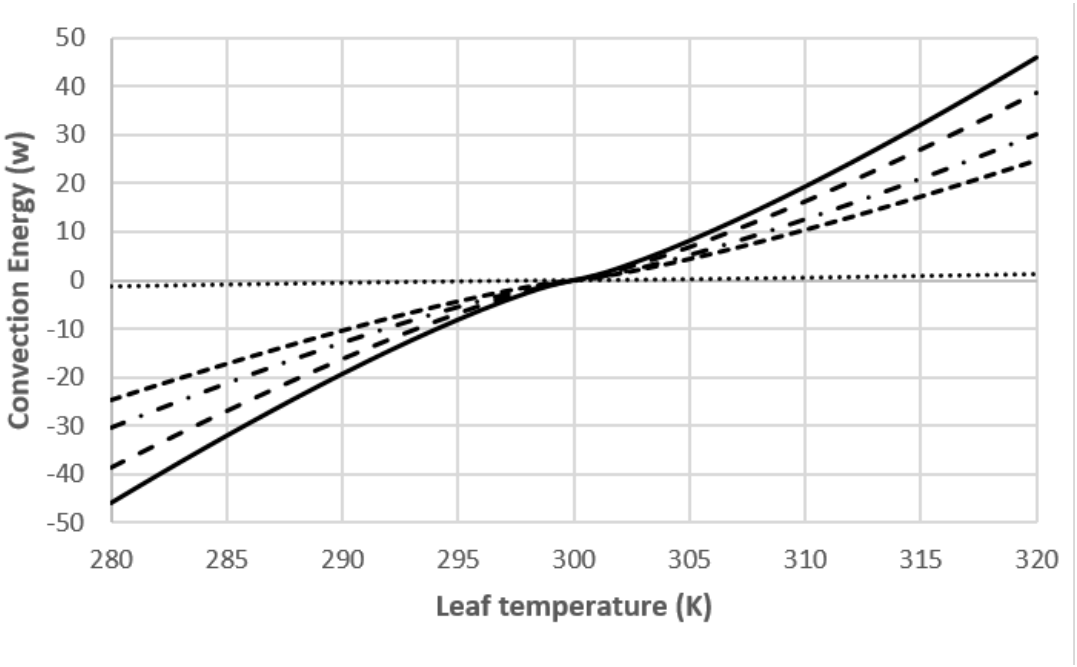

Figure 2.2: Convection heat flux with no forced convection at 2g (straight line), 1g (long dashes), 0.38g (dashes and dots), 0.16g (small dashes), and 0g (dots).

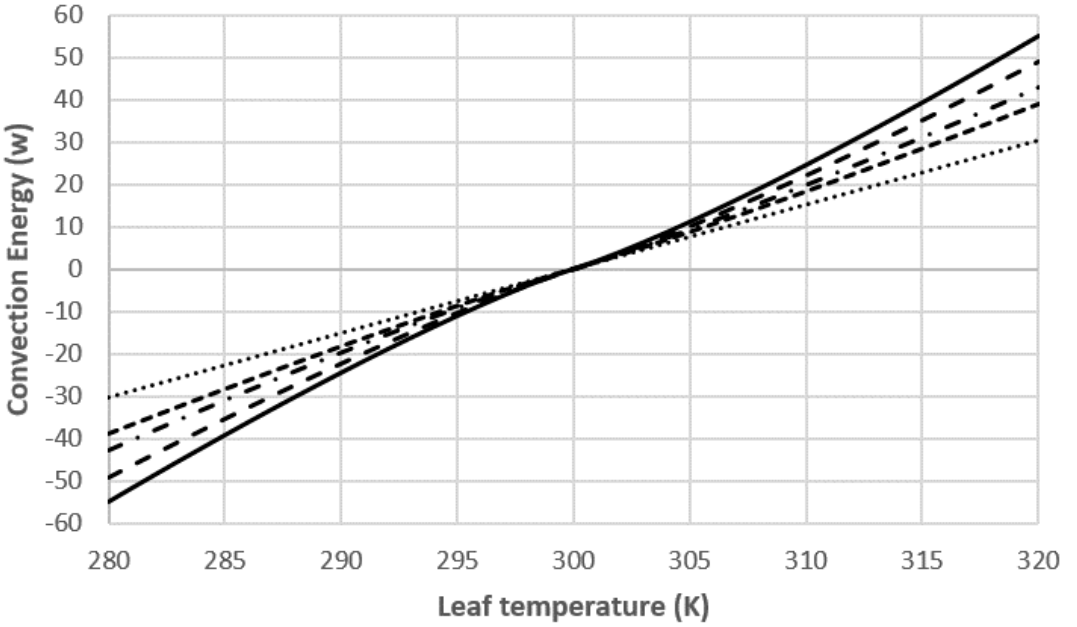

Figure 2.3: Convection heat flux with a forced convection velocity of 0.5 m/s at 2g (straight line), 1g (long dashes), 0.38g (dashes and dots), 0.16g (small dashes), and 0g (dots).

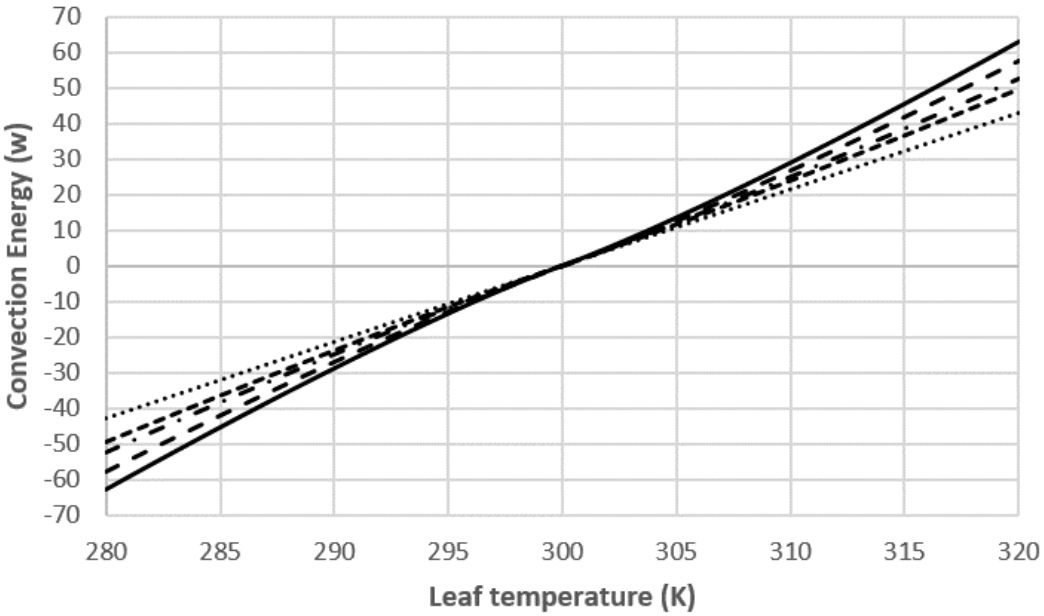

Figure 2.4: Convection heat flux with a forced convection velocity of 1 m/s at 2g (straight line), 1g (long dashes), 0.38g (dashes and dots), 0.16g (small dashes), and 0g (dots).

2.4.4 Transpiration energy

Leaf transpiration involves liquid water evaporation at the leaf surface and thus an energy consumption (W.m^{-2}), corresponding to the heat flux associated to the leaf transpiration, as defined in section 2.3:

$$\phi_{transpi} = \lambda_{mol}\, \varphi_{H_2O} \tag{2.14}$$

λ_{mol} is the latent heat of vaporization. φ_{H_2O} (mol.m^{-2}s^{-1}) is the water flux exchanged between the leaf and the surrounding air:

$$\varphi_{H_2O} = \frac{D_w\, d_s\, a_s}{\delta_X\, d_s\, a_s + l_s} \frac{P^0(T_{leaf}) - P^0(T_b)}{R\, T_b} \tag{2.15}$$

D_w is the diffusion coefficient for water vapor, d_s is the stomatal density on a leaf, a_s is the average cross-sectional area of a stomata, l_s the average depth of a stomatal pore, R the gas constant, and $P^0(T)$ the vapor pressure of water at T. Again, δ_X is the characteristic boundary layer thickness accounting for mass transfer resistance to the diffusion of water vapor form the leaf surface to the gas bulk.

The corresponding heat per time unit (W) is:

$$E_{transpi} = \phi_{transpi}\, LA = \lambda_{mol}\, \varphi_{H_2O}\, LA \tag{2.16}$$

The transpiration flux is driven by water vapor partial pressures gradient between the leaf surface and the surroundings, as detailed in section 2.2 (ICES paper). Partial pressures are computed using the Antoine equation, which is derived from the Clausius-Clapeyron relation and gives a semi-empirical relationship between temperature and vapor pressure of pure components:

$$log_{10}(P^0(T)) = A - \frac{B}{T + C} \tag{2.17}$$

with $P^0(T)$ in bar and T in Kelvin (National Institute of Standards and Technology, 2017). The values of the coefficients A, B, and C are (Bridgeman and Aldrich, 1964; National Institute of Standards and Technology, 2017): A = 5.4, B = 1838.675, C = -31.737. Hence the partial pressures (bar) here are computed with:

$$P^0(T) = 10^{5.4 - \frac{1838.675}{T - 31.737}} \tag{2.18}$$

In the transpiration rate equation, the partial pressures are in Pascal, so:

$$P^0(T) = 10^5\, 10^{5.4 - \frac{1838.675}{T - 31.737}} \tag{2.19}$$

Using a bulk temperature of 300 K, the transpiration heat flux is plotted for a surface temperature varying from 280 to 320 K, a convection velocity of 0 m/s, 0.5 m/s, and 1 m/s, and for 5 different gravity values: 2g, 1g, 0.38g (Mars), 0.16g (Moon), and 0g (Figure 2.5, Figure 2.6, Figure 2.7). Although $T_{leaf} > 303$ K in some of the calculations, the coefficients A, B, and C in the Antoine equation were kept constant as detailed above in the equation giving the partial pressure computation.

As for the convection heat flux, but less marked, there is an inflexion point at $T_{leaf} = T_b$ = 300 K, which tends to disappear for higher values of the forced convection velocity (compare Figure 2.5 and Figure 2.7). Again, this shows the lower impact of g on heat exchange at high forced convection velocities, which remains significant 0 m/s, since the transpiration heat flux is very low and varies between -2.5 W and 6.8 W at 0g (Figure 5). At higher forced convection velocities, the values of the transpiration heat flux are also

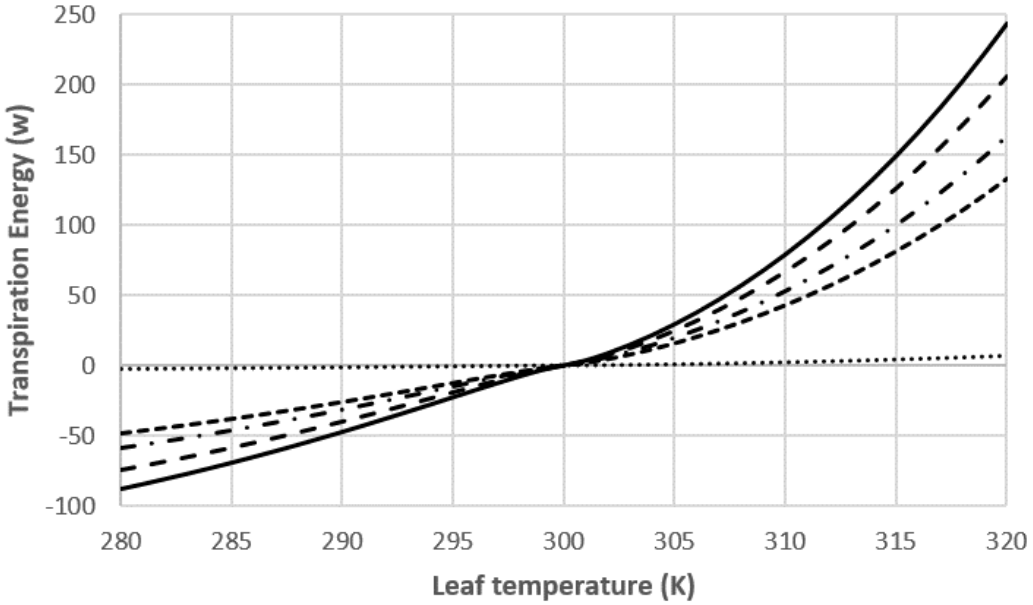

Figure 2.5: Transpiration heat flux with no forced convection at 2g (straight line), 1g (long dashes), 0.38g (dashes and dots), 0.16g (small dashes), and 0g (dots).

higher (about 100 W higher at 1m/s than at 0m/s in 1g and more than 200 W higher in 0g, when the T_{leaf} is the highest). It is to be noted that transpiration heat flux values for $T_{leaf} > T_b$ are more spread than for $T_{leaf} < T_b$ and also much higher in intensity.

2.4.5 Energy balance at steady state

From the previous sections, the energy balance at steady state is written in the following way:

$$\begin{aligned} &E_{photons} - E_{ray} - E_{conv} - E_{transpi} \\ &= I^{max}\, N_A\, h\, c \sum_{i=300}^{700} \frac{\alpha_i}{\lambda_i} - \varepsilon\, \sigma\, (T_{leaf}^4 - T_b^4)\, LA - \frac{k_t}{\delta_X}\, (T_{leaf} - T_b)\, LA - \lambda_{mol}\, \varphi_{H_2O} \end{aligned} \quad (2.20)$$

With the thickness of the boundary layer is:

$$\delta_X = 4.64 \sqrt{\frac{L\,\nu}{\sqrt{g\,\beta\,H\,(T_b - T_{leaf})} + v_{forced}}}$$

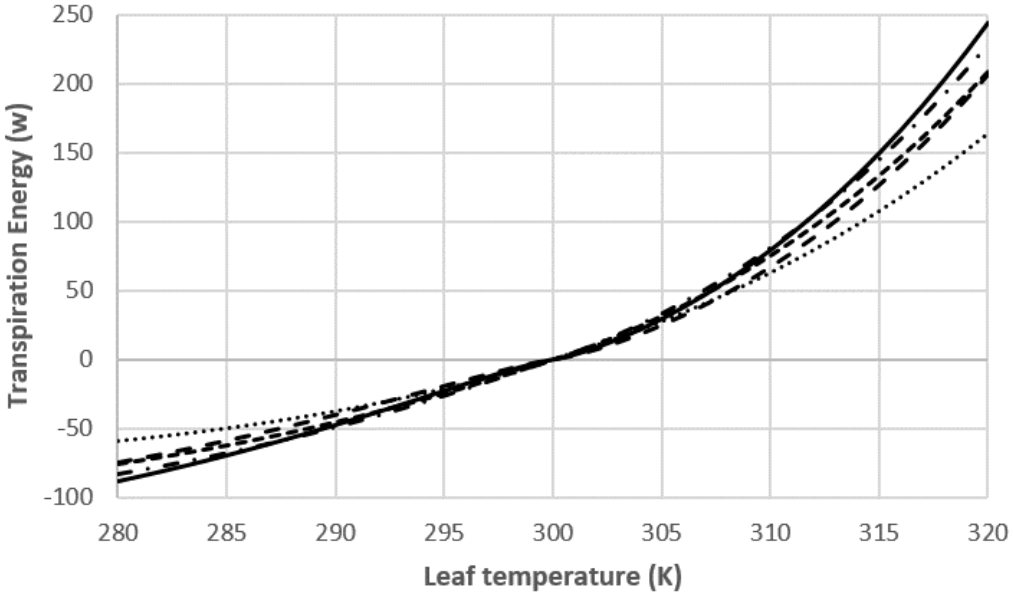

Figure 2.6: Transpiration heat flux with a forced convection velocity of 0.5 m/s at 2g (straight line), 1g (long dashes), 0.38g (dashes and dots), 0.16g (small dashes), and 0g (dots).

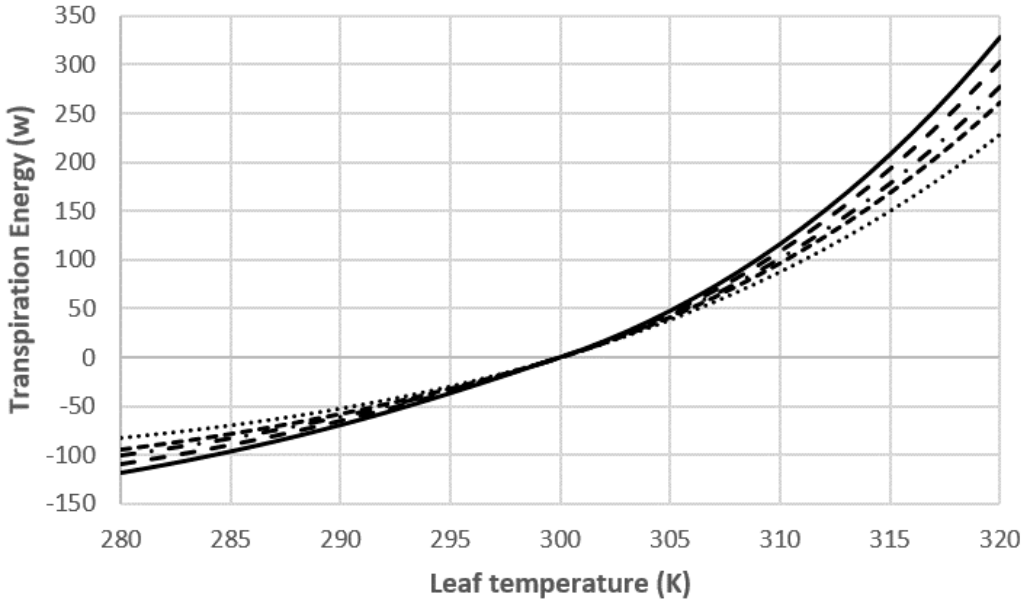

Figure 2.7: Transpiration heat flux with a forced convection velocity of 1 m/s at 2g (straight line), 1g (long dashes), 0.38g (dashes and dots), 0.16g (small dashes), and 0g (dots).

And the transpiration flux is:

$$\varphi_{H_2O} = \frac{D_w\, d_s\, a_s}{\delta_X\, d_s\, a_s + l_s} \frac{P^0(T_{leaf}) - P^0(T_b)}{R\, T_b}$$

With the parameters detailed previously, a numerical solution is found for T_{leaf} for different values of g and V_{forced}, for T_b=300 K (Table 2.1) and T_b = 293 K (Table 2.2). The results presented hereafter are more detailed than those presented in the papers (sections 2.2 and 2.3) and can be considered as supplementary data.

	2g	**1g**	**0.38g**	**0.16g**	**0g**	
V_{forced} = 0 m/s	302.86	303.32	303.98	304.54	309.33	
V_{forced} = 0.5 m/s	301.74	301.92	302.13	302.27	302.60	T_{leaf} (K)
V_{forced} = 1 m/s	301.06	301.15	301.25	301.31	301.44	
$\lvert T_{leaf}$(0.5 m/s)-T_{leaf}(0 m/s)$\rvert$	1.12	1.40	1.84	2.27	6.72	
$\lvert T_{leaf}$(0.5 m/s)-T_{leaf}(1 m/s)$\rvert$	0.68	0.77	0.88	0.96	1.16	ΔT_{leaf} (K)
$\lvert T_{leaf}$(0 m/s)-T_{leaf}(1 m/s)$\rvert$	1.79	2.16	2.73	3.23	7.89	

Table 2.1: Values of T_{leaf} for different values of forced convection and gravity when T_b = 300 K.

	2g	**1g**	**0.38g**	**0.16g**	**0g**	
V_{forced} = 0 m/s	298.28	298.67	299.21	299.66	303.18	
V_{forced} = 0.5 m/s	297.58	297.77	297.99	298.14	298.50	T_{leaf} (K)
V_{forced} = 1 m/s	297.14	297.26	297.39	297.47	297.64	
$\lvert T_{leaf}$(0.5 m/s)-T_{leaf}(0 m/s)$\rvert$	0.70	0.90	1.21	1.52	4.68	
$\lvert T_{leaf}$(0.5 m/s)-T_{leaf}(1 m/s)$\rvert$	0.44	0.51	0.61	0.67	0.85	ΔT_{leaf} (K)
$\lvert T_{leaf}$(0 m/s)-T_{leaf}(1 m/s)$\rvert$	1.14	1.41	1.82	2.19	5.53	

Table 2.2: Values of T_{leaf} for different values of forced convection and gravity when T_b = 293 K.

For a given T_b and gravity levels of 1g and 2g, the gradient between T_{leaf} at 0 m/s and T_{leaf} at 0.5 m/s is 1.6 to 1.8 times greater than between T_{leaf} at 0.5 m/s and T_{leaf} at 1 m/s (Table 1 and 2). It is more than twice as large for gravity levels 0.38g and lower. This again demonstrates the higher dependence to the forced convection velocities of the leaf surface temperature, for low forced convection values.

It is also to be noted that for $T_b = 293$ K, the leaf surface temperature at 0g and 1 m/s (resp. 0.5 m/s) is slightly above to the one at 1g and 0.5 m/s (resp. 0 m/s). This shows that it would be possible in weightlessness to have convection regimes with similar effects on leaf temperature as those on Earth and that it is possible to predict and anticipate them through calculations.

	$\mathbf{V_{forced} = 0\ m/s}$	$\mathbf{V_{forced} = 1\ m/s}$	
$\lvert T_{leaf}(1g)\text{-}T_{leaf}(0g)\rvert$	6.01	0.29	ΔT_{leaf} (K)
$\lvert T_{leaf}(1g)\text{-}T_{leaf}(0.16g)\rvert$	1.22	0.16	
$\lvert T_{leaf}(1g)\text{-}T_{leaf}(0.38g)\rvert$	0.66	0.10	
$\lvert T_{leaf}(1g)\text{-}T_{leaf}(2g)\rvert$	0.46	0.09	

Table 2.3: Gradients $|\Delta T_{leaf}|$ depending on gravity levels for values of forced convection of 0 and 1 m/s when $T_b = 300$ K.

	$\mathbf{V_{forced} = 0\ m/s}$	$\mathbf{V_{forced} = 1\ m/s}$	
$\lvert T_{leaf}(1g)\text{-}T_{leaf}(0g)\rvert$	4.51	0.38	ΔT_{leaf} (K)
$\lvert T_{leaf}(1g)\text{-}T_{leaf}(0.16g)\rvert$	0.99	0.21	
$\lvert T_{leaf}(1g)\text{-}T_{leaf}(0.38g)\rvert$	0.54	0.13	
$\lvert T_{leaf}(1g)\text{-}T_{leaf}(2g)\rvert$	0.39	0.12	

Table 2.4: Gradients $|\Delta T_{leaf}|$ depending on gravity levels for values of forced convection of 0 and 1 m/s when $T_b = 293$ K.

For a given T_b and no forced convection, the gradient between T_{leaf} at 1g and T_{leaf} at 0g is 11.5 to 13 times larger than the difference between T_{leaf} at 1g and T_{leaf} at 2g (Table 3 and 4). This shows the variability in leaf temperature value for low convection regime at low gravity levels. For a forced convection velocity of 1 m/s, the gradient of T_{leaf} at different gravity levels is the lowest, compared to other values of the forced convection velocity. Thus, for higher values of forced convection, the leaf surface temperature is less dependent on the gravity levels. This is also shown on Figure 2.8.

Time-dependent energy balance and mass coupling A time-dependent representation of the energy balance of a leaf rather than a steady-state representation is necessary, since the distance to thermodynamic equilibrium is varying in a plant from one instant to the other (Raschke 1960). Indeed, the processes involved are complex and influence

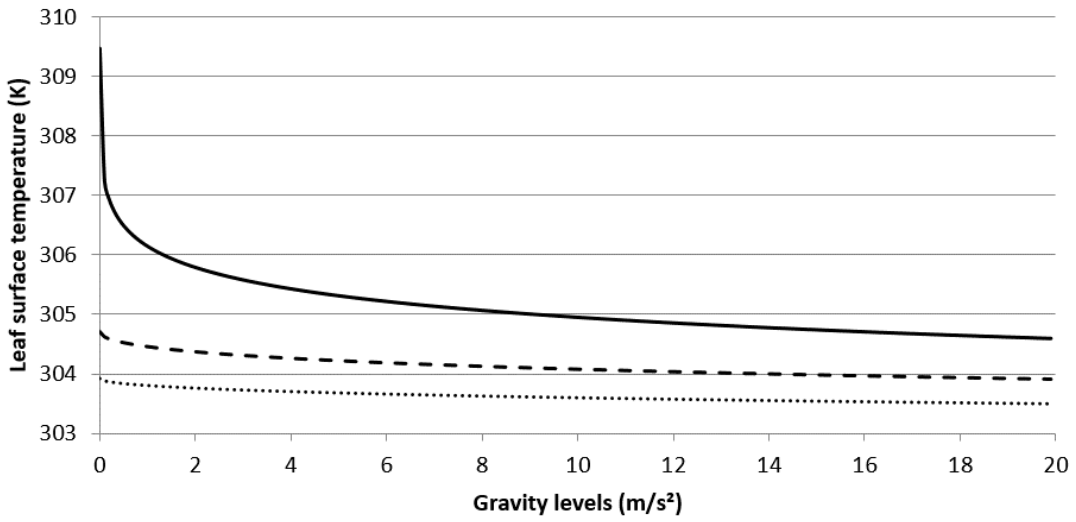

Figure 2.8: Leaf surface temperature as a function of gravity for different values of forced convection velocity: 0 m/s (line), 0.5 m/s (dashes), and 1 m/s (dots).

each other. The leaf surface temperature influences directly the heat exchanged through radiation to the outside, convection and transpiration; the transpiration rate depends on the water vapor content outside in the surrounding environment and inside the leaf; this depends on the water absorption rate in the roots but also on the leaf surface temperature which influences the saturation vapor pressure. The heat exchanged through convection is proportional to the temperature gradient between the leaf surface and the surroundings but inversely proportional to the boundary layer thickness, which depends on the leaf surface temperature. The heat radiated varies with the fourth power of the leaf surface temperature. Heat damage depends on two parameters: the critical temperature reached during steady state and the time to reach this temperature. The first one is directly linked to evaporative cooling, which prevents leaves from reaching damaging temperatures and depends on leaf water content; and the second one depends on the leaf heat capacity, which depends on the leaf water content as well (Schymanski, Or, and Zwieniecki 2013). Thus, although leaf water content does not affect steady-state leaf surface temperature, it does affect the rate of temperature increase when submitted to a sunfleck (Schymanski, Or, and Zwieniecki 2013).

Therefore Schymanski et al. (2013) propose a transient leaf energy balance, which depends on the rate of temperature change and on the leaf water content (Schymanski, Or, and

Zwieniecki 2013):

$$E_{photons} - E_{ray} - E_{conv} - E_{transpi} = Cp_{leaf}\,\frac{dT_{leaf}}{dt} \tag{2.21}$$

$Cp_{leaf} = m^{mol}_{H_2O}\,Cp^{mol}_{H_2O}$ is the leaf heat capacity (J.K^{-1}). $Cp^{mol}_{H_2O}$ is the molar liquid water heat capacity at constant pressure (J.mol^{-1}.K^{-1}) and $m^{mol}_{H_2O}$ the leaf water content (mol):

$$\frac{dm^{mol}_{H_2O}}{dt} = U_{H_2O} - \varphi_{H_2O} \tag{2.22}$$

U_{H_2O} is the water absorption rate (mol.s^{-1}) by the roots as defined in section 2 and φ_{H_2O} the transpiration rate (mol.s^{-1}).

This establishes a link between the mass balance presented in section 2.2 and the energy balance of the leaf, since the water absorption and transpiration rate are included in the energy balance. The computation of the biomass production is now linked to the energy balance, which affects the value of the leaf area and stem length, which in return will influence the CO_2 uptake rate, and transpiration rate and change the leaf surface temperature.

The global equation linking energy fluxes and mass balance in the leaf is thus:

$$I^{max}\,N_A\,h\,c\sum_{i=300}^{700}\frac{\alpha_i}{\lambda_i} - \varepsilon\,\sigma\,(T^4_{leaf} - T^4_b)\,LA - \frac{k_t}{4.64\sqrt{\frac{L\,\nu}{\sqrt{g\,\beta\,H\,(T_b - T_{leaf})} + v_{forced}}}}\,(T_{leaf} - T_b)\,LA$$

$$- \lambda_{mol}\,\frac{D_w\,d_s\,a_s}{4.64\sqrt{\frac{L\,\nu}{\sqrt{g\,\beta\,H\,(T_b - T_{leaf})} + v_{forced}}}\,d_s\,a_s + l_s}\,\frac{P^0(T_{leaf}) - P^0(T_b)}{R\,T_b}$$

$$= Cp^{mol}_{H_2O}\,\frac{dT_{leaf}}{dt}\int_{t_0}^{tf}\left[N_{vessel}\,\frac{\pi\,\rho_{mol}\,R^4_{vessel}}{8\,\mu\,L_{stem}}(\Psi_{ext} - \Psi_{int})\right.$$

$$\left. - \varphi_{H_2O} = \frac{D_w\,d_s\,a_s}{4.64\sqrt{\frac{L\,\nu}{\sqrt{g\,\beta\,H\,(T_b - T_{leaf})} + v_{forced}}}\,d_s\,a_s + l_s}\,\frac{P^0(T_{leaf}) - P^0(T_b)}{R\,T_b}\right] \tag{2.23}$$

The parameters are defined previously. Ψ_{int} and Ψ_{ext} are respectively the water potential

gradient in the roots and in the nutrient solution, R_{vessel} is the radius of the sap vessel, μ_{xylem} is the xylem sap dynamic viscosity, L_{stem} is the stem length, and N_{vessel} is the sap vessel number.

From the above, this approach structurally permits to account for gravity and forced convection crossed influences on the growth kinetics of plants. The two previous publications were written with the objective to show that a physical / physiological approach could be driven to tackle these phenomena.

However, we also clearly demonstrate in the above that a thorough understanding of coupled heat / mass / momentum transfer through the boundary layer at a solid surface (i.e. leaf surface in this case) is a clue for a complete mechanistic modeling. In turns, this calls for a more detailed definition of the physical transport mechanisms at the leaf surface. This is the objective of the following section.

2.5 Detailed model of the boundary layer

2.5.1 Assessment of the previous model

The heat and mass transfer problem geometry

The leaves of plants can be considered as horizontal or inclined plates, with a varying surface temperature but a constant heat flux between the surface and the environment (Schuepp 1993). This heat flux is linked to the transpiration of leaves, which exchanges latent energy with the surrounding environment, to the convective regime, to the photon flux received by the leaf, and to the radiation energy exchange (section 2.4). It is coupled to a mass transport due to gas exchanges during photosynthesis. Both heat transfer and mass transport cause natural convection within the boundary layer (Figure 2.9).

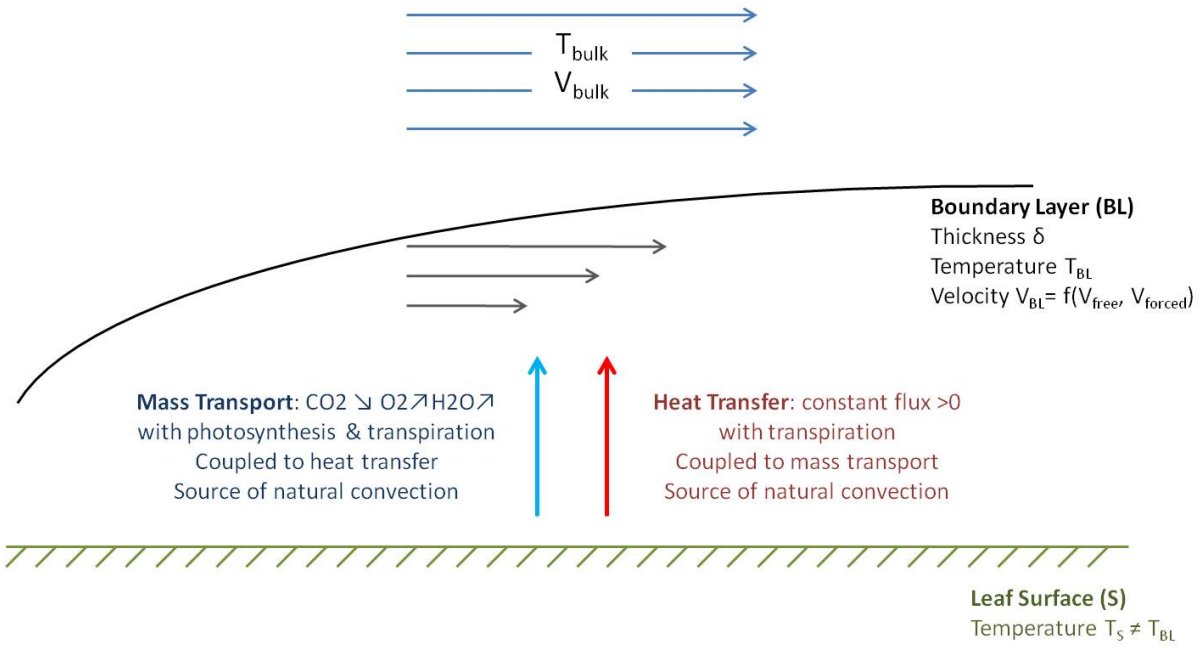

Figure 2.9: Schematic of heat and mass transfer in the boundary layer

Dimensionless numbers

The dimensionless numbers associated with mass transport and heat transfer are summarized in Table 2.5, depending on if they are associated to mass transport or heat transfer. These dimensionless numbers support a dimensionless vision of physical transports, leading to relevant comparisons between different systems in size and in nature. The characteristics of the phenomena we are investigating involve mass transfer (CO_2, O_2 and water), heat transfer and momentum transfer. The main specificity of this study is to incorporate the influence of gravity that can only be done by assessing the density gradients that generate mass flows depending on gravity.

	MASS Transport	LEWIS (Le)	**HEAT Transfer**
Viscosity vs.	SCHMIDT (Sc)		PRANDTL (Pr)
Convection vs.	**Diffusion** SHERWOOD (Sh)	**vs.**	**Conduction** NUSSELT (Nu)
Viscosity vs.	**Inertial** REYNOLDS (Re)		**Buoyancy** GRASHOF (Gr)

Table 2.5: Dimensionless numbers associated with mass transport and heat transfer

The dimensionless numbers associated with mass transport are Schmidt (Sc), Sherwood

(Sh), and Reynolds (Re):

- Schmidt number compares viscosity effects to mass transport by diffusion:

$$Sc = \frac{\nu}{D} \tag{2.24}$$

  ν is the kinematic viscosity and D the mass diffusion coefficient.

- Sherwood number compares convection effects to diffusion effects:

$$Sh = \frac{K\,L}{D} \tag{2.25}$$

  K is the mass transport coefficient, L the characteristic length, and D the mass diffusion coefficient.

- Reynolds number compares viscosity effects to inertial effects:

$$Re = \frac{V\,L}{\nu} \tag{2.26}$$

  V is the characteristic fluid velocity, L the characteristic length, and ν the kinematic viscosity.

Their heat transfer counterparts are respectively Prandtl (Pr), Nusselt (Nu), and Grashof (Gr):

- Prandlt number compares viscosity effects to heat transfer:

$$Pr = \frac{\nu}{\kappa} \tag{2.27}$$

  ν is the kinematic viscosity and κ the fluid thermal diffusivity.

- Nusselt number compares convection effects to conduction effects:

$$Nu = \frac{h\,L}{\lambda} \tag{2.28}$$

  h is the heat transfer coefficient, L the characteristic length, and λ the fluid thermal conductivity.

- Grashof number compares viscosity effects to buoyancy effects:

$$Gr = \frac{g\,\beta\,\Delta T\,L^3\,\rho^2}{\mu^2} = \frac{g\,\beta\,\Delta T\,L^3}{\nu^2} \tag{2.29}$$

  g is the gravity parameter, β the thermal expansion coefficient, v the thermal gradient, L the characteristic length, ρ the fluid density, and μ the dynamic viscosity.

The dimensionless number comparing heat and mass transfer is the Lewis number (Le):

$$Le = \frac{\kappa}{D} \tag{2.30}$$

The Rayleigh number (Ra) was introduced to compare the effects of forced and free convection within a heat transfer:

$$Ra = Gr\,Pr = \frac{g\,\beta\,\Delta T\,L^3}{\nu\,\kappa} \tag{2.31}$$

The Peclet number (Pe) compares convection and conduction times for a heat transfer and convection and diffusion times for a mass transport:

$$Pe = Re\,Pr = \frac{V\,L}{\kappa} \tag{2.32}$$

The Richardson number (Ri) expresses the ratio of the buoyancy forces over the inertial forces and gives the domain of mixed convection:

$$Ri = \frac{Gr}{Re^2} = \frac{g\,\beta\,\Delta T\,L}{V^2} \tag{2.33}$$

Hypotheses

The results published in the two papers exhibit a strong dependency on the gravity level of the transpiration rate, on the CO_2 uptake rate, and thus on the biomass production. This comes from the role played by the free convection in the model and the geometry chosen to model the leaves. In this section we discuss these modeling choices and hypotheses.
As first approximations, we have made three main hypotheses:

a. The air-flow (bulk and boundary layer) above the leaf is laminar.

Let us write U(x,y) and V(x,y) the tangential and perpendicular velocity components of

an incompressible fluid in a stationary flow above an infinite horizontal plate, which are bound by Prandtl equations (V«U and $\frac{\partial V}{\partial x} << \frac{\partial V}{\partial y}$):

$$\begin{aligned} U\,\frac{\partial U}{\partial x} + V\,\frac{\partial U}{\partial y} &= -\frac{1}{\rho}\,\frac{\partial p}{\partial x} + \nu\,\frac{\partial^2 U}{\partial y^2} \\ U\,\frac{\partial V}{\partial x} + V\,\frac{\partial V}{\partial y} &= -\frac{1}{\rho}\,\frac{\partial p}{\partial y} + \nu\,\frac{\partial^2 V}{\partial y^2} \end{aligned} \tag{2.34}$$

The following variable change enables to simplify those equations:

$$x \longrightarrow \beta(x)$$

$$y \longrightarrow y$$

We introduce the dimensionless variable: $\theta = \frac{y}{\beta(x)}$. Thus, the tangential velocity can be written:

$$u(x,y) = U_{bulk}\, f(\theta) \tag{2.35}$$

U_{bulk} is the bulk velocity. In addition, we introduce the following function:

$$F(\theta) = \int_0^\theta f(t)\,dt + F(0) \tag{2.36}$$

Thus:

$$F'(\theta) = f(\theta) = \frac{u(x,y)}{U_{bulk}} \tag{2.37}$$

The dimensionless function F is a solution of the Blasius equation:

$$F''(\theta) + \frac{1}{2}\,F'(\theta) \int_0^\theta F(t)\,dt = 0 \tag{2.38}$$

This equation is solved with the limit conditions:

- On the surface where $y = 0$ and $\theta = 0$: U = 0, so F'(0)=0 and V = 0, so F(0)=0.
- Far from the surface, were y and θ tend to infinity: $U = U_{bulk}$ so $F'(\infty) = 1$

$$\beta(x) = sqrt\frac{\nu\,x}{U_{bulk}} \tag{2.39}$$

And:

$$\theta = y\,\sqrt{\frac{\beta(x)}{\nu\,x}} \tag{2.40}$$

The numerical computation of F' as a function of θ using two methods, the Euler method and a fourth order Runge Kutta method, is given in Table 2.6.

θ	$F'(\theta)$ (Runge Kutta 4)	$F'(\theta)$ (Euler)
4.65	0.984	0.983
4.75	0.987	0.986
4.85	0.989	0.988
4.95	0.991	0.991

Table 2.6: Values of $F'(\theta)$ computed for two different numerical methods.

The boundary layer is the region of the flow where the velocity is smaller or equal to $0.99U_{bulk}$, i.e. where $F'(\theta) = 0.99$. According to Table 2.6, this is the case for $4.65 < \theta_\delta < 4.95$. And from the definition of θ:

$$\theta_\delta = \frac{\delta}{\beta(x)} \tag{2.41}$$

Thus:

$$\delta = \theta_\delta \, \beta(x) = \theta_\delta \sqrt{\frac{\nu \, x}{U_{bulk}}} \tag{2.42}$$

The pressure gradient is neglected in the boundary layer, leading to the following approximations in Prandtl equations:

- The continuity equation leads to $\frac{V}{\delta} \approx \frac{U}{L}$ with δ the boundary layer thickness, and L the characteristic length.

- Since convection and diffusion are of same order of magnitude on the top of the boundary layer ($y \approx \delta(x)$):

$$\frac{U_{bulk}^2}{L} \approx \frac{\nu \, U_{bulk}}{\delta^2} \tag{2.43}$$

  U_{bulk} is the bulk velocity, ν the air kinematic viscosity, L the characteristic length and δ the boundary layer thickness.

This leads to the definition of an average the boundary layer thickness, depending on the length of the leaf and not on the abscissa x on the leaf:

$$\delta = \theta_\delta \sqrt{\frac{\nu \, L}{U_{bulk}}} \tag{2.44}$$

In the literature, two values were found for θ_δ: 4.92 (Boulard et al. 2002; Marchio and Reboux 2008; Hézard 2012) and 4.64 (Bird, Stewart, and Lightfoot 1965; Vesala 1998; Holmberg, Paille, and Lasseur 2013). We chose $\theta_\delta = 4.64$ for our model. This is the current value of the constant coefficient used for δ_X expression. It must be kept in mind that, from one hand, the constant coefficient results from numerical simulations and approximations and, from the other hand, that this expression of δ_X is identical form characterizing heat, mass and momentum boundary layer thicknesses.

b. The air-flow velocity is the sum of the free convection velocity and of the forced convection velocity.

This assumes that free and forced convection are collinear vectors, parallel to the leaf surface, which is not the case in real configurations (see general case on Figure 2.10):

- The free convection vector is opposed to the direction of gravity, which can be perpendicular to the leaf surface or parallel, depending on the inclination of the leaf (Figure 2.10).
- The forced convection vector is more likely to be horizontal than parallel to the leaf surface. The case we considered for our previous approximations is given in case 2 on Figure 10: forced and free convection velocity vectors are parallel, which can only happen in the case of a vertical leaf with a vertical forced convection (parallel to the leaf surface).

The common representation used in the literature considers a horizontal leaf with a parallel air flow above it (Boulard et al. 2002). In the following development we will consider a horizontal forced convection, with a leaf that can be either horizontal or inclined. The remaining question that needs to be addressed is about the value of V_{bulk} used in the expression of the thickness of the boundary layer. Should it be the norm of V_{tot}, or the component of V_{tot} that is parallel to the leaf surface (V_{tot_X})? The relative effects of free and forced convection on the thickness of the boundary layer need to be more accurately characterized.

c. We assumed a mixed convection regime.

We considered that the Richardson number was in the order of magnitude of unity. This means that inertial and buoyancy forces are also of the same order of magnitude, i.e. the

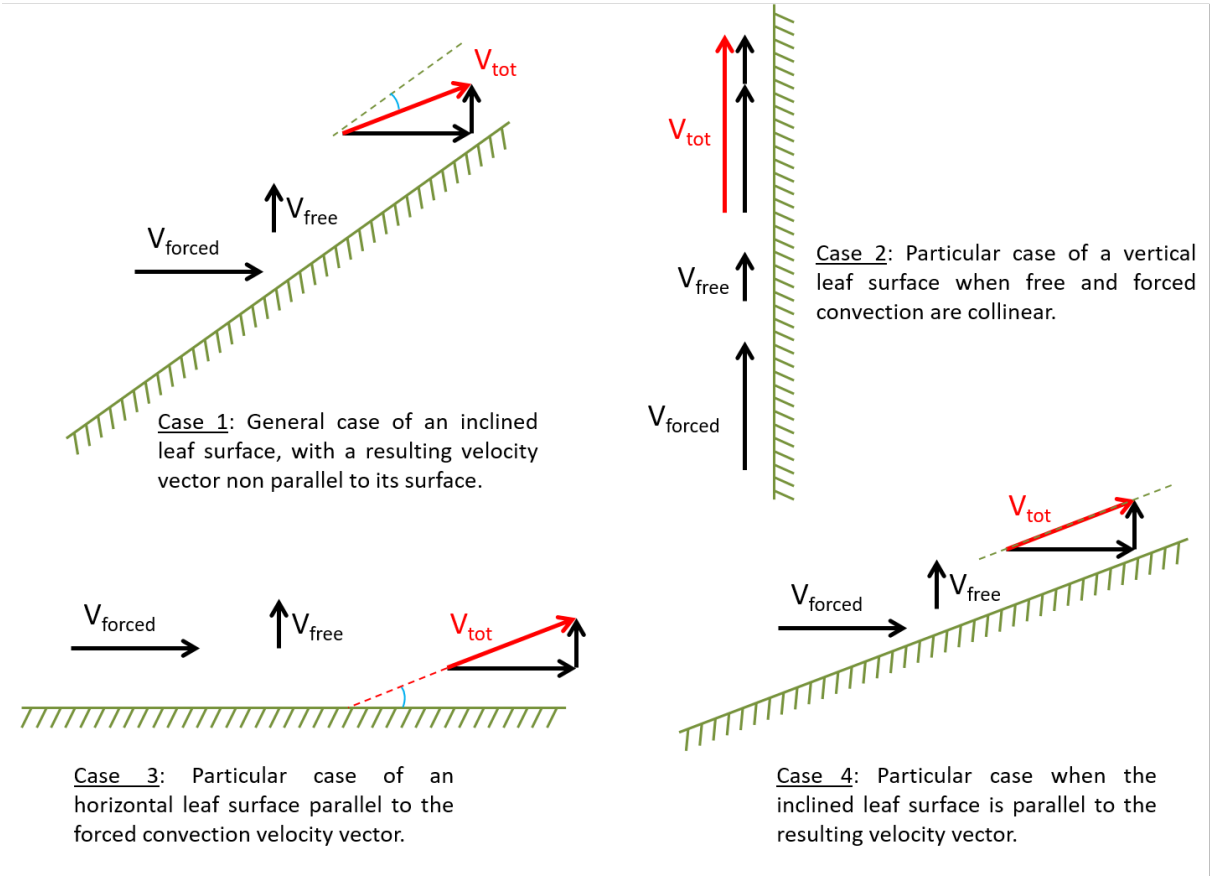

Figure 2.10: Schematic of the leaf surface with the free and forced convection vectors and the resulting vector V_{tot} for four different cases.

free and forced convection effects have comparable influences (mixed convection). This led to an expression of the free convection velocity, as a function of the gravity g, as expressed in sections 2.2 and 2.3:

$$v_{free} = \sqrt{g\,\beta\,H\,(T_b - T_{leaf})} \tag{2.45}$$

g is the gravity, β the thermal expansion coefficient, H the characteristic length of the plant chamber, T_b the temperature of the surrounding air far from the leaf, and T_{leaf} the temperature of the leaf surface. A discussion about the conditions leading to free, forced, or mixed convection regimes is provided in section 3.4.7.

2.5.2 Leaf geometry

Characteristic length and leaf inclination

As detailed previously (sections 2.2 and 2.3), the single round leaf model is used for the leaf geometry. The characteristic distance is hence:

$$L = 2\sqrt{\frac{A}{\pi}} \tag{2.46}$$

where A is the leaf area, which grows with the biomass production over time. Consequently, the characteristic length varies in time, with the biomass production. However, as seen previously, this length does not vary in space (according to the abscissa), i.e. the position on the leaf is not considered. This is in accordance to the literature where the characteristic length used to compute the mean boundary layer thickness is the weighted mean distance from the leading edge (Schuepp 1993). A commonly accepted definition for most leaf shapes is between 50% and 80% of the maximum leaf dimension in the direction of the flow (Parkhurst et al. 1968; Schuepp 1993).

With this model of characteristic length, edge effects, such as the forming and shedding of eddies at the surface of leaves, are not considered. The consequence of these effects for downwind leaves is the separation of the boundary layer from the surface (Schuepp 1993). Schuepp gives an 8 Hz frequency of eddy shedding behind a 5-cm leaf, inclined at 45° in a wind flowing at 1 m/s. According to Schuepp (1993), these effects account for less than 10% of total transfer for leaves larger than 5 mm, because of the low conductivity

of leaves.

The leaf is often modeled as a horizontal flat plate, but as seen previously, this is just a particular case. It is in fact very rare that leaves are inclined parallel to the airflow, so the effects of leaf inclination on the boundary layer transfer need to be addressed (Schuepp 1993). In particular, the effects of turbulence on a leaf highly depend on its orientation.

Single leaf

In an actual plant another effect to be considered is the mutual aerodynamic interference between leaves, which is not considered in the present model. This is characterized with a shelter factor, translating the decreased exposure to the free stream velocity of leaves within a canopy, leading to a decrease in heat and mass transfers (Landsberg and Thom 1971; Thom 1972; Schuepp 1993). However, turbulence and eddy effects induced by leaves, as well as flow channeling may counteract this shelter factor and induce specific aerodynamic regime locally (Schuepp 1993).

The roughness of the leaves also impacts the transfer; a high roughness is associated with a better transfer because it contributes to the boundary layer separation from the leaf surface (Schuepp 1993) and leads to turbulent transfer.

2.5.3 Modeling the boundary layer

The boundary layer is the region of the flow where viscous effects are of the same order of magnitude as inertial effects, conventionally defined as the region where the velocity of the air flow is less than 0.99 of the velocity of the bulk velocity, as stated previously. This is also called the cinematic or hydrodynamic boundary layer (Marchio and Reboux 2008; Marty 2012). It results from two effects: a diffusion phenomenon, perpendicular to the plate and a convection phenomenon, usually parallel to the flow (Marty 2012).

For other parameters of the air-flow, such as temperature and concentration, we define the thermal and mass boundary layers. They correspond to the region of the flow where these parameters gradually change from their surface value to their bulk value (Dussap 2016).

Thermal boundary layer

The thermal boundary is the region of the flow where the gradient between the leaf surface temperature and its temperature is less than 99% of the gradient between the leaf surface temperature and the bulk temperature (Marchio and Reboux 2008):

$$\frac{|T_{leaf} - T_{BL}|}{|T_{leaf} - T_b|} \leq 0.99 \tag{2.47}$$

T_{leaf} is the temperature of the leaf surface, T_b the temperature of the surrounding air far from the leaf, and T_{BL} the temperature in the boundary layer, which varies with the position.

Mass boundary layer

The mass boundary layer can be defined in the same way (Boulard et al. 2002):

$$\frac{|C_{leaf} - C_{BL}|}{|C_{leaf} - C_b|} \leq 0.99 \tag{2.48}$$

C_{leaf} is the concentration of a certain compound on the leaf surface, C_b the concentration in the surrounding air far from the leaf, and C_{BL} the concentration in the boundary layer.

Relationship between the different boundary layers

The mathematical relations between the different boundary layers thicknesses are linked to the dimensionless numbers previously defined (Dussap 2016):

$$\frac{\delta_{hydro}}{\delta_{thermal}} = Pr^{1/3} \tag{2.49}$$

$$\frac{\delta_{hydro}}{\delta_{mass}} = Sc^{1/3} \tag{2.50}$$

$$\frac{\delta_{mass}}{\delta_{thermal}} = Le^{1/3} \tag{2.51}$$

δ_{hydro}, δ_{mass}, $\delta_{thermal}$ are the respective thicknesses of the hydrodynamic, mass, and thermal boundary layers. The exponents 1/3 are derived from developments in statistical physics considering that in 3D, the variance of the 3D distance against the diffusion time

t is:

$$r^2 = 6\,D\,t \tag{2.52}$$

D is the diffusivity and r is the 3D distance:

$$r^2 = x^2 + y^2 + z^2 \tag{2.53}$$

The motions along the three directions x, y, and z are uncorrelated with each other. Equation 2.52 shows that for each direction the variance involves $D^{1/3}$ and since boundary layers thicknesses are defined as 1D distances to the surface, the ratios of the different boundary layer thicknesses involve the associated diffusivities at the power 1/3, leading to the previous relationships.

The Prandlt and Schmidt numbers in gases are around 0.7, which makes the thermal and mass boundary layer thicknesses be similar and equal to 89% of that of the hydrodynamic boundary layer. The Lewis number for air at 300 K is 1, consequently the thermal and mass boundary layers can be considered of equal thickness, which means that the resistances to heat and mass transfer at the leaf surface are similar, differing by less than 10% (Schuepp 1993). This justifies the previous assumptions. We have considered a unique thickness of the boundary layer for characterizing mass, heat and momentum transfer resistances

Boundary layer in preliminary MELiSSA plant growth models and their limits

Holmberg (2013) reported the following range for boundary layer thickness: from 50 µm on small leaves in strong winds to 10 mm for large leaves in still air (Holmberg, Paille, and Lasseur 2013). In the first version of MELiSSA plant growth model, the boundary layer thickness is set constant, defined from empirical values in the literature, varying from 7 mm to 12 mm, depending on the characteristic length of the leaf and bulk air speed that were considered (Boulard et al. 2002; Hézard 2012).

Kitaya et al. (2003) found a strong correlation between air flow velocity and conductance of the boundary layer in an experiment on tomato seedlings and on sweet potato leaves in a plant chamber: the larger the velocity the larger the conductance (Kitaya et al. 2003a). The conductance of the boundary layer is directly linked to its thickness: a thick boundary layer has a lower conductance (higher resistance) that decreases gas exchanges with the

surroundings. Kitaya et al. found that the net photosynthesis rate was 1.8 times higher at 0.9 m/s than at 0.01 m/s and the transpiration rate was 2.2 times higher (Kitaya et al. 2003a). Martin et al. (1999) showed that the boundary layer conductance measured in the field on a conifer increased with the wind speed: it doubled between 0 m/s and 2 m/s. These results were replicated in a wind tunnel and followed the same trend (Martin et al. 1999). The leaf structure also influences the thickness of the boundary layer: lobed leaves have smaller boundary layer thickness, since the distance from leaf edges is smaller on average (Schuepp 1993).

Considering the boundary layer thickness as a constant of the model is an acceptable hypothesis for plants growing in very specific configurations, in Earth gravity. But as mentioned previously it depends on the air velocity surrounding the leaves, as well as on the leaf shape. Since the intensity of free convection influences the air velocity around the leaves and is directly influenced by the gravity levels, it is crucial to bring gravity as a parameter in the model, used to compute the boundary layer thickness or conductance.

Turbulent boundary layer

The heat and mass transfer in the boundary layer are highly dependent on its hydrodynamic regime, laminar or turbulent. A significant part of the boundary layer becomes turbulent for high values of the bulk air velocities, but it is also affected by the shapes of leaves, their inclination, and their surface roughness (Schuepp 1993). The expression of the turbulent boundary layer thickness over a flat plate, suggested by Prandtl experimental data is following (Gunes 2010):

$$\delta = \frac{0.370}{Re_x^{1/5}}\, x \tag{2.54}$$

Re_x is the local Reynolds number at abscissa x.

Temperature profiles and vapor density on both sides of leaves have shown a dependence on free stream turbulence (Schuepp 1993). However, turbulence effects on heat and mass transfer are different depending on the side of an inclined leaf; the downwind is the wake of the flow and effective eddies are of the size of the leaf whereas on the upwind side effective eddies for transfer are small compared to the size of the leaf (Schuepp 1993).

Several factors are known to favor the transition from laminar to turbulent in the boundary layer around the leaves, such as the leaf surface roughness, free stream turbulence,

or other canopy elements that will trigger instability near the surface (Schuepp 1993). Rougher leaves show a transition to turbulence for smaller Reynolds numbers (Re $<$ 11000) (Schuepp 1993). However the boundary layer over a leaf surface is often composed of a laminar part very close to the surface, where heat and mass transfer results from diffusion processes, and of a turbulent part further away from the surface, where transfer is due to eddies (Beek, Muttzall, and Heuven 1999; Schuepp 1993). Indeed, when the boundary layer thickness exceeds a certain level, the transfer becomes turbulent. In the transition region, both diffusion and eddies equally contribute to the transfer (Beek, Muttzall, and Heuven 1999).

Influence of the free convection in the boundary layer due to the photosynthetic activity

Free convection as introduced in sections 2, 3, and 4 is only caused by temperature differences, but it can also be caused by concentration differences (Beek, Muttzall, and Heuven 1999). Indeed, gas exchanges at the leaf surface will locally change the partial pressures of CO_2, water vapor and O_2, leading to different gas densities of air at the leaf surface. The slice of air at the leaf surface being depleted of CO_2 and CO_2 gas being denser than air, this slice of air becomes less dense than the surrounding air and will rise, triggering free convection movements. This is very simply accounted using the ideal gas law. For example, a 400 ppm CO_2 difference in air (M_{air}= 29.10^{-3} kg.mol^{-1}) at 25 °C and constant total pressure of 1 bar results in a density difference given by (Figure 2.11):

$$x_{air} = \frac{1}{1 + 4.10^{-4}}\, x_{CO_2} = \frac{4.10^{-4}}{1 + 4.10^{-4}} \tag{2.55}$$

$$M = x_{air}\, M_{air} + x_{CO_2}\, M_{CO_2} \tag{2.56}$$

$$\Delta\rho = \frac{P_{tot}}{R\,T}\,(M_{400ppm} - M_0) = 2.42 g.m^{-3} \tag{2.57}$$

Of course, if there are other gas partial pressures gradients, the above expression is generalized accordingly.

The quantity $\beta\,\Delta\,T$ that is used to calculate the Grashof number can also be expressed

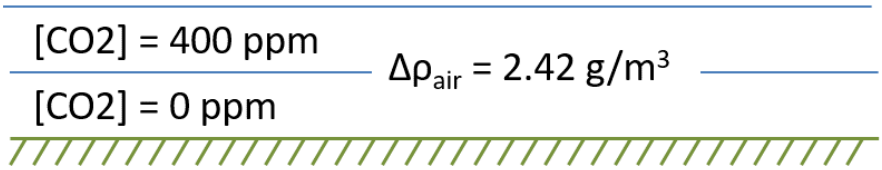

Figure 2.11: Schematic of the difference in CO_2 concentration at the leaf surface

in density ρ (Beek, Muttzall, and Heuven 1999):

$$\beta \left| T_{BL} - T_b \right| = \frac{\left| \rho_b - \rho_{BL} \right|}{\rho_{BL}} \tag{2.58}$$

This enables the establishment of correlations for free convection due to temperature gradients as well as density differences resulting from photosynthesis itself incorporating the two contributions in the same expression.

2.6 Conclusions and model improvements

The plant growth model as defined in sections 2.2 and 2.3 gives accurate preliminary results on gas exchanges and biomass production in low gravity environments. To include gravity in the plant growth model, mass and heat transfers in the boundary layer must be accurately described and heat (radiative and thermal) and mass balances must be coupled. As detailed in sections 2.4 and 2.3, the coupled heat and mass balance, and thus the variations of the leaf surface temperature with respect to gravity levels and forced convection values, could be more accurately modeled by improving some definitions in the model. In particular:

- The expression of the boundary layer can be refined and consider the inclination of the leaf with respect to the incident flow and to the vertical direction (i.e. considering U_{bulk} in the expression of the boundary layer thickness as the component that is parallel to the leaf, instead of the sum of the forced and free convection as it is currently done), as well as the different sides of the leaves (upper and lower); the new definition could also consider the laminar and the turbulent part of the boundary layer, instead of using Blasius approximation.

- Free convection caused because of gas concentration gradients should be implemented to give a more accurate definition of the free convection velocity.

- The leaf energy balance enables the coupling of the mass and heat transfer fluxes. To do so, the derivative of the leaf temperature with respect to time needs to be introduced, and the new model does not describe a steady state anymore, as it was the case in the original MELiSSA plant growth model established by Hézard et al. (2012). This enables to work on very short time frames and account for local gas exchanges in the boundary layer.

In the next chapter, discussions about boundary layer modeling are continued and the new mechanistic model including these improvements and coupling mass, heat and radiative transfers is presented.

2.7 Chapter's outcomes

- Conference article presented at the 47$^{\text{th}}$ International Conference on Environmental Systems in July 2017:
  - The leaf's conductance to water vapor is a combination of stomatal and boundary layer conductances.
  - Free convection velocity can be expressed as a function of gravity and temperature gradients.
- Article accepted for publication in Astrobiology, Volume 18 Issue 9 (September 2018):
  - There is a threshold value for forced convection, under which boundary layer thickness and gas exchanges rates depend on gravity levels and above which it depends on the value of forced convection velocity.
  - It is crucial to study the intricate relationships between forced convection, gravity levels and biomass production.
- To be more complete, the plant growth model needs to couple the initial mass balance to an energy balance, leading to a new variable in the model, namely the leaf surface temperature.
- The inclusion of gravity in plant gas exchanges models requires accurate mass and heat transfer descriptions in the boundary layer.

Chapter 3

Development of a mechanistic model accounting for gravity influence and coupled mass, heat, and radiative transfers

3.1 Introduction

The first MELiSSA plant growth model is a holistic model, with three main modules, morphological, physical, biochemical, corresponding to three scales of study, whole plant, organ level, and cell level. This global scheme was developed in Pauline Hézard's PhD thesis (Hézard 2012) and is maintained here. Nevertheless a fourth module, the energy balance module, is added in order to account for surface temperature of the leaves as detailed in section 2.4. This also allows to address gas exchanges in reduced gravity environments leading to adding gravity as a parameter of the model, which is one of the final objectives of this work. The studied system is a leaf, which is a photoreactive system and can thus be characterized by stoichiometric and kinetic reactions. Our main hypothesis lies in the fact that global kinetics of the leaf are guided by coupled radiative transfer, heat transfer, and mass transport, that can be limiting. Consequently, to get insights about these heat and mass transfers, the boundary layer dynamics at the leaf surface and its modeling was studied. The model presented hereafter assembles the different parts that have been previously described, coming back to a more detailed description of physical

transfer limitations, all these parts being included in the global framework of MELiSSA compartments models, with mass and energy balances at the core of the description. The main differences between this new model and the initial MELiSSA plant growth model lie in the fact that gravity is now a parameter of the model, that the conductance to water vapor is a combination of the boundary layer conductance and the stomatal conductance (which is species-dependent), that the surface temperature of the leaf is not a fixed parameter of the model but changes in time and according to gravity levels and ventilation, that the energy balance is addressed and coupled to the mass balance, and that the model is time-dependent. The main results from the previous chapters and publications are summarized as follows:

- The boundary layer model is the suitable concept for supporting the description of transfer resistances at the leaf surface.

- When a heat, mass or radiative transfer is limiting, the associated physical rate drives all the rates, and in turns all the kinetic rates, either physical or biological. The representation of this rate-limiting step as function of physical variables is the clue for modeling all the processes.

- The hydrodynamic, mass and heat transfer boundary layers have different thicknesses related to the definition of dimensionless numbers, (Prandtl, Schmidt, Lewis) with a dependency at power 1/3. For resistances in the gas phase, the order of magnitude of these dimensionless numbers is unity, showing that the different boundary layer thicknesses take almost the same value. This has been the basis of the previous modeling.

- The influence of gravity has been taken through the calculation of the free convection velocity, which depends on the difference of temperature through the boundary layer. In fact, this temperature difference is related to a density gradient that might lead to a more general expression of gravity influence.

- The influence of the bulk convective velocity has been accounted through an estimation of the hydrodynamic boundary layer thickness given by the Blasius model.

- The mixed influence of both free and forced convection (bulk convection) is accounted to by combining the two velocity vectors in a plan parallel to the leaf

surface.

- The energy balance throughout the boundary layer has demonstrated the capability to model the transient evolution of the temperature at the leaf surface. This consequently allows a more detailed assessment of water transfer through transpiration and more generally the water exchange between the plant and the surroundings. This leads to represent potential water transport limitation and a more thorough understanding of local water transport.

- The integration of these local transport phenomena in the higher plant MELiSSA model has demonstrated that the structure of the physical model, including a detailed description of water transport, enables to tackle the influence of gravity on the overall growth characteristics of the higher plant.

The objective is now to come back on the main elements of the previous approach. This requires considering the integration of the model over short periods of time, during the illuminated periods. In the initial version of the model, respiration was included. It was removed here to focus mainly on photosynthesis and, in the next chapter, validation of the model over short periods of day-time in various gravity and ventilation levels. This is the primary objective of this chapter rather than the theoretical representation of the entire plant life cycle that has been previously treated. For simulation on longer periods, respiration and a holistic integration will be included again (not part of this document). The stoichiometry guiding the model is presented first; then comes the the morphological module, that is computed proportionally to the biomass produced. Then heat and mass transfer in the boundary layer are discussed with different modeling approaches. After that, kinetic aspects are presented, followed by radiative transfer. Finally a presentation of the whole model is given and this chapter ends with a sensitivity study.

3.2 Stoichiometric module

3.2.1 Dry mass synthesis

A higher plant, and more specifically a leaf, must be considered as a reacting system, fixing carbon from atmospheric CO_2 through photosynthesis, producing O_2, and consuming other elements (nitrogen and phosphorus sources, minerals, etc.) as well as water

that is part of fresh biomass. The approach that is adopted for all MELiSSA compartments must be translated for higher plant growth, considering that the stoichiometric approach contains the information assessing the conversion yields that are the core of any quantified model of mass conversion. Consequently, following the modeling concepts enunciated by Dussap (2018) for control system architecture of regenerative systems, such as MELiSSA, the description of the reacting system represented by a plant must start with a stoichiometric formulation (Dussap 2018).

For the purposes of the present study we limit the description to the leaf behavior during illuminated periods, knowing that other descriptions would have to be developed for other organs and also for dark periods. Therefore, this stoichiometric description only concerns the photosynthetic metabolism of the leaf. For the following developments we only consider photosynthesis that is the fixation of CO_2 and the production of glucose units. As a first approximation, we can consider that the basic equation relevant for leaf metabolism is as follows:

$$CO_2 + 0.833\, H_2O \rightarrow CH_{1.667}O_{0.833} + O_2 \tag{3.1}$$

As a first approximation, we have considered that the biomass composition is a polymer of glucose, i.e.: $CH_{1.667}O_{0.833}$. This is sufficient to assess that the molar ratio between CO_2 uptake, O_2 production and C-molar production of dry mass is 1 at the leaf level. This is in accordance with the results obtained by Hézard (2012) based on experiments on lettuce growth in controlled environment. Further developments should include a thorough assessment of the metabolic behavior with at its core the ATP/NADP balance associated to photosynthesis and the cyclic phosphorylation, the synthesis of vegetal dry matter at the leaf level, and the exchanges of carbohydrates with the roots. The previous stoichiometric equation would be established with more accuracy on the basis of experimental results, provided that it would be possible to assess the CO_2 consumption, O_2 production and biomass production, and taking into account the age of the plant, since global stoichiometry may change. It would also be at that step of model development that the complete metabolic pathways analysis could be added in the description as metabolic maps for the different parts, accounting for the conversion yields, ATP, NAD/NADP yields at the leaf, roots and stem levels. This point is not investigated here.

From equation 3.1, the C-molar mass of the carbohydrate equivalent is: 27 g C-mol^{-1}, the

photosynthetic ratio (on a molar basis) is unity, and the consumption of water for dry mass synthesis is 0.56 g H_2O g_X^{-1}. The values of the yields are therefore given by:

$$Y_{H_20\,X} = 0.56\, g_{H_2O} g_X^{-1} \tag{3.2}$$

$$Y_{CO_2\,X} = 1.63\, g_{CO_2} g_X^{-1} \tag{3.3}$$

$$Y_{O_2\,X} = 1.19\, g_{O_2} g_X^{-1} \tag{3.4}$$

$$Y_{C\,X} = 0.444\, g_C g_X^{-1} \tag{3.5}$$

Dry mass is referred to by the subscript X and Y_{iX} is the mass yield associated to dry mass. Equation 3.5 is the mass fraction of carbon contained in the dry mass.

3.2.2 Photosynthetic yield

CO_2 absorption is the result of photosynthesis, through CO_2 consumption by the enzyme RuBisCO. Plants and other autotrophs synthesize carbohydrates from atmospheric CO_2 by reducing H^+ at the expense of ATP and NADPH. The assimilation of CO_2 occurs in three stages: carboxylation, reduction, and regeneration. The first stage involves the incorporation of CO_2 and water into five-carbon acceptor: ribulose 1, 5-biphosphate ($RuBP^{4-}$) that is catalyzed by the enzyme ribulose 1, 5-biphosphate carboxylase. This is often considered as the limiting step catalyzed by RuBisCO. Sasidharan (2012) performed a complete study of the mechanisms of light reactions in the chloroplast coupled to the Calvin cycle and RuBisCO functioning. The elementary flux mode analysis (EFM) leads to the main result that the maximum photon carbon yield, also called quantum yield, is:

$$Y_{C_{photon}} = \frac{1}{14} = 0.071\, mol_C\, mol_{Photon}^{-1} \tag{3.6}$$

The value classically found in the literature for the quantum yield is in the same order of magnitude (Sasidharan et al. 2010; Hézard 2012):

$$Y_{C_{photon}} = \frac{1}{18.5} = 0.054\, mol_C\, mol_{Photon}^{-1} \tag{3.7}$$

This value of the quantum yield accounts for losses in energetic coupling that have not been completely considered in the work of Sasidharan (2012). A more detailed metabolic

pathways analysis would include the coupling efficiency at the chloroplast level, leading to the conversion yields at the leaf, roots and stem levels. In this work, the value of Equation 3.7 is used and the resulting mass yield for dry biomass synthesis is:

$$Y_{X_{photon}} = \frac{0.054 \times 12}{0.444} = 1.46\, g_X\, mol^{-1}_{Photon} \tag{3.8}$$

3.2.3 Fresh mass synthesis

In order to assess the volume and geometrical parameters of a plant, it is necessary to account for fresh mass synthesis rather than dry mass synthesis solely, as it is done for submerged microbial cultures. In the subsequent sections, the computations are based on Hézard (2012) assessment for fresh mass: 91 % of the plant fresh mass is free water and 9 % of fresh mass is dry biomass (Hézard 2012). Plant fresh mass is referred to with the subscript FX:

$$\omega_X = \frac{m_X}{m_{FX}} = 0.09 \tag{3.9}$$

$$m_{FX} = \frac{m_X}{0.09} \tag{3.10}$$

Water used for total biomass synthesis is the sum of water used for dry biomass synthesis and free water in the plant, which is the difference between fresh biomass and dry biomass. Water consumption associated with the synthesis of fresh biomass corresponding to 1g of dry biomass is thus:

$$Y^*_{H_2O\,X} = 0.56 + \frac{1}{0.09} - 1 = 10.67\, g_{H_2O}\, g_X^{-1} \tag{3.11}$$

3.2.4 Total Water consumption

Total water consumption corresponds to the total amount of water absorbed by the plant. This encompasses the water consumption for dry biomass synthesis, free water in the plant, and transpired water. In the literature, transpired water by plants is classically 10 times the amount of fresh biomass (Hézard 2012):

$$\omega_{W/FX} = \frac{m_W}{m_{FX}} = 10 \tag{3.12}$$

m_W is the mass of transpired water. This leads to the computation of the mass of

transpired water with respect to the dry biomass:

$$m_W = 10\, m_{FX} = \frac{\omega_{W/FX}}{\omega_X} = \frac{10}{0.09}\, m_X = 111.1\, m_X \tag{3.13}$$

The ratio of transpired water over total absorbed water for 1g of dry biomass, is thus:

$$\omega_{W/H_2O\,X} = \frac{m_W}{m_W + m_{H_2O\,X}} = \frac{111.1}{111.1 + 10.67} = 0.87 \tag{3.14}$$

In Hézard work this ratio was set to 0.5, computed from experimental value on lettuce growth in controlled environment. Water transpired by plants is not only a function of photosynthesis but also depends on outside relative humidity and stomata opening at night. In controlled environments this ratio can be adjusted with the relative humidity value of bulk air. This is especially of interest for regenerative LSS applications where water recycling is needed.

3.3 Morphology module

The morphological components needed to compute mass transport and heat exchange fluxes, are proportional to the biomass produced, which is similar to the previous MELiSSA plant growth model. The fresh biomass is split between dry biomass and water mass. The morphological components are set proportional to the carbon biomass to better reflect the reality. Indeed, the water content in a leaf constitutes a buffer that can protect the leaf from overheating through evaporative cooling and through increasing the leaf heat capacity (Schymanski, Or, and Zwieniecki 2013). Hence, the leaf area is:

$$LA = k_1\, m_{FX} = \frac{k_1}{\omega_{FX}}\, m_X = \frac{k_1}{Y_{CX}\, \omega_{FX}}\, m_C \tag{3.15}$$

k_1 is the ratio between the canopy surface and the biomass produced (m^2/g_{Fx}), empirically determined by Hézard et al. (2012).

When several plants are growing on a defined surface, it is necessary to introduce a parameter that quantifies the number of plants per soil surface unit: n_{plants} (m^{-2}). This permits to extend the description from one plant to an entire canopy. This has been used

in the previous chapter for defining the leaf area index (LAI):

$$LAI = n_{plants}\, LA \tag{3.16}$$

The parameter n_{plants} is the plant density in the plant chamber. The variable LAI has been further used to compute the averaged photon flux to an entire canopy, following a Beer Lambert law (see chapter 2). The leaf characteristic length L is given by:

$$L = 2\sqrt{\frac{LA}{\pi}} \tag{3.17}$$

The characteristic length of the leaf is the diameter of a circular single leaf, as detailed in chapter 2, and it increases with the leaf area (i.e. with biomass production), which is new compared to the initial MELiSSA plant growth model where L was an entry parameter of the model.

The stem length and the number of sap vessels are:

$$L_{stem} = k_2\, m_{FX} = \frac{k_2}{\omega_{FX}}\, m_X = \frac{k_2}{Y_{CX}\, \omega_{FX}}\, m_C \tag{3.18}$$

$$N_{vessel} = k_3\, m_{FX} = \frac{k_3}{\omega_{FX}}\, m_X = \frac{k_3}{Y_{CX}\, \omega_{FX}}\, m_C \tag{3.19}$$

k_2 defines the total length of the stems as a function of the fresh biomass produced (m/g_{FX}); k_3 is the ratio between the number of sap vessels and the fresh biomass (g_{FX}^{-1}), a sap vessel being a channel between the root and the leaf, such as the phloem or the xylem, transporting sap. Hézard et al. (2012) empirically determined both k_2 and k_3 for lettuce growth. These parameters enable the establishment of a growth model incorporating in a first approach the growth of the basic plant structures (leaves and stems).

3.4 Heat and Mass transfer at a solid surface boundary

In the previous chapter, we demonstrated that the estimation of the boundary layer thickness is of crucial importance when examining potential transfer limitations, affecting both heat and mass transfer. The influence of different gravity levels can also be assessed by studying heat and mass transfer at the boundary layer, considering that the thickness of the boundary layer depends on both bulk convective velocity and on density gradients

across the boundary layer. In this paragraph, different boundary layer models, that are classically used in chemical engineering, are reviewed in order to achieve a physically consistent description of heat and mass transfer characteristics at the leaf surface. This enables to develop a modeling approach of higher plant growth behavior in non classical conditions, i.e. in reduced gravity environments, in modified partial pressures conditions, in non-standard total pressure, etc.

3.4.1 The stagnant boundary layer model

The stagnant boundary layer model is the most basic model, in which the diffusion flux is defined as a function of the concentration gradient, given a boundary layer of thickness δ_X, with the general form:

$$\Phi_X = \frac{D_X}{\delta_X} \left(C_{X_i} - C_{X_b}\right) = k_X \left(C_{X_i} - C_{X_b}\right) \tag{3.20}$$

In the case of heat transfer by convection, the former expression takes the form:

$$\Phi_{conv} = \Phi_T = \rho\, C_p \frac{D_T}{\delta_T} \left(T_{X_i} - T_{X_b}\right) = \rho\, C_p\, k_T \left(T_{X_i} - T_{X_b}\right) \tag{3.21}$$

with:

$$D_T = \frac{\lambda}{\rho\, C_p} \tag{3.22}$$

Φ_X and Φ_T are respectively the mass flux of the quantity X ($mol.m^{-2}.s^{-1}$) and the energy flux ($W.m^{-2}$). D_X is the diffusivity or diffusion coefficient of X ($m^2.s^{-1}$). k_X is the transfer coefficient ($m.s^{-1}$). C_{X_i} and C_{X_b} are respectively the interface and bulk concentrations. ρ is the density ($kg.m^{-3}$). C_p is the heat capacity ($J.kg^{-1}.K^{-1}$). λ is the thermal conductivity ($W\ m^{-1}.K^{-1}$). δ_X and δ_T are respectively the boundary layer thickness associated to the transport of quantity X and the thermal boundary layer, i.e. depending on the diffusivity at the power 1/3 (chapter 2 paragraph 5.3.3) and they are related to the hydrodynamic boundary layer:

$$\delta_X = \delta_h\, Sc_X^{-1/3} \tag{3.23}$$

$$\delta_T = \delta_h\, Pr^{-1/3} \tag{3.24}$$

With Schmidt and Prandtl numbers defined as the ratio of mass and thermal diffusivities

to the kinematic viscosity (momentum diffusivity):

$$Sc_X = \frac{\nu}{D_X} \tag{3.25}$$

$$Pr = \frac{\nu}{D_T} = \frac{\nu\,\rho\,C_p}{\lambda} \tag{3.26}$$

In summary, the equivalent boundary layer representation requires being able to determine the hydrodynamic boundary layer thickness δ_h with respect to external variables in order to correlate other boundary layers thicknesses and transfer fluxes in terms of fluid and components physical properties. The main advantage of the stagnant boundary layer model is that it is the simplest way to link in a single model momentum, heat and mass transfers.

3.4.2 The laminar boundary layer model

The boundary layer is now supposed to be in a laminar flow (laminar at the leaf surface) rather than in stagnant state as it was the case in the previous model. The integration of Navier Stockes equations was presented in section 5.1.3 in chapter 2. Bird et al. (1965) have obtained this result by analytic integration with suitable simplifying assumptions from a work published by Schlichting (1955) (Bird, Stewart, and Lightfoot 1965; Schlichting 1955). The equivalent boundary layer thickness is given as a function of the abscissa x from the edge of a plate:

$$\delta_{hx} = \sqrt{\frac{280}{13}\,\frac{\nu\,x}{U_{bulk}}} = 4.641\,\sqrt{\frac{\nu\,x}{U_{bulk}}} = 4.64\,x\,Re_x^{-1/2} \quad \text{with:} \quad Re_x = \frac{x\,U_{bulk}}{\nu} \tag{3.27}$$

The thickness of the boundary layer increases as the square root of the distance from the edge of the plate. For larger surfaces, other phenomena are considered, since this equation cannot be extrapolated to infinity. The analytic integration enables the derivation of the expression of the shear stress at the wall, given by Bird et al. (1965):

$$\tau_{W_X} = -\mu\,\frac{du}{dy}|_{y=0} = \frac{3}{2}\,\rho\,\nu\,\frac{U_{bulk}}{\delta_{hx}} = 0.323\,\rho\,U_{bulk}^2\,Re_x^{-1/2} \tag{3.28}$$

The factor 3/2 comes from the velocity profile inside the boundary layer. Bird et al. (1966) have assumed that x component of the velocity depends on the depth with at

power 3 (parabolic profile of the shear stress). Also, the continuity equation leads to a velocity perpendicular to the plate. This leads to the definition of an apparent thickness of the boundary layer:

$$\tau_{W_X} = \rho\,\nu\,\frac{U_{bulk}}{\delta_{hx}^{app}} \quad \Rightarrow \quad \delta_{hx}^{app} = 3.10\sqrt{\frac{\nu x}{U_{bulk}}} \tag{3.29}$$

The average shear stress at the wall for the total length is then obtained:

$$\tau_W = \frac{1}{L}\int_0^L \tau_{W_X}\,dx = 0.646\,\rho\,U_{bulk}^2\,Re^{-1/2} \tag{3.30}$$

This value results from averaging the value of $\frac{1}{\delta_{hx}}$, hence:

$$\tau_W = \rho\,\nu\,\frac{U_{bulk}}{\delta_h} \quad \Rightarrow \quad \delta_h = 1.55\sqrt{\frac{\nu\,L}{U_{bulk}}} \tag{3.31}$$

The friction factor is also determined:

$$\tau_W = \frac{1}{2}\,f\,\rho\,U_{bulk}^2 \quad \Rightarrow \quad f = 1.29\,Re^{-1/2} \tag{3.32}$$

More recently, with a slightly different analysis, Schlichting and Gersten (2017) report a very close correlation for the friction coefficient (Schlichting and Gersten 2017):

$$f = 1.328\,Re^{-1/2} \tag{3.33}$$

With a similar analysis, the thicknesses of the mass and heat transfer boundary layers are determined at the abscissa x (Schlichting 1955):

$$\delta_{X_x} = 3.01\sqrt{\frac{\nu\,x}{U_{bulk}}}\,Sc_x^{-1/3} = 3.01\,x\,Re_x^{-1/2}\,Sc_x^{-1/3} \tag{3.34}$$

This leads to the expression of the Sherwood number at abscissa x:

$$Sh_{X_x} = \frac{x\,k_{X-x}}{D_X} = \frac{x}{\delta_{X_x}} = 0.332\,Re_x^{1/2}Sc_x^{1/3} \tag{3.35}$$

It must be noticed that this representation using a laminar boundary layer model allows for estimating the local transfer coefficients onto the surface. This possibility is not used in

this work but it must be noted that future work could map exchange coefficients onto the surface giving potentially access to local properties. The average value of the Sherwood number for a rectangular plate of length L is given by calculation of the average value of the local transfer coefficient, i.e. the average value of $\frac{1}{\delta_{h_x}}$:

$$Sh_X = 0.664\, Re^{1/2} Sc_X^{1/3} \tag{3.36}$$

Similarly, we obtain:

$$Nu = 0.664\, Re^{1/2} Pr^{1/3} \tag{3.37}$$

These relations are the reference correlations for Sherwood and Prandtl numbers and result from approximations. The integration for averaging the transfer coefficient onto the surface becomes more difficult for complex geometries of the flat plate, resulting in different constant coefficients. This coefficient is subject to numerous debates and considerable work and varies in the literature from 0.4 to 0.75 (Bird, Stewart, and Lightfoot 1965).

3.4.3 The Chilton Colburn analogy

The Chilton and Colburn analogy between mass (respectively heat) transfer and momentum transfer (respectively friction losses) is formulated defining the coefficients J_T and J_X as follows:

$$Nu = J_T\, Re\, Pr^{1/3} \tag{3.38}$$

$$Sh_X = J_X\, Re\, Sc_X^{1/3} \tag{3.39}$$

In order to finalize the Chilton Colburn analogy between the different forms of transfers, the friction factor f is defined:

$$\tau_W = \frac{1}{2} f\, \rho\, U_{bulk}^2 \tag{3.40}$$

Leading to the following relation:

$$J_T = J_X \approx \frac{f}{2} \quad \text{with} \quad f = 1.29\, Re^{-1/2} \tag{3.41}$$

The friction factor found here is similar to the one found with the laminar boundary layer model. This demonstrates that once the fluid properties are known, the remaining

question is to correlate the friction coefficient. This is also summarized as follows:

$$\frac{Nu}{Re\,Pr} = St_T = \frac{k_T}{U_{bulk}} = J_T\,Pr^{-2/3} \approx \frac{f}{2}\,Pr^{-2/3} \tag{3.42}$$

$$\frac{Sh_X}{Re\,Sc_X} = St_X = \frac{k_X}{U_{bulk}} = J_X\,Sc_X^{-2/3} \approx \frac{f}{2}\,Sc_X^{-2/3} \tag{3.43}$$

St is the Stanton number, which is defined for thermal (St_T) and mass transfer (St_X). This is the most compact definition of the Chilton-Colburn analogy and a convenient starting point for correlating different heat and mass transfer limitations.

3.4.4 The penetration theory model

The previously presented boundary layer models are suitable for extrapolating the behavior of the exchanges with respect to gravity only as first approximations. The penetration theory model changes the reference frame and considers a plate moving in a quiescent fluid, instead of a fluid moving along a plate. In this context, the transfer of momentum from the surface to the bulk fluid obeys a classical Wiener process, which is characteristic of diffusion (result reported in most chemical engineering textbooks). The solution is given by the distribution of a quantity (here momentum) into a semi-infinite medium. The velocity distribution is given by:

$$U = U_0 - \frac{2}{\sqrt{\pi}}\,U_0 \int_0^{\frac{y}{\sqrt{4\,\nu\,t}}} e^{-\xi^2}\,d\xi \approx U_0\left[1 - \frac{y}{\sqrt{\pi\,\nu\,t}}\right] \tag{3.44}$$

U_0 is the velocity of the plate, y the ordinate normal to the plate, t the time of contact. The term $\sqrt{\pi\,\nu\,t}$ represents the penetration depth, i.e. the distance the momentum has penetrated during time t. The shear stress constraint at the wall is therefore given by:

$$\tau_{W_x} = \mu\,\frac{U_0}{\sqrt{\pi\,\nu\,t}} \tag{3.45}$$

Since the time of contact is given by $t = \frac{x}{U_0}$, after averaging x between 0 and L, i.e. onto the total length, the shear stress constraint is:

$$\begin{aligned} &\tau_W = 2\,\mu\,\frac{U_0^{3/2}}{\sqrt{\pi\,\nu\,L}} = \frac{2}{\sqrt{\pi}}\,\rho\,U_0^2\,(\,\frac{\mu}{L\,U_0\,\rho}\,)^{1/2} = \frac{2}{\sqrt{\pi}}\,\rho\,U_0^2\,Re^{-1/2} = 1.13\,\rho\,U_0^2\,Re^{-1/2} \\ &\text{and} \quad f = 2.26\,Re^{-1/2} \end{aligned} \tag{3.46}$$

The form of the expression obtained for τ_W is similar to the one obtained for a laminar boundary layer. The constant coefficient is 1.7 times higher in the case of the penetration theory, resulting in an apparent hydrodynamic boundary layer thickness that is 1.7 times lower. These discrepancies can be explained by the fact that no fluid velocity normal to the surface occurs because the plate is moving instead of the fluid.

A similar approach for mass transfer leads to the expression of the average mass transfer coefficient:

$$k_X = 2\sqrt{\frac{D_X}{\pi\, t_c}} = 2\sqrt{\frac{D_X\, U_0}{\pi\, L}} \tag{3.47}$$

t_c is the contact time between a fluid element and the surface.
The Higbie model considers that this averaged contact time is given by: $\frac{L}{U_0}$. Using this expression, the Stanton number becomes:

$$St_X = \frac{k_X}{U_0} = 1.13\, Sc_X^{-1/2}\, Re^{-1/2} \tag{3.48}$$

This expression can be applied to compute mass and heat transfer coefficients. It must be outlined that the Chilton Colburn analogy still applies. However, the exponent of the Schmidt number is now -1/2 instead of the previous -1/3. The estimation of the transfer coefficients is thus about 1.6 times higher than with the boundary layer approach, considering that the Schmidt number is close to unity. Hence, several estimations of both the average friction factor and the transfer coefficient derived from the Higbie model involve correlations that are 50 to 70 % higher than the ones obtained with the laminar boundary model. This highlights the many uncertainties surrounding the definition and correlation of the time of contact and more precisely the average contact time to consider.

3.4.5 The surface renewal model

In 1951, Danckwerts proposed an important extension of the penetration theory model (Danckwerts 1970; Sherwood, Pigford, and Wilke 1975; Beek, Muttzall, and Heuven 1999). While the Higbie model takes the exposure time of the fluid element with the surface as a constant (t_c in section 3.4.4), the Danckwerts model considers a wide spectrum of times and averages the varying degrees of penetration. This is justified by the fact that the previous time t_c is hardly correlated with the global hydrodynamic characteristics. In the interface region, mass transfer takes place according to the penetration theory and

elements of this region are exchanged with the bulk region. When considering a fractional rate of renewal s of the area exposed to transfer, the surface age distribution (probability distribution that an element of surface is exposed during a time t) is shown to be:

$$\zeta = s\, e^{-st} \tag{3.49}$$

$1/s$ is a characteristic constant equivalent to the average residence time of an element in the interface (surface) region. After taking the average for all times, the transfer coefficient is equal to:

$$k_X = \sqrt{D_X\, s} \tag{3.50}$$

The fractional surface renewal rate s (s^{-1}) may be correlated from mass transfer data as a function of hydrodynamic characteristics of the system. In this model, the parameter s plays the same role as t_c for the penetration theory model and δ_h for the hydrodynamic boundary layer thickness: they are the adjustable parameters of the different models.
The current trend of research on transfer coefficients addresses the correlation of s with external variables rather than with the use of other models. The fundamental reason is that this enables to account for both laminar and turbulent boundary layers and finally relates physical transport to statistical physics. As first approximation the fractional surface renewal rate can be given by:

$$s = \frac{U_0}{L} \tag{3.51}$$

Formally, this corresponds to a perfectly mixed boundary layer, which is intuitively a correct assumption, considering that a fluid element entering the boundary layer has a mean residence time that is the volume of the boundary divided by the flow rate. The average mass transfer coefficient is then given by:

$$k_X = \sqrt{\frac{D_X}{t_c}} = \sqrt{\frac{D_X\, U_0}{L}} \tag{3.52}$$

Using this expression, the Stanton number becomes:

$$St_X = \frac{k_X}{U_0} = Sc_X^{-1/2}\, Re^{-1/2} \tag{3.53}$$

This leads to the friction coefficient:

$$f = \sqrt{Re} \tag{3.54}$$

Although the previous assumption is very simple, it provides an estimation that is an intermediate between Higbie and the other boundary layer models. The Danckwerts model provides the clue for developing simple interpretations of fluid behavior in the vicinity of the wall. The comparison between the Danckwerts and the Higbie models leads to consider that the surface renewal theory corresponds to a perfectly mixed situation, whereas the penetration theory is a plug flow model, and the other boundary layer approaches are an intermediate between these two. The distribution of ages of the fluid elements in the vicinity of the wall is the most accurate way to characterize the transfer (Mondal and Chatterjee 2017) considering that when the degree of turbulence is increasing in the boundary layer, the surface renewal model provides the most realistic results. However, it must also be considered that the surface renewal model provides a global estimation of the transfer coefficient (without any local estimation), which is not the case for the other two models.

3.4.6 Influence of free convection

Free convection is the result of fluid movements due to Archimedes forces, caused by the variation of fluid density with temperature gradients and gas concentration gradients (in the order of 1 to 5 g/m^3). Dynamics and thermal transfer are coupled: heat is transferred along the velocity field; this affects fluid temperature and thus fluid density; these changes in density in return generate movements with Archimedes forces (Marty 2012). As detailed in chapter 2, a first estimation of the free convection velocity that is generally considered for free convection in an open space is:

$$v_{free} = \sqrt{g\,H\frac{\Delta T}{T}} \tag{3.55}$$

g is the gravitational acceleration, H is the height of the chamber, and ΔT is the temperature gradient. This comes from the mixed convection case, when the Richardson number is equal to unity and enabled us to derive first assessments of the influence of gravity on plant growth. This expression can be fine-tuned for a closed chamber. Apply-

ing a global mechanical energy balance between two points with different densities and different heights leads to:

$$\frac{1}{2}\,\rho\, v_{free}^2 = g\,\Delta\rho\, H \tag{3.56}$$

Then:

$$v_{free} = \sqrt{2g\,H\,\frac{\Delta\rho}{\rho}} \tag{3.57}$$

There is a factor $\sqrt{2}$ difference between equation 3.57 and equation 3.55. This comes from the fact that friction losses are neglected in this approach, which is justified in a confined environment. Equation 3.57 is more general than equation 3.55 because it accounts both for temperature and concentration gradients leading to density differences. This expression is therefore chosen for the free convection in subsequent developments.
This free convection velocity is accounted for in the expression of the boundary layer thickness through U_{bulk} (bulk air velocity). As detailed in chapter 2, U_{bulk} is a combination of v_free and v_forced and first tests were performed with a simple addition of the two velocities to obtain U_{bulk}. Later on, only the component of the bulk velocity that is parallel to the leaf surface was included. This implies the inclusion of the leaf inclination with respect to the vertical direction, with an angle α:

$$U_{bulk} = v_{free}\,cos\alpha + v_{forced}\,sin\alpha \tag{3.58}$$

In reality, the combination of mixed effects of free and forced convection is complicated and little is known about it (Beek, Muttzall, and Heuven 1999).
To account for free convection and thus study the influence of gravity on heat and mass transfer at the leaf surface, a deeper mechanistic formalism for free convection at the boundary layer level is developed. Let us consider a flat plate of length L with a boundary layer of thickness δ_{free} with no forced convection and a density gradient throughout the height of the boundary layer $\Delta\rho$. The basic assumption is that the vertical pressure gradient created by density gradient balances the shear stress constraint created by the onset of a free convection velocity parallel to the plate. At the abscissa x on the plate, the system to solve is:

$$g\,\Delta\rho\,\delta_{free\,x} = \frac{1}{2}\,\rho\, f\, U_{free\,x} = 0.323\,\rho\, U_{free\,x}^2\, Re_x^{-1/2} \tag{3.59}$$

$$\rho\,\nu\,\frac{U_{free\,x}}{\delta_{free\,x}} = \frac{1}{2}\,\rho\,f\,U_{free\,x} \tag{3.60}$$

Given the expression of the friction factor, this system involves two unknowns: $\delta_{free\,x}$ and $U_{free\,x}$ with the boundary layer model. Considering that the surface renewal model applies for the overall correlation of the drag coefficient into the boundary layer ($f = Re^{-1/2}$) we obtain:

$$\delta_{free\,x} = \left[\frac{\rho\,\nu^2\,x}{0.323^2\,g\,\Delta\rho}\right]^{1/4} \quad \Rightarrow \quad \frac{\delta_{free\,x}}{x} = 1.76\left[\frac{x^3\,g\,\Delta\rho}{\rho\,\nu^2}\right]^{-1/4} \tag{3.61}$$

Taking the average of $1/\delta_{free\,x}$ on the length of the plate leads to:

$$\frac{\delta_{free}}{L} = 1.32\left[\frac{L^3\,g\,\Delta\rho}{\rho\,\nu^2}\right]^{-1/4} \tag{3.62}$$

This relation is in agreement with a classical correlation linking the Nüsselt number with the Grashof and the Prandtl numbers (Beek, Muttzall, and Heuven 1999):

$$Nu = 0.55\,Gr^{1/4}\,Pr^{1/3} \tag{3.63}$$

$$Nu = \frac{h\,L}{D_T} \quad Gr = \frac{L^3\,g\,\Delta\rho}{\rho\,\nu^2} \quad Pr = \frac{\nu}{D_T} \tag{3.64}$$

The difference here with the previous theoretical demonstration is on the constant coefficient of value 0.55 instead of 0.76.

Intuitively, a correct approach of mixed free and forced convection effects would consider that the global transfer resistance (inverse of the transfer coefficient) is obtained by the sum of parallel transfer resistances. In fact this assumption has already been used when integrating $1/\delta$ for assessing the average transfer coefficient. Consequently, the sum of parallel resistances equals the sum of transfer coefficients and for example, using the surface renewal model for convective transfer, we obtain:

$$Sh_X = \frac{L}{\delta_X} = \sqrt{\frac{L\,U_{bulk}}{D_X}} + 0.76\left[\frac{L^3\,g\,\Delta\rho}{\nu^2\,\rho}\right]^{1/4}\left[\frac{\nu}{D_X}\right]^{1/3} = Re^{1/2}\,Sc^{1/2} + 0.76\,Gr^{1/4}\,Sc^{1/3} \tag{3.65}$$

For an air velocity at 1 m/s and a density gradient of 0.5 %, the free convection term accounts for 10 % of the transfer coefficient. If we use the boundary layer model for the first right-hand term, we obtain:

$$Sh_X = \frac{L}{\delta_X} = 0.664\, Re^{1/2}\, Sc^{1/3} + 0.76\, Gr^{1/4}\, Sc^{1/3} \tag{3.66}$$

The difference between the two approaches is rather small and is essentially due to the first term of the right-hand side.

3.4.7 Overview of the influences of different types of convection

The goal of the previous analysis was to install the basis mechanisms that are at the root of the experimental correlations that are frequently used. The main conclusion is that if we take the thickness of the boundary layer as a descriptive image, it is subject to controversial estimations. Semi-empirical expressions based on dimensionless numbers associated with mass transport and heat transfer have been derived for heat and mass transfers in free and forced convection on a leaf (flat plate) and are given in Table 3.1 (Schuepp 1993; Beek, Muttzall, and Heuven 1999). An important extension of these correlations compared to the previous analysis is that they include both laminar boundary layer and the turbulent sub-layer that has not been considered except implicitly in the surface renewal model.

Table 3.1: Correlations with dimensionless numbers for heat and mass transfer in forced and free convection.

	Mass Transport	Heat Transfer
Forced	$Sh = c_M\, Sc^{0.33}\, Re^n$	$Nu = c_H\, Pr^{0.33}\, Re^n$
Free	$Sh = k_M\, Sc^m\, Gr^n$	$Nu = k_H\, Pr^m\, Gr^n$

c_M, c_H, k_M, and k_H are empirical constants (resulting from the Chilton Colburn analogy) determined for mass transport (subscript M) and heat transfer (subscript H) for forced and free convection respectively. The exponent n and m depend on the convective regime of the flow (laminar or turbulent), as well as on the inclination of the plate. The different cases are discussed hereafter.

Thermal exchanges in natural convection depend on the shape and dimension of exchange surfaces, but also on the orientation of these surfaces according to the vertical. Unlike in forced convection, the dimensionless number used to characterize the transition between turbulent and laminar flow in natural convection is the Rayleigh number: above $Ra = 10^9$ the flow is turbulent (Marty 2012; Rattner and Bohren 2008). In the cases of flat plates (both horizontal and vertical) submitted to a constant flux φ, like what it is assumed

for the leaves, the dimensionless number is a modified Rayleigh number (Marchio and Reboux 2008):

$$Ra^* = \frac{g\,\beta\,L^3\,\varphi}{\nu\,\kappa} \tag{3.67}$$

A threshold value is at $Ra^* = 10^{13}$. In the case of a vertical plate, the convective regime depends on the length of the plate: for small plates, the regime is laminar, for large plates ($\sim$ 1 m), the regime is turbulent.

- For laminar flows in the air, the literature gives $n = m = 0.25$ and $k_H = k_M = 0.5$ (Schuepp 1993. Hence an average Nüsselt number: $Nu = 0.5Ra^{0.25}$. This is quite in agreement of theoretical correlation that have been previously derived.

- For turbulent flows, McAdams formulas are used:

$Nu = 0.13\,Ra^{1/3}$ for plates with a constant temperature
$Nu = 0.568\,Ra^{*^{0.22}}$ for plates with a constant flux
In the case of a horizontal plate, a distinction must be made between upper and lower surfaces, as well as when the plate is hotter or colder than the surrounding air. Indeed, for a plate hotter than the surrounding air, on the lower side, we face a stable thermal stratification as hotter air that is less dense than surrounding air will be blocked by the plate and will not be able to rise, so free convection will be limited. In the same way, on the upper side of a plate colder than the surroundings, colder air that is denser than surrounding air will be blocked by the plate and will not sink, thus limiting free convection movements. This case is not tackled by the previous theoretical analysis, which is a weakness of the previous developments. Table 3.2 gives correlations of the Nüsselt number (heat transfer), for a laminar or turbulent regime, for a hot or a cold horizontal plate, and upper or lower surfaces (Rattner and Bohren 2008).
The expressions for the Sherwood number (mass transport) are similar to the Nüsselt number expressions. These correlations stay the same for an inclined leaf but in the expression of Ra, g is replaced by $g\,cos\theta$, where θ is the angle of the leaf with the vertical axis (Marty 2012):

$$Ra^* = \frac{g\,cos\theta\,\beta\,\Delta T\,L^3}{\nu\,\kappa} \tag{3.68}$$

Table 3.2: Correlations of the Nüsselt number for upper and lower faces of hot and cold horizontal plates.

		Laminar	Turbulent
Hot	Upper	$Nu = 0.54\,Ra^{0.25}$ $Sh = 0.54\,(Sc\,Gr)^{0.25}$	$Nu = 0.15\,Ra^{1/3}$ $Sh = 0.15\,(Sc\,Gr)^{1/3}$
	Lower	/ /	$Nu = 0.27\,Ra^{0.25}$ $Sh = 0.27\,(Sc\,Gr)^{0.25}$
Cold	Upper	/ /	$Nu = 0.27\,Ra^{0.25}$ $Sh = 0.27\,(Sc\,Gr)^{0.25}$
	Lower	$Nu = 0.54\,Ra^{0.25}$ $Sh = 0.54\,(Sc\,Gr)^{0.25}$	$Nu = 0.15\,Ra^{1/3}$ $Sh = 0.15\,(Sc\,Gr)^{1/3}$

3.5 The kinetic model for higher plant growth

Up to here the focus was set on the physical transfer limitation at leaf surface during illuminated periods. It must be outlined that there are other physical determinants, such as water movements inside the plant, nutrients transport in the root compartment, etc. They are not described in detail in this chapter and will be reconsidered in chapter 5.

The logic followed is the same as the one used in the MELiSSA initial plant growth model (Hézard 2012). Potential physical limiting rates are computed and converted into global CO_2 uptake rates: overall water transport into the plant, light energy transfer using a Lambert Beer model, CO_2 availability assessed as a global transfer capacity at the leaf level, and water transpiration capacity considering water vapor transfer at the surface of the leaf. They correspond to the maximum biomass growth rate in a given situation characterized by the leaf surface, the height of the plant, the transfer resistance in the gas phase (transfer coefficients) and potential differences of the species in the gas phase and light energy input.

The limiting rate is set as the real CO_2 uptake flux and the other rates are calculated accordingly, using the conversion yields that are given by the previous stoichiometric approach (paragraph 3.1). This simplified approach permits to simply integrate the model and to compute the different observable variables. The important input of this work is to consider the mass transfer limitations at the leaf level in more mechanistic way than what was previously used by Hézard (2012) who considered for the simulation a unique mass transfer coefficient for all species equal to: $k = 10^{-4} m.s^{-1}$. Here the mass transfer coefficient is given as a function of overall degree of gas turbulence (characterized by the bulk velocity in the vicinity of the exchange areas) in the growth chamber and of gravity.

As detailed in chapter 2 part 2, we include an additional transfer resistance of water at the leaf surface related to the stomatal resistance. We consider that the total water diffusion conductance at the leaf surface is a combination of the two conductance associated with the two diffusion processes occurring at the leaf surface: stomatal conductance and boundary layer conductance. The boundary layer conductance for water is a function of the diffusion coefficient for water vapor D_w, as it has been demonstrated previously and thus the water flow rate through the boundary layer is:

$$\Phi_W^{BL} = \frac{D_W}{\delta_W}\left(C_{W_i} - C_{W_b}\right) = k_W\left(C_{W_i} - C_{W_b}\right) = \frac{k_W}{RT}(p_{W_i} - p_{W_b}) \tag{3.69}$$

The conductance (inverse of the resistance) of the boundary layer is therefore:

$$g_W^{BL} = \frac{D_W}{\delta_W} \tag{3.70}$$

The transfer resistance inside the stomatal pore, as detailed in chapter 2, is:

$$g_W^s = \frac{D_W\, d_s\, a_s}{l_s} \tag{3.71}$$

l_s is the depth of a stomatal pore and since the surface offered to vapor transfer inside the pore is not equal to the surface of the leaf, the stomatal cross-sectional area a_s and the stomatal density d_s need to be included in the expression of the stomatal resistance. Thus, the water flow rate through the stomatas of one leaf is:

$$N_W = \frac{D_W}{l_s}\, a_s\, d_s\left(C_W^* - C_{W_i}\right) = \frac{1}{RT}\,\frac{D_W}{l_s} a_s\, d_s\left(P^0 - p_{W_i}\right) \tag{3.72}$$

This water flow rate equals the diffusion at the leaf surface:

$$N_W = \frac{D_W}{\delta_W}\,\frac{1}{RT}\left(p_{W_i} - p_{W_b}\right) \tag{3.73}$$

And this leads to the total water flow rate through the leaf, with the global conductance G:

$$\Phi_W = G\,\frac{1}{RT}\left(P^0 - p_{W_b}\right) \tag{3.74}$$

With:

$$G = \frac{D_W\, a_s\, d_s}{l_s + \delta_W\, a_s\, d_s} \tag{3.75}$$

This expression for water conductance was used in both publications in part 2.2 and 2.3. We have here reported the demonstration and the link with the detailed mass transfer model we have previously developed. The main consequence of this vision is that the global water transfer at the leaf level depends on physiological parameters l_s, a_s, and d_s indicating that the transfer of water is adapted to physiology and is species-dependent.

3.6 The new MELiSSA plant growth model - Summary

As stated in the introduction of this chapter, the structure of the initial MELiSSA plant growth model laid down by Hézard (2012) was kept and a fourth module dedicated to the energy balance was added. In this section, a summary of the equations discussed in the previous parts is given and equations used for computations are presented.

3.6.1 The morphological module

This was presented in section 3.3. The morphological components are proportional to the carbon biomass produced and to the species-dependent empirical constant parameters k_1, k_2, and k_3:

$$LA = \frac{k_1}{Y_{CX}\,\omega_{FX}}\,m_C \tag{3.76}$$

$$LAI = n_{plants}\,LA \tag{3.77}$$

$$L = 2\sqrt{\frac{LA}{\pi}} \tag{3.78}$$

$$L_{stem} = \frac{k_2}{Y_{CX}\,\omega_{FX}}\,m_C \tag{3.79}$$

$$N_{vessel} = \frac{k_3}{Y_{CX}\,\omega_{FX}}\,m_C \tag{3.80}$$

3.6.2 Free convection, conductance, and boundary layer

As detailed in part 3.4.6, the velocity associated with free convection is:

$$v_{free} = \sqrt{2g\,H\,\frac{\Delta\rho}{\rho}} \tag{3.81}$$

This vertical velocity is combined with the horizontal forced convection velocity to com-

pute the bulk velocity, which is the vectorial sum of these two velocities. As a result, the component of the bulk velocity that is parallel to the leaf (inclined of an angle α with the vertical direction) and used in the calculation of the boundary layer thickness is:

$$U_{bulk} = v_{free}\, cos\alpha + v_{forced}\, sin\alpha \tag{3.82}$$

The two options for the boundary layer thickness are the laminar boundary layer model and the surface renewal model:

$$\delta_{BL} = \frac{L}{0.664\, Re^{\frac{1}{2}}\, Sc^{\frac{1}{3}} + 0.76\, Gr^{\frac{1}{4}}\, Sc^{\frac{1}{3}}} \quad \text{Boundary Layer Model} \tag{3.83}$$

$$\delta_{SR} = \frac{L}{Re^{\frac{1}{2}}\, Sc^{\frac{1}{2}} + 0.76\, Gr^{\frac{1}{4}}\, Sc^{\frac{1}{3}}} \quad \text{Surface Renewal Model} \tag{3.84}$$

The surface renewal model is chosen and thus the boundary layer thickness computed in the model is:

$$\delta_X = 2\sqrt{\frac{\nu\, L}{U_{bulk}}} \tag{3.85}$$

For ease of computation in this study, a single boundary layer thickness is considered for all mass and heat transfers. The transfer coefficients are calculated from the thickness of the boundary layer.

$$k_X = \frac{D_X}{\delta_X} \tag{3.86}$$

The transfer coefficient of water at the leaf surface has an additional term accounting for stomatal resistance:

$$k_W = G = \frac{D_W\, a_s\, d_s}{l_s + \delta_W\, a_s\, d_s} \tag{3.87}$$

When considering heat transfer, Pr number replaces Sc number and the diffusivity is the thermal diffusivity in equations 3.83 and 3.84. The diffusion coefficients are taken from Sherwood, Pigford, and Wilke 1975:

$$D_{CO_2} = \frac{0.177\, 10^{-4}}{P} \left[\frac{T}{317}\right]^{3/2} \tag{3.88}$$

$$D_{O_2} = \frac{0.176\, 10^{-4}}{P} \left[\frac{T}{298}\right]^{3/2} \tag{3.89}$$

$$D_{H_2O} = \frac{0.242\, 10^{-4}}{P} \left[\frac{T}{293}\right]^{3/2} \tag{3.90}$$

$$D_T = \frac{\lambda}{\rho\, C_p} = \frac{0.2207\, 10^{-4}}{P} \left[\frac{T}{300}\right]^{1.81} \tag{3.91}$$

The diffusion coefficients are in $m^2.s^{-1}$, P is the total pressure in bars, T is the temperature in K. With these relations, partial pressures and temperature gradients in the vicinity of the surface are linked to the rates by:

$$N_X = \Phi_X\, LA = k_X\, \frac{LA}{R\, T}\, (p_{X_{leaf}} - p_{X_b}) \tag{3.92}$$

$$N_T = \Phi_T\, LA = k_T\, LA\, (T_{leaf} - T_b) \tag{3.93}$$

Partial pressures and temperature gradients are used to compute the density gradient, which is used to get the free convection velocity.

3.6.3 The physical and biochemical modules

As explained in part 3.5, in a first step, the maximum mass exchange rates are computed; they correspond to the mass exchange rates that would be occurring without any metabolic limitations. Then in a second step, stoichiometric tests enable to determine the limiting rate. Finally the real mass exchange rates are computed and used to compute the biomass production as well as the transpiration energy rate. As detailed in chapter 2, the maximum light absorption rate I^{max} (mol/s) is derived from the Beer-Lambert law and depends on the dimensionless light extinction coefficient k, the incident light flux I_0 (µmol/m^2/s), and the leaf area index LAI:

$$I^{max}_{canopy} = I_0\, (1 - e^{-k\, LAI}) LA \tag{3.94}$$

This equation is valid for a whole plant canopy, where light is intercepted by upper leaves. In the case where a single leaf model is used, the light absorption rate becomes:

$$I^{max} = I_0\, LA \tag{3.95}$$

In order to determine which rate is limiting, the CO_2 uptake rate is expressed according to the maximum light absorption rate, using the maximum quantum yield as determined in equation 3.7:

$$U^{Max_1}_{CO_2} = Y_{C_{photon}}\, I^{max} \tag{3.96}$$

This is valid for a single leaf model. When integrating over a whole canopy, it is necessary to divide the previous rate by the plant density n_{plants}:

$$U_{CO_{2_{canopy}}}^{Max_1} = Y_{C_{photon}} \frac{I^{max}}{n_{plants}} \tag{3.97}$$

The CO_2 maximum uptake rate (mol/s) depends on the leaf area LA, on the CO_2 diffusion coefficient D_{CO_2} in still atmosphere, and on the boundary layer thickness δ_X, and is driven by the CO_2 concentrations gradient (C_{int} is the internal concentration and C_{ext} is the bulk concentration):

$$U_{CO_2}^{Max_3} = \frac{D_{CO_2}}{\delta_X} LA\,(C_b - C_{leaf}) = \frac{D_{CO_2}}{\delta_X} \frac{LA}{R\,T_b}\,(p_b - p_{leaf}) \tag{3.98}$$

The maximum transpiration rate (mol/s) is driven by the water vapor concentration gradient and depends on the water vapor conductance as defined in equation 3.75 and on the leaf area:

$$\varphi_{H_2O}^{max} = G\,\frac{LA}{R\,T_b}(P^0(T_{leaf})\,RH_{leaf} - P^0(T_b)\,RH_b) \tag{3.99}$$

$P^0(T)$ is the saturating water vapor pressure at T, and RH_{leaf} and RH_b are respectively the leaf and bulk air relative humidity. This rate is also expressed as a CO_2 uptake rate in order to determine which rate is limiting.

$$U_{CO_2}^{Max_3} = \frac{1 - \omega_{W/H_2O\,X}}{\omega_{W/H_2O\,X}} \frac{\omega_X}{1 - \omega_X} \frac{M_{mol}^{H_2O}}{M_X}\,\varphi_{H_2O}^{max} \tag{3.100}$$

Finally the maximum water absorption rate (mol/s) is driven by the water potential gradient, and depends on the the stem length L_{stem}, on the number of sap vessels N_{vessel}, and on the vessels radius R_{vessel}:

$$U_{H_2O}^{max} = N_{vessel}\,\frac{\pi\,\rho_{mol}\,R_{vessel}^4}{8\,\mu\,L_{stem}}(\Psi_{ext} - \Psi_{int}) \tag{3.101}$$

μ is the nutrient solution dynamic viscosity, Ψ_{ext} and Ψ_{int} are respectively the water potential at the leaf surface and at the root interface. Since the favored plant growth technique for life-support systems is hydroponics, the water absorption flux shall never be limiting in these conditions, so the water potential gradient is taken very large with an order of magnitude difference between the two potentials. In the case of our parabolic

flight experiments, the plants are grown in agar, which provides all needed nutrients and water the plants need, so water absorption is not limiting in this case either. This rate is also converted to a CO_2 uptake rate:

$$U_{CO_2}^{Max_4} = (1 - \omega_{W/H_2O\,X})\,\frac{\omega_X}{1-\omega_X}\,\frac{M_{mol}^{H_2O}}{M_X}\,U_{H_2O}^{max} \tag{3.102}$$

The four rates $U_{CO_2}^{Max_i}|_{i=1..4}$ are compared and the lowest rate is set to be the CO_2 uptake rate. Then, the other rates (light absorption, water transpiration, and water absorption) are computed with respect to this limiting rate and using the same yields issued from the metabolic reactions analysis. This way, the stoichiometric limitations are taken into account within the model.

3.6.4 The energy balance module

The different terms accounting for the thermal energy balance at the leaf surface have been presented in Chapter 2. This is summarized as follows (in W):

$$E_{photons} = I^{max}\,N_A\,h\,c\,\sum_{i=300}^{700}\frac{\alpha_i}{\lambda_i} \tag{3.103}$$

$$E_{ray} = \varepsilon\,\sigma\,(T_{leaf}^4 - T_b^4)\,LA \tag{3.104}$$

$$E_{conv} = \frac{k_t}{\delta_X}\,(T_{leaf} - T_b)\,LA \tag{3.105}$$

$$E_{transpi} = \lambda_{mol}\,\varphi_{H_2O} \tag{3.106}$$

λ_{mol} is the latent heat of vaporization of water and φ_{H_2O} is the recalculated transpiration rate considering the selected limiting CO_2 uptake rate.The steady state thermal balance is obtained by solving the following equation:

$$Bilan = E_{photons} - E_{ray} - E_{conv} - E_{transpi} \tag{3.107}$$

The quantity "Bilan" is the energy balance of the leaf, later used to computed the leaf

temperature.

3.6.5 The transient state balance

Different time constants need to be considered. The most rapid phenomenon enables an interpretation of the transient evolution of the leaf surface temperature, given a morphological situation (fixed surface, length, planting density) and results from solving the energy balance in transient mode. As detailed in chapter 2 part 2.4:

$$\frac{dT_{leaf}}{dt} = \frac{Bilan}{Cp_{leaf}} = \frac{Bilan}{m_{H_2O}\, Cp_{H_2O}} \tag{3.108}$$

Cp_{H_2O} is the liquid water specific heat capacity at constant pressure (J.kg^{-1}.K^{-1}) and m_{H_2O} the leaf water mass (kg)
This equation is the basic equation for interpreting the effects of transient gravity levels on the leaf surface temperature. The second time constant is linked to plant growth itself. This is given considering the different yields, as it was done in the initial MELiSSA plant growth model:

$$\frac{dm_X}{dt} = M_X\, U_{CO_2} \quad (M_X = 27g.C - mol^{-1}) \tag{3.109}$$

$$\begin{aligned}\frac{dm_{H_2O}}{dt} &= M_{H_2O}\,(U_{H_2O} - \varphi_{H_2O}) \\ &= (Y^*_{H_2O\,X} + \frac{\omega_{W/FX}}{\omega_X})\, Y_{X\,CO_2}\, M_{CO_2}\, U_{CO_2} \quad (M_{CO_2} = 44g.mol^{-1})\end{aligned} \tag{3.110}$$

The yields here are for illuminated periods:

$$Y_{X\,CO_2} = \frac{1}{Y_{CO_2\,X}} = \frac{1}{1.63} \text{ and } Y^*_{H2_{O}\,X} + \frac{\omega_{W/FX}}{\omega_X} = 10.67 + \frac{10}{0.09}$$

These equations are then integrated using the function ode45 in Matlab, which is uses the method Runge-Kutta 4 or 5. This enables the computation of the morphological variables, leading to the transfer variables (light energy, surface temperature, mass transfer) and the integration continues on the given time frame. This code can be found in Appendix A.

3.7 Sensitivity analysis

Using the equations presented in section 3.6, we perform a sensitivity study on two time frames of certain variables to the forced convection velocity, to the gravity levels, to the light levels, to the leaf inclination, and to the transpiration ratio. The tested parameters are summarized in Table 3.3 and the parameters used or this study are summarized in Table 3.4. The initial state of the system is not necessary at equilibrium and the kinetic leading to a dynamical equilibrium of transfer velocities is studied. As shown through the results presented in this section, the variations of the boundary layer thickness and the free convection velocity are linked: indeed the boundary layer is computed as a function of the free convection velocity (Equation 3.85).

Table 3.3: Tested parameters in the sensitivity study.

Parameters	**Value**	**Unit**	**Comments**
Gravity	1.10^{-5}	$m.s^{-2}$	Weightlessness
	3.711	$m.s^{-2}$	Mars Gravity
	4.9035	$m.s^{-2}$	Half Earth Gravity
	9.807	$m.s^{-2}$	Earth Gravity - **Standard**
	19.614	$m.s^{-2}$	Twice Earth Gravity
Forced Convection	0	$m.s^{-1}$	No forced convection
	0.1	$m.s^{-1}$	
	0.5	$m.s^{-1}$	**Standard**
	1	$m.s^{-1}$	
Light Intensity	25	$\mu mol.m^2.s^{-1}$	Parabolic Flight
	400	$\mu mol.m^2.s^{-1}$	**Standard**
Leaf Inclination	0	rad	0°, Vertical Leaf
	0.52	rad	30° from vertical direction
	0.79	rad	45° from vertical direction - **Standard**
	1.05	rad	60° from vertical direction
	1.57	rad	90°, Horizontal Leaf
Transpiration Ratio	0.1	/	
	0.5	/	
	0.8	/	**Standard**
	0.99	/	

Table 3.4: Parameters used for the sensitivity study.

Parameters	**Value**	**Unit**
Bulk Air		
Temperature, T_b	293	K
Pressure, P_b	101300	Pa
Relative Humidity, RH	50	%
CO_2 concentration, $[CO_2]$	1000	ppm
Water vapor saturating pressure at T_b, $P^0(T_b)$	$2.3\ 10^3$	Pa

Parameters	**Value**	**Unit**
Air kinematic viscosity, ν	$1.8\ 10^{-5}$	$m^2.s^{-1}$
Ideal gas constant, R	8.314	$J.mol^{-1}.K^{-1}$
Bulk O_2 partial pressure, $p^b_{O_2}$	$0.2093\, P_b = 2.12\, 10^4$	Pa
Bulk CO_2 partial pressure, $p^b_{CO_2}$	$[CO_2]\, P_b = 101.3$	Pa
Bulk H_2O partial pressure, $p^b_{H_2O}$	$RH\ P^0(Tb) = 1.15\, 10^3$	Pa
Bulk N_2 partial pressure, $p^b_{N_2}$	$P_b - p^b_{O_2} - p^b_{CO_2} - p^b_{H_2O} = 7.88\, 10^4$	Pa
Molar mass O_2, M_{O_2}	$32\, 10^{-3}$	$kg.mol^{-1}$
Molar mass CO_2, M_{CO_2}	$44\, 10^{-3}$	$kg.mol^{-1}$
Molar mass H_2O, M_{H_2O}	$18\, 10^{-3}$	$kg.mol^{-1}$
Molar mass N_2, M_{N_2}	$28\, 10^{-3}$	$kg.mol^{-1}$
Morphology		
Ratio leaf area / fresh biomass, k_1	0.0044	$m^2.g^{-1}$
Ratio stem length / fresh biomass, k_2	$4.9\, 10^{-4}$	$m.g^{-1}$
Ratio number sap vessels / fresh biomass, k_3	0.0979	g^{-1}
Stomatal density, d_s	$1.4\, 10^8$	m^{-2}
Stomatal cross-sectional area, a_s	$170\, 10^{-12}$	m^2
Stomatal pore depth, l_s	$11\, 10^{-6}$	m
Physical		
Standard plant chamber length, H	1	m
Sap vessel radius, R_{vessel}	$4.8\, 10{-}5$	m
Leaf water potential, Ψ_{int}	-5000	Pa
Nutrient solution water potential, Ψ_{ext}	-120	Pa
Nutrient solution dynamic viscosity, μ	$1.3\, 10^{-3}$	Pa.s
Molar water vapour density, ρ_{mol}	41.58	$mol.m^{-3}$
Molar water heat capacity at P_b, Cp_w	75.327	$J.mol^{-1}.K^{-1}$
Diffusion coefficient of water vapour, D_w	$2.42\, 10^{-5}$	$m^2.s^{-1}$
Diffusion coefficient of CO_2, D_c	$1.7\, 10^{-5}$	$m^2.s^{-1}$
Diffusion coefficient of O_2, D_o	$1.76\, 10^{-5}$	$m^2.s^{-1}$

Parameters	Value	Unit
Biochemical		
Quantum Yield, $Y_{C_{photon}}$	0.054	$mol_C.mol_h^{-1}$
Dry matter content in plant, ω_X	0.09	$g_X.g^{-1}_{FX}$
C-molar mass, $BCmol$	27	$g.mol_C^{-1}$
Energy		
Avogadro number, N_A	$6.02\,10^{23}$	mol^{-1}
Planck Constant, h	$6.63\,10^{-34}$	J.s
Light speed, c	$3.0\,10^{8}$	$m.s^{-1}$
Emissivity, ϵ	0.97	/
Boltzmann constant, σ	$5.67\,10^{-8}$	$W.m^{-2}.K^{-4}$
Conduction coefficient, k_t	0.025	$W.m^{-1}.K^{-1}$
Latent Heat of vaporization, λ	40788.3276	$J.mol^{-1}$

3.7.1 Transient mode: two minutes

At first, the model sensitivity is studied on two-minute simulations. The leaf surface temperature, the boundary layer thickness, the free convection velocity, and the partial pressures of CO_2 and H_2O are computed for different values of the parameters listed above.

Sensitivity to the forced convection

The final leaf surface temperature varies linearly with respect to the forced convection value and it raises faster and reaches a higher value for lower values of forced convection (Figure 3.1). Indeed, for lower values of forced convection, the final boundary layer thickness is larger: with 0 m/s it is 47% higher than the one with 1m/s. This is correlated with CO_2 and H_2O partial pressures at the leaf surface: with lower forced convection and a higher boundary layer above the leaf, there are less gas exchanges with the bulk air leading to a depletion in CO_2 and a raise in water vapor. The graphs of the partial pressures show 2 distinct phases: the first one corresponds to a limitation through transpiration and in the second one the limiting rate is water absorption (Figure 3.1). The duration of the first

phase is shorter for higher values of forced convection. Since the free convection velocity depends on temperature and concentration gradients that are linked to gas exchanges rates, it is higher for lower values of forced convection. In all cases, the steady state value for the boundary layer thickness is reached after 2 minutes and it decreases faster for lower values of forced convection velocity (Figure 3.1).

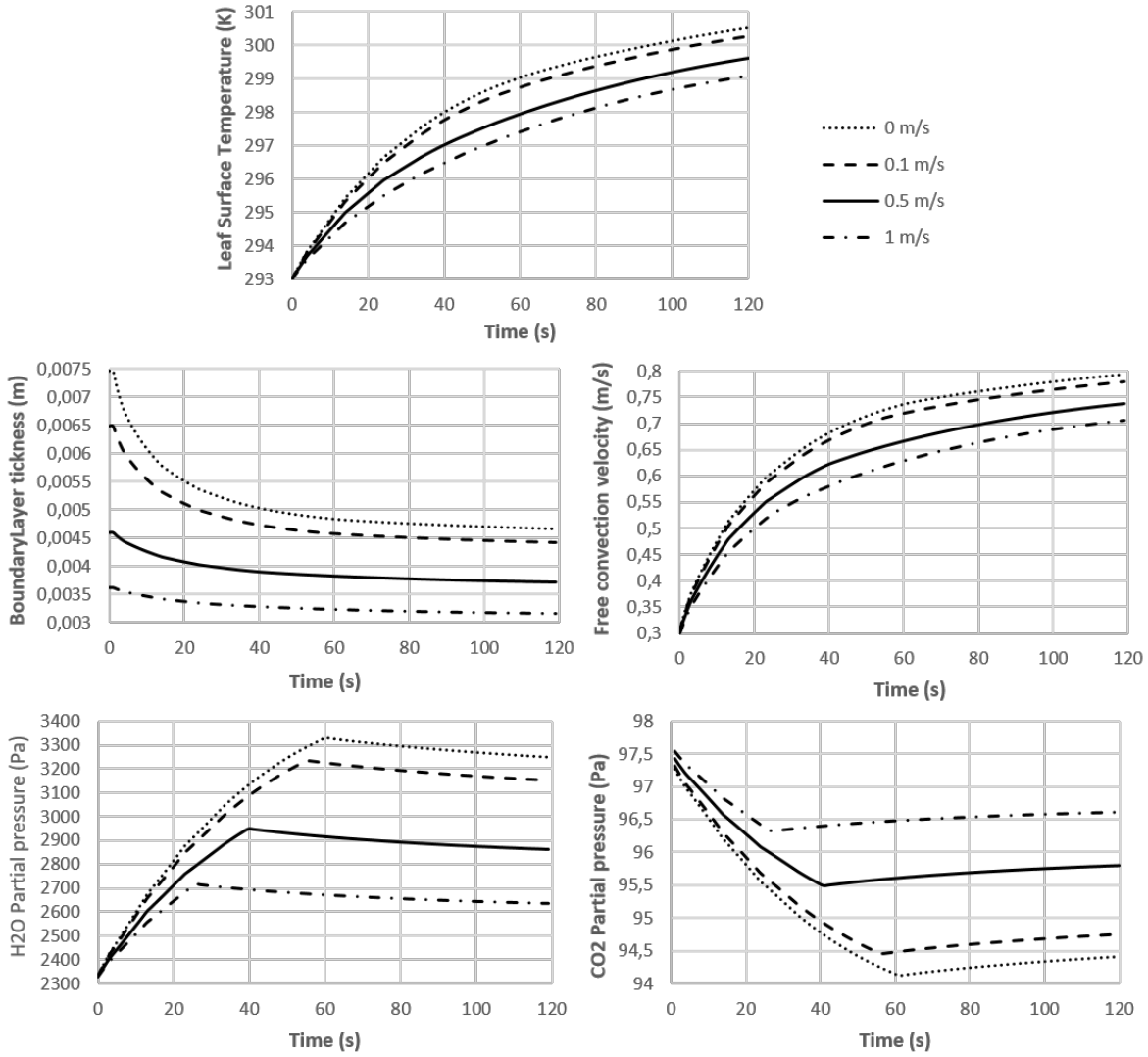

Figure 3.1: Leaf surface temperature, boundary layer thickness, free convection velocity and CO_2 and H_2O partial pressures evolution over 2 minutes for different forced convection velocity values.

Sensitivity to the gravity levels

The leaf surface temperature after 2 minutes is 1.8 K higher (0.6% more) in 0g than in 1g and 2.1 K higher (0.7% more) in 0g than in 2g (Figure 3.2). The difference in leaf surface temperature between the final temperature at 0.5g and 1g is equal to the one between the

final temperature at 1g and 2g, although the difference in gravity levels is twice as big. Hence the gravity influence is more significant for lower values and tends to be erased above 0.5g. The boundary layer thickness in 0g increases very slowly from 5.824 mm to 5.834 mm over the course of 2 minutes, whereas for other gravity levels, they decrease and reach their steady state value at 100 s. The difference between the various boundary layer thicknesses tends to decrease with higher levels of gravity (0.35 mm difference between the one at 1g and the one at 2g and between the one at 0.5g and the one at 1g). At 0g the final free velocity convection is in the order of 10^{-4} m/s while it is 0.7 m/s at 1g and 1 m/s at 2g, which is in accordance with results for the partial pressures (Figure 3.2). In 0g, the CO_2 (resp. H_2O) partial pressure decreases (resp. increases), which is due to the large thickness of the boundary layer and corresponding very low value of free convection, resulting in stagnant air above the leaf surface in which CO_2 is depleted and water vapor saturated because of poor convection. It is to be noted that the depletion of CO_2 and the increase of water vapor is more important in the case of 0g than in the case of no forced convection. In the partial pressures, the same trend is observed as in section 3.7.1: the limiting rate is transpiration and then water absorption and the transition time is reached later in 0g than for higher gravity levels (Figure 3.2).

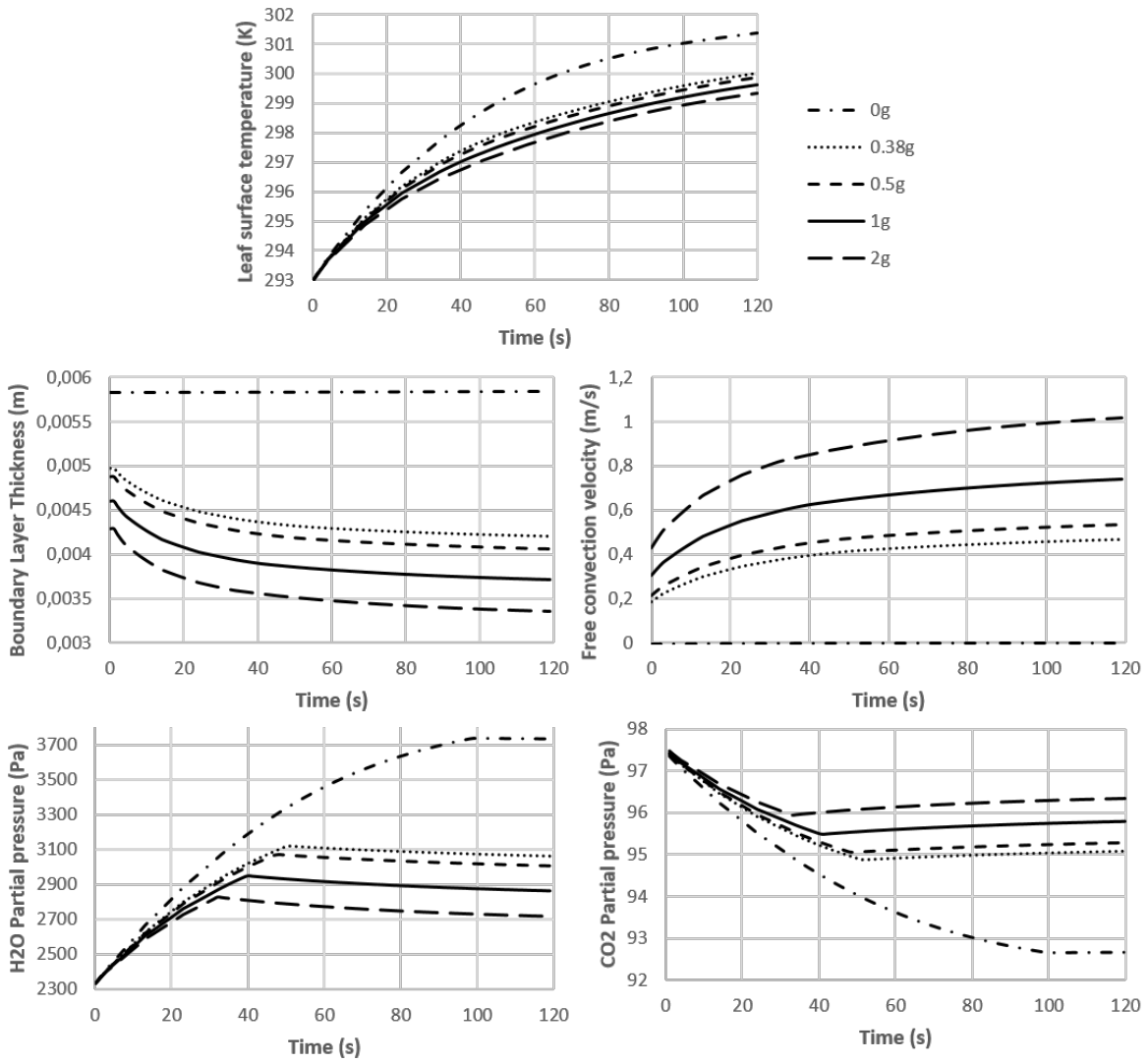

Figure 3.2: Leaf surface temperature, boundary layer thickness, free convection velocity and CO_2 and H_2O partial pressures evolution over 2 minutes for different gravity levels.

Sensitivity to the light levels

The leaf surface temperature barely changes and oscillates around the initial leaf temperature over the course of 2 minutes when light levels are 25 µmol.m^2.s^{-1}, whereas at 400 µmol.m^2.s^{-1}, it reaches 299.6 K following a trend that can be approximated to a second order polynomial with an R^2 of 0.99 (Figure 3.3). The boundary layer thickness (resp. free convection velocity) decreases (resp. increases) in both cases but is higher (resp. lower) for the lower light level case and they can be approximated to a linear decrease (resp. increase) with R^2 of 0.97 (resp. 0.99). In the lower light case, the limiting rate is the light absorption and hence the partial pressures of CO_2 and H_2O are constant, whereas the ones in the case of the higher light level follow the same trend as before: limited by

transpiration and then limited by water absorption (Figure 3.3).

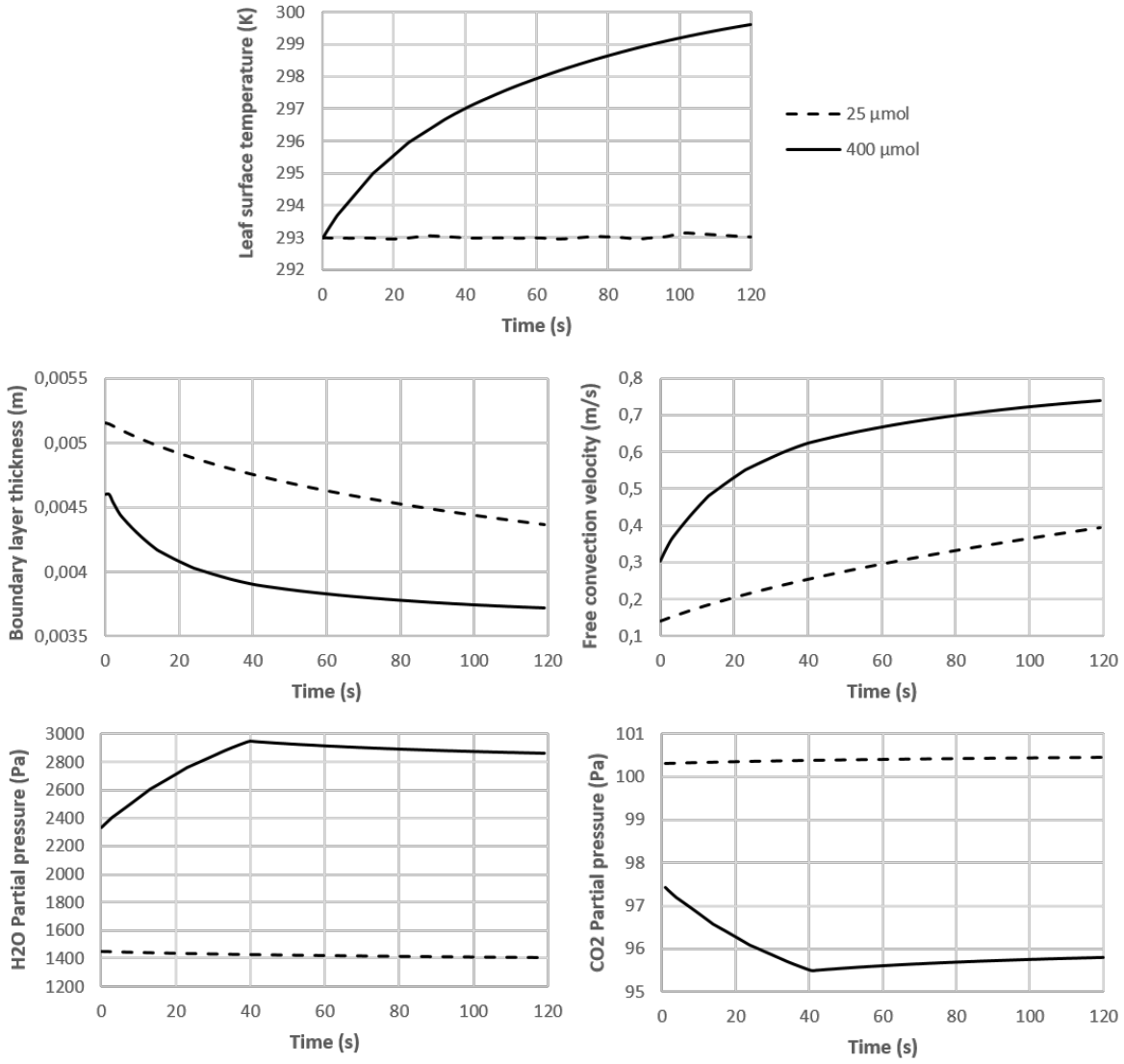

Figure 3.3: Leaf surface temperature, boundary layer thickness, free convection velocity and CO_2 and H_2O partial pressures evolution over 2 minutes for different light values.

Sensitivity to the leaf inclination

At 90° inclination, the leaf is horizontal, so the component of the bulk velocity that is parallel to the leaf surface is the forced convection only, and is thus smaller than for other leaf inclination values. Hence, the boundary layer thickness is constant over the course of 2 minutes and at the end is larger than all the other ones and the leaf surface temperature raises faster and reaches a larger final temperature, above 300 K (Figure 3.4). In the same fashion, when the leaf is vertical (0° inclination), the component of the bulk velocity that is parallel to the leaf is the free convection only, hence a final leaf surface temperature

higher and a faster raise in the leaf surface temperature. In this specific case, the free convection velocity reaches a value equal to the forced convection velocity at 15 seconds and is then higher than the forced convection velocity, hence a higher temperature for a horizontal leaf than for a vertical leaf (Figure 3.4). The boundary layer thickness of a vertical leaf becomes also smaller than for a horizontal leaf at 15 seconds. In terms of partial pressure, the depletion of CO_2 and increase in water vapor is most important for the horizontal leaf. The evolution of the leaf surface temperature for leaf inclinations from 30° to 60° are almost identical, with a relative difference of less than 0.05% in the final leaf surface temperature (Figure 3.4).

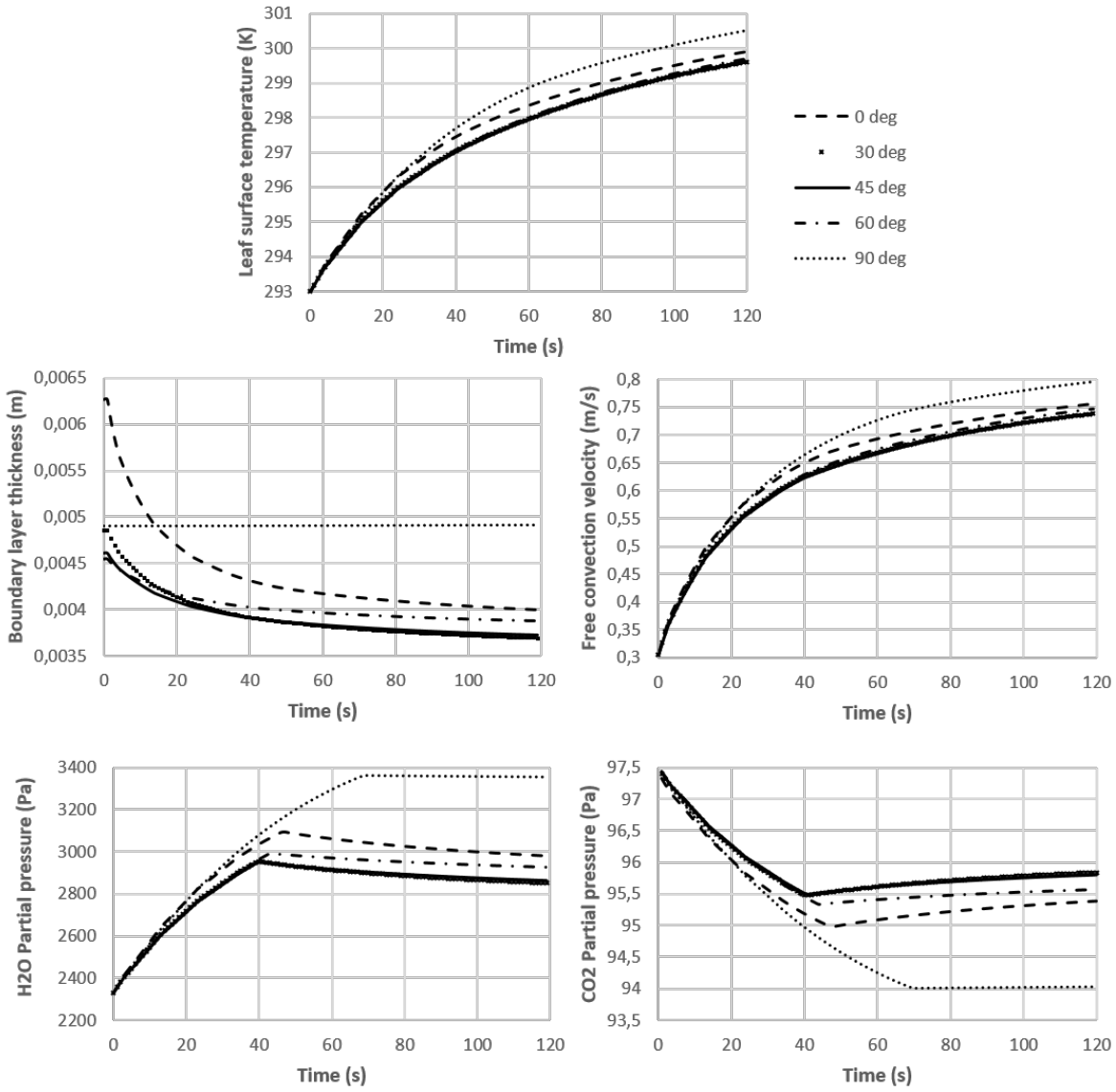

Figure 3.4: Leaf surface temperature, boundary layer thickness, free convection velocity and CO_2 and H_2O partial pressures evolution over 2 minutes for different leaf inclination values.

Sensitivity to the transpiration ratio

For a transpiration ratio of 0.99, the steady state leaf surface temperature is reached after 100 s, while for other ratio values, the steady state temperature is not reached after 120 s (Figure 3.5). Although the difference between the ratios 0.5 and 0.8 is smaller than between the ratios 0.1 and 0.5, the difference between the final temperatures for 0.1 and 0.5 is similar to the one between the final temperatures for 0.5 and 0.8. The evolution of the leaf surface temperature is hence not linear with respect to the transpiration ratio. The final temperature is highest for a transpiration ratio of 0.1, which also corresponds to the lowest partial pressure in water vapor at the leaf surface, barely varying over the course of 2 minutes (Figure 3.5). The free convection is highest and the boundary layer the smallest for this ratio. This underlines the two cooling mechanisms of a leaf: convection and transpiration and when the latter is too weak, the first one is not sufficient for cooling the leaf. For a transpiration ratio of 0.1, the limiting rate is first the CO_2 absorption (2 seconds) and it then switches to a light absorption limitation; for a ratio of 0.5 the light absorption rate is limiting, which explains the behaviour of the partial pressures at the leaf surface; for Tr = 0.99, the limiting rate is the transpiration; and for Tr = 0.8, it is first transpiration and then water absorption (Figure 3.5).

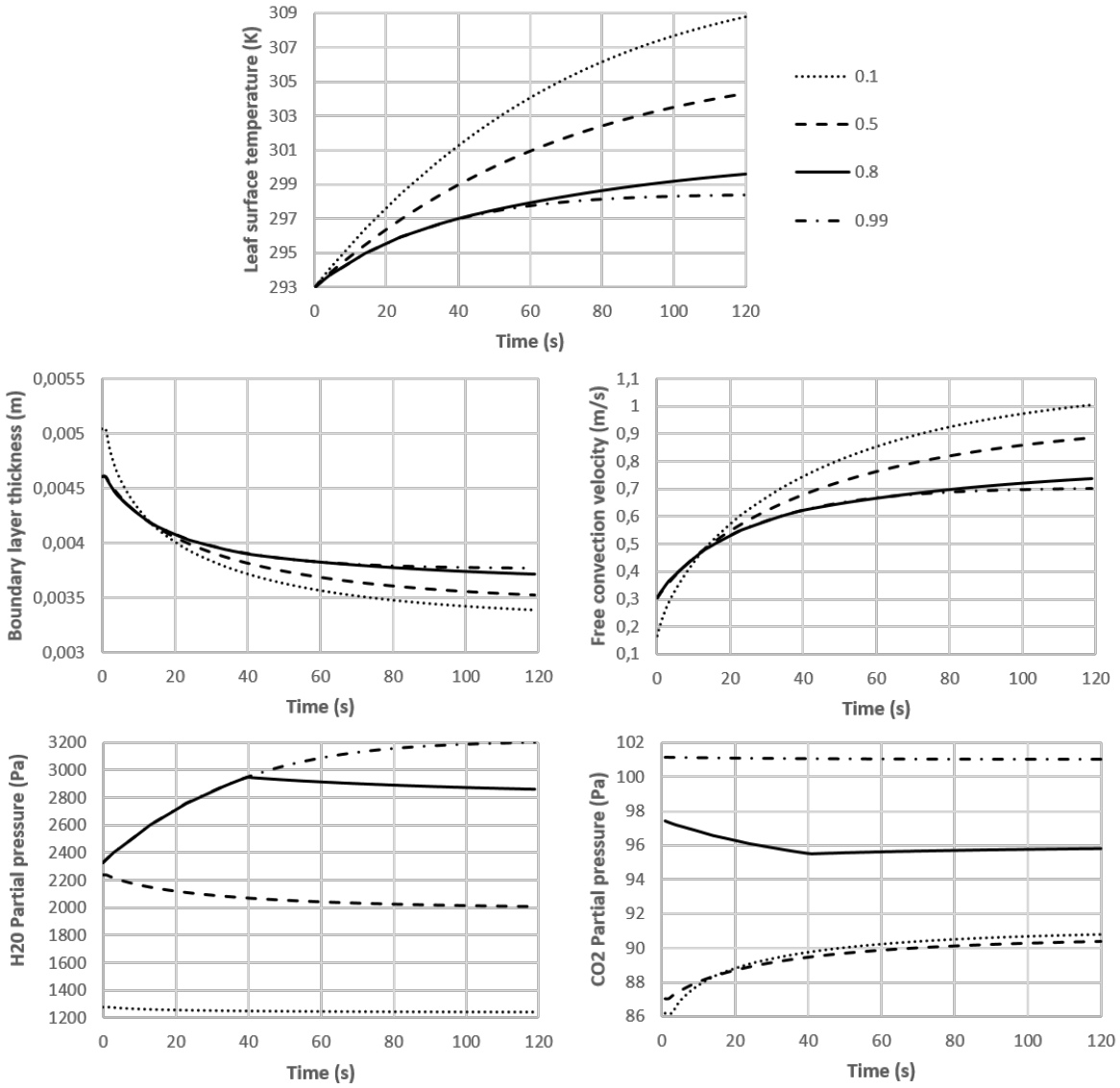

Figure 3.5: Leaf surface temperature, boundary layer thickness, free convection velocity and CO_2 and H_2O partial pressures evolution over 2 minutes for different transpiration ratios.

3.7.2 Steady-state mode: one hour

Following the same approach, the model sensitivity is studied on on-hour simulations. The leaf surface temperature, the boundary layer thickness, the free convection velocity, and the partial pressures of CO_2 and H_2O are computed for different values of the parameters listed above.

Sensitivity to the forced convection

As observed in the transient analysis, the limiting rate is first the transpiration rate and then the water absorption rate, explaining the evolution of partial pressures at the leaf surface (Figure 3.6). The amplitudes in partial pressures are larger for the lowest forced convection velocities, which increases the density gradient and thus the free convection velocity. However, this increase of the free convection for low values of forced convection is in the order of magnitude of the highest values of forced convection tested here, consequently the total bulk velocity is still smaller for low values of forced convection, and hence the boundary layer thickness is larger (Figure 3.6). For all values tested, the leaf surface temperature shows a rapid increase followed by a steady increase over the course of an hour, the highest values occurring for the lowest values of forced convection.

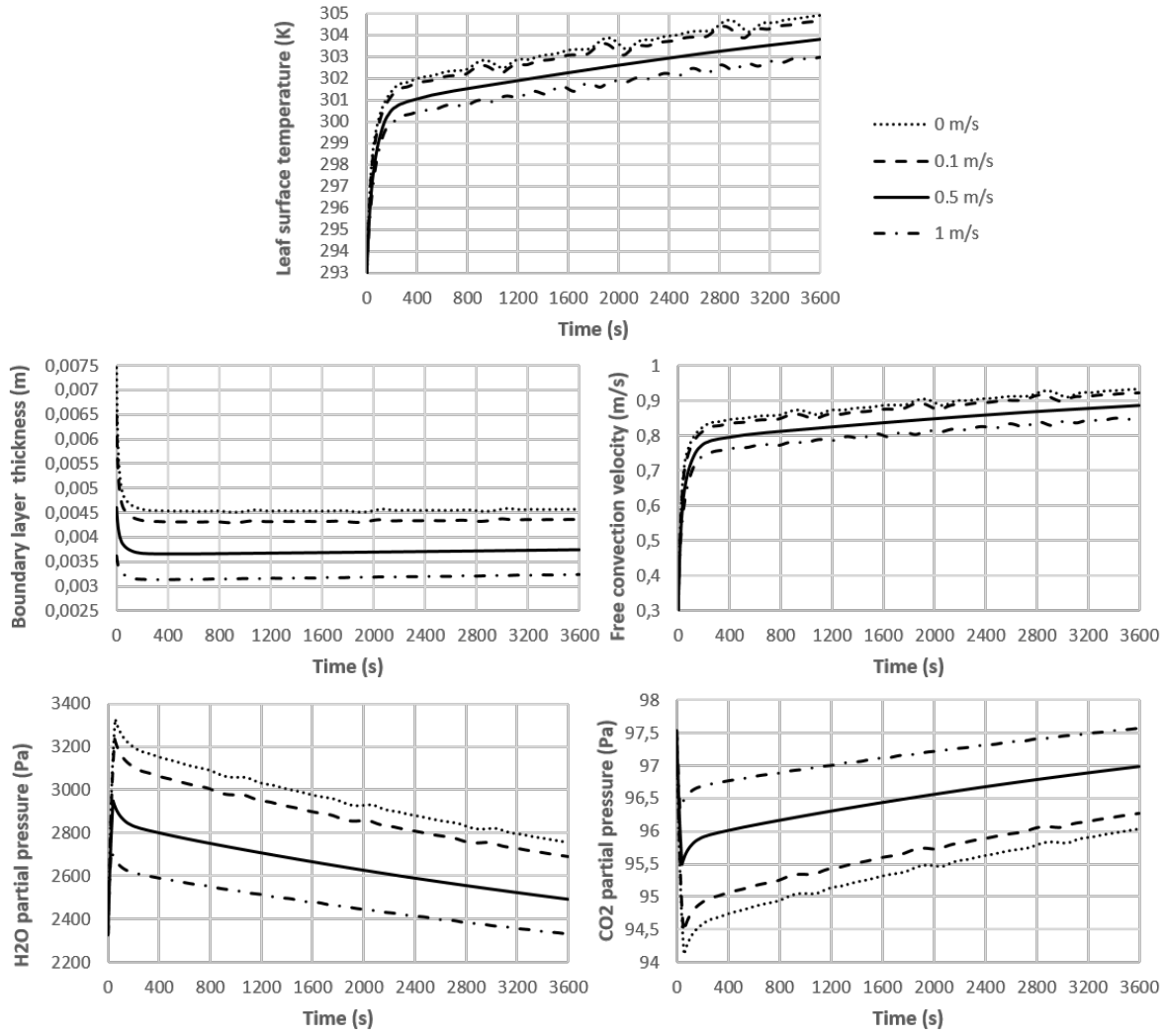

Figure 3.6: Leaf surface temperature, boundary layer thickness, free convection velocity and CO_2 and H_2O partial pressures evolution over one hour for different forced convection velocity values.

Sensitivity to the gravity levels

The evolution of the boundary layer thickness is the same as the one over two minutes: all thicknesses decrease and reach a steady-state value except the one at 0g, which steadily increases (Figure 3.7). It is twice as big in 0g than in 2g and is about 50% larger in 0g than in 0.38g and 0.5g. The free convection velocity remains in the order of magnitude of 10^{-4} at 0g, whereas it steadily increases in other gravity levels, after a rapid increase over the first 140 to 200 seconds (Figure 3.7). The limiting rates are similar, as reflected by the partial pressures of CO_2 and water vapor: first the transpiration and then the water absorption. The final leaf surface temperature after an hour in 0g is about 2K higher than the ones for other gravity levels. Oscillations in the leaf surface temperature correspond

to the same oscillations observed in the free convection velocity (Figure 3.7).

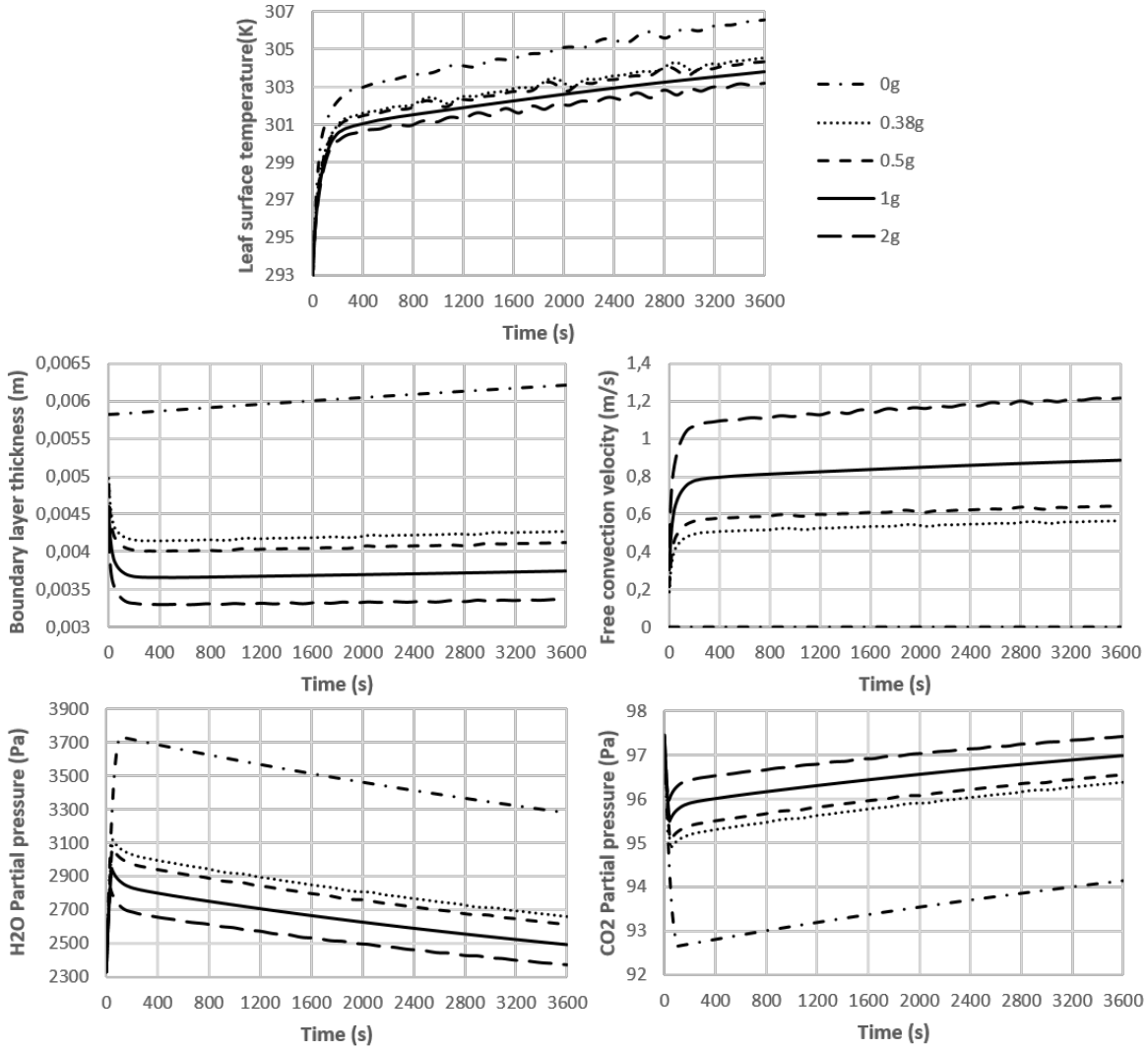

Figure 3.7: Leaf surface temperature, boundary layer thickness, free convection velocity and CO_2 and H_2O partial pressures evolution over one hour for different gravity levels.

Sensitivity to the light levels

At 25 µmol.m^2.s^{-1}, the limiting rate remains the light absorption over an hour, hence the quasi constant partial pressures of CO_2 and water vapor at the leaf surface (Figure 3.8). The free convection velocity oscillates around 0.15 m/s while the one at 400 µmol.m^2.s^{-1} starts at 0.3 m/s and steadily increases; the boundary layer thickness at the lower light level oscillates around 5 mm, while it decreases under 4 mm at the higher light level. Finally, the leaf surface temperature oscillates around 293.4 K for the lower light level and increases exponentially until 250 s then steadily for the higher light level (Figure 3.8).

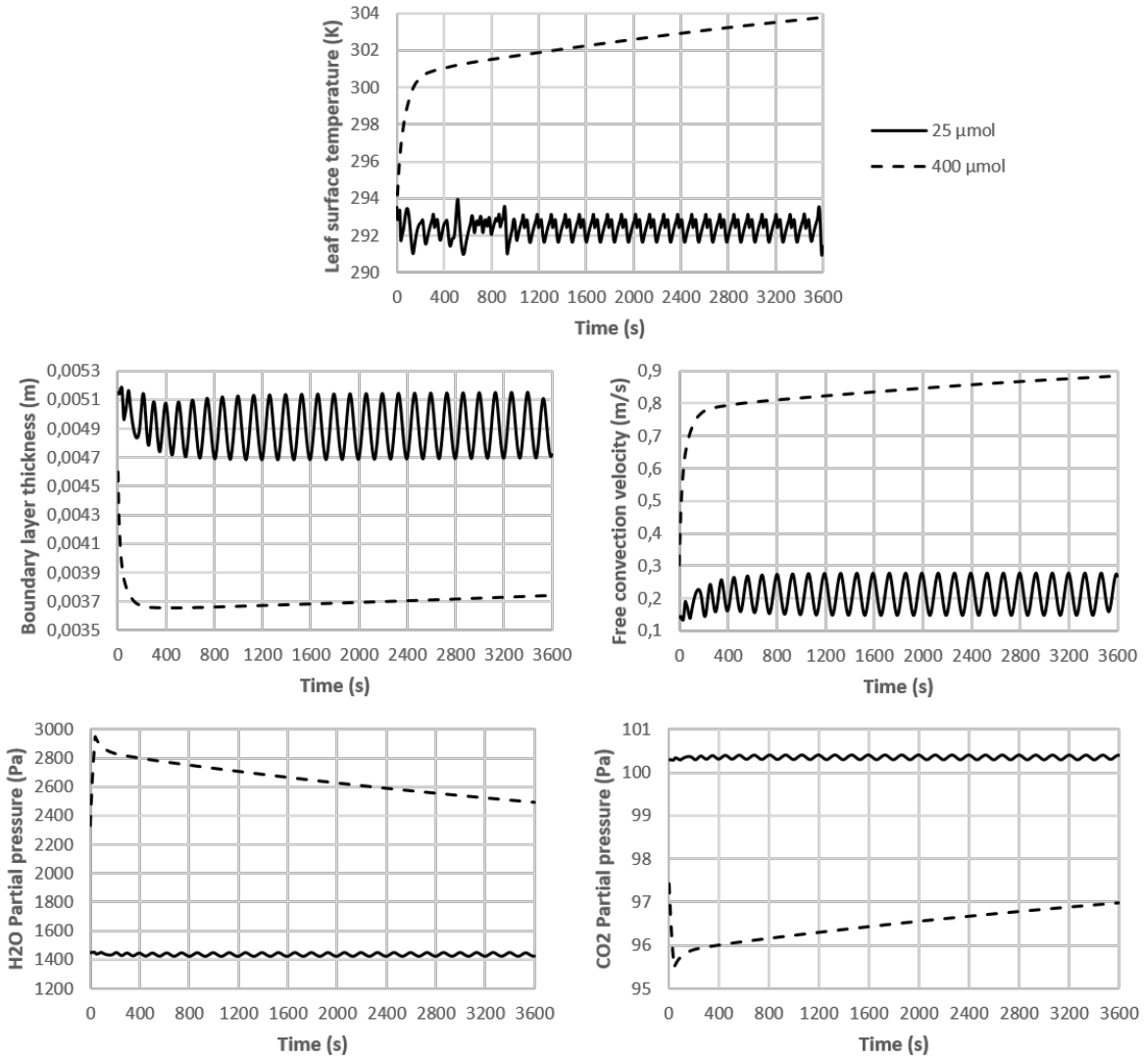

Figure 3.8: Leaf surface temperature, boundary layer thickness, free convection velocity and CO_2 and H_2O partial pressures evolution over one hour for different light values.

Sensitivity to the leaf inclination

Like it was highlighted in the transient analysis, the highest leaf surface temperature is for a horizontal leaf, with about 2 K more than temperatures for other inclinations (Figure 3.9). In all cases the leaf surface temperature increases exponentially and a steady increase follows starting at 220-250 seconds. The boundary layer thickness is 1mm larger than for all other inclinations and when all other decrease until a steady-state value, the boundary layer thickness on a horizontal leaf steadily increases, which is similar to its behaviour in 0g. The free convection is also highest for a horizontal leaf (0.1 m/s more than for other inclinations), since it is linked to concentration and temperature gradients and the variations in CO_2 and H_2O partial pressures are the largest for a horizontal

leaf. The limiting rates are the same as before: transpiration and then water absorption (Figure 3.9).

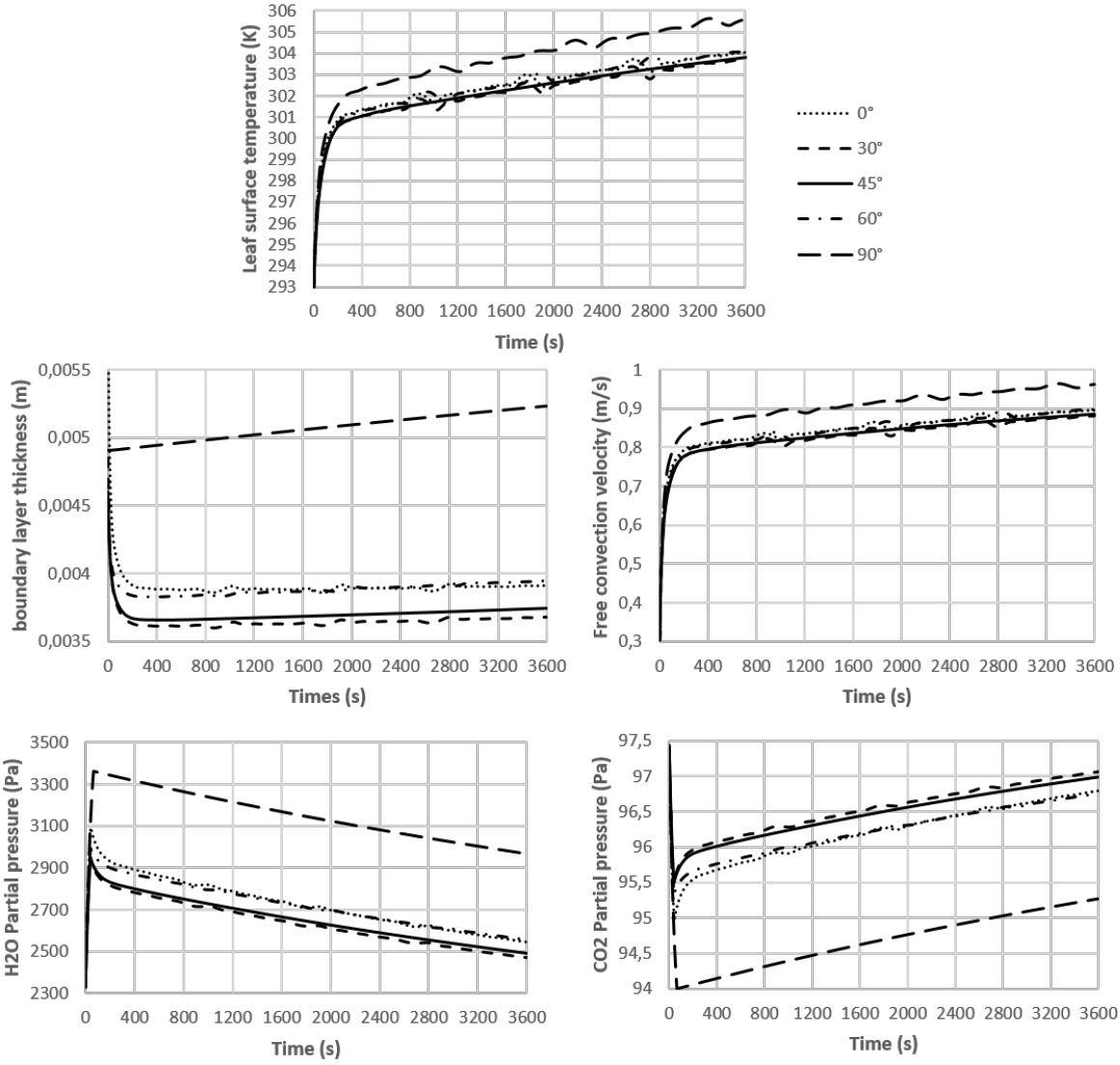

Figure 3.9: Leaf surface temperature, boundary layer thickness, free convection velocity and CO_2 and H_2O partial pressures evolution over one hour for different leaf inclination values.

Sensitivity to the transpiration ratio

The limiting rate for the ratio at 0.1 is the light absorption; at 0.5, the CO_2 absorption rate is limiting until 1090s, then by the water absorption rate; at 0.8 the transpiration rate is limiting and then the water absorption rate; and at 0.99, the transpiration rate is limiting. This explains the different behaviours of the partial pressures at the leaf surface (Figure 3.10). The highest temperature is reached for the lowest transpiration ratio and

the behavior is similar for all ratios: a rapid increase and then a steady increase (0.1 to 0.8) or an oscillation around the steady state value (0.99). These oscillations around a steady-state value are also found in the water vapor partial pressure, in the boundary layer thickness, and in the free convection velocity, for a ratio of 0.99. It is interesting to note that after an hour, the boundary layer thicknesses for all ratios reach the same value of 3.8 mm, which was not the case in any of the simulations before (Figure 3.10). This highlights the fact that even though the boundary layer thickness plays a crucial role in gas exchanges at the leaf surface, the phenomena of heat and mass transfer are multi-factor phenomena, depending on the temperature gradient between the leaf surface and the bulk air, on the free convection velocity generated by concentration gradients resulting from gas exchanges dependent on the transpiration ratio.

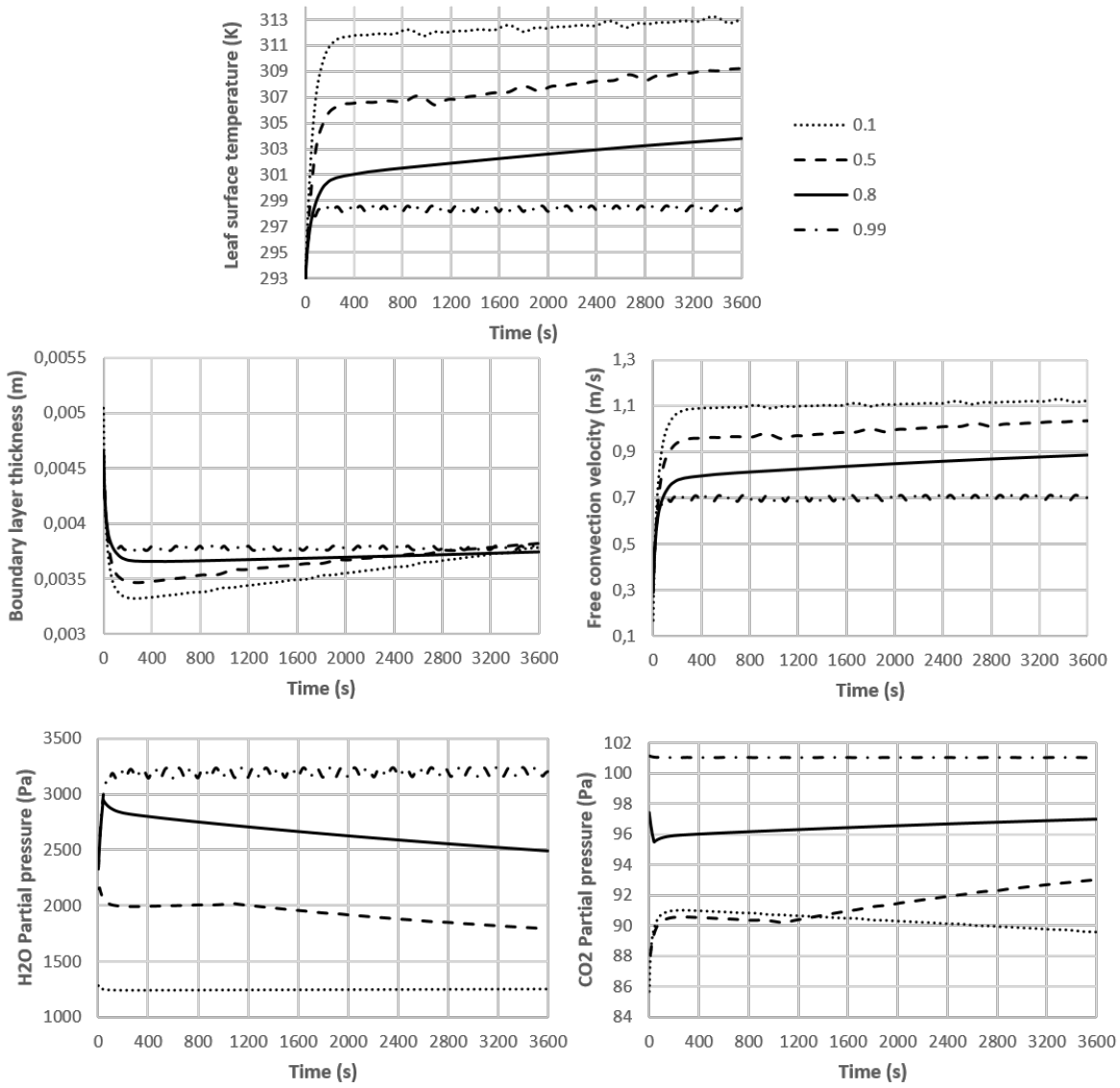

Figure 3.10: Leaf surface temperature, boundary layer thickness, free convection velocity and CO_2 and H_2O partial pressures evolution over one hour for different transpiration ratios.

3.8 Conclusion

The new model developed here is a mechanistic model and an update of the initial MELiSSA plant growth model. Many parameters that were previously empirically defined are now defined with a mechanistic expression. It enables to take into account the influence of gravity on plant growth and to account for physical limitations due to the convection regime, the light intensity, the transpiration of water movements in the stem. In chapter 2, the boundary layer was modelled in a very basic way and here we explored

new ways of modeling it in order to have a more detailed description, leading also to a more detailed expression of the free convection velocity. The sensitivity analysis revealed that leaf surface temperature, boundary layer thickness, free convection velocity, and leaf partial pressures are not sensitive to leaf inclination, unless the leaf is horizontal. It also revealed that these variables are more sensitive to a weightless environment (with a standard forced convection velocity) than to an environment with no forced convection (but in 1g). The sensitivities to light and transpiration ratio are also very high, since these parameters have direct influences on transfer limitations. Finally, this model puts into light the leaf surface temperature, which is a new variable of the model that is sensitive to gravity levels and can be directly measured, giving information about local gas exchanges. This is what is detailed in chapter 4.

3.9 Chapter's outcomes

- Mechanistic physical transfer models are generally averaged on a surface but they can be used for accurate local transfer studies.
- The new model presented in this chapter is mechanistic.
- Changes compared to the initial MELiSSA plant growth model include:
  - The definition of the boundary layer with the surface renewal model and not as an empirical entry parameter of the model;
  - This implies the explicit definition of the free convection velocity, which is a function of gravity and of gas density gradients.
  - The coupling of mass and energy balances introduces time-dependent variations of the leaf surface temperature.
- The sensitivity analysis of the model revealed a strong sensitivity to leaf inclination and to low gravity levels.

Chapter 4

Model validation

4.1 Introduction

As stated in chapters 1 and 2, past experiments on different space stations such as MIR or the ISS (Monje et al. 2000; Monje, G. Stutte, and Chapman 2005) and in parabolic flights (Kitaya et al. 2001; Hirai and Kitaya 2009) have show that poor ventilation or lack of ventilation in spaceflight induces stagnant air boundary layers with decreased conductance around the leaves due to the lack of natural convection in weightlessness. The mechanisms of natural convection were also reviewed in chapter 2 (part 2.9) and it was established that natural convection is the result of buoyancy gradients, which are direct consequences of Earth gravity and hence decrease in lower gravity levels and disappear in weightlessness. The resulting deficiency in optimal gas exchange is directly linked to photosynthetic activity (CO_2 uptake and O_2 release) and also to transpired water that regulates leaf temperature. Kitaya et al. observed a 1°C increase when gravity levels decreased from 1g to 0.01g during a parabolic flight experiment in 2001 (Kitaya, Hirai, and Shibuya 2010). On the contrary in 2g, the boundary layer around the leaf is smaller, promoting gas exchanges compared to 1g, and leading to a decrease in the leaf surface temperature. Later experiments on the ISS showed that plant gas exchange processes and photosynthesis occur normally in weightlessness when adequate ventilation is provided (Monje, G. Stutte, and Chapman 2005). A ground experiment showed that above a certain threshold of 0.2 m/s air current velocity, leaf gas exchange is not limited by convection (Kitaya et al. 2003b). But in large-scale plant production in space, it will be impossible to have a homogeneous airflow distribution and thus a perfectly ventilated

chamber. Therefore, locally, there will be regions with reduced convection and thus slower gas exchange, leading to leaf temperature increase.

The gas exchanges model described in chapter 3 needs to be validated locally at the leaf scale, in time-dependent and in steady state, for different ventilation and gravity levels. The available data on plant gas exchanges in 0g is quite limited and the one available is not quantitative enough on local gas exchanges to enable a thorough validation (Monje et al. 2000; Monje, G. Stutte, and Chapman 2005; G. W. Stutte et al. 2005). Hence, an experiment in parabolic flight that enables local measurements was imagined and flew in October 2017.

The objective of this chapter is to validate a complete detailed model of coupled radiative, mass and heat transfers and their potential crossed limitations at the leaf level. Ultimately this is linked to the initial MELiSSA holistic plant growth model, but the objective here is to experimentally verify that the onset of the different limitations, including gravity induced limitations, are correctly represented by the modeling approach that has been previously proposed.

Inspired from the experiments of early 2000s done by Kitaya et al. with a thermal camera measuring leaf surface temperature of barley and sweet potato leaves, the aim of the experiment presented hereafter was to measure the surface temperature of spinach leaves using infra-red (IR) cameras. These measurements are commonly used in agronomy (Jones et al. 2009) to indirectly assess stomatal conductance and relate to drought tolerance and water stress. Indeed stomatal conductance is directly linked to stomatal aperture, i.e. water vapor release, and thus leaf surface temperature. Originally stomatal conductance was assessed with porometer measurements but IR measurements have been proved to give accurate measurements of stomatal conductance using some corrections for air temperature, leaf angle, etc., are less time-consuming, and can be automated, leading to the analysis of a greater number of replicates. Leaf surface temperature can be linked to the leaf evaporation and knowing the Water Use Efficiency (WUE), it can be linked to CO_2 assimilation and thus photosynthesis, i.e. gas exchanges.

IR cameras have made progresses in the past 20 years and their sizes have drastically decreased, from 30 cm long and 3 kg in 2000 to 6 cm long and 500 g nowadays. The IR cameras used in this experiment weight 100 g and are operated via an Android phone. Consequently, when early experiments could only study one replicate in one flight, this

experiment enabled the study of four spinach plants simultaneously. Using Android devices, which are daily used items, and commercial-of-the-shelf (COTS) IR cameras for data acquisition is the novelty and originality of this experiment.

This study is the result of the fruitful collaboration between two PhD candidates of University of Bremen (Helia Sharif in Space robotics and Vasiliki Kondyli in Human-centered habitat design) and two candidates at University Clermont Auvergne, from two different laboratories, Antoine Vernay from INRA-PIAF (Physique et Physiologie Integrative de l'Arbre en environement Fluctuant) and Lucie Poulet from CNRS-Institut Pascal. The wide range of skills and background in the team enabled to design an experiment that could give accurate physiological results, while using cutting-edge measurement technologies.

The participation in CNES 131th parabolic flight campaign in October 2017 was enabled by the program CNES Paraboles through which the team was selected. The project was also selected to participate in ESA 69th and 70th parabolic flight campaigns in April and November 2018. Between the first two campaigns, the design of the experiment was improved but only results from the first campaign are presented here, since the second campaign happened at the moment of this manuscript writing.

The primary aim of this study was to expand on results obtained in the past by quantifying spinach plants' leaf surface temperature (directly linked to local leaf gas exchanges) as a function of gravity levels and different low airflow velocities, in order to validate the gas exchanges mechanistic model presented in chapter 2, accounting for local conditions of convective heat and mass transfer rates. We hypothesized that (i) leaf surface temperature would increase in weightlessness and (ii) a higher air flow velocity would decrease boundary layer thickness, fostering heat and gas exchanges which would lead to decrease leaf surface temperature.

The experimental set-up and the results, which can mainly validate some trends in the model and identify phenomena and parameters, are presented in this chapter. Finally lessons learned from the flaws of this experiment are discussed and a new design is presented.

4.2 Materials and Methods

4.2.1 Parabolic Flight

The experiment took place onboard the Novespace A310 ZEROG aircraft (modified A310), in the frame of the CNES Parabole program, in October 2017. The flight lasted 3 hours from takeoff to landing. The total pressure during the flight was on average 850.7 hPa with a standard deviation of 1.3 hPa. There were a total of 31 parabolas (see flight pattern on Figure 4.1), during which there was about 20 seconds of weightlessness, preceded and followed by two phases (about 20 seconds) at 1.8g (see acceleration data for a single parabola on Figure 4.2).

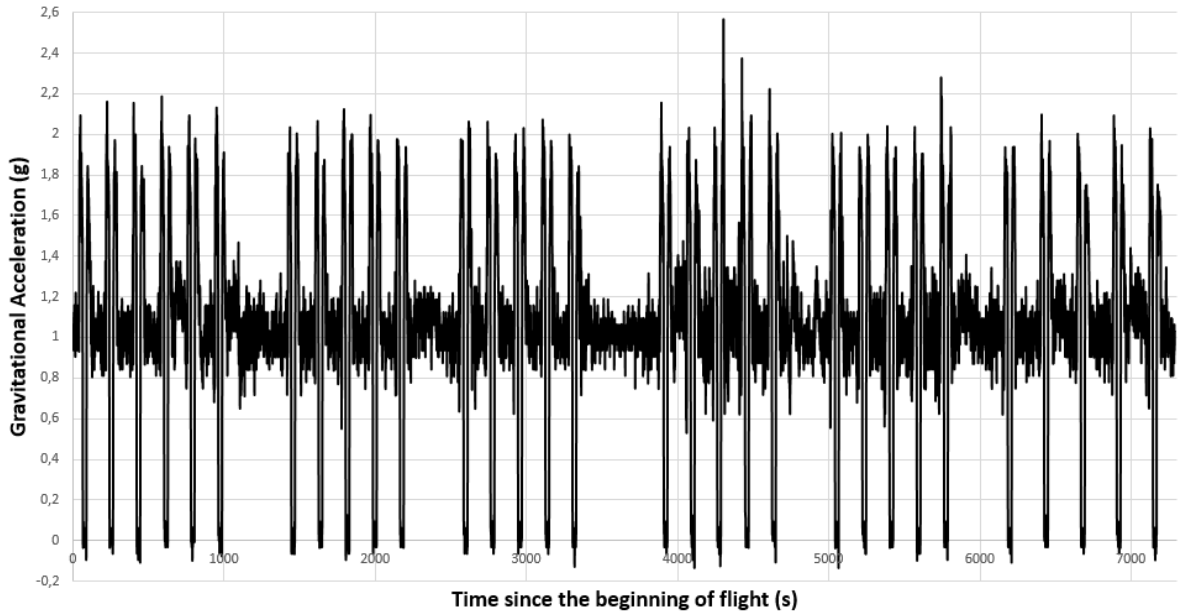

Figure 4.1: Whole flight gravity profile with the 31 parabolas.

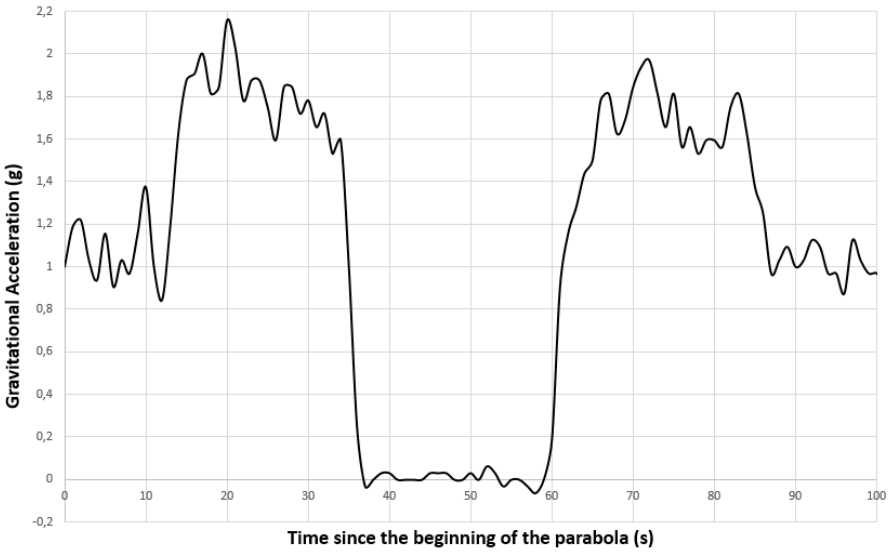

Figure 4.2: Gravitational acceleration during the second parabola.

4.2.2 Experimental set-up

An enclosure with dimensions 50 cm x 40 cm x 30 cm was custom-built by the company EJM Plastic® (Cournon d'Auvergne, France). It is made of 1-cm thick opaque black polyethylene (0.96 g/cm^3) and a lid of 1-cm thick transparent polycarbonate (1.20 g/cm^3) equipped with handles and latch clamps (Figure 4.3).

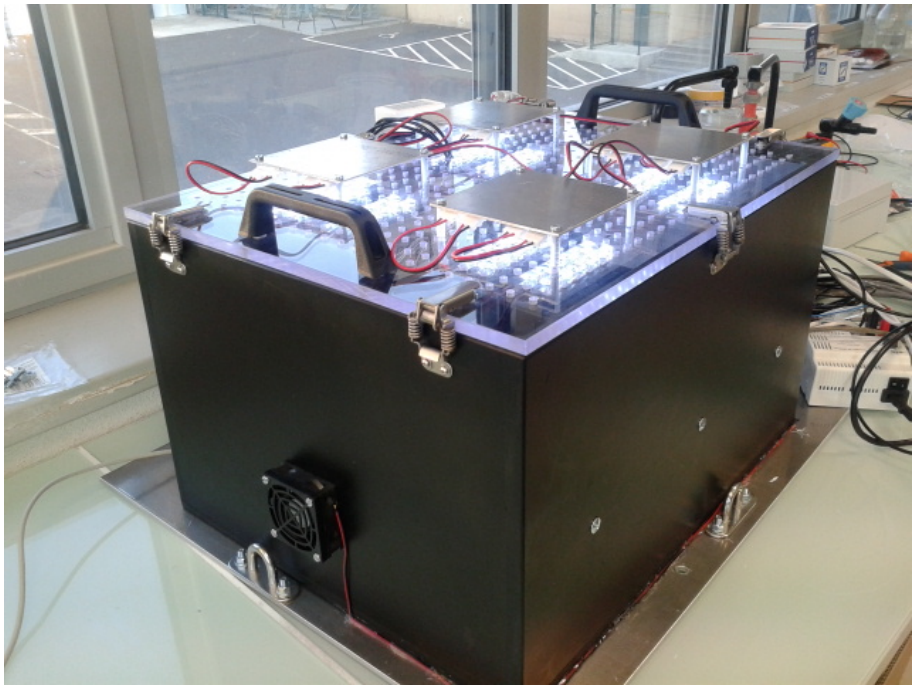

Figure 4.3: Experimental set-up with lights on. Enclosure from EJM Plastic with fans on the side and LED lighting system on top of the lid.

Two inlet fans (San Ace 60 9GA0612P7H01) bring cabin-air inside the enclosure, which is homogenized thanks to perforated plates located 5 cm from each fan and exits the enclosure through the perforated lid. This way, the ventilation inside the enclosure can be modified to 5 different values according to the input voltage (0V, 4.5V, 6V, 7.5V, and 12V). The holes of the perforated plates and of the lid measure 5 mm in diameter and are spaced of 2 cm. LED lights (see part 4.2.5) for detailed description) are placed outside of the enclosure on top of the lid and the inside of the enclosure is covered with aluminum tape for a better light diffusion. Inside the enclosure, four 3D-printed frames containing a grid of nylon thread to keep leaves horizontal during the flight and hygrometer holders, are held on two aluminum bars. Each of the four pots containing spinach plants is set centered under a 3D-printed frame and under an Infra-Red (IR) camera, so that the studied leaves are 13 cm under the IR cameras (Figure 4.4).

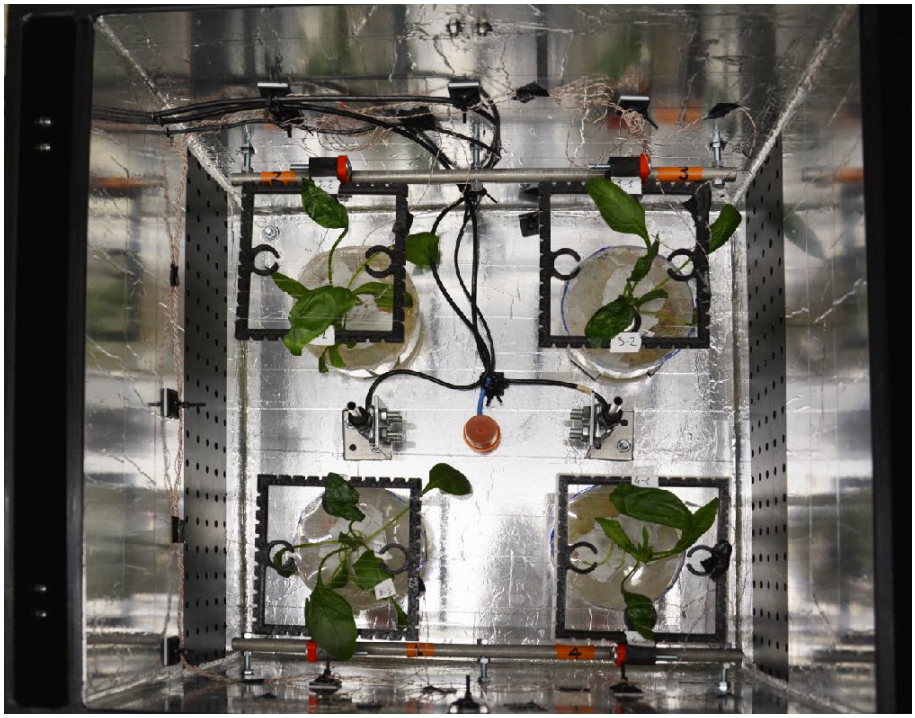

Figure 4.4: Inside the enclosure: Spinach plants under 3D printed frames equipped with hygrometer holders and nylon thread to hold the leaves horizontally. On both sides, the perforated plates are shown.

For safety reasons, the enclosure was strapped with two ropes (Figure 4.5) and the experimental set-up as a whole (enclosure plus Campbell data logger and power supplies) was set onto an aluminum plate (5mm thick) with dimensions 750 mm x 545 mm in a sealed rack (800 mm X; 600 mm Y; and 600 mm Z) provided by CNES Education (Figure 4.6).

All items were secured with 3M Velcro Dual lock (ref SJ3550).

Figure 4.5: Inside the rack: the enclosure is wrapped in ropes and fixed on a aluminum plate.

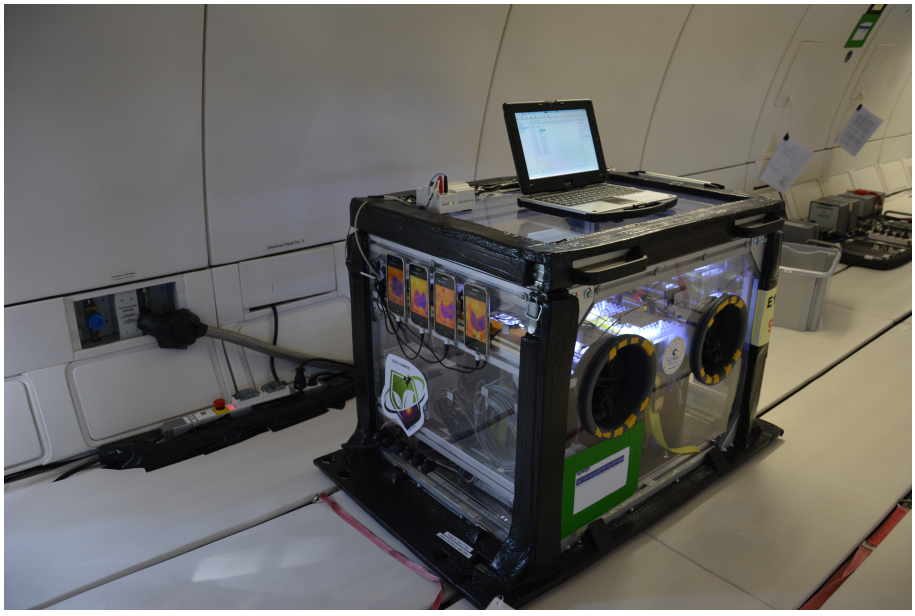

Figure 4.6: Experimental rack in the A310 ZEROG plane. The whole experimental set-up is inside, except for the phones and the laptop computer.

4.2.3 Spinach plants and agar gel

Based on criteria of i) photosynthesis efficiency, ii) size and shape of leaves, iii) easiness to grow, iv) size of the plant, and v) edibility, the choice of plant has been set on spinach (Spinacia Olerasea L.), cultivar “Monstrueux de Viroflay” (batch XD 545).

To avoid any fungi or bacterial contamination, the plants were cultivated under sterile conditions and seeds were sterilized before being sowed into each pot, in accordance with the following protocol:

- One-minute washing in a 70% ethanol solution
- Ten-minute washing in a bleach solution
- Three times five-minute rinsing in sterile water solutions

The plants were grown for 5 weeks within a growth chamber (photoperiod: 16h day/8h night, constant temperature of 21°C) in a solid agar solution (see Appendix B for agar recipe), which provides a good control of nutrient release to the roots thus preventing nutrient stress, while enabling them to absorb the needed water. One seed per pot was sowed into 60 sterile pots (diameter 11cm, height 14cm) containing 400 mL of agar solution and each pot was closed with lids equipped with filters which allowed gas exchanges and prevented external contamination 4.7.

Figure 4.7: Agar-grown 6-week old spinach plants. On the lid the filter enables gas exchanges and blocks potential contamination.

The twenty best-developed spinach plants were brought to the parabolic flight campaign site in Novespace (Bordeaux, France) and from these twenty plants, only four were used in the parabolic flight, the ones with the largest leaves. One leaf per plant was covered

on both sides with nail polish to prevent gas exchanges and block transpiration (non-transpiring leaf). The procedure was as follows:

- Five days before the flight: lids opening to allow the plants for acclimation to ambient air conditions.
- Three days before the flight: pots cutting to agar level (height of about 4 cm) to allow the spinach shoots to straighten in ambient air conditions.
- One day before the flight: lids sealing around the plants' stem using thermo-glue and Terostat (Teroson ®) to prevent water evaporation from the agar solution to the enclosure air.
- Morning of the flight: nail polish applied on one leaf per plant to stop gas exchanges on this leaf so that it serves as a control.

A contamination happened in the pots between the step of puts cutting and the step of lid sealing, which was removed before the flight.

4.2.4 Sensors

Air speed inside the enclosure was measured using two hot wire anemometers (air velocity transducer TSI ®, model 8465, accuracy ± 2% of the measure, range of measures = 0.125m.s-1 to 1m.s-1) set between two plant pots, on the fan axis, measuring air speed with a time step of 1s, integrating multi-directional air flow. The air velocity measurements are summarized in Table 4.1.

Table 4.1: Average total velocity measured by the anemometers during the flight.

Voltage (V)	**Anemometer 1 (m/s)**		**Anemometer 2 (m/s)**		**Average velocity (m/s)**
	Average	St. Deviation	Average	St. Deviation	
4.5	0.110	0.022	0.161	0.015	0.135
7.5	0.140	0.026	0.299	0.031	0.219

Light intensity and spectrum inside the enclosure was characterized prior to the flight (see section 4.2.5) but in addition a light quantum sensor (Solems CBE 80) was set in the center of the enclosure to quantify Photosynthetically Active Radiations (PAR, $\mu mol.m^{-2}.s^{-1}$) during the flight.

Temperature and relative humidity were measured on the lower side of each leaf (transpiring and non transpiring) with eight thermocouples (acquisition every 250 ms) and eight hygrobutton ProgesPlus® (acquisition every 3 s with an accuracy accuracy ± 5%). In addition, two thermocouples were set in two positions (bottom and top) inside the enclosure to acquire a measure of the air temperature.

A data logger Campbell Scientific® associated to the software Logger Net collected synchronized data of the thermocouples, light quantum sensor and anemometers and an MSR 145 data logger recorded cabin air parameters: temperature, relative humidity, total pressure, as well as gravity levels.

During the flight a problem was experienced with the thermocouples, probably due to a varying electrical ground of the plane during the flight, which caused the measures to fluctuate with a range of 4°C. Outliers were removed from data.

4.2.5 LED lighting system, light spectrum and patterns

Four 10-cm white LED stripes (RS Pro SMD3528 60LED/M) are mounted on thin (1 mm) square aluminum plates, screwed outside of the polycarbonate lid (Figure 4.8). There are four aluminum plates all connected together, relying on one power supply and heat is evacuated passively through these plates. The colour temperature of the LEDs is 5500 to 7000 K and their light spectrum was characterized using an Ocean Optics USB 2000+ spectrometer with an optical fibre (QP 400-2-SR) and a cosine corrector (Ocean Optics CC-3) coupled to the fibre, see (Figure 4.9).

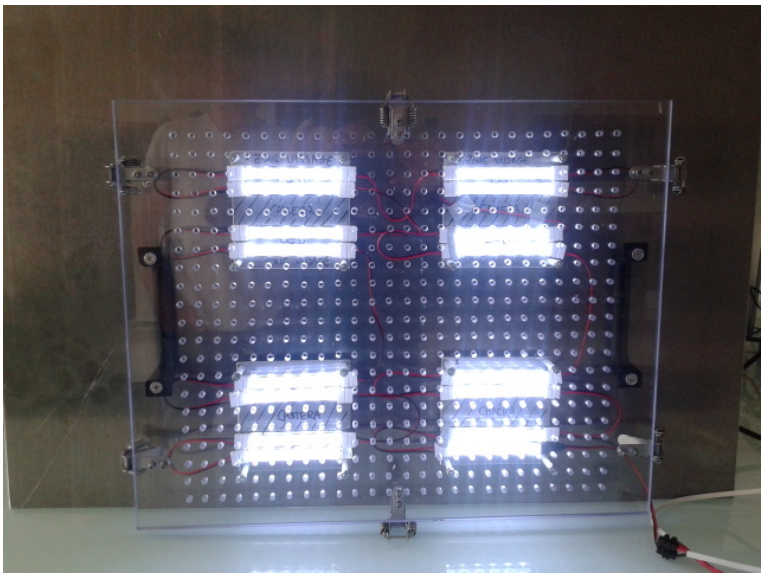

Figure 4.8: LED lighting system seen through the polycarbonate lid.

The light intensity under each plate, at the height of the studied leaves was measured prior to the flight using a LI-COR quantum sensor (LI-190) mounted on a portable meter LI-COR Quantum/Radiometer/Photometer LI-189. The light intensity is 25.51 µmol/m²/s on average with a standard deviation of 0.76 µmol/m²/s. The light intensity measured in the center of the enclosure during the flight varied from 12.3 to 18.3 µmol/m²/s (mean = 17.1 ± 0.8 µmol/m²/s (standard deviation)).

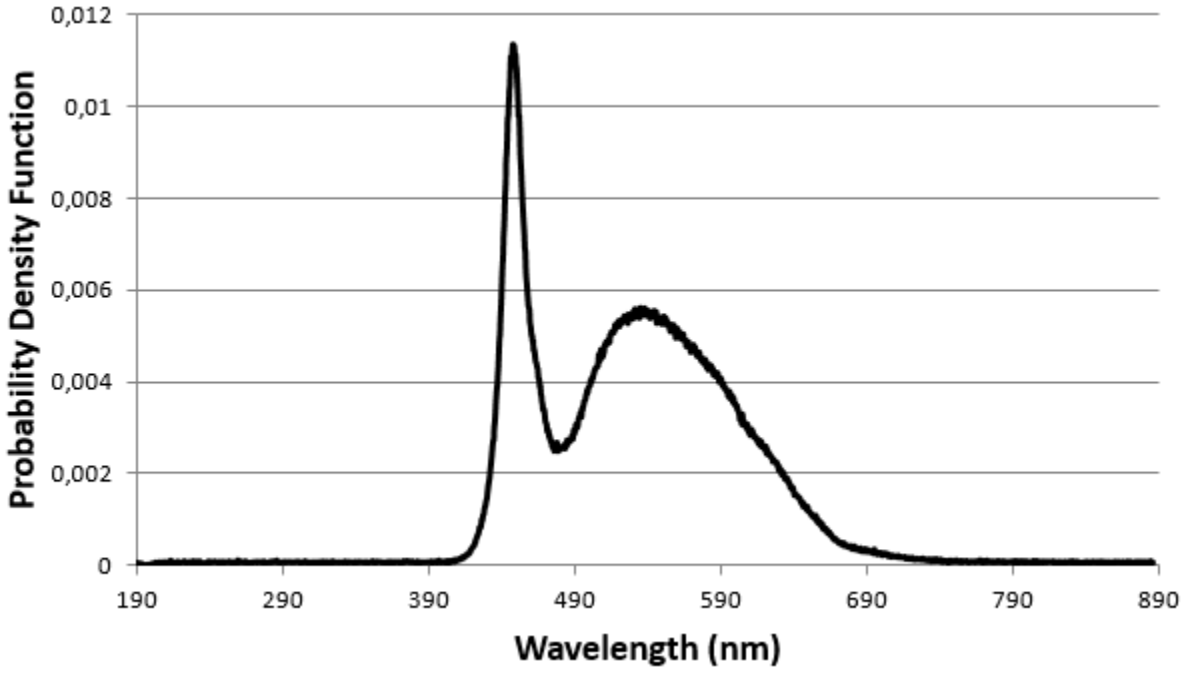

Figure 4.9: Probability Density Function of the LED lighting system used in October 2017.

4.2.6 Thermal cameras and Android phones

The four IR cameras used for this experiment are FLIR ONE cameras from FLIR® which take images at wavelengths ranging from 8 to 15 µm. They are operated using a custom-made application on four Android devices, placed outside of the sealed rack for ease of operations. During the flight the cameras were linked to the Android devices via a USB cable and were continuously charging on a USB hub which provided up to 2.0 Am at each of its ports. The application is compatible with Android Programming Interface (API) 20 platform and allows autonomous acquisition of IR images of spinach leaves. The initial code did not enable an IR image acquisition at regular time step, so the images acquired during October 2017 parabolic flight campaign were acquired at a frequency varying from 1 to 5 per second. The Android devices were equipped with 64 Gb SD cards, which enabled the storage of more than 50000 images per phone.

4.2.7 IR images analysis

The analysis of the Infra-Red (IR) images was performed using the Atlas System Development Kit developed by Flir® , enabling to do radiometric analysis of IR images. The environmental parameters were set to an emissivity of 0.95 and a distance of 13 cm. The temperature of external optics was given by the thermocouple set in the upper part of the enclosure and averaged for each parabola (Table 4.2). The air temperature was calculated from the measure of the two thermocouples inside the enclosure, the reference temperature by the Campbell data logger, and the MSR 145 data logger and averaged for each parabola (Table 4.2 below and in the supplementary material in appendices). The relative humidity measured by the MSR 145 was averaged for each parabola (Table 4.2). The standard deviation for relative humidity is high because the rack was opened briefly before the 30th parabola and the relative humidity dropped from 70% to 31%. Without these two outliers, the standard deviation is 2.45.

Table 4.2: Average temperatures and relative humidity during the flight of 31 parabolas.

	External Optics Temperature (°C)	**Air Temperature in the Enclosure (°C)**	**Relative Humidity (%)**
Average	22.0	22.4	70.6
Standard Deviation	0.20	0.15	9.92

Each IR image acquired shows the transpiring leaf and the non transpiring leaf. For each IR image, the environmental parameters were adjusted to those given in Table 4.2. The minimum, maximum, average, and standard deviation of pixel temperature was extracted, both for the transpiring leaf and the non transpiring leaf, as well as for an inert part in the image, acting as our baseline.

The delta between the measured transpiring (resp. non transpiring) leaf surface temperature and the measured baseline temperature is calculated for each leaf and each parabola. This physical quantity is used for the subsequent statistical analysis. Another problem experienced during the flight was the fact that the cameras recalibrated themselves every 2 min 16 s, causing regular temperature jumps that did not allow for data analysis on some parabolas. Hence parabolas where this happened were automatically removed from the data pool.

4.2.8 Statistical analysis

Tested air velocities were randomized among the different sets of parabolas to eliminate a potential time and acclimation effect of plants and the position of transpiring and non transpiring leaves were also randomly distributed into the enclosure with respect to the fans positions, to remove any position effect in the enclosure (see Figure 4.12). The statistical analysis was performed by A. Vernay, using the R software version 3.3.2 (R Core Team, 2016).

A Linear Mixed Effect (LME) model was used to determine simple effects and interactions between different factors. The first factors tested were the transpiring and non-transpiring status of the leaf and it was found significant: non-transpiring leaves showed significantly higher surface temperature than transpiring leaves. Hence the next tests were performed only on the transpiring leaves and the factors studied were three different airflow distributed over 2 sets of 5 parabolas (6 parabolas for the first set of the flight), the parabola number, the picture number, and three gravity levels. Parabola number and pictures number were embedded as random effect in the model. Analyses of variance (using the Restricted Maximum Likelihood Method (REML) method (Pinheiro and Bates 2000) with linear mixed effects models were performed on each plant separately. Indeed, preliminary tests displayed significantly different responses between plants, requiring a distinct statistical analysis per plant. The differences could be due to morphological and/or functional

variability highlighted by the small replicate number. All factors and factor-factor were simultaneously included in the model for each plant. It was later simplified by removing insignificant higher-order interactions.

For each test, the coefficients p and F are calculated: the difference is significant if p is lower than 0.05 and the highest F, the more significant the difference (F value compared the variability between all data and the variability inter treatment). This enabled to say if there were differences between the different gravity treatments, between the different ventilation treatments, or if there were interactions between gravity and ventilation. Then a multiple pairwise comparison (Tukey's HSD test) using the LSMEANS package (Lenth 2016) was performed to determine the quantitative significance of difference between each treatment modality.

4.2.9 Post flight biological analyses

The following measures were performed by A. Vernay on the plants after the flight: shoot and root fresh and dry weight, leaf area, root length, surface, and diameter.

Fresh mass was measured using a laboratory scale (Sartorius BP2015), as soon as feasible after the flight and after washing away agar from both the shoot and the roots and dry them with absorbent paper.

Leaf area was obtained by scanning the leaves with an Epson scanner (professional mode, 16 bits, dpi 600, stored in TIF formatting) and measuring leaf area with the ImageJ software, after storing them in plastic bags in a freezer and thawing them when the equipment was available. In the same way, roots were stored in plastic bags and frozen until subsequent measurements could be made. After thawing they were coloured with methylene blue for better contrast and scanned with the same Epson scanner. Later the pictures were analyzed with the WinRHIZO® software (V2005a, Regent Instruments, Canada) to obtain root length, surface and diameter.

Dry mass was obtained after drying the different organs at 60°C for 72 h, then weighing them using the same Sartorius BP2015 scale.

From these measurements, the following values were determined: the Specific Root Length (SRL) (in cm g^{-1}), which is the root length divided by the root dry mass; the shoot to root ratio, which is the ratio of the shoot to root dry mass; the specific Leaf Area (SLA), which is the ratio of the leaf surface to the leaf dry mass; and the Leaf (resp. Root) Dry

Matter Content (LDMC, resp. RDMC), which is ratio of the leaves (resp. roots) dry mass to the leaves (resp. roots) fresh mass.

4.3 Computational Fluid Dynamics study

4.3.1 Evaluation of the fan flow rate

The fans used are San Ace 60 mm x 60 mm x 15 mm (9GA0612P7H01). They were controlled with an ELC DC power supply (AL 841C), ranging from 3 V to 12 V. During the flight, the three voltage values used were 0 V, 4.5 V, and 7.5 V. Their maximum static pressure is 55.6 Pa, which corresponds to a flow rate of 0 m^3/s at 12V. The datasheet of this fan only gives the relationship between airflow, static pressure, and voltage for 10.2 V, 12 V, and 13.8 V. Trials and errors CFD simulations enabled us to determine the air flow rate of the fans for 4.5 V and 7.5 V, in order to have the same velocities at the simulated anemometers than the ones measured by the anemometers in the enclosure during the flight. This corresponded to volume flow rates of 0.069 m^3/min = 0.00115 m^3/s for a voltage of 4.5 V and of 0.074 m^3/min = 0.00123 m^3/s for a volatage of 7.5 V.

4.3.2 Work hypotheses

The software PHOENICS 2017 (CHAM Ltd) was used to perform a study of computational fluid dynamics inside the enclosure. This was done to get local velocity values at the leaf surface, which could not be determined using only the two anemometers.

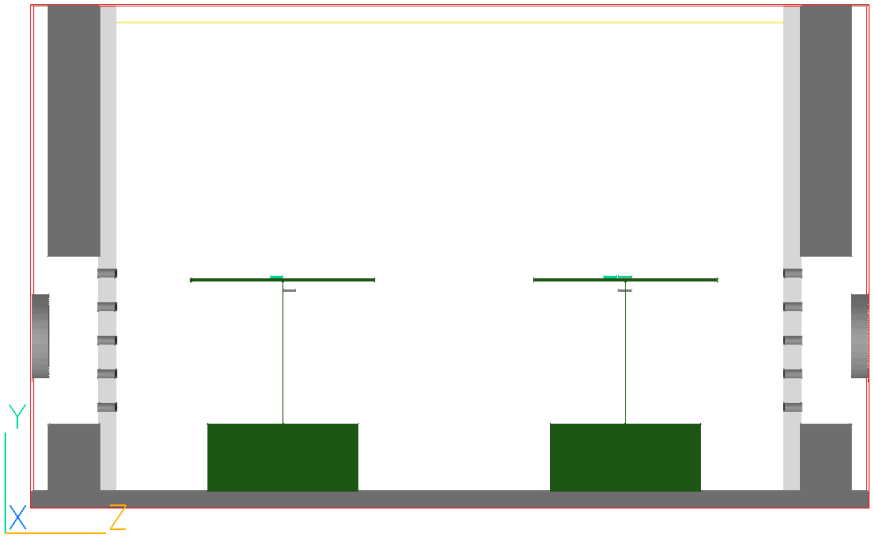

Figure 4.10: 3D model of the enclosure - Front View.

A 3D model of the enclosure was developed using the actual dimensions of the one that flew in the aircraft (Figure 4.10). The length direction is Z; the width is X; and the height is Y. The walls and the unused empty spaces of the enclosure are modelled using blockage objects. The porous plates are modeled using the exact number of holes (19 x 5 per plate) and the outlet is modeled using a porous plate, which makes the file encompassing model geometry less heavy (Figure 4.11).

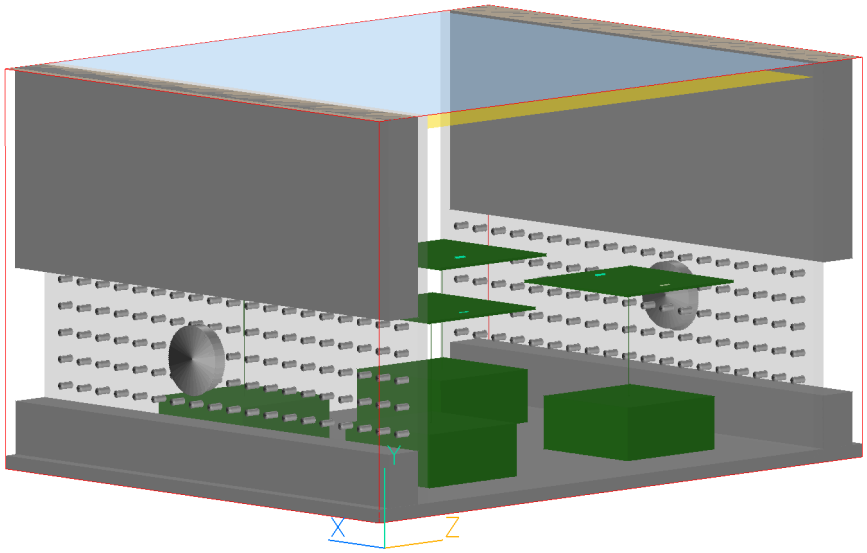

Figure 4.11: 3D model of the enclosure - Side View.

The pots are modeled with cubic blockages of dimensions 9 cm (X) x 4 cm (Y) x 9 cm (Z) to represent the 9-cm diameter and 4-cm height cylindrical pots. The studied leaves are

modeled together with the 3D printed frames, using plates of the dimensions of the 3D printed frames (11 cm x 11 cm). Blockage of 4 mm length and width and 8.5 cm height are used to model the stems of the plants. Point history objects are used to follow the evolution of the air velocity at specific points in the enclosure, one placed for each studied leaf and one for each anemometer, as indicated on Figure 4.12.

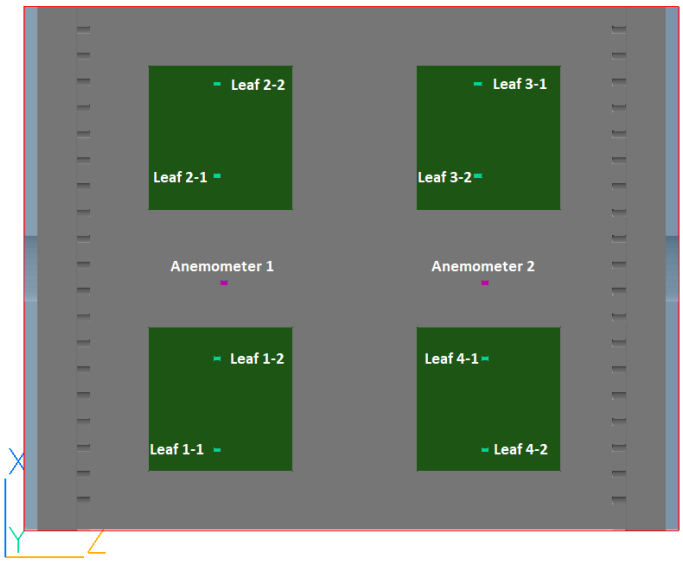

Figure 4.12: Diagram showing the position of the different leaves in the enclosure.

The mesh used is illustrated in Figure 4.13. It contains a total of 1022868 meshes: 164 in the X direction, 81 in the Y direction, and 77 in the Z direction.

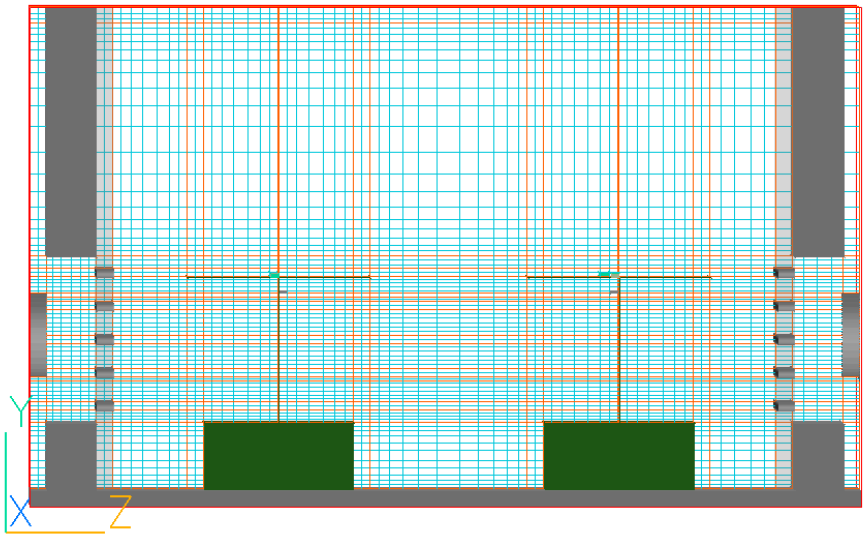

Figure 4.13: 3D model of the enclosure with the mesh used for the computations.

The air velocity experimentally measured by the anemometers during the flight is 0.10-

0.15 m/s and 0.14-0.30 m/s for a fan voltage of 4.5 V and 7.5 V respectively. Taking a characteristic length of the leaf of 0.1 m, an air temperature of 293 K, a temperature gradient of 3 K, an air density of 1.204 kg/m^3, an air viscosity of 1.8.10^{-5} m^2/s, an air specific heat capacity of 1004 J/K/kg, and an air thermal conductivity of 0.0262 W/m/K, the computation of the associated dimensionless numbers in 0g, 1g, and 2g is given in Table 4.3.

Table 4.3: Dimensionless numbers in the enclosure during the parabolic flight.

Dimensionless numbers	**Air Velocity**	**0g**	**1g**	**2g**
Prandtl	/	0.689	0.689	0.689
Grasshof	/	0.458	449000	897900
Rayleigh	/	0.316	310000	619000
Nusselt	/	0.394	49.29	62.80
Reynolds	Low	668.9	668.9	668.9
	High	1672	1672	1672
Richardson	Low	0.000001024	1.004	2.007
	High	0.0000001638	0.1607	32.11

These numbers indicate that the air flow is laminar for all gravity levels (Re $<$ 3000). Consequently, a laminar model is used to run the CFD simulations. Additionally, in 1g, it is a mixed convection regime (Ri $>$ 0.1), whereas in 0g, as expected, forced convection is dominant (Ri $\ll$ 0.1), and in 2g, it remains a mixed convection regime with 0.1 $<$ Ri $<$ 2.

The air follows the ideal gas law and is set to ambient temperature and pressure. The simulations were run in steady mode over 2500 iterations.

4.3.3 Simulation results

For each simulation case, the air velocity in the three directions is computed. On the points of interest (leaves and anemometers), the norm of the total velocity is computed and it is the one that is kept for the following analyses. The vertical component of the air velocity is close to zero on all leaves. The velocities computed at the position of the anemometers are always compared to the experimentally measured air velocities by anemometers during the parabolic flight.

Lower air flow rate

The lower air flow rate, corresponding to an input voltage of 4.5V, is 0.00115 m^3/s and is set at each fan as the inlet flow rate. The velocity profile in the enclosure is displayed on Figures 4.14, 4.15, and 4.16.

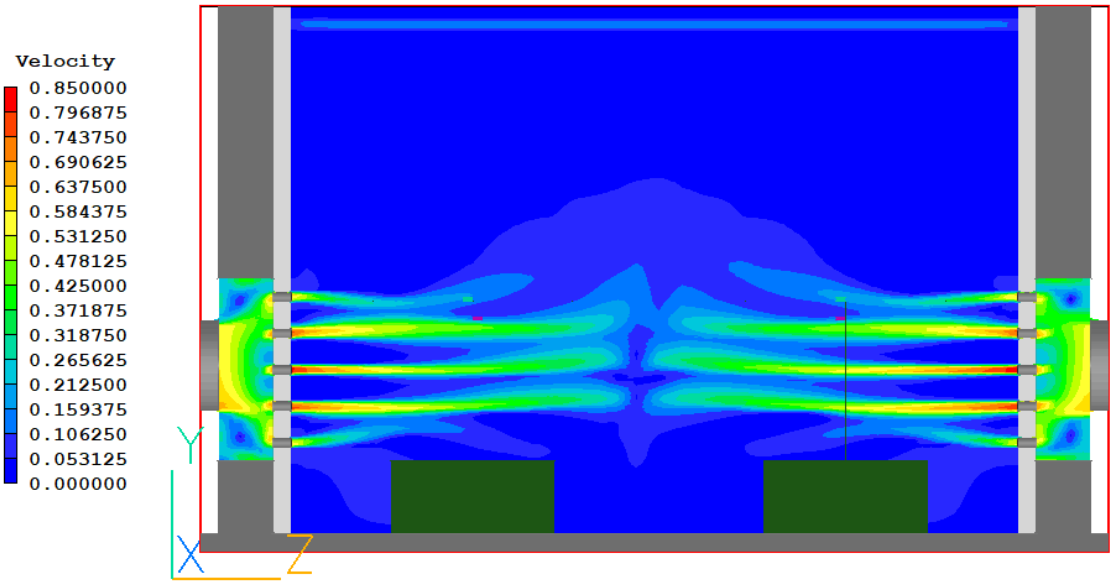

Figure 4.14: Velocity profile into the enclosure at the lower air flow rate (in m/s) - Front View.

The simulation gives an air velocity of 0.137 m/s for anemometer 1 and 0.138 m/s for anemometer 2, which is similar to the experimental air velocities measured by the anemometers. The air velocities on the leaf surface are given in Table 4.4. The number of the leaves correspond to their position in the enclosure, as indicated on Figure 4.12.

Table 4.4: Simulation results of the air velocity at the leaves surfaces for the lower air flow rate.

Leaf #	**Leaf status**	**Air Velocity (m/s)**
1-1	Transpiring	0.0225
1-2	Non Transpiring	0.00895
2-1	Transpiring	0.00198
2-2	Non Transpiring	0.0667
3-1	Transpiring	0.0789
3-2	Non Transpiring	0.00755
4-1	Transpiring	0.00624
4-2	Non Transpiring	0.0336

These results show that the value of the air velocity above the leaves can vary from one

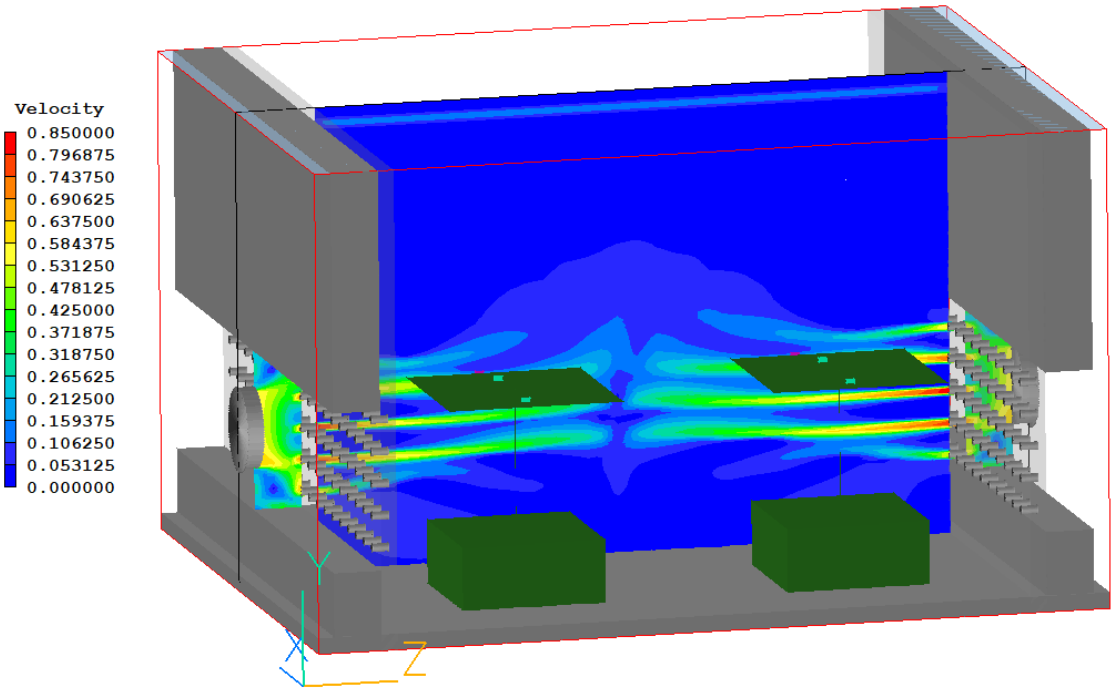

Figure 4.15: Velocity profile into the enclosure at the lower air flow rate (in m/s) - Side View.

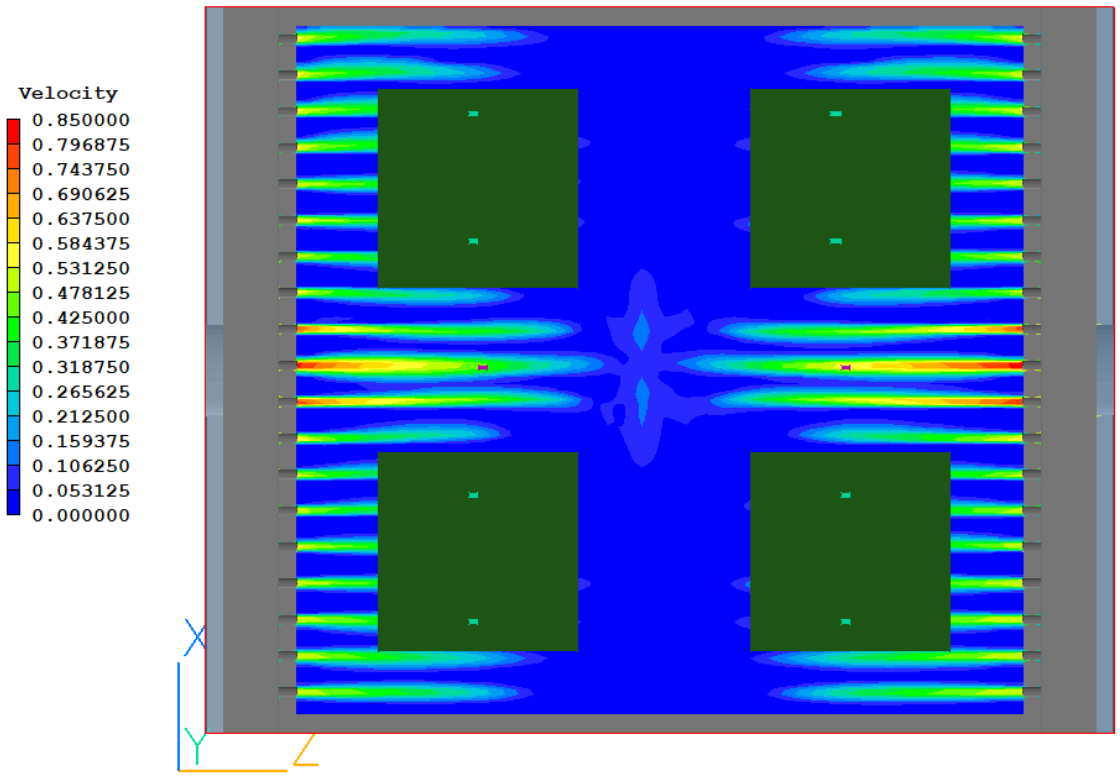

Figure 4.16: Velocity profile into the enclosure at the lower air flow rate (m/s) - Top View.

order of magnitude depending on the position of the leaf inside the enclosure. Leaves 1-1, 2-2, 3-1, and 4-2, which are next to the wall of the enclosure have an air velocity at their surface in the range 0.02 - 0.08 m/s, while other leaves, towards the center of the enclosure have an air velocity at their surface in the range 0.002 - 0.009 m/s.

Higher air flow rate

The higher air flow rate, corresponding to an input voltage of 7.5V, is 0.00123 m^3/s and is set at each fan as the inlet flow rate.The velocity profile in the enclosure is displayed on Figures 4.17, 4.18, and 4.19.

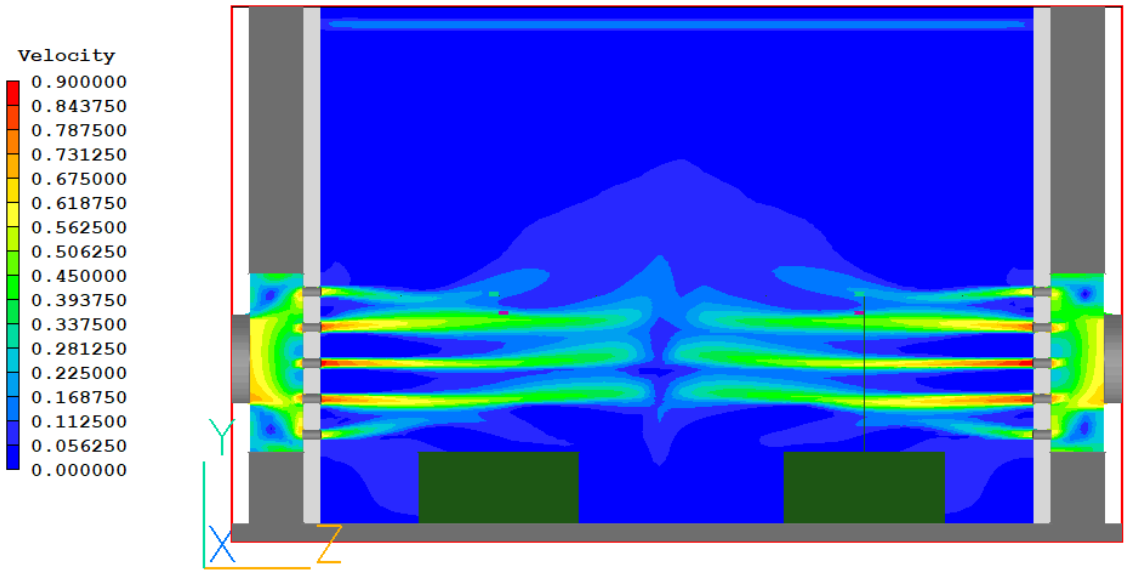

Figure 4.17: Velocity profile in the enclosure at the higher air flow rate - Front View.

The simulation gives an air velocity of 0.315 m/s for anemometer 1 and 0.248 m/s for anemometer 2, which is similar to the experimental air velocities measured by the anemometers. The air velocities on the leaf surface are given in Table 4.5. The number of the leaves correspond to their position in the enclosure, as indicated on Figure 4.12.
As observed for the lower flow rate, the position of the leaf inside the enclosure strongly influences the order of magnitude of the air velocity at the leaf surface: 0.02 - 0.08 m/s for leaves at the wall and 0.004 - 0.01 m/s at the center of the enclosure. The values of the air velocity found in these CFD simulations are used as parameters in the model for the forced convection velocity.

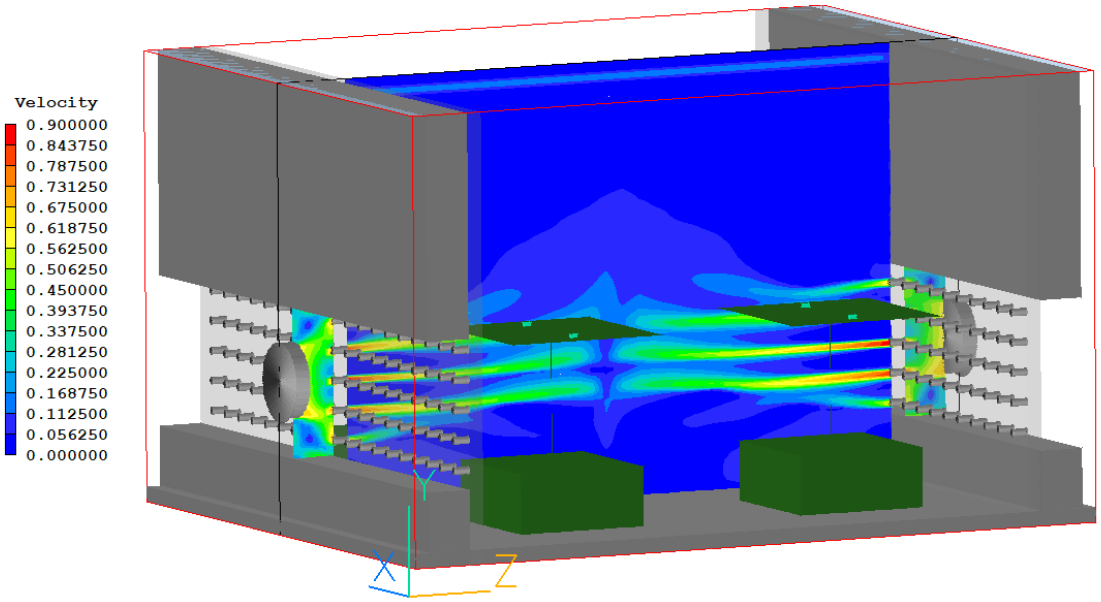

Figure 4.18: Velocity profile in the enclosure at the higher air flow rate - Side View.

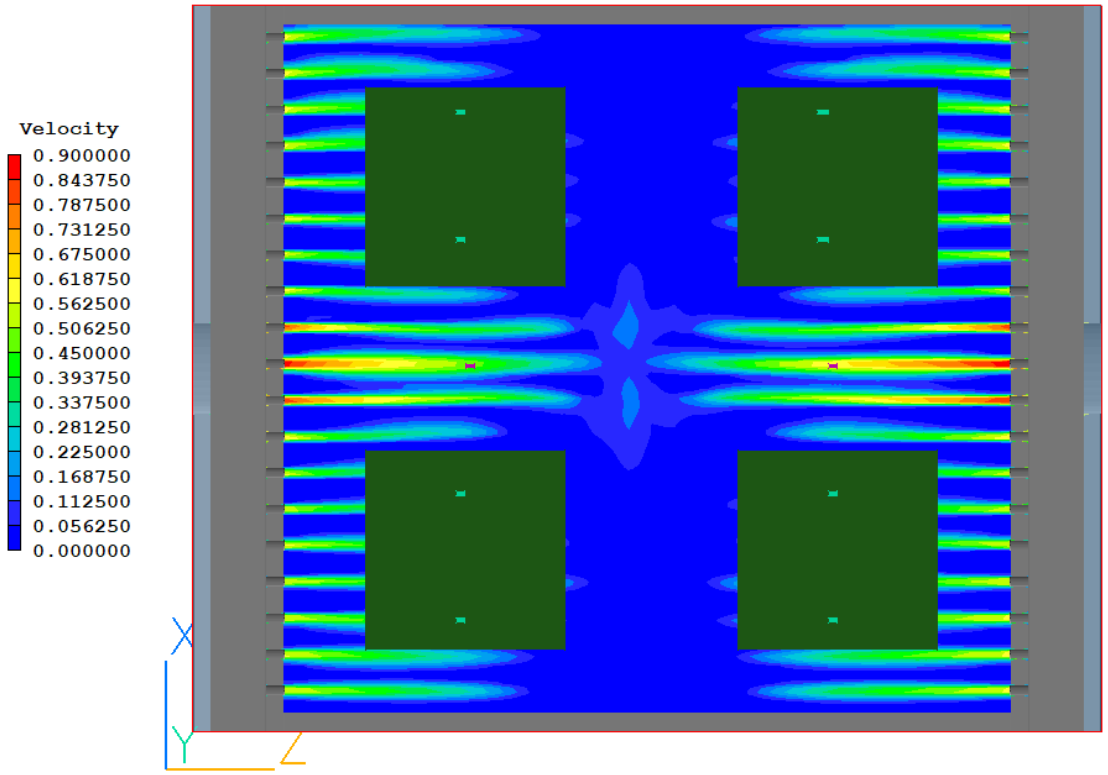

Figure 4.19: Velocity profile in the enclosure at the higher air flow rate - Top View.

4.4 Preliminary results

4.4.1 Results of the statistical analysis

The results of the LME test obtained with R software are given in Figure 4.21. As detailed in section 4.2, these results were obtained by testing the gravity and ventilation

Table 4.5: Simulation results of the air velocity at the leaves surfaces for the higher air flow rate.

Leaf #	**Leaf status**	**Air Velocity (m/s)**
1-1	Transpiring	0.0243
1-2	Non Transpiring	0.00687
2-1	Transpiring	0.00586
2-2	Non Transpiring	0.0700
3-1	Transpiring	0.0786
3-2	Non Transpiring	0.0121
4-1	Transpiring	0.00433
4-2	Non Transpiring	0.0336

effects on the gradient between the measured transpiring leaf surface temperature and the measured baseline temperature. Indeed, as detailed in section 4.2, the experiment was not performed in a controlled environment, but the air temperature and relative humidity were measured during the flight. Also the effect of the cameras recalibration could sometimes be cancelled by looking at the gradient between the measured transpiring leaf surface temperature and the measured baseline temperature.

The baseline chosen as equivalent to the air temperature was the bottom aluminum floor (Figure 4.20).

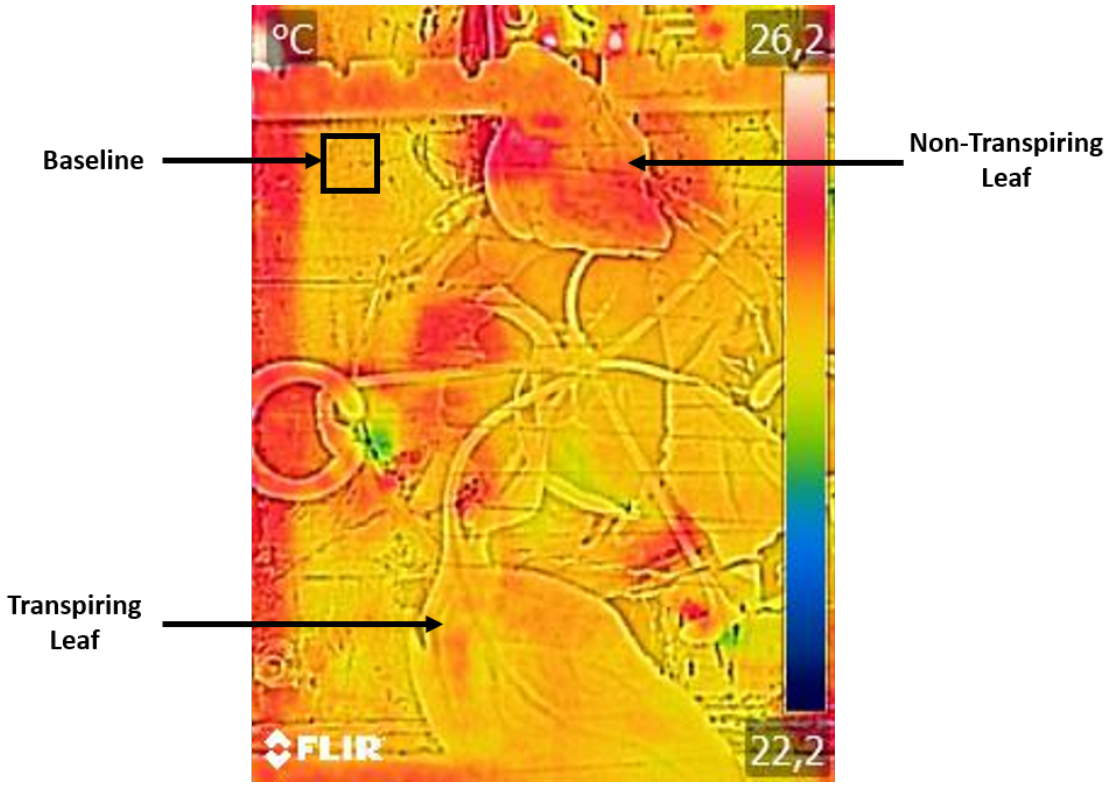

Figure 4.20: IR image collected with the FLIR ONE cameras showing the baseline, the transpiring leaf and the non-transpiring leaf for plant 1.

The results are presented for each plant/phone and give a qualitative and quantitative overview of the effects in steady state, since the data are pooled for all parabolas at a given ventilation and gravity level. Note that the transpiring leaf temperature was always lower than the baseline temperature, so the the gradients between the leaf surface temperature and the baseline are negative.

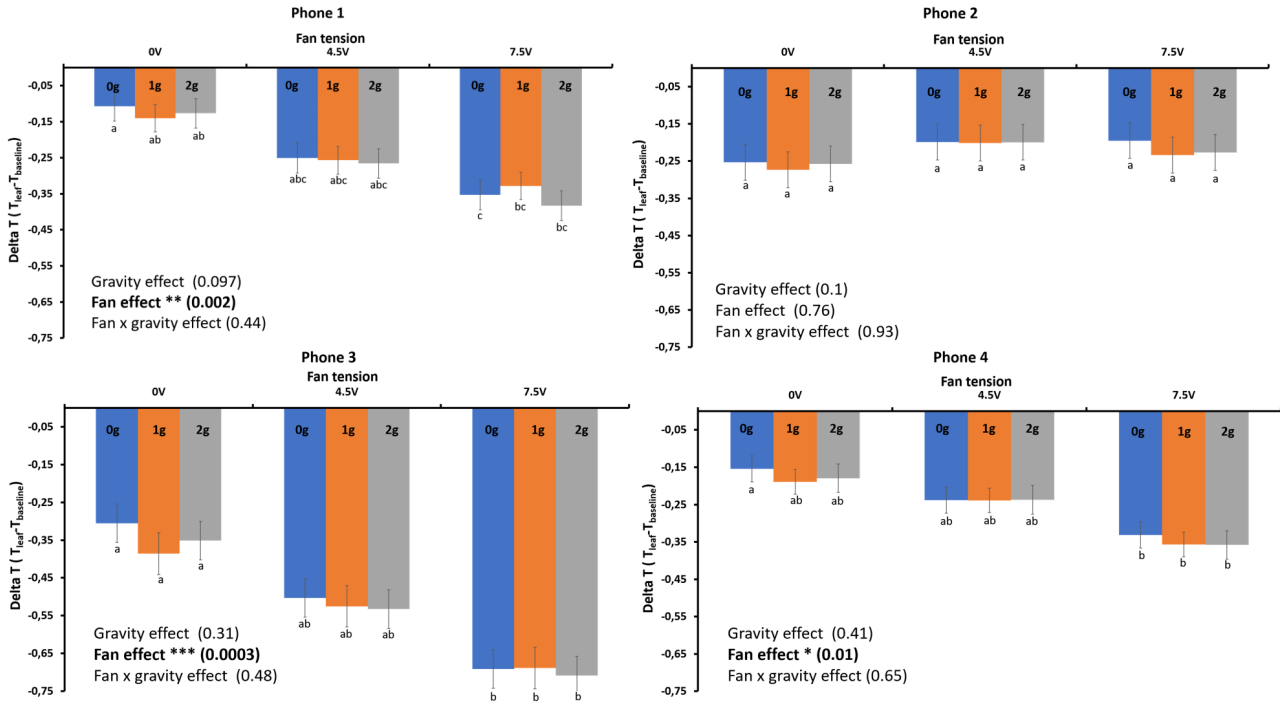

Figure 4.21: Results of the LME test for each phone computed in R.

These results indicate that for three plants out of four, there is a significant ventilation effect: p = 0.002 for phone 1, p = 0.0003 for phone 3 and p = 0.01 for phone 4. In other words, the leaf surface temperature of the transpiring leaf changes significantly in different ventilation settings. This is in accordance to the literature, since a study by Kitaya et al. (2003) demonstrated that the net photosynthesis rate of a tomato seedling canopy was doubled between an air current of 0.1 m/s and one of 1 m/s (Kitaya et al. 2003b). However this statistical analysis does not show a significant effect of gravity on any plant.

With no ventilation, the trend is the same for the four phones: the temperature gradient is largest in 1g and the one in 2g is larger than in 0g, although these differences are not statistically significant.

At the lower ventilation (4.5 V), the trends are the same for the plants 1 and 3, and for the plants 2 and 4 (no difference between the three gravity treatments). Interestingly, the transpiring leaves of plants 1 and 3 are in the same configuration, close to the enclosure wall, and the transpiring leaves of plants 2 and 4 are also in the same configuration, towards the center of the enclosure (see Figure 4.12). According to the CFD data of section 4.3.3, leaves 1-1 and 3-1 are under an airflow of respectively 2.3 10^{-2} m/s and 7.9 10^{-2} m/s, whereas leaves 2-1 and 4-1 are respectively under an airflow of 2.0 10^{-3} m/s

and 6.2 10^{-3} m/s. A similar trend is observed for the highest ventilation (7.5 V): plants 1 and 3 and plants 2 and 4 display similar trends. More generally, except for plant 2, the temperature gradients between the transpiring leaf and the baseline temperature are larger at the highest ventilation (-0.35 °C for plant 1, -0.7 °C for plant 3, and -0.4 °C for plant 4) and are smaller with no ventilation (-0.15 °C for plant 1, -0.35 °C for plant 3, and -0.15 °C for plant 4). Indeed, at higher ventilation, the leaf is expected to transpire more and thus its temperature to decrease more than with a lower or no ventilation. Hence the gradients increase (become more negative) with the ventilation level. Therefore the trend given by the model (higher exchange rates when increasing the forced ventilation) is experimentally verified.

It is also to be noted for the four plants, with no ventilation, that the temperature gradients between the three gravity treatments are more different (even though not significantly different) than in the cases with ventilation. This was expected since when there is forced convection, the effects of free convection are less visible and the free convection is a direct expression of the gravity levels.

This statistical analysis demonstrates that the results are similar to expected trends and that the results for the four plants cannot be pooled but need to be studied independently for model validation.

4.4.2 Results of the dynamical analysis

In this section we study the leaf surface temperature variations in 0g and 2g in different ventilation settings compared to the simulations results obtained with the model presented in the previous chapter. The parameters used for these simulations, which differ from those used in section 3.7 for the sensitivity analysis are summarized in Table 4.6. The air temperature was set at 295.6 K, which is the average air temperature in the enclosure during the flight. The initial leaf surface temperature was set at 296.15 K, which is also an average value during the flight. The morphological and biochemical parameters of spinach stomatal densities, cross-sectional area and leaf area / fresh biomass ratio were determined experimentally on our spinach plants. It is to be highlighted that our model integrates the influence of total pressure on the different entry parameters and within gas exchanges equations, which is crucial since the total pressure in the plane is 0.85 bar, and not 1 bar like standard atmospheric pressure.

Table 4.6: Parameters used for the parabolic flight simulations.

Parameters	Value	Unit
Bulk Air		
Temperature, T_b	295.6	K
Pressure, P_b	85000	Pa
Relative Humidity, RH	70	%
CO_2 concentration, $[CO_2]$	700	ppm
Bulk O_2 partial pressure, $p^b_{O_2}$	$0.2093\,P_b = 1.7791\,10^4$	Pa
Bulk CO_2 partial pressure, $p^b_{CO_2}$	$[CO_2]\,P_b = 59.5$	Pa
Bulk H_2O partial pressure, $p^b_{H_2O}$	$RH\,P^0(Tb) = 1.8915\,10^3$	Pa
Bulk N_2 partial pressure, $p^b_{N_2}$	$P_b - p^b_{O_2} - p^b_{CO_2} - p^b_{H_2O} = 6.5259\,10^4$	Pa
Morphology		
Spinach stomatal density, d_s	$2.51\,10^8$	m^{-2}
Spinach stomatal cross-sectional area, a_s	$4.34\,10^{-10}$	m^2
Physical		
Standard plant chamber length, H	0.3	m
Leaf water potential, Ψ_{int}	-1800	Pa
Diffusion coefficient of water vapour, D_w	$2.8850\,10^{-5}$	$m^2.s^{-1}$
Diffusion coefficient of CO_2, D_c	$1.8751\,10^{-5}$	$m^2.s^{-1}$
Diffusion coefficient of O_2, D_c	$2.0456\,10^{-5}$	$m^2.s^{-1}$
Biochemical		
Spinach dry matter content, ω_X	0.015	$g_X.g^{-1}_{FX}$

For 0g phases, the gravity parameter was set to 0.001 m/s^2, in accordance to the data collected by our MSR145 sensor. Indeed, microgravity in parabolic flights is not as pure as the one achieved on a drop tower (or on ISS) and the acceleration is on average of 10^{-3} m/s^2.

Unlike for the statistical analysis, what is of interest here is the leaf temperature variation during short periods of time (about 20 seconds), during which the air temperature remains constant. For each plant, the difference between the transpiring leaf temperature during a 20-second phase and its temperature at the beginning of the phase is computed and pooled between ventilation and gravity levels. For each ventilation level, there are 2 sets

of parabolas (i.e. a total 11 for the no ventilation case, and 10 for the two other values), but since there was the calibration issue mentioned in section 4.2.7, not all parabolas could be used for data analysis. Table 4.7 summarizes which parabolas were used for which analysis.

Table 4.7: Usable parabolas for each plant, gravity level, and ventilation level.

Phases	**Fan**	**Plant 1**	**Plant 2**	**Plant 3**	**Plant 4**
0g	0 V	Parabolas 1, 2, 4, 5, 23, 24, 26			Parabolas 2, 3, 5, 6
	4.5 V	Parabolas 7, 8, 10, 11, 17, 19, 20	Parabolas 7, 9, 10, 11, 17, 18	Parabolas 7, 9, 10, 11, 17, 19, 20	Parabolas 7, 8, 11, 17, 18, 20,21
	7.5 V	Parabolas 14, 27, 30, 31			Parabolas 14, 15, 30, 31
2g before	0 V	Parabolas 2, 5, 24			Parabolas 3, 6, 22, 25
	4.5 V	Parabolas 8, 10, 11, 17, 20	Parabolas 7, 10, 17	Parabolas 7, 10, 17, 20	Parabolas 8, 11, 17, 18, 21
	7.5 V	Parabolas 14, 27, 30, 31			Parabolas 12, 15, 30
2g after	0 V	Parabolas 1, 4, 5, 23, 26	Parabolas 1, 4, 23, 26		Parabolas 2, 5, 24, 25
	4.5 V	Parabolas 7, 10, 19, 20	Parabolas 7, 9, 10	Parabolas 9, 10, 19	Parabolas 7, 8, 11, 17, 20
	7.5 V	Parabolas 14, 27, 31	Parabolas 16, 27, 31		Parabolas 14, 30, 31

0g Phase

Figure 4.22 presents the results obtained per plant for the case without ventilation, in 0g, compared to the simulation results expected using the parabolic flight parameters presented in Table 4.6.

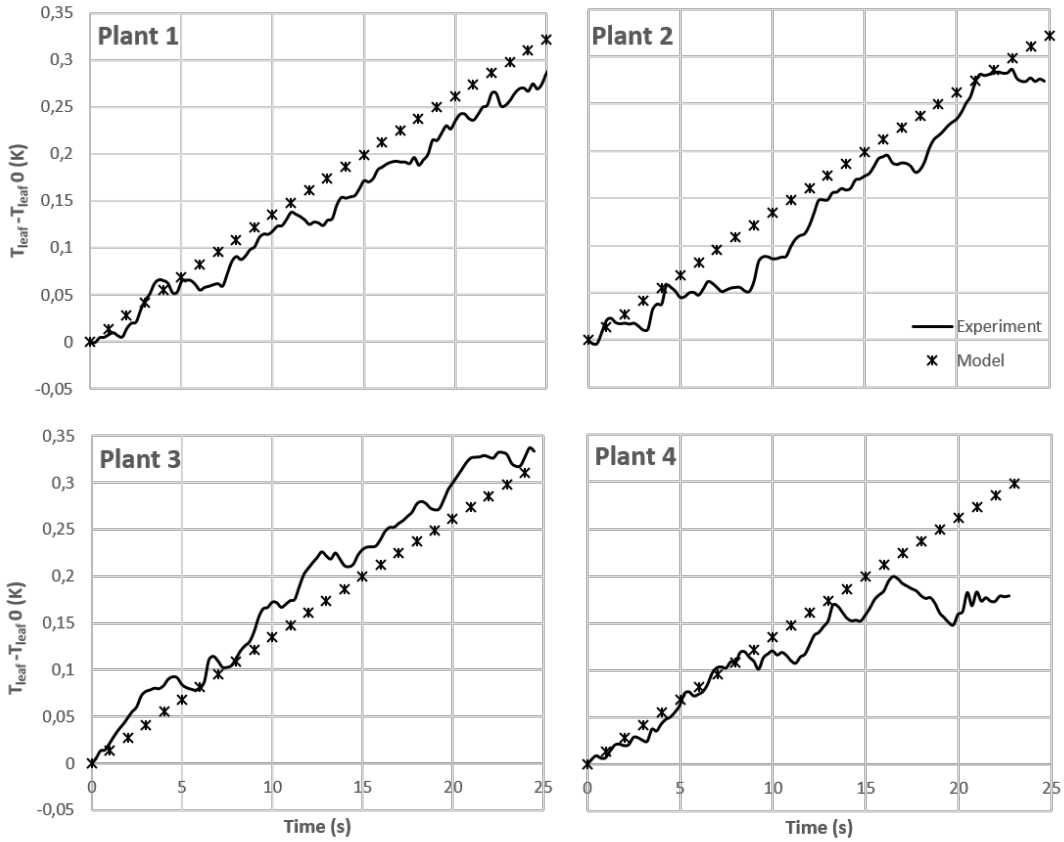

Figure 4.22: Temperature evolution over 25 seconds in 0g without ventilation, model simulation and experimental results for the 4 plants. Average on all usable parabolas (see Table 4.7).

For the four plants the model simulations are very close to the experimental results, showing that the model gives accurate predictions for the temperature evolution in 0g without ventilation. To our knowledge, this is the first time that it was shown that a complete predictive mass and heat transfer model, based on mechanistic principles issued from a chemical engineering approach, was capable to reproduce experimental temperature transient profiles in parabolic flights. It is also interesting to underline that all four plants show a similar temperature increase of about 0.3 K. Kitaya et al. (2001) had shown an increase of 1°C in the leaf surface temperature of sweet potato in 20 seconds of weightlessness using an irradiance of 260 W/m^2 (Kitaya et al. 2001). Our irradiance during this parabolic flight was much lower, about 16.6 W/m^2, which explains a lower increase observed in leaf surface temperature.

The same analysis is performed in 0g with ventilation and given in Figures 4.23 and 4.24. The values used for the forced ventilation velocities are the ones computed in section 4.3. They are summarized in Table 4.8.

Table 4.8: Air velocity at the leaves surfaces used as the forced convection velocity parameter (in m/s).

Fan Voltage	**Plant 1**	**Plant 2**	**Plant 3**	**Plant 4**
4.5 V	0.023	0.002	0.079	0.0062
7.5 V	0.024	0.0059	0.079	0.0043

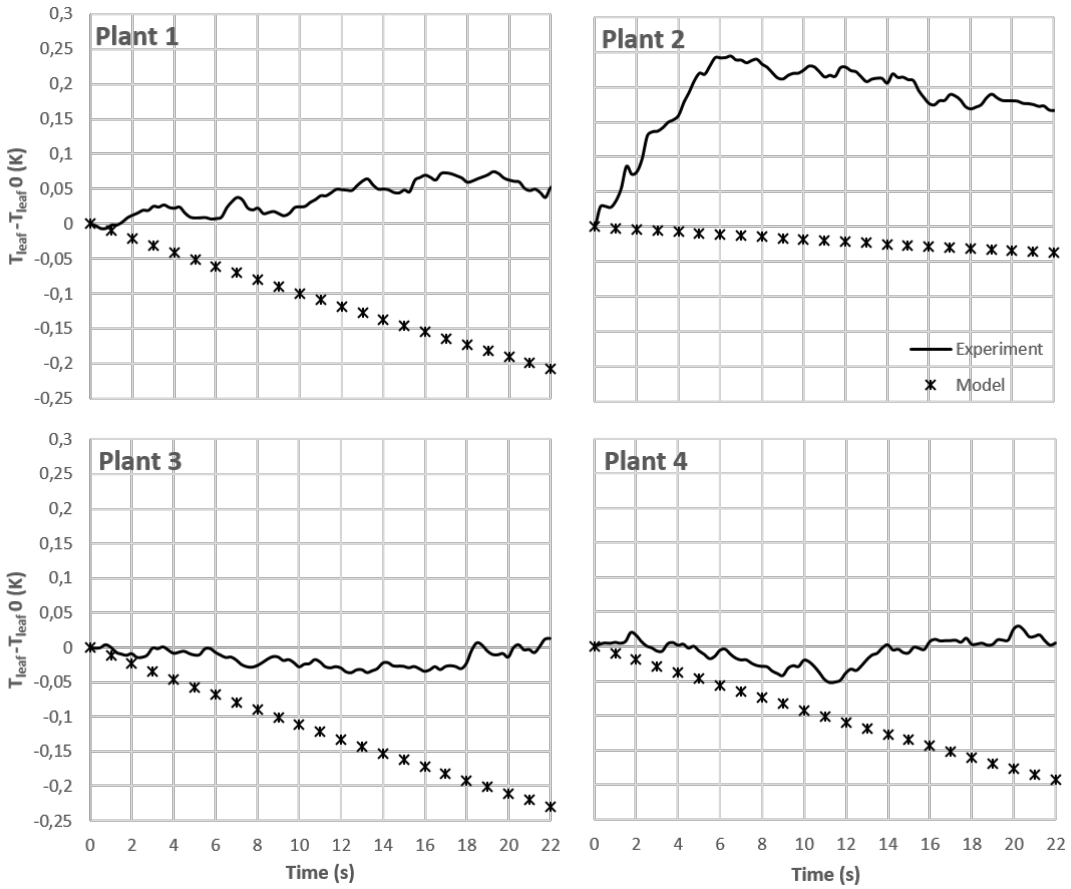

Figure 4.23: Temperature evolution over 25 seconds in 0g with the lower ventilation level (plant 1: 0.0225 m/s; plant 2: 0.00198 m/s; plant 3: 0.0789 m/s; plant 4: 0.00624 m/s), model simulation and experimental results for the 4 plants. Average on all usable parabolas (see Table 4.7).

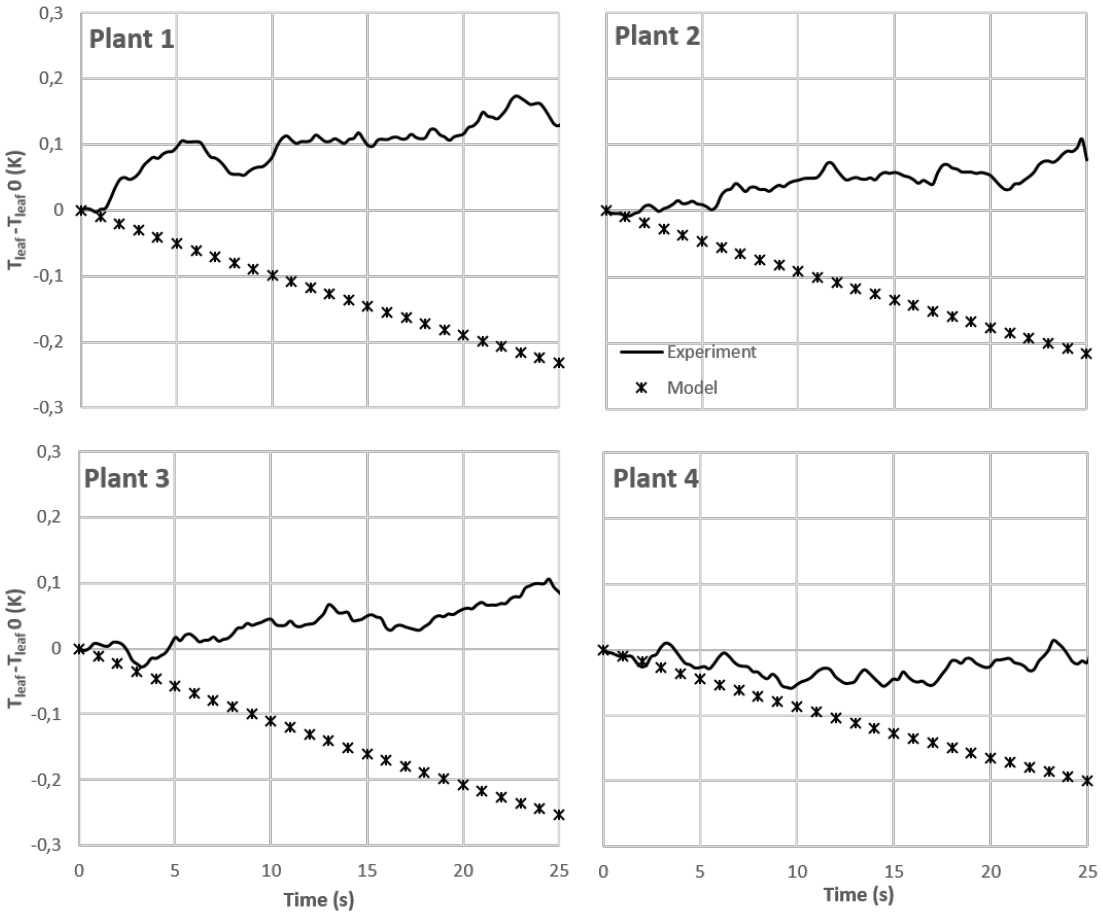

Figure 4.24: Temperature evolution over 25 seconds in 0g with the higher ventilation setting (plant 1: 0.0243 m/s; plant 2: 0.00586 m/s; plant 3: 0.0786 m/s; plant 4: 0.00433 m/s), model simulation and experimental results for the 4 plants. Average on all usable parabolas (see Table 4.7).

Compared to the case without ventilation, the simulations provided by the model do not fit the experimental results, nor qualitatively (the trends are not the same), nor quantitatively (the variation amplitudes are different). Hence, in the case with the lower ventilation the model predicts a decrease in leaf surface temperature ranging from 0.05 to 0.25, while experimentally we observe a stagnation of the leaf surface temperature, or, in the case of plant 2, an increase of 0.2 K. In the case with the higher ventilation setting, the model predicts a decrease in leaf surface temperature ranging from 0.2 to 0.25 K, while experimentally, the leaf surface temperature increases from 0.1-0.2 K or stays around its initial value.

These results that differ from the model depending on the ventilation level can be explained by different reasons. First of all, for the simulations, we made the hypothesis of a constant air temperature over a 20-second phase within a parabola, which is an ap-

proximation, since in reality it varies a little and the air temperature in the enclosure is inhomogeneous, which might have influenced the leaf surface temperature variations. Hence, the air ventilated above the leaves might be warmer than what is set in the model and this could cause the leaf surface temperature to follow a different trend than the simulations. Secondly, the weight given to the parameter of forced convection velocity in the current version of the model might be too important, which would explain the responses of the model to such values of forced convection. Thirdly, these discrepancies could also come from the fact that the data we are working with show defects, due to the calibration issue, and although we have removed the problematic parabolas, some might have remained. Finally, there might be another physical effect, like the the shape of the leaf, that we neglected to include in the model, but whose influence cannot be neglected. As highlighted by the statistical analysis of the data, the influence of ventilation on the leaf surface temperature is significant, although not in the same order of magnitude as the one predicted by the model.

2g Phase

The same approach as detailed in paragraph 4.4.2 is followed to analyze the leaf surface temperature variations in 2g, before and after the 0g-phase. However, some parabolas, that were usable for the 0g-phase analysis, were not necessarily suitable for the 2g-phase analysis and the ones used for the analysis are summarized in Table 4.7.
Figures 4.25 and 4.26 present the results obtained per plant for the case without ventilation, in 2g before and after the 0g phase, compared to the simulation results expected using the parabolic flight parameters presented in Table 4.6.

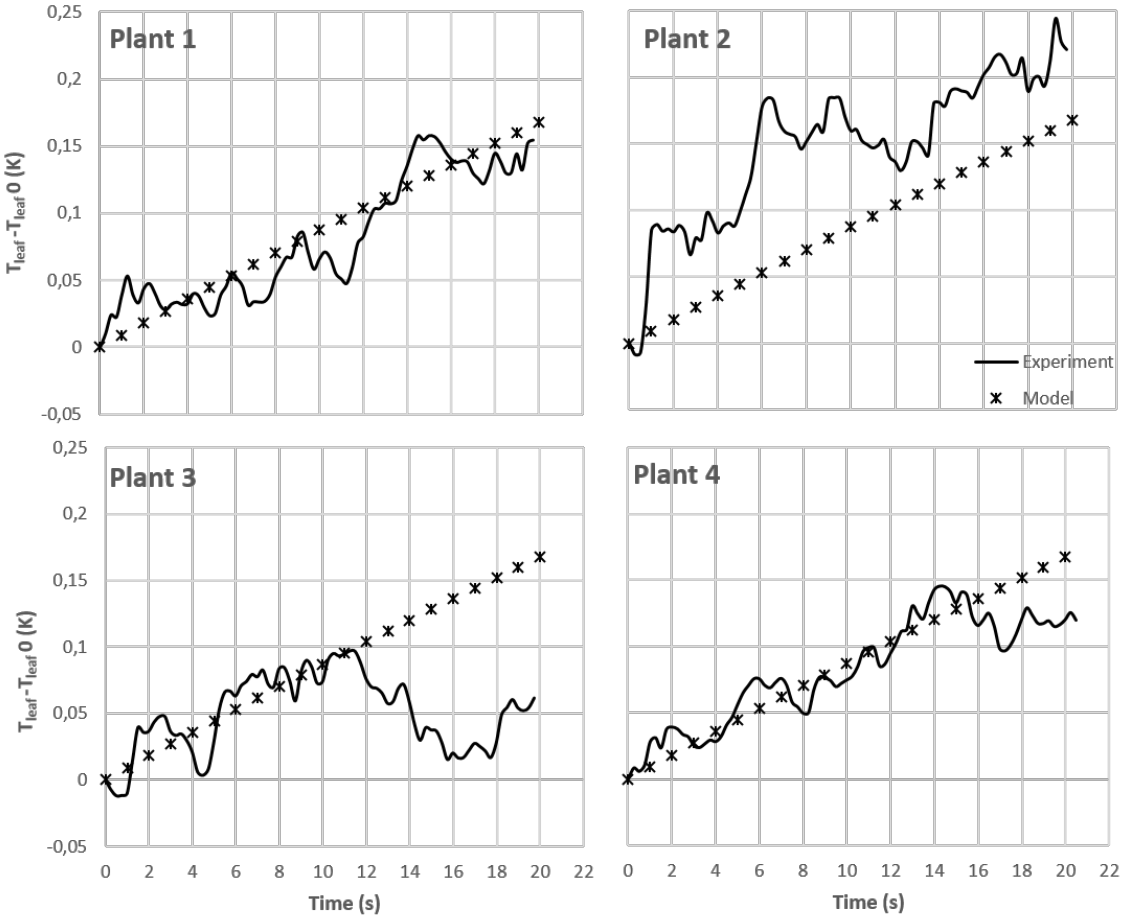

Figure 4.25: Temperature evolution over 25 seconds in 2g before the 0g phase, without ventilation, model simulation and experimental results for the 4 plants. Average on all usable parabolas (see Table 4.7).

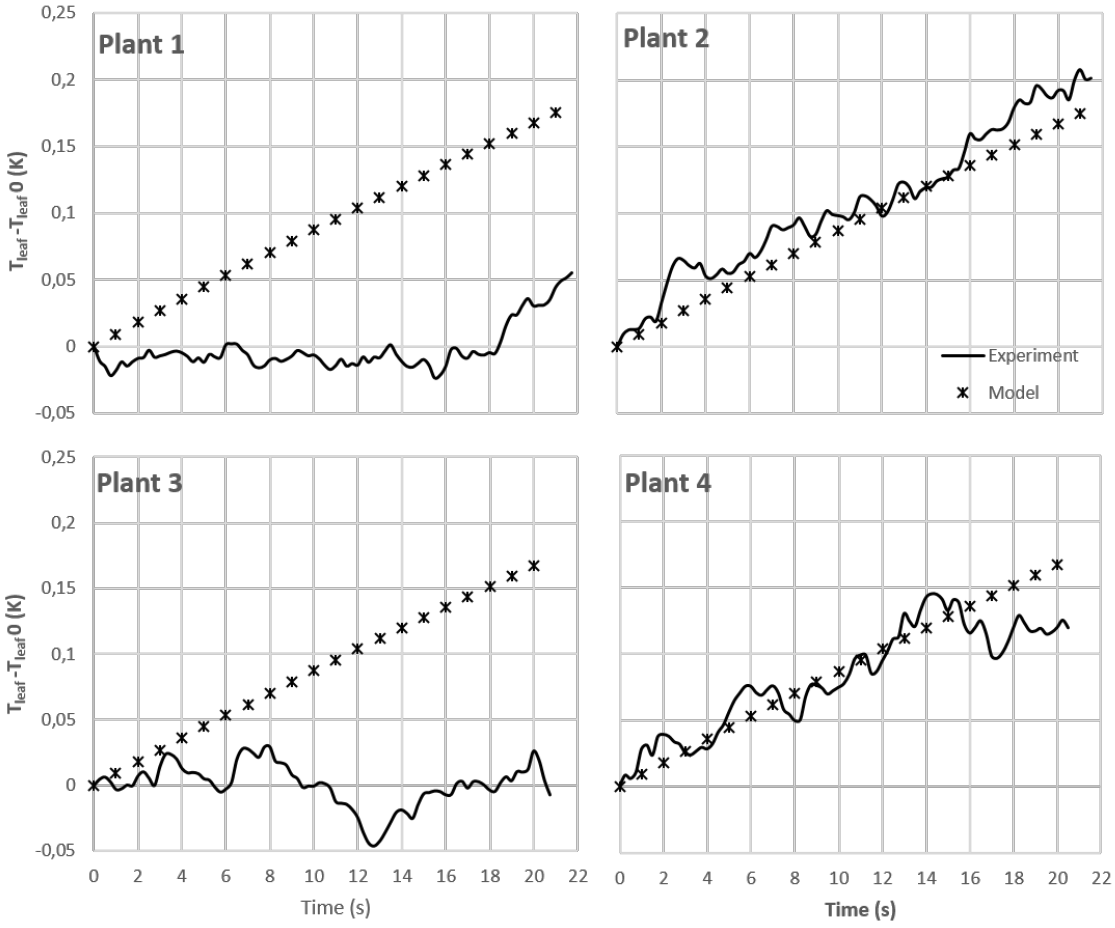

Figure 4.26: Temperature evolution over 25 seconds in 2g after the 0g phase, without ventilation, model simulation and experimental results for the 4 plants. Average on all usable parabolas (see Table 4.7).

The model simulation results and experimental results are in accordance on the 2g-phase before the 0g-phase, for all plants. However they differ for plants 1 and 3 in the 2g-phase after the 0g-phase. It is to be highlighted that the studied leaf of plant 1 and 3 are geometrically similarly positioned, close to the walls of the enclosure, while the studied leaf of plant 2 and 4 are positioned towards of the enclosure. These results differ from the one found in the literature, which reported a decrease in leaf surface temperature in 2g, more important on the "after" 2g-phase than on the "before" (Kitaya, Hirai, and Shibuya 2010). Indeed, the results presented by Kitaya et al. included an air velocity of 0.2 m/s, while in this case we had no ventilation. The model predicts an increase of 0.17 K in 20 seconds, without forced ventilation in 2g, which is about half the temperature increase predicted an observed in 0g. Consequently, without ventilation, the leaf surface temperature in 2g does not decrease, but it increases less than in 0g.

The sequence: 2g - 0g - 2g, using average data presented previously for each plant, is studied and compared to the simulation results (Figure 4.27).

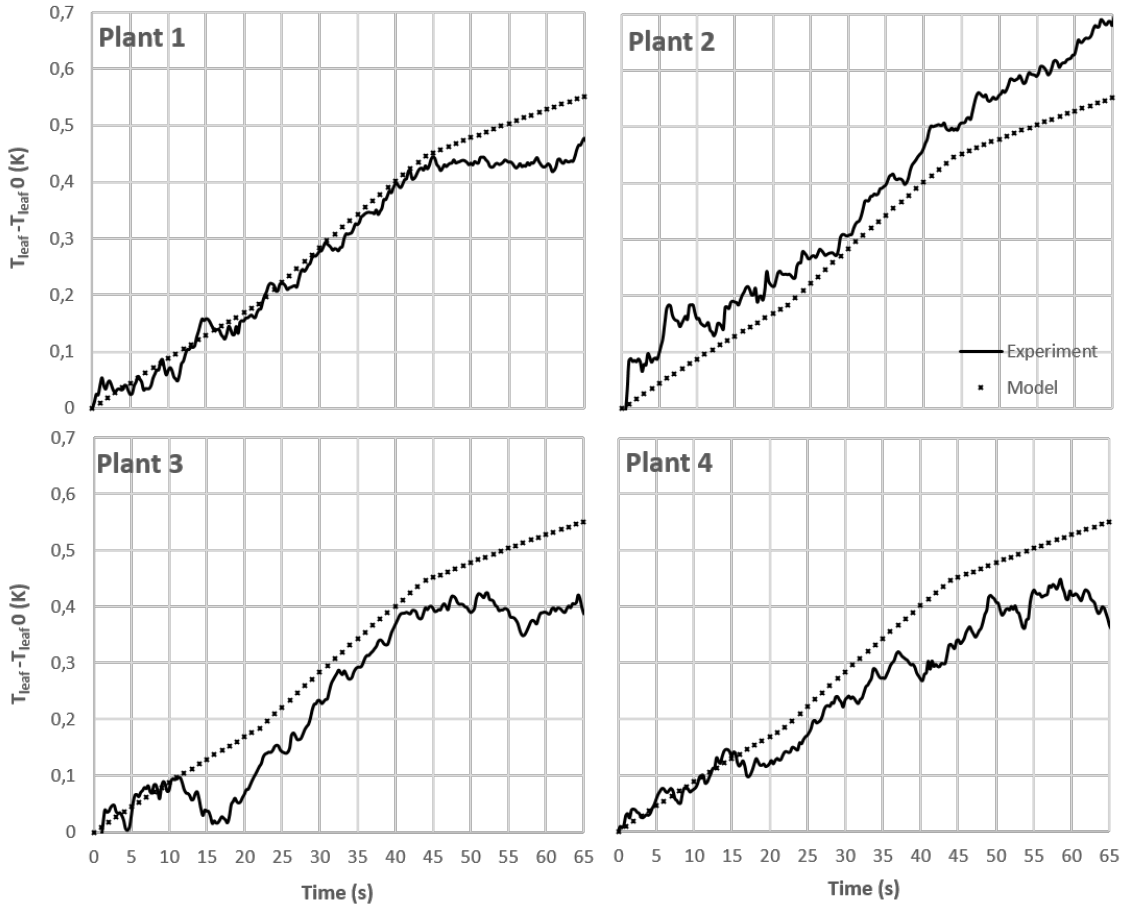

Figure 4.27: Temperature evolution over an average parabola of 65 seconds, without ventilation, model simulation and experimental results for the 4 plants. Average on all usable parabolas (see Table 4.7).

The experimental and simulation results follow similar trends, although the different phases are not as visible on the experimental results as on the model simulation results. Quantitatively the leaf surface temperature increase are of the same range, experimentally and from the simulation. As seen previously, the "after" 2g-phase is flatter experimentally than from the simulation (except for plant 2).

The analysis is now performed on the parabolas for which a ventilation was set on the two 2g phases, before and after the 0g phase, at the lower setting (Figures 4.28 and 4.29) and higher setting (Figures 4.30 and 4.31).

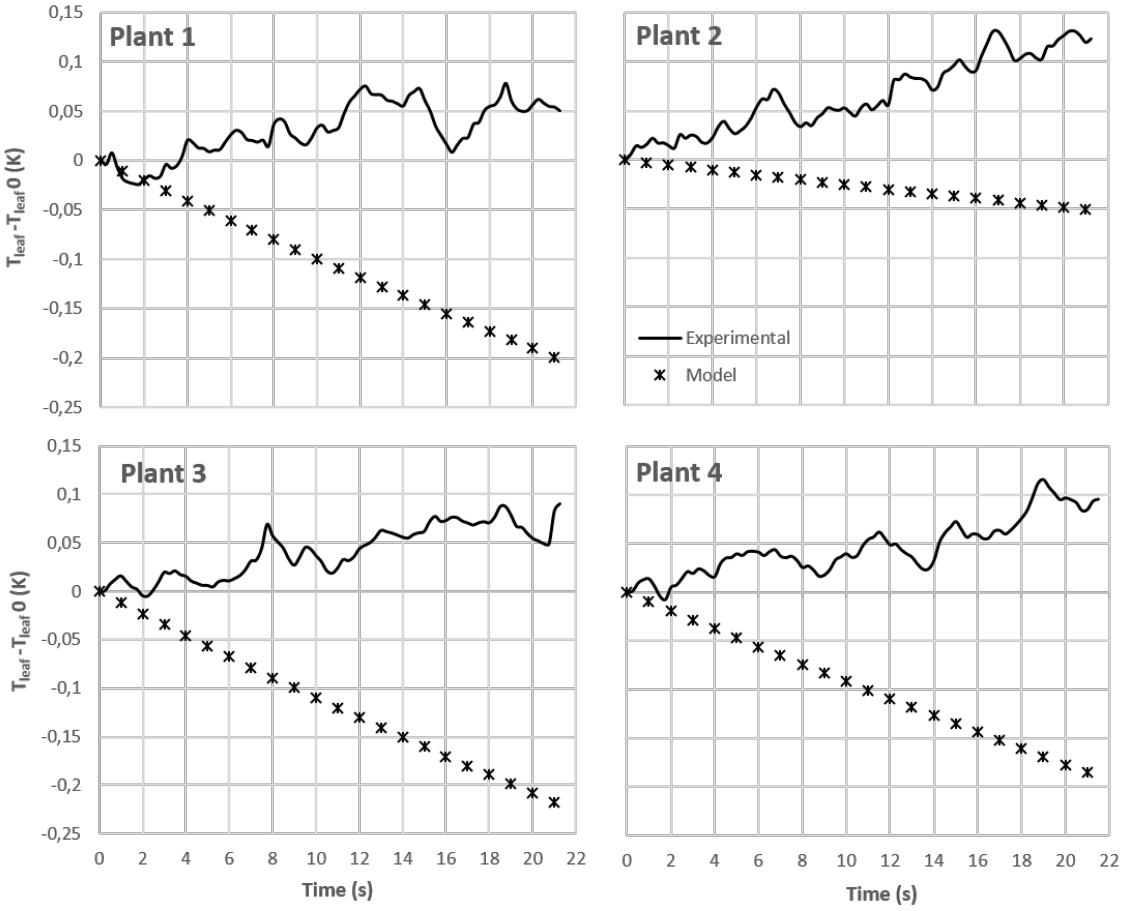

Figure 4.28: Temperature evolution over 22 seconds in 2g before the 0g phase, with the lower ventilation setting (plant 1: 0.0225 m/s; plant 2: 0.00198 m/s; plant 3: 0.0789 m/s; plant 4: 0.00624 m/s), model simulation and experimental results for the 4 plants. Average on all usable parabolas (see Table 4.7).

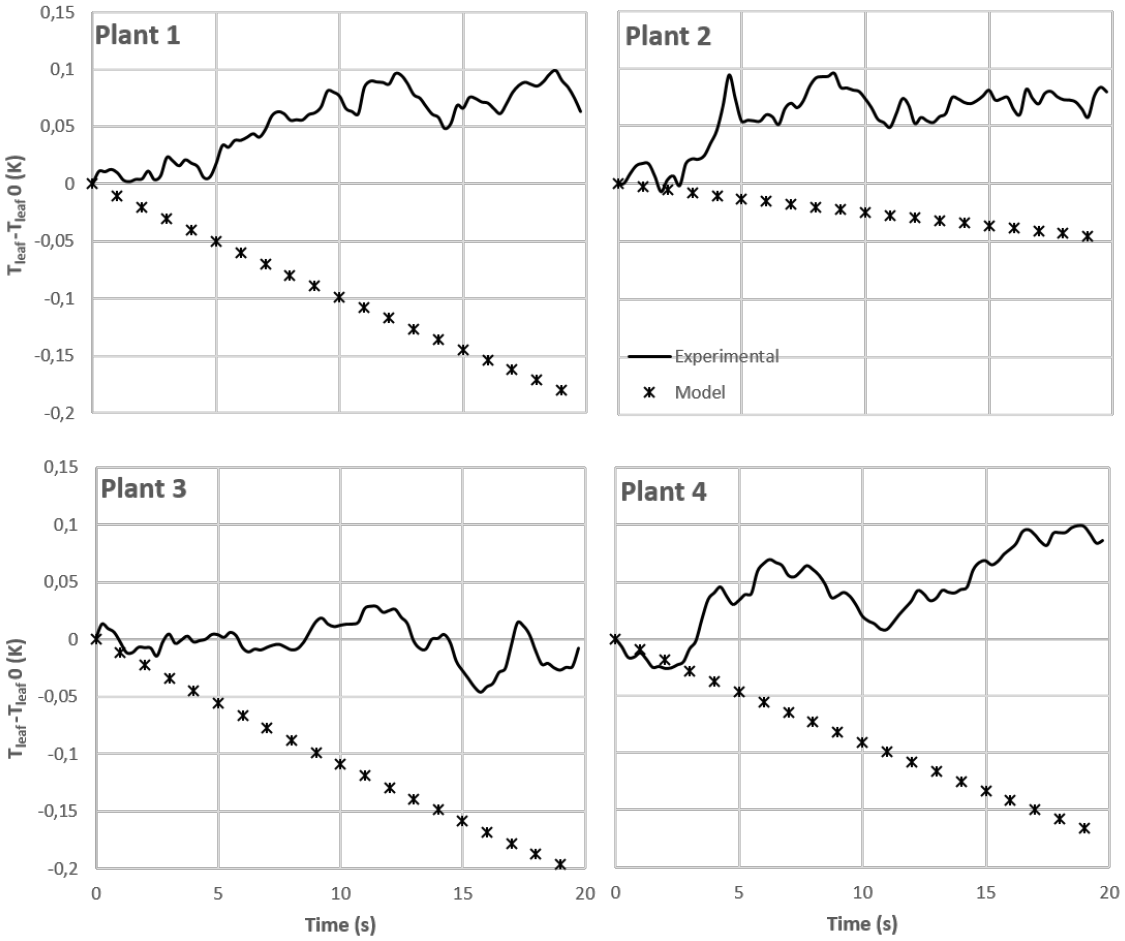

Figure 4.29: Temperature evolution over 20 seconds in 2g after the 0g phase, with the lower ventilation setting (plant 1: 0.0225 m/s; plant 2: 0.00198 m/s; plant 3: 0.0789 m/s; plant 4: 0.00624 m/s), model simulation and experimental results for the 4 plants. Average on all usable parabolas (see Table 4.7).

Like in the 0g phase, the experimental and simulation results are not in accordance, compared to the case without ventilation. The model predicts a decrease in leaf surface temperature in the range of 0.05 - 0.2 K, while experimentally the leaf surface temperature rises from 0.05 to 0.1 K.

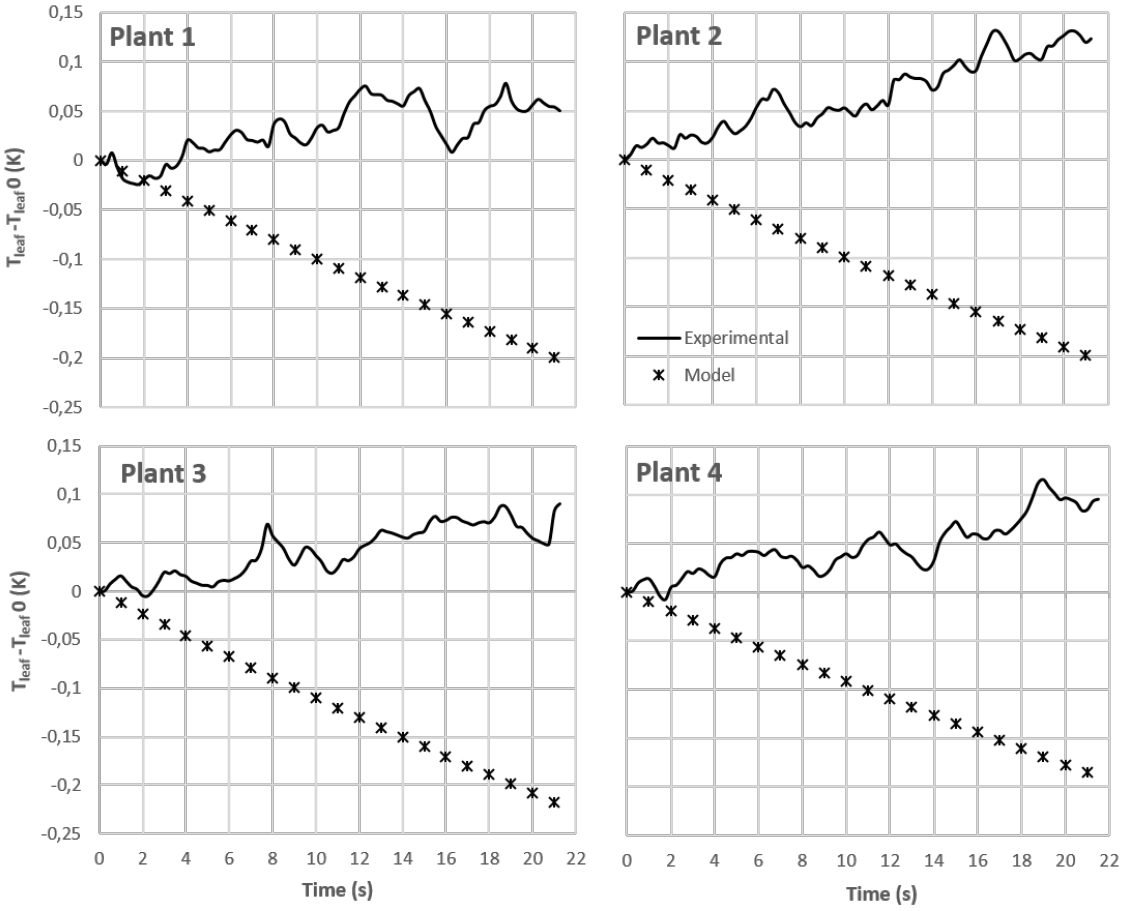

Figure 4.30: Temperature evolution over 22 seconds in 2g before the 0g phase, with the higher ventilation setting (plant 1: 0.0243 m/s; plant 2: 0.00586 m/s; plant 3: 0.0786 m/s; plant 4: 0.00433 m/s), model simulation and experimental results for the 4 plants. Average on all usable parabolas (see Table 4.7).

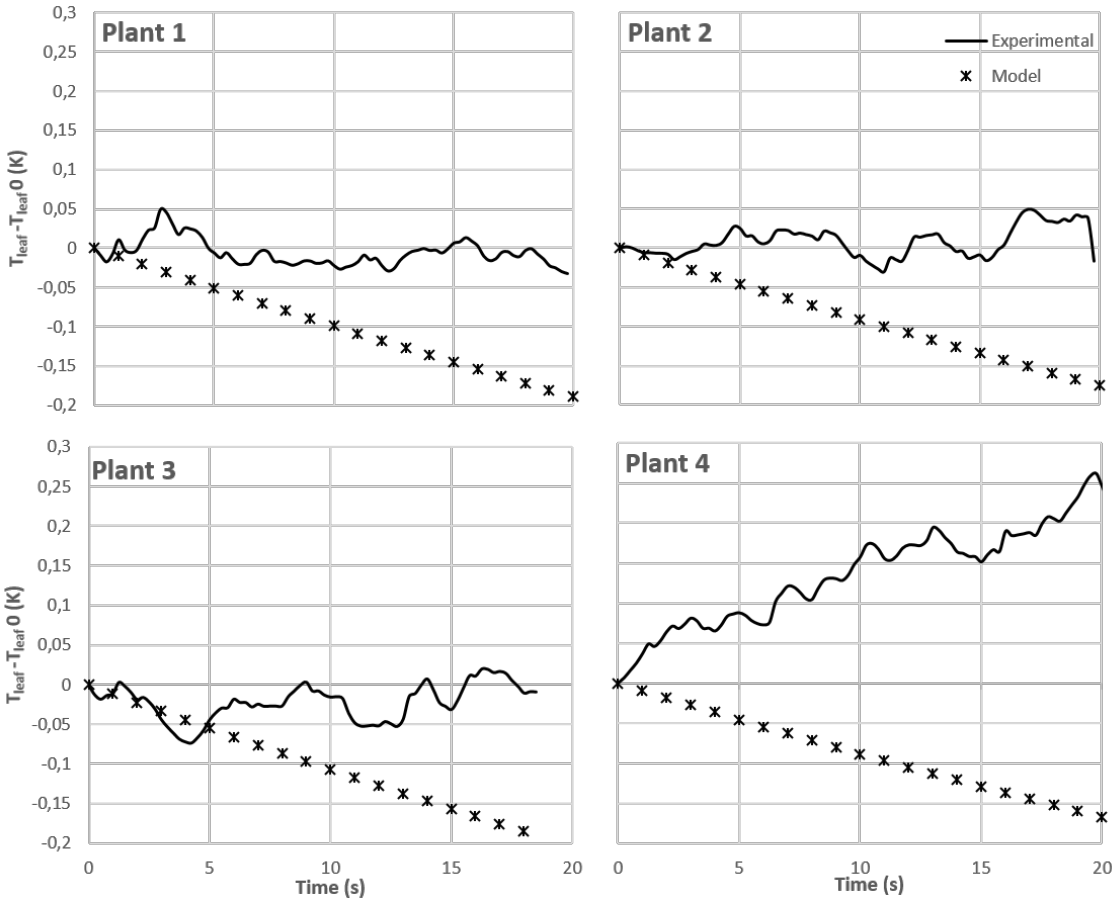

Figure 4.31: Temperature evolution over 20 seconds in 2g after the 0g phase, with the higher ventilation setting (plant 1: 0.0243 m/s; plant 2: 0.00586 m/s; plant 3: 0.0786 m/s; plant 4: 0.00433 m/s), model simulation and experimental results for the 4 plants. Average on all usable parabolas (see Table 4.7).

The observations are similar for the case with the higher ventilation level: the experimental and simulation results do not match. However, in the case after the 0g phase, the trends observed experimentally are closer to the ones predicted by the model, since the measured leaf surface temperature stagnates or slightly decreases (except for plant 4).

4.4.3 Conclusion

The results obtained from the statistical analysis correspond to what was expected from the literature review and enabled to identify main trends in the phenomena observed. They also confirmed that the temperature variations between the transpiring leaf and the non-transpiring leaf are significant. The dynamical analysis enabled to partially validate the model, in 0g and 2g, when there is no forced convection. However, the model predictions are not validated experimentally with forced ventilation. In any case, these results

and validation will need to be confirmed and the model further validated with a new experiment, which completed three flights in April 2018 and will fly again in November 2018. The changes performed in the experimental set-up and procedures are detailed in section 4.5.

4.5 Lessons learned and new set-up

The data analysis of the experiment performed in October 2017 led to the improvements of many sub-systems of the experimental set-up, from sensors to procedures, for the following ESA parabolic flight campaigns of April and November 2018.

4.5.1 Anemometers

The measurement range lower value of the anemometers used in the initial experimental set-up was 0.1 m/s. Since the lowest air velocities we working with are in the range 0.05-0.15 m/s, as seen in section 3.3, it was decided to change the hot wire anemometers for Intertek® TRANSDUCER 8475 model, whose measurement range goes from 0.05 to 2.5 m/s. The new data acquisition frequency is once every 4 seconds but the gain in precision is great.

4.5.2 Lighting system

The light provided to the spinach in the initial experimental set-up was very little, in comparison to what is recommended for plant growth (25 µmol/m^2/s in average against 400 µmol/m^2/s recommended) (Dougher and Bugbee 2001, 2001; personal communication with INRA sicentists, 2018). This might explain the results obtained, a low photosynthesis rate induced low transpiration rates and thus low temperature variations at the leaf surface.

The lighting system was thus replaced by a custom-made one, especially designed for our needs and set-up by DLS Lighting (St-Georges-de-Mons, France) (Figure 4.32 and 4.33). Like the previous system, it is composed of four modules all connected to the same driver, each of them containing four warm (3000 K) white LED lamps mounted on aluminum plates equipped of fins that dissipated the heat generated by the LEDs (Figure 4.34).

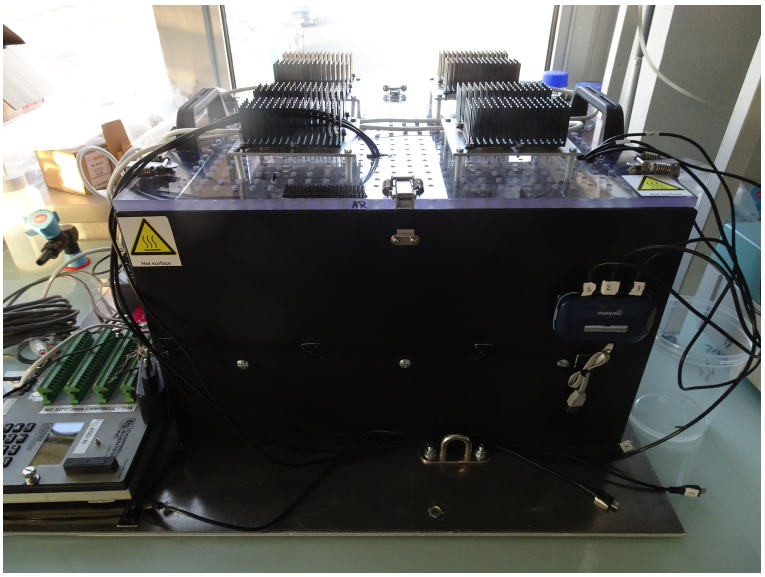

Figure 4.32: New lighting system installed on the enclosure - Side View

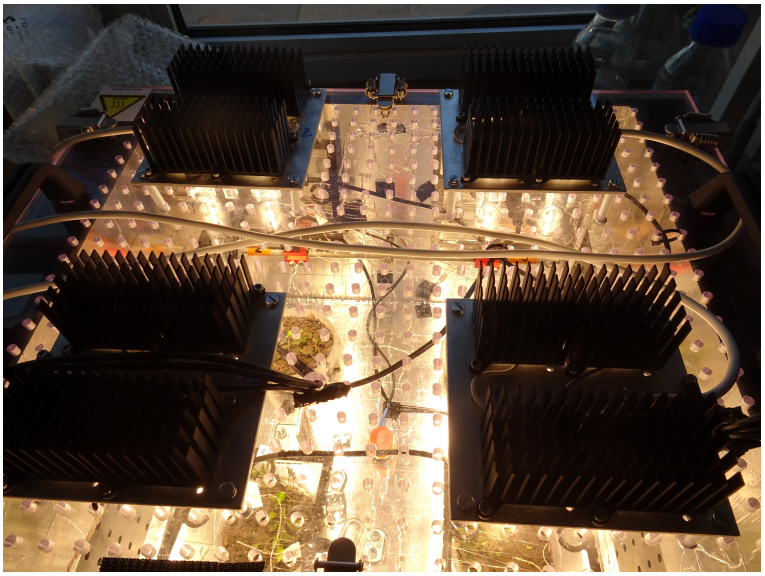

Figure 4.33: New lighting system installed on the enclosure - Top View

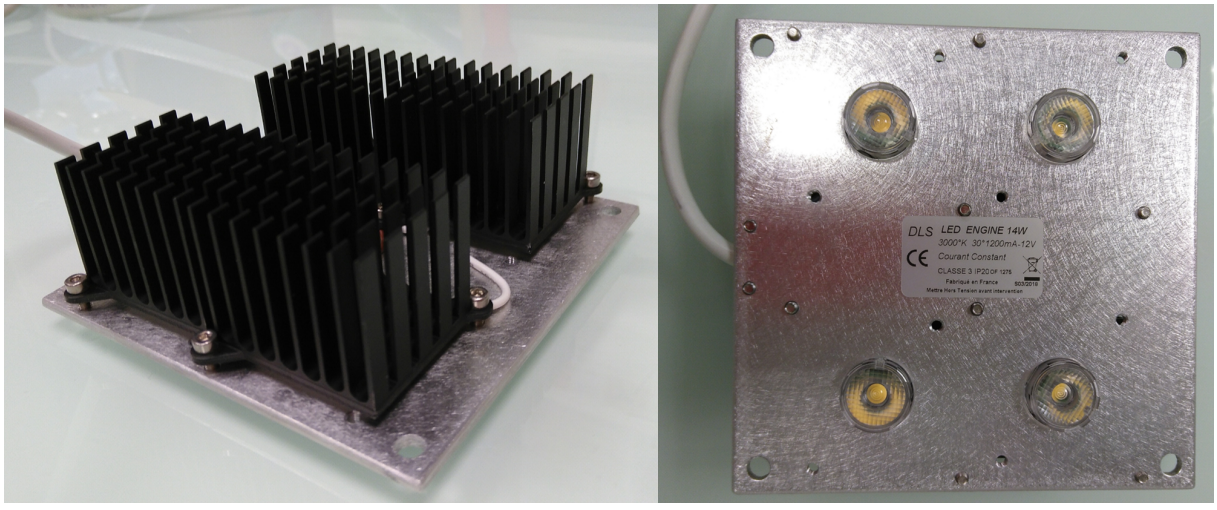

Figure 4.34: New LED module back (left) and front (right)

The light intensity was measured, at the height of the studied leaves, using using a LI-COR quantum sensor (LI-190) mounted on a portable meter LI-COR Quantum/ Radiometer/ Photometer LI-189 and provides from 363.2 to 768.1 µmol.m^{-2}.s^{-1} to the plants, with an average of 539 µmol.m^{-2}.s^{-1} and a standard deviation of 116 µmol.m^{-2}.s^{-1}. The light spectrum, as characterized using a an Ocean Optics USB 2000+ spectrometer with an optical fibre (QP 400-2-SR) and a cosine corrector (Ocean Optics CC-3) coupled to the fibre, is given in Figure 4.35.

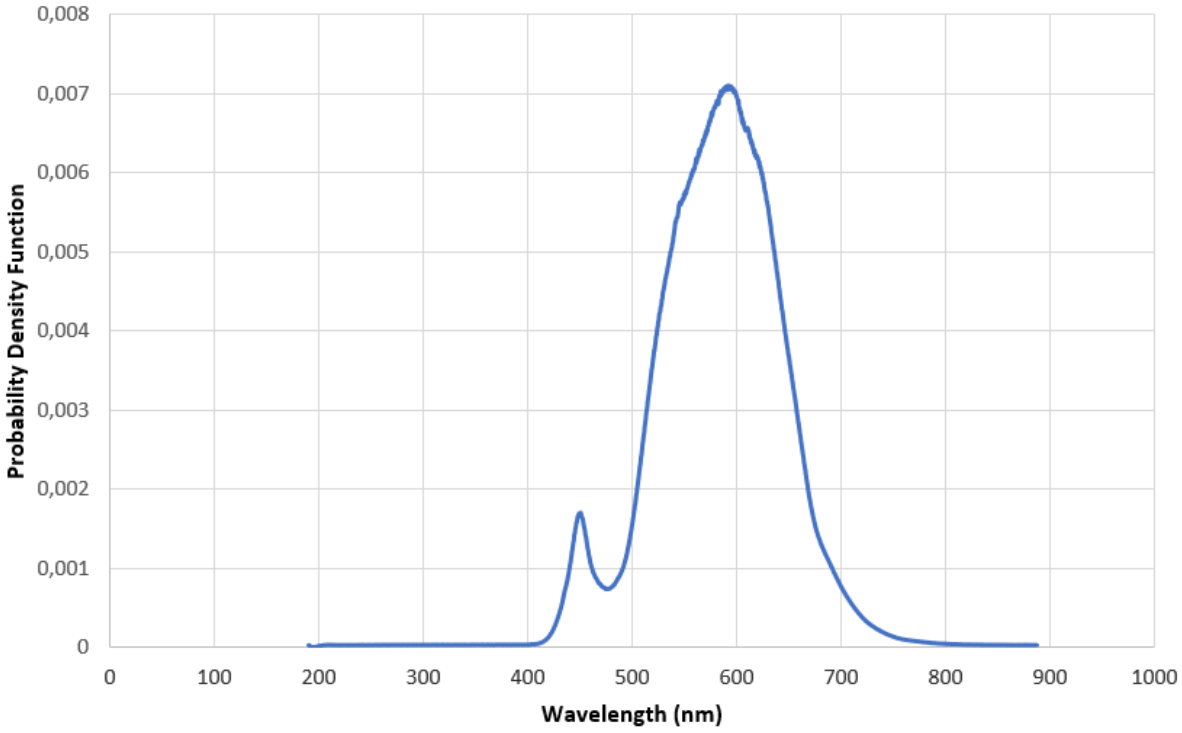

Figure 4.35: Probability Density Function of the new LED lighting system

4.5.3 Thermocouples

An issue that could not be anticipated before the flight was the temperature jumps of the thermocouples, which only occurred during the flight, and were likely due to electromagnetic perturbations but the cause of the issue could not be accurately identified. Hence, it was decided to replace the thermocouples for PT100 temperature sensors (Heraeus, M1020 (-50/+300°C)). They are linked to the Campbell data logger via a Wheastone bridge.

4.5.4 New procedures

To avoid any fungi contamination, the ground procedures before the flight were modified. The opening of the lid and cutting of pots will be done under a sterile hood with laminar flux. Some tests of this new procedure were performed on the ground and succeeded in avoiding any contamination. To provide a better acclimation to the plants, pots will be opened more than a week before the flight, instead of a few days ahead.
An alternative to the agar medium was used during the campaign of April 2018, which consisted in growing spinach hydroponically within rockwool medium. No contamination was observed and the spinach plants did not need a thorough acclimation like it was the case with in-vitro culture. Since the set-up of this growth method is practically easier to handle, this method was preferred for the future campaign of November 2018.

4.5.5 New application for cameras

The application used to acquire IR images with the Android devices was modified to avoid any unwanted calibration during data acquisition. Additionally, the number of IR images acquired during flight was set to one per second. Preliminary tests in the laboratory were successful and demonstrated that the application enabled a stable and reliable acquisition of IR images.

4.5.6 IRGA tests

Additional tests in laboratory using an infra-red gas analyzer (IRGA) will enable the quantification of CO_2 uptake and H_2O transpiration of spinach plants for different airflow velocities, leading to the determination of the WUE and linking this to IR images of the leaves.
A 5-week old spinach plant is set into a sealed Plexiglas enclosure equipped with a controlled air inlet, CO_2 injection, and outlet, and a fan allowing to change the air velocity. A custom-made Infra-Red Gas Analyser (IRGA) using two Li-820 (Lincoln, USA) measures the CO_2 and H_2O concentration differences between the inlet and the outlet tubes, which corresponds to the total CO_2 uptake and water transpiration of the plant. A Flir One IR camera is set inside the enclosure to acquire IR images of the plant and connected to the Android device, outside the enclosure. An anemometer and a light quantum sensor are

also set in the enclosure to assess air velocity and light intensity.
Measurements are acquired for multiple spinach plants and air flow velocities. Assimilation rate and stomatal conductance are inferred from the total CO_2 consumption and their total leaf area (measured with areameter Licor 3000A ®), leading to the calculation of the Water Use Efficiency (WUE).

4.6 Conclusion

Although the phenomena are studied in transient state for short time constants (20s), the observed and simulated effects are locally representative of the phenomena that would be observed in a large-scale cultivation module in reduced gravity environments. The CFD analysis enabled to put in light air dynamics within the enclosure and estimate forced convection velocities at the surface of the leaves. The experiment performed in the parabolic flight of October 2017 contributed to validate the model in 0g and 2g without ventilation, as well as identify main trends. These results will need a refly to be confirmed and deepened, in the cases with ventilation. To be further validated, a comparison of the results obtained with the first version of the MELiSSA plant growth model and this new one including gravity as a parameter should be made, supported by experimental data obtained on lettuce growth in growth chambers at Guelph university, offering a validation of the model in steady state. This flights also enabled to identify flaws and problems of the experiment, which allowed us to improve the experimental setting for the upcoming two campaigns.
This work with COTS IR cameras inspired the project Astroplant Challenge, supported by the MELiSSA project, to include IR sensors in their plant cultivation citizen kit, in order to monitor plant transpiration. These pieces of equipment are easy to handle for non scientists and IR images of plants are very interesting outreach material, offering multi-disciplinary aspects.
Outreach and multi-disciplinary dimensions are two things that were very dear to me during this PhD project, which is why I co-created the project "Retour A l'Ecole", with other PhD students from Université Clermont Auvergne, which consists in making outreach in primary schools about a broad range of scientific topics, focusing on making rather than learning, and following the scientific method. The details of this project are given in a

paper presented at the 68th International Astronautical Congress in Appendix C.

4.7 Chapter's outcomes

- We performed the whole design, assembly, and implementation of a parabolic flight experiment capable of acquiring 120 Gb in one flight, using simple and COTS equipment. This data was aimed at validating the model presented in the previous chapter.
- Velocities at the leaf surface can be estimated with a CFD analysis.
- Trends in the leaf surface temperature variations revealed by the statistical analysis are in accordance with the literature.
- This experiment enabled us to validate local gas transfer models in 0g and 2g without ventilation.
- From one local measure (the leaf surface temperature), we are able to derive realistic trends on global phenomena.
- The study of transient states for short time constants (20s) tells us a lot about local gas transfer.
- These results will be confirmed by six additional parabolic flights and deserve to be extrapolated for physiological interpretations.
- Local transfer justifies all CFD computations in 1g and 0g to establish velocity, temperature, and concentration profiles.

Chapter 5

Sap transport and plant morphology

5.1 Introduction

In the previous chapters, the focus was set on gas exchanges modeling in reduced gravity environment and this detailed model has been included into the initial version of the MELiSSA plant growth model. Hence, the gas exchanges part of the physical module in this model is now better detailed than the biochemical and morphological modules and is mechanistically described for inclusion of gravity as a model parameter. Although part of the physical module, the flux associated with water absorption was not investigated further in this study. However, this flux can be limiting and inhibit photosynthesis, it becomes thus crucial in the frame of a realistic plant growth model to include sap transport mechanisms and study their potential alterations in low gravity settings.

The inclusion of a realistic morphology module based on mechanistic equations is also mandatory to thoroughly understand plant development in space and is necessary when transitioning from a single leaf model to a multiple leaves and organs plant. In the current version, morphology is quantitatively taken into account with empirical proportional equations with the produced biomass, which allows the computation of a coupled mass and energy balance of the plant.

Further steps in the MELiSSA plant growth model will need to include detailed sap transport and detailed plant architecture, enabling the inclusion of gravity as a model parameter. Consequently in this chapter, the mechanisms of sap transport in the xylem and the phloem are reviewed along with the associated existing models, plant growth models including a detailed morphology linked to plant physiology are assessed, and the conse-

quences for our model are detailed. Lastly, a discussion about leaf senescence mechanisms and the possibilities of modeling them is included.

5.2 Sap transport: mechanisms and existing models

There are two types of vascular tissues in plants: the xylem, pulling water and nutrients from the soil to the transpiring leaves and the phloem, transporting photosynthates through the plant to non-photosynthetic organs (Knoblauch and Peters 2017).

5.2.1 Xylem transport

The xylem in plants' stem is made of dead cells, hence the transport is passive and ensured by two mechanisms: transpiration at the exit and root pressure at the entrance.

Transpiration and the cohesion-tension theory

Evaporation from the surfaces of mesophyll cells in the leaves form concave menisci in mesophyll cell walls, leading to high surface tension. According to Laplace's law, with this curvature of menisci, it is possible to have a pressure jump between the outside atmospheric pressure and the low pressure in the xylem (Caupin and Herbert 2006). This results in the concavity of these menisci pulled outwards generating a very low pressure in the xylem, in turn pulling water from the roots. This is often referred to as "negative pressure". In fact, as Caupin explains in his review of 2006, according to the classical nucleation theory, this concept refers to a liquid density that is reduced compared to the equilibrium one, when intermolecular distances become larger and water in the xylem is in a metastable state because of water molecules' mutual attraction (Caupin and Herbert 2006).

This mechanism of sap ascent, ensuring continuity in the water column, is called the cohesion-tension theory. Capillarity balances gravity and also provides the force that moves water upwards. Indeed, the xylem conduits are hydrophilic, hence providing adhesion between water and their surface. The attractive force creating surface tension in liquid water comes from the fact that water is a polar molecule and a negatively charged oxygen atom of one water molecule bonds with a slightly positively charged hydrogen atom of another molecule (Caupin and Herbert 2006).

Cavitation

Cavitation in plants influences their anatomy, physiology and ecology in many ways and corresponds to a critical aspect of water relations (Cochard et al. 2013). When water is limiting, stomata close to prevent cavitation (Cochard 2002). During a drought, the succession of cavitation events can lead to plant death (Brodribb and Cochard 2009; Brodribb Tim J. et al. 2010).

Mechanism of cavitation

To understand the causes of cavitation, it is essential to go back to the cohesion-tension theory. When water molecules density drops below the spinodal density, which corresponds to a spinodal pressure, the system becomes unstable and allows perturbations to develop without limit, leading to cavitation, as predicted by the density functional theory, since this phenomenon is not described by the classical nucleation theory (Caupin and Herbert 2006). This drop in water molecule density finds its origin in the emergence of air bubbles inside the xylem, that grow until they are as wide as the xylem width, preventing water to circulate. Let us consider an air bubble of radius r_{bubble} and, according to the ideal gas law, of pressure (Figure 5.1):

$$P_{bubble} = \frac{n_{bubble} RT}{V_{bubble}} \tag{5.1}$$

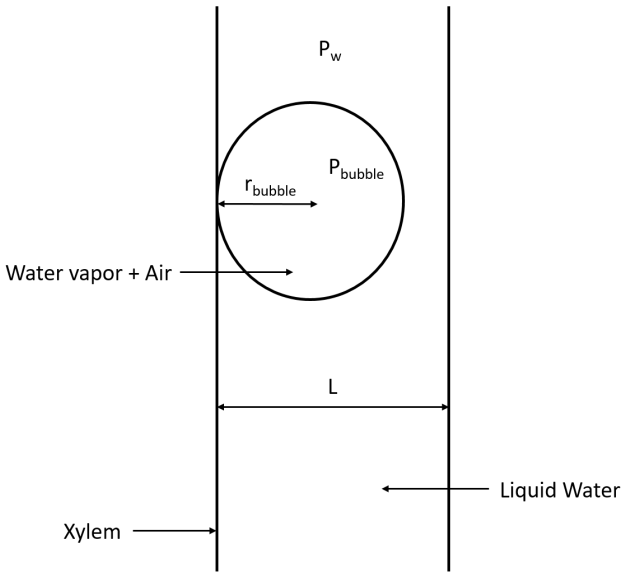

Figure 5.1: Diagram of cavitation mechanism in the xylem.

The tendency to collapse of the bubble makes the volume V_{bubble} decrease, leading to an

increase of the pressure P_{bubble}, which balances the collapsing force. As P_{bubble} increases, the gas inside the bubble becomes more soluble in water (Henry's law) and thus the bubble slowly collapses as air dissolves and n_{bubble} decreases (Tyree 1997). In this case, cavitation does not occur. But when this happens with a high transpiration rate, the pressure P_w inside the xylem decreases (cohesion-tension theory), thus the air bubble expands, and according to Laplace's law:

$$P_{bubble} - P_w = \frac{2\tau}{r_{bubble}} \tag{5.2}$$

The right-side term decreases until r_{bubble} reaches the width of the xylem, which corresponds to a maximum volume V_{bubble} and a minimum pressure P_{bubble} (Tyree, 1997):

$$P_{bubble_{min}} = \frac{nbubble\, R\, T}{V_{bubble_{max}}} \tag{5.3}$$

Hence:

$$P_w = \frac{6\, n_{bubble}\, R\, T}{\pi\, L^3} - \frac{2\,\tau}{L} \tag{5.4}$$

At this point when the bubble has expanded to the width of the conduit, no more water transport occurs and the conduit is thus dysfunctional. When the pressure inside the xylem is smaller than a critical pressure, the air bubble is sucked to an adjacent vessel thus embolizing adjacent vessels and creating a new cavitation. Stability exists if the radius of the meniscus is bigger than the radius of the pores. Thus, the porosity of pit-membrane (section of the cell wall through which adjacent cells can exchange fluids) is critical to prevent dysfunction of adjacent vessels to embolized vessels (Tyree 1997).
Small diameter vessels are needed to avoid cavitation which breaks the water column, preventing parts of the plant to receive sap. Indeed, from equation 5.4, we deduce that, because $P_w > 0$:

$$L < \sqrt{\frac{3\, n_{bubble} RT}{\pi\tau}} \tag{5.5}$$

Pressures down to 15 MPa can be sustained by pores about 20 nm diameters. Under this pressure threshold, meniscus is sucked through the cell wall and will generate embolism

in adjacent xylem conduits (Tyree 2003).

Causes for cavitation

Cavitation or embolism can be caused by many events like drought, freezing stress, foliar abscission due to herbivory or wind damage (Tyree 1997; Cochard 2006). But more generally air bubbles inside the xylem can originate from the pores, from a hydrophobic crack, from homogeneous nucleation (when cohesion between water molecules is lost because of frost), or from hydrophobic adhesion failure (i.e. loss of adhesion between water molecules and walls of the xylem) (Tyree 1997; Cochard 2006).

Dry soils and viscous flow generate very low pressure in the xylem, even at smaller heights, that might induce cavitation (Caupin and Herbert 2006). Fast-growing species usually have large very efficient conduits, which are highly vulnerable to cavitation, making them less adapted for drought climates. Slow-growing species however have small inefficient conduits which are very resistant to cavitation and thus perform better under drought conditions (Tyree 2003).

In frozen xylems, bubbles of gas can form in ice, since gas is insoluble in ice, which can then spread and induce cavitation in the xylem when ice thaws, depending on how large the bubble is and how low the xylem pressure is (Cochard 2006).

Observation and measures of cavitation

There are many ways to observe cavitation: by direct observation cutting a branch and using a colored liquid; by acoustic emissions, although it was shown that acoustic waves in trees can also be due to other mechanisms; by calculating the percent of loss of hydraulic conductance and establishing vulnerability curves (already established for hundreds of tree species) (Cochard 2006).

The three main methods used to induce cavitation in the xylem are: bench dehydration, air pressurization, and centrifugation (Cochard et al. 2013). To measure cavitation and embolisms, the following methods are used: acoustic detection of cavitation, observations of xylem water content (direct and indirect), and hydraulic detection of embolisms (Cochard et al. 2013). Any of these methods can be combined together to establish a vulnerability curve (VC) of the xylem. These are two-dimensional graphs giving the percentage of cavitation according to the xylem pressure.

Cavitation and recovery from it occurring daily were observed in the past but it turned

out that this was a bias in the sampling procedure (Cochard and Delzon 2013; J. K. Wheeler et al. 2013). According to Cochard et al., the analysis of exponential curves is associated to defective techniques used world-wide, which overestimates the vulnerability to cavitation of the xylem (Cochard et al. 2010; Cochard and Delzon 2013). Trees might not be able to refill their pipes that easily and that often as suggested by previous studies; the "high cavitation resistance" paradigm is the only reasonable structure to understand water relations within plants (Cochard and Delzon 2013).

Positive water pressure in the roots

When water potential of root cells is more negative than that of the soil, water moves to the root from soil by reverse-osmosis (i.e. selective and active ions uptake from soil solution) which generates positive pressure in the roots forcing sap through the xylem to the leaves. This sometimes results in the phenomenon of guttation and may refill cavitated conduits (Cochard 2006).

Two reasons explain the fact that sap flow is directed to the symplasm in roots (Cochard 2006). First of all, casparian strips located into the endodermis cells are made of hydrophobic suberin, preventing water to take the apoplasmic pathway; and second, aquaporins (water channels) in the plasmalemma membrane make it more porous and thus less resistive, so water flows through the less resistive pathway which is the symplasm (Cochard 2006).

5.2.2 Phloem transport

Mechanism of sap flow in the phloem

Unlike the xylem, the phloem has been less extensively studied and thus less quantitative data about transport in the phloem is available, making the modeling effort quite difficult (Carvalho, Losada, and Niklas 2018). The phloem is a group of multiple conduits that are composed of living cells called sieve elements or sieve tubes (Carvalho, Losada, and Niklas 2018). Sap in the phloem can move through sieve tubes in both direction, following an osmotic gradient, from sugar sources (parts of the plant producing carbohydrates, such as photosynthesizing leaves or roots releasing carbohydrates when the plant grows) to sugar sinks (parts of the plant that are growing and storage organs, including young leaves, fruits, seeds, and roots): this is known as the Münch pressure-flow hypothesis (Münch

1927; Knoblauch and Peters 2017; Carvalho, Losada, and Niklas 2018) (see Figure 5.2). There are two mechanisms for loading and unloading sugars into and from the phloem (Carvalho, Losada, and Niklas 2018):

- the symplastic path: passive diffusion following a concentration gradient that is sometimes assisted by an active mechanism of polymer trapping;
- the apoplastic path: active transport of sugars via H+/sucrose antiporters.

At sugar sources (e.g. photosynthetizing leaves), high photosynthates concentrations result in water coming from the xylem by osmosis increasing hydrostatic pressure (Knoblauch and Peters 2017; Carvalho, Losada, and Niklas 2018). At sugar sinks, once sugars are converted to starch (for storage in roots or in tubers), it is insoluble in water and thus has no more osmotic effect. Pure water left in the phloem leaves it by osmosis or is pulled to the xylem by the transpiration pull, lowering the hydrostatic pressure (Knoblauch and Peters 2017) (see Figure 5.2). Phloem transport also enables the provision of carbohydrates to the plant's tissues on the way, generating a lateral leakage in the phloem (Minchin and Lacointe 2017).

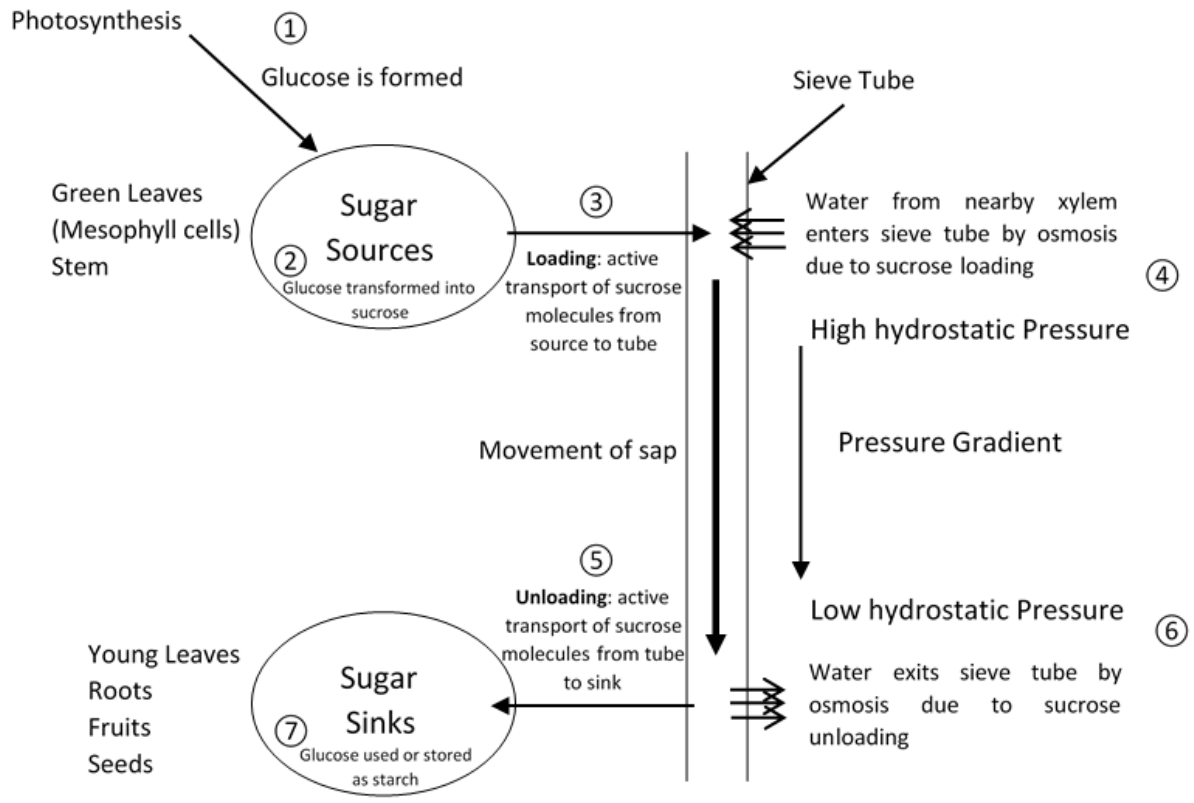

Figure 5.2: Diagram of sugar translocation in the phloem.

The Münch hypothesis

There was a controversy on the Münch hypothesis for transport of assimilates through tall trees, arguing that the hydraulic resistance would be too important and prevent sap from moving from the leaves to the roots (Knoblauch and Peters 2017; Ryan and Robert 2017). Indeed resistance in phloem vessels is ten times larger than in the xylem because of their small diameters (Ryan and Robert 2017). But recent measurements showed that from the top to the bottom of trees, phloem vessels and pores on the sieve plates get larger, which increases the area of the conduits and decreases their resistance, giving a cone shape resistance to the phloem (Ryan and Robert 2017). This requires a smaller pressure to generate flow in the phloem, thus also explaining sugar transport in very tall trees (Ryan and Robert 2017). A recent study on morning glory plants found that pressure differentials increased with the distance between a source and a sink, which is predicted by Münch hypothesis (Knoblauch et al. 2016; Knoblauch and Peters 2017). They also found that larger plants also have an increased sieve tube conductivity, since sole pressure gradients would not have enabled such mass flow rates observed in trees (Knoblauch et al. 2016). These measurements in plants' phloem have shown that models of Da Vinci and Murray about phloem flow, which considered a closed hydraulic system and the conservation of cross sectional areas of conduits, are not adapted for modeling flow through the phloem (Carvalho, Losada, and Niklas 2018).

5.2.3 Modeling sap transport

Modeling sap flow into the xylem and the phloem

As seen in the previous section, the cohesion-theory describes sap ascent in the xylem as the surface tension at the leaf surface being transferred to the roots by an uninterrupted column of water, making water potential in the roots lower than the soil potential and thus leading to water uptake. Water flowing upwards in the xylem, from the absorption in the soil to the transpiration in the atmosphere, can be modeled using analogies to Ohm's law (Thornley and Johnson 1990; Tyree 1997). It can be considered that the soil is composed of multiple resistances in parallel, which can be combined into a global soil resistance; this global soil resistance is in series with root resistances (Tyree 1997) and when there is a large water storage in trees, it can be seen as a capacitor. Transpiration

is then the analogous to the electric current, initiated by a vapour pressure difference leading to stomata opening (Williams, Bond, and Ryan 2001). Hence, the water flow through each xylem vessel can be written with an analogous to Ohm's law, driven by a potential gradient:

$$F_x = -\frac{\Delta\psi}{r_x} \tag{5.6}$$

Where F_x is the water flow in the xylem, r_x is the resistance of the xylem vessels determined thanks to Hagen-Poiseuille equation and $\Delta\psi$ the gradient in water potential (Daudet et al. 2002).

Sap concentrated in sugars moves downwards along a turgor gradient, which is aided by gravity on Earth, unlike water flowing in the xylem going against the direction of gravity (Ryan and Robert 2017). To study sap flow in the phloem alone without taking into account radial water fluxes and the dynamics of solute transport, Navier-Stokes equations are used for the fluid motion and Van't Hoff equation is used to calculate the osmotic pressure (Henton et al. 2002). Henton et al. (2002) and Daudet et al. (2002) assumed that all carbohydrates were soluble sugars and expressed the osmotic potential π as a linear function of the sucrose concentration C:

$$\pi = -R\,T\,C \tag{5.7}$$

where R is the ideal gas constant and T the temperature. Henton et al. (2002) demonstrated via time-dependent numerical simulations that solute and water can simultaneously travel in opposite directions within the phloem. The sap flow in the phloem, F_p, can also be modelled using an Ohm's law analogy, but with a gradient of osmotic pressure (Daudet et al. 2002):

$$F_p = -\frac{\Delta P}{r_p} \tag{5.8}$$

where P is the osmotic pressure and r_p the resistance of the phloem vessels determined thanks to Hagen-Poiseuille equation.

The first analytical solution for phloem transport was given by Hall and Minchin 2013; previous phloem modelings were solved numerically only (Minchin and Lacointe 2017).

Phloem lateral leakage is usually not integrated into phloem and plant hydraulic models, because it is complex to model and it is also difficult to gather experimental data on this process (Minchin and Lacointe 2017). Therefore Minchin et al. have proposed an

addition to the already existing PIAF model (Lacointe and Minchin 2007) described here after in the paragraph "Modeling a coupled phloem and xylem transport" using a single-source single-sink system connected by a phloem element and showed that phloem lateral leakage has a greater effect on the hydrostatic pressure than on the gradient (Minchin and Lacointe 2017). Accurate modeling of the phloem requires more than a description with a Poiseuille's law, since it is a leaky pipe and its flow rate cannot be determined using only a local pressure gradient (Minchin and Lacointe 2017).

Modeling a coupled phloem and xylem transport

To have a complete plant hydraulic model, it is necessary to couple phloem and xylem flows, which are represented in a simple diagram on Figure 5.3. Earlier models used to have 1-D description following a continuous partial differential equation approach (Christy and Ferrier 1973; Thompson and Holbrook 2003). The research group at INRA/PIAF in Clermont-Ferrand has been implementing a numerical model for a little over 15 years, which describes xylem and phloem elements as finite elements using electrical analogies, enables a coupling between phloem and xylem flows and allows for a mechanistic modeling of the loading and unloading processes.

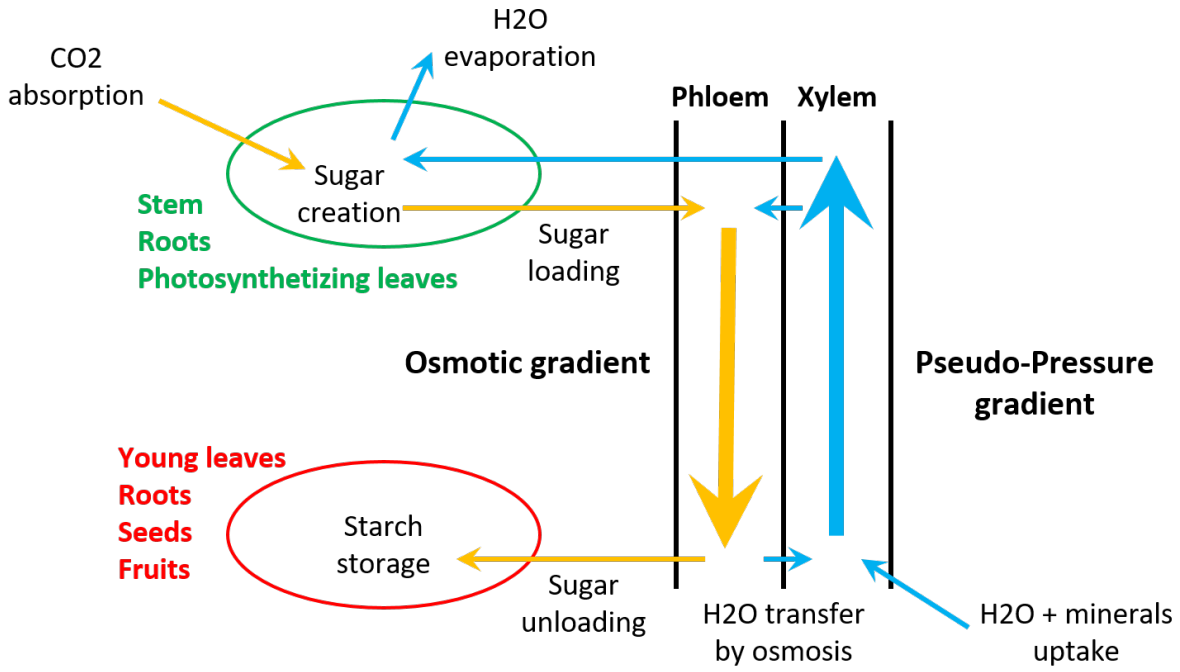

Figure 5.3: Simplified scheme of sap ascent and resources allocation in plants.

The bases of this model were laid down by Daudet et al. (2002) who expanded work started by Minchin et al. in 1993 and represented plant's hydraulic system as a branched struc-

ture, where both phloem and xylem are represented as discretized resistive elements in series, described by their xylem water potential and phloem sucrose concentration and turgor pressure, based on source-sink interactions, also known as transport-resistance modelling. This modular approach allowed a great flexibility in the plant geometries, as well as a quantitative description of water and carbon fluxes, through dynamic xylem/phloem interactions (Minchin and Thorpe 1993; Daudet et al. 2002). It was programmed with the software P-Spice, which is usually used to simulate electrical circuits and the most complex architectures they could achieve involved a network of three leaves, three fruits, one root, and eight stem segments (Daudet et al. 2002). Lacointe et al. expanded on work from Daudet et al. and implemented the model in C++ with a graphical interface allowing the modeling of more complex architectures and they were the first to model xylem/phloem interactions for a multi-sink system (Lacointe and Minchin 2008). The equations used for the axial flows are the ones described in the paragraph "Modeling sap flow into the xylem and the phloem", analogous to Ohm's law, where the driving force is a pressure gradient. The lateral flow is driven by a water potential gradient between the xylem and the phloem. The purpose of this model was to study the dynamics of flow in a coupled xylem/phloem system, rather than estimate realistic flow rates in the xylem and phloem. They have demonstrated that with two sinks, changes in transpiration rates can influence phloem translocation rates (Lacointe and Minchin 2008).

Hölttä et al. (2006) implemented a "discrete" generalized model of xylem/phloem transport in the trees, axially dividing them into N elements where the flow can circulate axially and radially between the phloem and the xylem (Hölttä et al. 2006). Water pressure gradient in the xylem comes from water removal at the top element and water uptake at the bottom element. Compared to the model developed by Lacointe et al. (2008), this one is simpler because it does not consider complex architectures and different organs such as leaves, stems, and roots. This model only considers two conduits and is built on a mass balance equation between incoming and outgoing radial and axial fluxes for each element. Then the equations driving the different flows are analogous to the ones developed by Lacointe et al.(2008):

- The link between pressure gradient and water flow in a given element of the phloem and of the xylem is computed with Darcy's law, which is analogous to Ohm's law.
- The radial flow is driven by a water potential gradient.

- The relationship between mass and pressure variations in time follows Hooke's law.
- The osmotic pressure in the phloem follows Van't Hoff's law.

Their simulations showed that the translocation mechanism in the phloem can happen without transpiration, generating flow movement in the xylem with phloem water only, allowing nutrient transport from the roots at night and in low transpiration conditions (Hölttä et al. 2006).
Both models made the hypothesis of sucrose as the sole solute transported in the phloem, when in reality other solutes are transported, such as potassium ions (Lacointe and Minchin 2008; Hölttä et al. 2006), which will have to be implemented in further versions. They provide a good mechanistic model of phloem/xylem interactions but it is a static description of the plant at a given point in time, which does not allow changes in plant structure and organ growth modeling or branching (Seleznyova and Hanan 2018).

5.3 Functional-structural models: linking sap transport and plant morphology

Functional-structural models enable to link plant physiology and plant morphology, using principles of carbon partitioning and resource allocations in a plant, as well as plant architectural languages, such as L-Systems. Lindenmayer-Systems or L-Systems are a formal language based on a grammar that enables a modular approach of plant modeling, allowing to outline a fixed plant morphology and the functions within this plant (Prusinkiewicz and Lindenmayer 1990; Vos et al. 2010). Functional-structural models are composed of two parts: the plant structure, defining organogenesis and its dynamic, as well as geometrical parameters of a plant; and the plant function defining processes and mechanisms driving plant growth and development. They can be either static or dynamic, depending on the studied type of interactions; static models are well adapted to investigate a given process of plant growth while dynamic models enable a whole-plant integration of these processes and linking them to plant morphology and the environment (Vos et al. 2010). Functional-structural models enable to get a better understanding of the plant and are focused on individual plants rather than on a whole canopy of several plants. For more details about existing functional-structural models, see the review made by Hézard in 2012

(Hézard 2012). Models used for agronomy predictions need to account for dynamics at crop level, taking multiple plants into account, and at this scale individual plant architecture and geometrical details are not as crucial as the organ growth and distribution over time (UVED 2018). Therefore the model of GreenLAB which aims at being an agriculture decision-making help and an agronomy prediction model is based on a common biomass pool and can be adapted for a large variety of plant species mostly oriented towards the study of organogenesis (De Reffye et al. 2003; Counède et al. 2006). The architecture of the plant is given following organogenetic rules and biomass growth and organogenesis are governed with source-sink interactions using dynamic equations (Counède et al. 2006; Mathieu et al. 2009). The feedback model where the plant development depends on the environment is still under development (UVED 2018). We will not detail more the GreenLAB model here, since its aims differ from those of a mechanistic plant growth model adapted for Life-Support Systems and we will focus on the functionnal-structural models.

5.3.1 Towards the inclusion of phloem/xylem interactions within functional-structural models

The models presented in the introduction of part 5.3 provide a mechanistic description of a coupled xylem / phloem carbohydrate transport and resource allocation between organs in a complex architecture but this plant structure is fixed in a given point in time and does not evolve with the production of biomass, making it impossible to model organ growth, shoot elongation and branching (Lacointe and Minchin 2008; Seleznyova and Hanan 2018). Therefore Prusinkiewicz et al. developed a model coupling carbon transport and allocation based on sink-source interactions as detailed in the introduction of part 5.3 with L-systems, in a model called Carbon Transport-Resistance Allocation Model (C-TRAM) (Prusinkiewicz 2007). It required to develop a special programming language allowing to model linear and branching structures (Prusinkiewicz et al. 2007). In C-TRAM the carbon transport is based on the phloem sap transport and is modeled with electrical analogies, internodes being resistances and organs represented as electromotive forces. The limit of this model is that lateral water fluxes between the xylem and the phloem are not taken into account, which may lead to a wrong computation of the phloem flux for long-distance transport (Thompson and Holbrook 2004; Seleznyova and Hanan

2018).

Other functional-structural models provide a link between plant morphology and plant physiology based on transport-resistance modelling. This is the case of the L-PEACH model, which is adapted to study the growth and development of peach trees, especially following water stress or fruit thinning, by coupling L-systems to environmental parameters and carbon partitioning within a peach tree, using electrical analogies (Allen, Prusinkiewicz, and DeJong 2005). The available resources in water and light define the carbohydrates production in the leaves and organ growth depends on the local carbohydrates distribution, based on source-sink interactions. The model can simulate different development stages and a 3D rendering of the tree is produced (Allen, Prusinkiewicz, and DeJong 2005). The limit of this model is that plant's hydraulic system, i.e. xylem and phloem interactions, is not taken into account. Therefore, Da Silva et al. included the model of a xylem circuit into an L-PEACH model, using an electrical analogy and a classical representation of xylem vessels as conductances in series, where the flow is driven by a pressure gradient. This model provided a link between water potentials, leaf net carbon assimilation, transpiration, and individual organ growth and thus established phloem-xylem interactions. The leaf was modeled as a sink in the xylem circuit whose flow was equal to leaf transpiration, which was computed with an independent L-PEACH leaf sub-model coupling photosynthesis and transpiration. This model included an interaction with the environment since the water available in the soil depended on the water transpired and was thus computed at each iteration (Da Silva et al. 2011).

In 2014, Nikinmaa et al. developed a model that linked phloem/xylem interactions, carbon transport and partitioning, and leaf gas exchanges for an 8-year-old Scots pine tree. The architecture model of the plant was developed in LIGNUM (using L-systems) and was static, which made it impossible to simulate dynamic interactions (Nikinmaa, Sievänen, and Hölttä 2014).

5.3.2 Towards an object-oriented modeling approach

Based on the C-TRAM model, Ciezlak et al. (2011) expanded on previous work and developed an aspect-oriented modelling approach based on the programming language L+C, integrating previously constructed or new distinct models examining a given aspect of plant growth and development, into comprehensive functional-structural plant growth

models, enabling the study of complicated processes (Cieslak et al. 2011). This modelling approach uses a multiscale approach (organ scale and source-sink scale), enabling each organ to have several sources or sinks attached to it, thus allowing the inclusion of growth, maintenance, storage, and carbon acquisition, as well as linking plant's morphology using L-systems, mechanistic carbon transport, environmental feedback loop, and horticultural management. They applied it on the study of kiwifruit vine development and the simulation results were similar to those obtained in experiments (Cieslak, Seleznyova, and Hanan 2011). However, this model did not take phloem/xylem interactions into account. In some of these models using the electrical analogy, the electromotive force found in source-sink interactions does not have a physiological reality and there can be a confusion between sap flow used for transport equations and carbohydrates flow used for organ growth equations (Seleznyova and Hanan 2017), making the transport mechanism used in these models closer to a stationary diffusion than the Münch flow (Seleznyova and Hanan 2018). Therefore Seleznova and Hanan (2017) proposed a new model, based on similar methods as C-TRAM, using the aspect-oriented approach used by Cieslak et al (2011), but without the electrical analogy (Seleznyova and Hanan 2017), enabling continuous solutions at the whole-plant level by applying analytical methods at an internode level (Seleznyova and Hanan 2018). This model offers the first mechanistic modeling approach of phloem/xylem interactions using Michaelis-Menten source-sink fluxes and transport equations based on the Münch hypothesis, within the structure of a developing tree (Seleznyova and Hanan 2017; Seleznyova and Hanan 2018). The model was tested on a system where the analytic solutions were known and available and it proved to be robust and accurate (Seleznyova and Hanan 2017; Seleznyova and Hanan 2018).

5.3.3 Consequences for our model

In the current version of our plant growth model, sap ascent is not differentiated between the phloem and the xylem and the root module is not included. Hence, water influx in the leaf is driven by the water potential gradients between the soil and the xylem and is function of the sap viscosity, of the sap vessel radius, and of their numbers. Moreover plant structure is not taken into account in our model, the plant is modeled as a single leaf with the properties of a whole plant in terms of leaf area, stem length and vessel numbers. The morphological module serves to give quantitative relationships between these parameters

and biomass production but does not include geometrical traits and organ differentiations. To include a more realistic sap transport and take into account phloem/xylem interactions, the water absorption flux arriving in the leaf should be written:

$$U_{H_2O}^{xylem} = U_{H_2O}^{phloem} + U_{H_2O}^{roots} \tag{5.9}$$

with:

$$U_{H_2O}^{phloem} = U_{H_2O}^{phloemIN} + U_{H_2O}^{phloemOUT} \tag{5.10}$$

The water flow within the phloem being driven by osmotic gradients, it can be linked to the carbohydrates production in the leaves. Indeed the lateral flow of water between the xylem and the phloem is linked to the carbohydrates concentration, which in our model corresponds to a mass of carbon being produced. Currently the fresh biomass is divided between biomass contributing to the leaf area, with the ratio k_1, the biomass contributing to the stem, with the ratio k_2, and the biomass contributing to the vessels multiplication, with the ratio k_3. The coefficients k_1, k_2, and k_3 are empirical and determined from the literature and from experimental data analysis provided by Hézard 2012. The biomass produced intended for the roots can thus be calculated as:

$$Biomass_{Roots} = (1 - k_1 - k_2 - k_3)Biomass \tag{5.11}$$

To include sap transport and carbon partitioning in our model, as a first approximation, the sucrose concentration in the leaf is equal to the carbon concentration corresponding to the biomass leaving the leaf, i.e. the biomass produced for the stem, the vessels, and the roots. This gives the osmotic potential at the source with the Van't Hoff equation and thus the lateral water flux. At the sink, being the roots, the concentration in sucrose is supposed to be negligible and thus the osmotic potential to be zero. This provides a link between our gas exchanges model and the plant's hydraulic system, and opens a possibility of adding a root module.

The fact that our model is intended for bioregenerative life-support systems means that the focus is not only set on the biomass production but also on gas exchanges, to gain understanding in air renewal, and on water absorption and transpiration, for water recycling. Consequently, even the latest functional-structural model developed by Seleznyova et al. (2018) is not detailed enough, in its current form, for an application in bioregenerative

life-support systems. Another specificity of the context of our plant growth model compared to classic functional-structural models, is that plants are grown hydroponically and not in the soil. As a result, our focus is not set on water stress or nutrient depletion since the nutrient solution in a bioregenerative LSS will be very much controlled, but we need to be able to account for these stressful situations to gain understanding of underlying mechanisms but also to develop predictive tools for future crewed missions.

The fact that the goal of our model is to gain understanding in plant growth in reduced gravity environment adds in some specificity. Indeed, all the models presented previously were adapted for plant growth in Earth gravity, so none of the equations describing sap transport include gravity as an explicit parameter. Consequently, in order to have a thorough description of plant growth mechanisms in reduced gravity environments, it is necessary to investigate the influence of gravity on sap transport and carbon partitioning and be able to include it in a plant growth model. In sap ascent, gravity is included in the computation of water potential. Indeed the total water potential ψ_w is the sum of an osmotic potential ψ_π due to solute concentration, a hydrostatic potential ψ_P due to turgor pressure, and a gravimetric potential due to gravity ψ_g:

$$\psi_w = \psi_P + \psi_\pi + \psi_g \tag{5.12}$$

In the xylem, water flows from a high hydrostatic potential at the roots to a lower hydrostatic potential at the leaves, due to transpiration, causing meniscus forming in very small pores and generating strong capillary forces and pulling water by suction. In a system at equilibrium, the water potential is constant along the xylem, so the water potential at the top is equal to the water potential at the bottom and since the osmotic potential is very low because the concentration in nutrients is very low in the xylem, we obtain the following relationship:

$$\psi_P{}^{top} + \psi_g{}^{top} = \psi_P{}^{bot} + \psi_g{}^{bot} \tag{5.13}$$

The gravimetric potential is equal to:

$$\psi_g = \rho g h \tag{5.14}$$

Thus:

$$\psi_P{}^{top} = \psi_P{}^{bot} - \rho g h \tag{5.15}$$

Hence in 1g, the hydrostatic potential at the top of the xylem is always lower than the one at the bottom. When the plant is transpiring, the system is not at equilibrium anymore and the hydrostatic potential at the top is even smaller. However, since the driving force in pulling the water column in the xylem is the capillary force, it still exists in weightlessness when $\psi_g = 0$. Capillary forces are actually the dominant forces in weightlessness and are problematic in the root zone for plant watering (see chapter 1).

Solutes and water in the phloem move along an osmotic gradient and on Earth they are also driven by the gravitational force. In reduced gravity environments, it is likely that solutes and water in the phloem will move slower and this could have incidences on plant's water hydraulic system, and even affect plant growth and its development.

5.3.4 Next steps

In order to include sap transport in our model, it will be necessary to study the effects of a reduced gravity on sap ascent and solute transport. Once these plant's hydraulic dynamics are linked to plant's gas exchanges, they can be included into a more complex plant morphology, going from single leaf to whole plant scale. This could be achieved by including our model into an aspect-oriented functional-structural model as the one developed by Seleznyova et al. (2018). The models described in this chapter are mostly adapted for tree growth so further development is needed to adapt them to MELiSSA candidate species. The light absorption will also be impacted by going from single leaf to whole plant, since multiple leaves shade one another, and this will need to be accounted for.

Lastly, these models lack a root module, but a mechanistic model of root growth and development in reduced gravity environments is crucial. Indeed, gravitropism is suppressed in weightlessness changing roots' shape (chapter 1), it is thus necessary to study the incidences of these changes on nutrient and water uptake. A recent survey and analysis on the roots of 369 species found that root morphology and development depend on the environment in which they evolved (Ma et al. 2018). It appears that thinner roots, which are more efficient in terms of photosynthetic carbon invested to explore the soil for nutrients and are less dependent on mycorrhizal fungi, are found in more evolved species, whereas thicker roots have a strong dependency to mycorrhizal fungi and are found in more ancestral species (Ma et al. 2018). These results suggest that root strategies and

morphology are strongly influenced by their environment and evolutionary genetic traits. Consequently a study in depth of the low gravity influence on the development of roots and the consequences for nutrient uptake for a wide variety of species is necessary to develop an accurate mechanistic model of root growth to be integrated into MELiSSA plant growth model.

As stated previously, capillary forces make water stick around roots in weightlessness, leading to hypoxia (chapter 1) and this also needs to be carefully studied and modelled in order to understand the mechanisms and be able to predict roots' behaviour for a wide range of parameters.

5.4 Leaf senescence

In these discussions about plant morphology and its link to the underlying physiological mechanisms, the phenomenon of leaf senescence was not discussed. However this is a crucial point in a plant's life and essential when we transition from a single leaf to a more complex plant architecture with many leaves.

5.4.1 Mechanisms of leaf senescence

When a leaf senesces, chloroplasts, which contain 70% of the leaf's proteins, are the first organelles of the leaf's cells to disintegrate and all cellular materials are directed to other organs of the plant (Lim, Kim, and Nam 2007). Causes for leaves senescence are multiple and can be internal (nutrients reallocation to younger leaves or seeds or fruits) or external (due to biotic or abiotic environmental conditions) (Quirino et al. 2000). All the processes involved in the metabolic pathway for leaf senescence have not yet been identified and more than 800 genes have been found associated to leaf senescence mechanisms (Lim, Kim, and Nam 2007), but it is always a decrease in photosynthetic activity that initiates the whole process (Quirino et al. 2000; Lim, Kim, and Nam 2007; Brouwer, Gardeström, and Keech 2014). In particular, this happens when sugar levels are too high above a certain threshold, which leads to a decrease in photosynthesis of the leaf leading to its senescence (Quirino et al. 2000; Lim, Kim, and Nam 2007). Elevated CO_2 does not affect leaf senescence, although it affects the amount of carbon gain by increasing photosynthesis (Herrick and Thomas 2003). Leaves do not react in the same way if they grow in the shade

or if they are partially shaded (Brouwer, Gardeström, and Keech 2014). In the first case, they adapt to low light and adopt a shade avoidance response, which includes a smaller leaf area and longer petioles (Brouwer, Gardeström, and Keech 2014). In the other case, which happens to lower leaves on a plant, they cannot adapt to a light intensity that is too low and end up to enter a senescence process and this process is accelerated on darkened leaves when other leaves on the plant are in the light (Brouwer, Gardeström, and Keech 2014).

5.4.2 Including leaf senescence in our model

As detailed here above, the main cause of leaf senescence is a decrease in photosynthetic activity, which can be shade-induced or caused by sugar levels above a certain threshold. Hence in our model, this can be translated in:

- A condition on the absorbed light intensity, I: if it stays under a certain threshold for a certain time, then the carbohydrates contained in the leaf would be reallocated to other organs in the plant. The values of this threshold and time would be species-specific and determined from experimental data.
- A condition on the amount of carbon produced by the leaf: above a certain threshold, like in the previous case, the carbohydrates contained in the leaf would be reallocated to other organs in the plant.

5.5 Chapter's outcomes

- Transpiration and root pressure generate a potential gradient, which ensures sap transport in the xylem.
- Sugar transport through the phloem is ensured through an osmotic gradient resulting from photosynthetic activity.
- Plant morphology and sap transport can be linked using aspect-oriented models based on the C-TRAM model.
- Sap transport needs to be studied in reduced gravity environments, along with root absorption and leaf senescence. This would lead to link our gas exchanges model to

plant morphology and resources allocations.

Conclusion

Plants are necessary for human space exploration, since the only way of being autonomous from Earth for food production is to use plants. Trials to grow plants in space conditions have been done since the 1950s and the astronauts regularly eat them as bonus food. However, space conditions induce modifications in plant development and functions, which can be direct, like the loss of gravitropism, or indirect, like the alteration of gas exchanges and photosynthesis because of modifications in the convection regime above the leaf in low gravity environments. To use plants for human survival, their growth mechanisms, biomass production, and gas exchanges processes need to be fully understood for a wide range of parameters. Hence the necessity of developing a mechanistic model of plant growth, which provides a multi-scale approach, enables the identification of knowledge gaps, and can be adapted to any plant species by tuning specific parameters.

The inclusion of gravity within such a model requires a very accurate description of heat and mass transfer in the boundary layer forming around plant leaves and to couple energy and mass balances in the plant. By doing so, the leaf surface temperature becomes a variable of the model and not a fixed entry parameter as it was the case in previous versions. This work was detailed in three articles: a review article published in Botany Letters in 2016, a conference paper presented at the 47^{th} International Conference on Envrionmental Sytems (ICES) in July 2017, and an article published in Astrobiology in September 2018.

The new model presented in this document is mechanistic and based on the initial version of the MELiSSA plant growth model. The main changes compared to this earlier version are:

- The inclusion of gravity as an entry parameter of the model through the definition of the free convection velocity, which is defined with respect to a density gradient of the surrounding gases, and the gravity.

- The definition of the boundary layer thickness is now based on the surface renewal model, depending on the free convection velocity, and hence on the gravity level, when in the initial version, the boundary layer thickness was a fixed entry parameter determined empirically from the literature.

- The leaf inclination is taken into account in the expression of the bulk velocity, which is used to compute the boundary layer thickness.

- The leaf conductance to water vapour is now defined as a composition between the stomatal conductance and the boundary layer conductance, while in the initial version of the MELiSSA plant growth model, the conductance was an empirical entry parameter.

- The previously defined mass balance is now coupled to an energy balance, which sets the leaf surface temperature as a variable of the model and also introduces a dependence to time.

The sensitivity analysis revealed a strong dependence to leaf inclination of the leaf surface temperature, the boundary layer thickness, free convection velocity, and CO_2 and water partial pressures. These parameters were also very sensitive to gravity levels, especially to low gravity levels, changing their behaviour the most.
A parabolic flight experiment was designed to validate the model, using thermal cameras to measure spinach leaf surface temperature, in various g levels and ventilation settings. This experiment enabled the acquisition of a large amount of data using daily COTS equipment. In addition, a CFD analysis enabled to estimate the air velocity (forced convection) above the leaves. The statistical analysis conducted on data collected during the flight showed a significant influence of the ventilation and trends similar to those reported in the literature. The dynamic analysis showed the adequacy between experimental and simulation results without ventilation, for the phases in 0g and 2g. However, the model does not fit experimental data when there is an added forced convection. This could be due to poor data acquisition or to a physical phenomenon that was wrongly neglected. These results are preliminary and not published yet; they will need to be confirmed with additional data, which is the case with the flight that happened in April 2018 and with the one that will occur in November 2018. Ultimately this model and approach could be used to compute the ventilation within a whole plant growth module.

This gas exchanges model needs to be coupled to a sap transport model, as well as to a morphology model and root growth model. Once this model is validated, a similar approach could be used for liquid dynamics within the root zone in reduced gravity. Aspect-oriented models based on the C-TRAM model enable linking plant morphology and sap transport. Sap transport, as well as nutrient absorption by roots and root growth need to be studied in reduced gravity environments and an accurate leaf senescence model should be added. Many groups around the world have been working on these topics for many years and joining their forces would allow for the development of a more complete and accurate plant growth model in reduced gravity environments.

Other aspects of space environment include high radiations, different magnetic fields, and low pressure. High radiations from cosmic rays and solar particles would disturb the energy balance established in a terrestrial environment and thus further modeling effort is needed here, coupled to dedicated experiments. Plants are sensitive to variations in magnetic field and respond with alteration in gene expressions and phenotypes. On Mars, for example, there is no magnetic field: how would the plants react? An accurate mechanistic model of plant growth should take this into account. Finally, it is admitted that habitation and greenhouse modules on other planetary habitats will likely be pressurized to less than Earth atmospheric pressure, to limit structural constraints on the habitat, leading plants to grow under a reduced total pressure. Hypobaric chamber plant growth has been studied already but it would be interesting to include low-pressure induced effects into the plant growth model.

Finally, Earth applications of this model are endless. Indeed, CO_2 levels are rising and the average Earth temperature is increasing, which changes the entry parameters of basic plant growth model used for agriculture on Earth. Being able to predict plant growth for a wide range of parameters in space means being able to predict plant growth and agricultural yields on a planet where climate change induces high CO_2 levels and temperature. Space research and sustainable development on Earth need to work together and inspire each other to ensure a brighter future to our beautiful planet Earth.

Bibliography

Ai, W., S. Guo, L. Qin, and Y. Tang (2008). "Development of a ground-based space micro-algae photo-bioreactor". *Advances in Space Research*. Space Life Sciences 41.5, pp. 742–747.

Allen, M. T., P. Prusinkiewicz, and T. M. DeJong (2005). "Using L-systems for modeling source-sink interactions, architecture and physiology of growing trees: the L-PEACH model". *The New Phytologist* 166.3, pp. 869–880.

Anderson, M. (2017). *Moon/Mars Life Support Systems – How far along are we?*

Anderson, M., M. K. Ewert, J. F. Keener, and S. A. Wagner (2015). *Life Support Baseline Values and Assumptions Document*. Tech. rep.

Ashida, A. and K. Nitta (1995). "Construction of CEEF is Just Started: CEEF: Closed Ecology Experiment Facilities". *SAE Transactions* 104, pp. 808–815.

Bastien, R., S. Douady, and B. Moulia (2015). "A Unified Model of Shoot Tropism in Plants: Photo-, Gravi- and Propio-ception". *PLoS Computational Biology* 11.2.

Beek, W. J., K. M. K. Muttzall, and J. W. v. Heuven (1999). *Transport phenomena*. 2nd ed. Chichester ; New York : Wiley.

Beihang University (2017). *Lunar Palace 365 Experiment Starts*.

Bird, R. B., W. E. Stewart, and E. N. Lightfoot (1965). *Transport Phenomena*. New ork. John Wiley & Sons.

Bluem, V. (1992). "C.E.B.A.S., a closed equilibrated biological aquatic system as a possible precursor for a long-term life support system?" *Advances in space research: the official journal of the Committee on Space Research (COSPAR)* 12.5, pp. 193–204.

Bluem, V., M. Andriske, F. Paris, and D. Voeste (2000). "The C.E.B.A.S.-Minimodule: Behaviour of an artificial aquatic ecological system during spaceflight". *Advances in Space Research*. Life Sciences: Space Life Support Systems and the Lunar Farside Crater SAHA Proposal 26.2, pp. 253–262.

Boulard, T., M. Mermier, J. Fargues, N. Smits, M. Rougier, and J. C. Roy (2002). "Tomato leaf boundary layer climate: implications for microbiological whitefly control in greenhouses". *Agricultural and Forest Meteorology* 110.3, pp. 159–176.

Brodribb Tim J., Bowman David J. M. S., Nichols Scott, Delzon Sylvain, and Burlett Regis (2010). "Xylem function and growth rate interact to determine recovery rates after exposure to extreme water deficit". *New Phytologist* 188.2, pp. 533–542.

Brodribb, T. J. and H. Cochard (2009). "Hydraulic Failure Defines the Recovery and Point of Death in Water-Stressed Conifers". *Plant Physiology* 149.1, pp. 575–584.

Brouwer, B., P. Gardeström, and O. Keech (2014). "In response to partial plant shading, the lack of phytochrome A does not directly induce leaf senescence but alters the fine-tuning of chlorophyll biosynthesis". *Journal of Experimental Botany* 65.14, pp. 4037–4049.

Bryce Space & Technology for The FAA's Office of Commercial Space Transportation (2018). *The Annual Compendium of Commercial Space Transportation: 2018*.

Cabello, F., N. Creus, J. Pérez, J. Albiol, F. Gòdia, and C. Lasseur (2001). *Connection Between Different Compartments of the MELISSA Biological Life Support System*. SAE Technical Paper 2001-01-2132. Warrendale, PA: SAE Technical Paper.

Carter, D., C. Brown, J. Bazley, D. Gazda, K. Takada, and R. Schaezler (2017). "Status of ISS Water Management and Recovery".

Carvalho, M. R., J. M. Losada, and K. J. Niklas (2018). "Phloem networks in leaves". *Current Opinion in Plant Biology*. 43 Physiology and metabolism 2018 43, pp. 29–35.

Caupin, F. and E. Herbert (2006). "Cavitation in water: a review". *Comptes Rendus Physique*. Nucleation 7.9, pp. 1000–1017.

Christy, A. L. and J. M. Ferrier (1973). "A Mathematical Treatment of Munch's Pressure-Flow Hypothesis of Phloem Translocation". *Plant Physiology* 52.6, pp. 531–538.

Chunxiao, X. and L. Hong (2008). "Crop candidates for the bioregenerative life support systems in China". *Acta Astronautica*. From Dream to Reality: Living, Working and Creating for Humans in Space - A selection of papers presented at the 16th IAA Humans in Space Symposium, Beijing, China, 2007 63.7, pp. 1076–1080.

Cieslak, M., A. N. Seleznyova, and J. Hanan (2011). "A functional-structural kiwifruit vine model integrating architecture, carbon dynamics and effects of the environment". *Annals of Botany* 107.5, pp. 747–764.

Cieslak, M., A. N. Seleznyova, P. Prusinkiewicz, and J. Hanan (2011). "Towards aspect-oriented functional–structural plant modelling". *Annals of Botany* 108.6, pp. 1025–1041.

Clauwaert, P., C. Ilgrande, M. Christiaens, R. Lindeboom, A. Luther, M. Muys, A. Alloul, C.-G. Dussap, F. Godia, B. Sas, N. Boon, K. Rabaey, N. Leys, D. Geelen, and S. Vlaeminck (2015). "The nitrogen cycle in Life Support Systems". *COSPAR, 2nd Symposium, Abstracts*.

Cochard, H. (2002). "A technique for measuring xylem hydraulic conductance under high negative pressures". *Plant, Cell & Environment* 25.6, pp. 815–819.

Cochard, H. (2006). "Cavitation in trees". *Comptes Rendus Physique*. Nucleation 7.9, pp. 1018–1026.

Cochard, H., E. Badel, S. Herbette, S. Delzon, B. Choat, and S. Jansen (2013). "Methods for measuring plant vulnerability to cavitation: a critical review". *Journal of Experimental Botany* 64.15, pp. 4779–4791.

Cochard, H. and S. S. Delzon (2013). "Misunderstanding sap ascent in trees". *Journal of Sigmoidal Plant Hydraulics* e0001, 3 p.

Cochard, H., S. Herbette, T. Barigah, E. Badel, M. Ennajeh, and A. Vilagrosa (2010). "Does sample length influence the shape of xylem embolism vulnerability curves? A test with the Cavitron spinning technique". *Plant, Cell & Environment* 33.9, pp. 1543–1552.

Cogne, G., J.-B. Gros, and C.-G. Dussap (2003). "Identification of a metabolic network structure representative of Arthrospira (spirulina) platensis metabolism". *Biotechnology and Bioengineering* 84.6, pp. 667–676.

Cornet, J.-F., C.-G. Dussap, and J.-B. Gros (1998). "Kinetics and energetics of photosynthetic micro-organisms in photobioreactors". *Bioprocess and Algae Reactor Technology, Apoptosis*. Advances in Biochemical Engineering Biotechnology 59. Springer Berlin Heidelberg, pp. 153–224.

Cornet, J.-F., C.-G. Dussap, J.-B. Gros, C. Binois, and C. Lasseur (1995). "A simplified monodimensional approach for modeling coupling between radiant light transfer and growth kinetics in photobioreactors". *Chemical Engineering Science* 50.9, pp. 1489–1500.

Cornet, J.-F., C.-G. Dussap, and J.-J. Leclercq (2001). "Simulation, Design and Model Based Predictive Control of Photobioreactors". *Engineering and Manufacturing for Biotechnology*. Focus on Biotechnology. Springer, Dordrecht, pp. 227–238.

Counède, P.-H., M. Z. Kang, A. Mathieu, J.-F. Barczi, H. P. Yan, B. G. Hu, and P. D. Reffye (2006). "Structural Factorization of Plants to Compute their Functional and Architectural Growth". *Simulation,Transactions of the society for modelling and simulation international* 82.7, pp. 427–438.

Cruvellier, N., L. Poughon, C. Creuly, C.-G. Dussap, and C. Lasseur (2016). "Growth modelling of Nitrosomonas europaea ATCC® 19718 and Nitrobacter winogradskyi ATCC® 25391: A new online indicator of the partial nitrification". *Bioresource Technology* 220.Supplement C, pp. 369–377.

Da Silva, D., R. Favreau, I. Auzmendi, and T. M. DeJong (2011). "Linking water stress effects on carbon partitioning by introducing a xylem circuit into L-PEACH". *Annals of Botany* 108.6, pp. 1135–1145.

Danckwerts, P. V. (1970). *Gas-liquid reactions*. New York. Chemical Engineering Series. McGraw-Hill Book Co.

Daudet, F. A., A. Lacointe, J. P. Gaudillère, and P. Cruiziat (2002). "Generalized Münch Coupling between Sugar and Water Fluxes for Modelling Carbon Allocation as Affected by Water Status". *Journal of Theoretical Biology* 214.3, pp. 481–498.

De Reffye, P., M. Goursat, J.-P. Quadrat, and B.-G. Hu (2003). "The dynamic equations of the tree morphogenesis GreenLab model".

Dong, C., G. Liu, Y. Fu, M. Wang, B. Xie, Y. Qin, B. Li, and H. Liu (2016). "Twin studies in Chinese closed controlled ecosystem with humans: The effect of elevated CO2 disturbance on gas exchange characteristics". *Ecological Engineering* 91.Supplement C, pp. 126–130.

Dougher, T. A. O. and B. Bugbee (2001). "Differences in the Response of Wheat, Soybean and Lettuce to Reduced Blue Radiation". *Photochemistry and Photobiology* 73.2, pp. 199–207.

Drayer, G. E. and A. M. Howard (2014). "Modeling and simulation of an aquatic habitat for bioregenerative life support research". *Acta Astronautica* 93, pp. 138–147.

Dunne, D. (2017). *China talking with European Space Agency about building a moon village*.

Dussap, C.-G. (2016). *Transfert de matière - Cours de Génie des procédés. Génie Mathématique et Modélisation, Polytech Clermont-Ferrand*. Polytech Clermont-Ferrand.

Dussap, C.-G. (2018). *Concept of the control system architecture of the MELiSSA loop*. Barcelona.

Dussap, C.-G., J.-F. Cornet, and J.-B. Gros (1993). *Simulation of Mass Fluxes in the MELISSA Microorganism Based Ecosystem*. SAE Technical Paper 932125. Warrendale, PA: SAE Technical Paper.

Eckart, P. (1996). *Spaceflight life support and biospherics*. Microcosm Press.

England, C. (2001). "Mars Atmosphere Resource Recovery System (MARRS)". *AIP Conference Proceedings* 552.1, pp. 10–15.

ESA (2015). *Exploring Together: ESA Space Exploration Strategy*. Tech. rep. ESA Human Spaceflight, Operations - Strategic Planning, and Outreach Office.

ESA Human Spaceflight (2017). *ESA and Chinese astronauts train together*. Website.

Ewert, M. K., A. E. Drysdale, J. A. Levri, B. E. Duffield, A. J. Hanford, K. E. Lange, and K. W. Stafford (2002). *Advanced Life Support Requirements, Assumptions and Reference Missions*. SAE Technical Paper 2002-01-2480. Warrendale, PA: SAE Technical Paper.

Fu, Y., L. Li, B. Xie, C. Dong, M. Wang, B. Jia, L. Shao, Y. Dong, S. Deng, H. Liu, G. Liu, B. Liu, D. Hu, and H. Liu (2016). "How to Establish a Bioregenerative Life Support System for Long-Term Crewed Missions to the Moon or Mars". *Astrobiology* 16.12, pp. 925–936.

Furfaro, R., G. Giacomelli, P. D. Sadler, and S. Gellenbeck (2017). "The Mars-Lunar Greenhouse (M-LGH) Prototype for Bio Regenerative Life Support: Current Status and Future Efforts".

Giacomelli, G., R. Furfaro, M. Kacira, L. Patterson, D. Story, G. Boscheri, C. Lobascio, P. D. Sadler, M. Pirolli, R. Remiddi, M. Thangavelu, and M. Catalina (2012). "Bio-Regenerative Life Support System Development for Lunar/Mars Habitats". *42nd International Conference on Environmental Systems*. American Institute of Aeronautics and Astronautics.

Gitelson, I. I., I. A. Terskov, B. G. Kovrov, G. M. Lisovskii, Y. N. Okladnikov, F. Y. Sid'ko, I. N. Trubachev, M. P. Shilenko, S. S. Alekseev, I. M. Pan'kova, and L. S. Tir-

ranen (1989). “Long-term experiments on man’s stay in biological life-support system”. *Advances in Space Research* 9.8, pp. 65–71.

Gitelson, I. I. and G. M. Lisovsky (2008). “Creation of Closed Ecological Life Support Systems: Results, Critical Problems and Potentials”. *Journal of Siberian Federal University Biology* 1.1, pp. 19–39.

Gòdia, F., J. Albiol, J. Pérez, N. Creus, F. Cabello, A. Montràs, A. Masot, and C. Lasseur (2004). “The MELISSA pilot plant facility as an integration test-bed for advanced life support systems”. *Advances in Space Research*. Space Life Sciences: Life Support Systems and Biological Systems under Influence of Physical Factors 34.7, pp. 1483–1493.

Goodliff, K., P. Troutman, D. Craig, J. Caram, and N. Herrmann (2016). “Evolvable Mars Campaign 2016 - A Campaign Perspective”. Long Beach, California.

Gros, J.-B., L. Poughon, C. Lasseur, and A. A. Tikhomirov (2003). “Recycling efficiencies of C,H,O,N,S, and P elements in a biological life support system based on microorganisms and higher plants”. *Advances in Space Research* 31.1, pp. 195–199.

Gunes, H. (2010). *Boundary Layer Theory*. Istanbul Technical University - Department of Mechanical Engineering.

Guo, S., Y. Tang, J. Zhu, X. Wang, Y. Yin, H. Feng, W. Ai, X. Liu, and L. Qin (2008). “Development of a CELSS Experimental Facility”. *Advances in Space Research*. Space Life Sciences 41.5, pp. 725–729.

Häder, D.-P., P. R. Richter, S. M. Strauch, and M. Schuster (2006). “Aquacells — Flagellates under long-term microgravity and potential usage for life support systems”. *Microgravity - Science and Technology* 18.3-4, p. 210.

Hall, A. J. and P. E. H. Minchin (2013). “A closed-form solution for steady-state coupled phloem/xylem flow using the Lambert-W function”. *Plant Cell Environ.* 36.12, pp. 2150–62.

Hauslage, J., M. Lebert, and H. Müller (2014). “Eu:CROPIS – Euglena and Combined Regenerative Organic-food Production in Space”. Waterloo, Canada.

Hendrickx, L., H. De Wever, V. Hermans, F. Mastroleo, N. Morin, A. Wilmotte, P. Janssen, and M. Mergeay (2006). “Microbial ecology of the closed artificial ecosystem MELiSSA (Micro-Ecological Life Support System Alternative): Reinventing and com-

partmentalizing the Earth's food and oxygen regeneration system for long-haul space exploration missions". *Research in Microbiology*. Space Microbiology 157.1, pp. 77–86.

Henton, S. M., A. J. Greaves, G. J. Piller, and P. E. H. Minchin (2002). "Revisiting the Münch pressure-flow hypothesis for long-distance transport of carbohydrates: modelling the dynamics of solute transport inside a semipermeable tube". *Journal of Experimental Botany* 53.373, pp. 1411–1419.

Herrick, J. D. and R. B. Thomas (2003). "Leaf senescence and late-season net photosynthesis of sun and shade leaves of overstory sweetgum (Liquidambar styraciflua) grown in elevated and ambient carbon dioxide concentrations". *Tree Physiology* 23.2, pp. 109–118.

Hézard, P. (2012). "Higher Plant Growth Modelling for Life Support Systems: Global Model Design and Simulation of Mass and Energy Transfers at the Plant Level." PhD thesis. Clermont-Ferrand: Doctoral school of Life Sciences, Health, Agronomy, Environment. Université Blaise Pascal, Université d'Auvergne.

Hézard, P., S. Sasidharan, C. Cruely, and C.-G. Dussap (2010). "Higher plants modeling for bioregenerative life support applications: general structure of modeling". *40th International Conference on Environmental Systems*. International Conference on Environmental Systems (ICES). American Institute of Aeronautics and Astronautics.

Hilbig, R., R. Anken, and D. Grimm (2010). "Modul.LES: a multi-compartment, multi-organism aquatic life support system as experimental platform for research in ?g". Vol. 38, p. 4.

Hilbig, R. and M. Lebert (2010). "OMEGAHAB-XP a bioregenerative aquatic life support system designed to be used in Bion-M1 long term space flight". Vol. 38, p. 3.

Hirai, H. and Y. Kitaya (2009). "Effects of Gravity on Transpiration of Plant Leaves". *Annals of the New York Academy of Sciences* 1161.1, pp. 166–172.

Holmberg, M., C. Paille, and C. Lasseur (2013). "Preliminary Modelling of Mass Flux at the Surface of Plant Leaves within the MELiSSA Higher Plant Compartments". *Uppsala Universitet, ESA*. Master's Thesis.

Hölttä, T., T. Vesala, S. Sevanto, M. Peramaki, and E. Nikinmaa (2006). "Modeling xylem and phloem water flows in trees according to cohesion theory and Munch hypothesis". *Trees* 20, pp. 67–78.

International Space Exploration Coordination Group (2013). *The Global Exploration Roadmap*. Tech. rep. ISECG NASA.

Jones, H. G., R. Serraj, B. R. Loveys, L. Xiong, A. Wheaton, and A. H. Price (2009). "Thermal infrared imaging of crop canopies for the remote diagnosis and quantification of plant responses to water stress in the field". *Functional Plant Biology* 36, pp. 978–989.

Kitaya, Y., M. Kawai, J. Tsuruyama, H. Takahashi, A. Tani, E. Goto, T. Saito, and M. Kiyota (2001). "The effect of gravity on surface temperature and net photosynthetic rate of plant leaves". *Advances in Space Research* 28.4, pp. 659–664.

Kitaya, Y., M. Kawai, J. Tsuruyama, H. Takahashi, A. Tani, E. Goto, T. Saito, and M. Kiyota (2003a). "The effect of gravity on surface temperatures of plant leaves". *Plant, Cell & Environment* 26.4, pp. 497–503.

Kitaya, Y., J. Tsuruyama, T. Shibuya, M. Yoshida, and M. Kiyota (2003b). "Effects of air current speed on gas exchange in plant leaves and plant canopies". *Advances in Space Research* 31.1, pp. 177–182.

Kitaya, Y., H. Hirai, and T. Shibuya (2010). "Important Role of Air Convection for Plant Production in Space Farming". *Biological Sciences in Space* 24.3_4, pp. 121–128.

Kliss, M. and R. MacElroy (1990). "Salad Machine: A Vegetable Production Unit for Long Duration Space Missions". *SAE Technical Paper 901280*.

Knoblauch, M., J. Knoblauch, D. L. Mullendore, J. A. Savage, B. A. Babst, S. D. Beecher, A. C. Dodgen, K. H. Jensen, and N. M. Holbrook (2016). "Testing the Münch hypothesis of long distance phloem transport in plants". *eLife* 5, e15341.

Knoblauch, M. and W. S. Peters (2017). "What actually is the Münch hypothesis? A short history of assimilate transport by mass flow". *Journal of Integrative Plant Biology* 59.5, pp. 292–310.

Lacointe, A. and P. E. H. Minchin (2007). "Mechanistic modelling of carbon allocation among sinks A generalised Münch model for branched architectures". *5th International Workshop on Functional Structural Plant Models*. Napier, New Zealand.

Lacointe, A. and P. E. H. Minchin (2008). "Modelling phloem and xylem transport within a complex architecture". *Functional Plant Biology* 35.10, pp. 772–780.

Landsberg, J. J. and A. S. Thom (1971). "Aerodynamic properties of a plant of complex structure". *Quarterly Journal of the Royal Meteorological Society* 97.414, pp. 565–570.

Lane, H. W., R. L. Sauer, and D. L. Feeback (2002). *Isolation: NASA Experiments in Closed-environment Living : Advanced Human Life Support Enclosed System Final Report*. American Astronautical Society.

Lasseur, C., J. Brunet, H. de Weever, M. Dixon, C.-G. Dussap, F. Godia, N. Leys, M. Mergeay, and D. Van Der Straeten (2011). "MELiSSA: the European Project of Closed Life Support System". *Gravitational and Space Research* 23.2.

Lenth, R. (2016). "Lsmeans: least-squares means". 69, pp. 1–33.

Lim, P. O., H. J. Kim, and H. G. Nam (2007). "Leaf Senescence". *Annual Review of Plant Biology* 58.1, pp. 115–136.

Lobascio, C., M. Lamantea, S. Palumberi, V. Cotronei, B. Negri, S. D. Pascale, A. Maggio, M. Maffei, and M. Foti (2008). *Functional architecture and development of the CAB bioregenerative system*. SAE Technical Paper 2008-01-2012. Warrendale, PA: SAE Technical Paper.

Lopez, G., R. R. Favreau, C. Smith, and T. M. DeJong (2010). "L-PEACH: A Computer-based Model to Understand How Peach Trees Grow". *HortTechnology* 20.6, pp. 983–990.

Ma, Z., D. Guo, X. Xu, M. Lu, R. D. Bardgett, D. M. Eissenstat, M. L. McCormack, and L. O. Hedin (2018). "Evolutionary history resolves global organization of root functional traits". *Nature* 555.7694, pp. 94–97.

MacElroy, R., M. Kliss, and C. Straight (1992). "Life support systems for Mars transit". *Advances in Space Research* 12.5, pp. 159–166.

Marchio, D. and P. Reboux (2008). *Introduction aux transferts thermiques*. Les Presses Mines ParisTech.

Marino, B. D. (1999). "Biosphere 2—The Special Issue". *Ecological Engineering* 13, pp. 1–359.

Martin, T. A., T. M. Hinckley, F. C. Meinzer, and D. G. Sprugel (1999). "Boundary layer conductance, leaf temperature and transpiration of Abies amabilis branches". *Tree Physiology* 19.7, pp. 435–443.

Marty, P. (2012). *Transferts Thermiques Convectifs - Génie des Procédés Master 2*. Grenoble: Université Joseph Fourier.

Massa, G. D. (2016a). "Veggie: Space Vegetables for the International Space Station and Beyond". *Spring Seminar Series*. Purdue Univ.; Dept. of Horticulture and Landscape Architecture; West Lafayette, IN, United States.

Massa, G. D. (2016b). *Veggies in Space: Salad Crop Production on the ISS*.

Massa, G. D., M. W. Romeyn, and R. F. Fritsche (2017). "Future Food Production System Development Pulling from Space Biology Crop Growth Testing in Veggie". *33rd American Society for Gravitational and Space Research*. Seattle, WA, United States.

Massa, G. D., R. M. Wheeler, R. C. Morrow, and H. G. Levine (2016). "Growth Chambers on the International Space Station for Large Plants". *8th International Symposium on Light in Horticulture*. East Lansing, MI; United States: International Society for Horticultural Science (ISHS); Korbeek-Lo, Belgium.

Mathieu, A., P. H. Cournède, V. Letort, D. Barthélémy, and P. de Reffye (2009). "A dynamic model of plant growth with interactions between development and functional mechanisms to study plant structural plasticity related to trophic competition". *Annals of Botany* 103.8, pp. 1173–1186.

Mergeay, M., W. Verstraete, G. Dubertret, M. Lefort-Tran, and C. Chipaux (1988). "MELISSA- a microorganisms based model for CELSS development". Noordwijk, the Netherlands, pp. 65–68.

Minchin, P. E. H. and A. Lacointe (2017). "Consequences of phloem pathway unloading/reloading on equilibrium flows between source and sink: a modelling approach". *Functional Plant Biology* 44.5, pp. 507–514.

Minchin, P. E. H. and M. R. Thorpe (1993). "Sink strength: a misnomer, and best forgotten". *Plant, Cell, and Environment* 16.9, pp. 1039–1040.

Mitchell, C. A. (1994). "Bioregenerative life-support systems". *The American Journal of Clinical Nutrition* 60.5, 820S–824S.

Mondal, C. and S. G. Chatterjee (2017). "A frequency quantum interpretation of the surface renewal model of mass transfer". *Royal Society Open Science* 4.7.

Monje, O., G. E. Bingham, J. G. Carman, W. F. Campbell, F. B. Salisbury, B. K. Eames, V. Sytchev, M. A. Levinskikh, and I. Podolsky (2000). "Canopy photosynthesis and transpiration in micro-gravity: Gas exchange measurements aboard Mir". *Advances in Space Research*. Life Sciences: Space Life Support Systems and the Lunar Farside Crater SAHA Proposal 26.2, pp. 303–306.

Monje, O., G. Stutte, and D. Chapman (2005). "Microgravity does not alter plant stand gas exchange of wheat at moderate light levels and saturating CO2 concentration". *Planta* 222.2, pp. 336–345.

Münch, E. (1927). *Versuche uber den Saftkreislauf*. Gebrüder Borntræger.

Muscatello, A. C. S.-M. (2011). "Evaluation of Mars CO2 Capture and Gas Separation Technologies". Long Beach, CA, United States.

NASA (2015a). *Human Exploration Destination Systems TA7*. NASA Technology Roadmaps.

NASA (2015b). *Human Health, Life Support, and Habitation SystemsTA6*. NASA Technology Roadmaps.

NASA (2015c). *Robotics and Autonomous SystemsTA4*. NASA Technology Roadmaps.

Nikinmaa, E., R. Sievänen, and T. Hölttä (2014). "Dynamics of leaf gas exchange, xylem and phloem transport, water potential and carbohydrate concentration in a realistic 3-D model tree crown". *Annals of Botany* 114.4, pp. 653–666.

Ordoñez, L., C. Lasseur, L. Poughon, and G. Waters (2004). *MELiSSA Higher Plants Compartment Modeling using EcosimPro*. SAE Technical Paper 2004-01-2351. Warrendale, PA: SAE Technical Paper.

Parkhurst, D. F., P. R. Duncan, D. M. Gates, and F. Kreith (1968). "Wind-tunnel modelling of convection of heat between air and broad leaves of plants". *Agricultural Meteorology* 5.1, pp. 33–47.

Pérez, J., L. Poughon, C.-G. Dussap, J. L. Montesinos, and F. Gòdia (2005). "Dynamics and steady state operation of a nitrifying fixed bed biofilm reactor: mathematical model based description". *Process Biochemistry* 40.7, pp. 2359–2369.

Pinheiro, J. and D. Bates (2000). *Mixed-Effects Models in S and S-PLUS*. Springer-Verlag New York.

Poughon, L., C.-G. Dussap, and J.-B. Gros (1999). "Dynamic model of a nitrifying fixed bed column: Simulation of the biomass distribution of Nitrosomonas and Nitrobacter and of transient behaviour of the column". *Bioprocess Engineering* 20.3, pp. 209–221.

Poughon, L., B. Farges, C.-G. Dussap, F. Godia, and C. Lasseur (2009). "Simulation of the MELiSSA closed loop system as a tool to define its integration strategy". *Advances in Space Research*. Life Sciences in Space 44.12, pp. 1392–1403.

Poughon, L. (1994). *MELiSSA: simulation and modelling: Spirulina modelling*. Technical note TN 17.3.

Poughon, L. (1998). *Towards a dynamic model of the MELiSSA loop*. Technical Note TN 39.2.

Poughon, L. (2005). *MELiSSA Loop Mass Balance Modelling with Matlab® / Simulink*. Technical Note TN 79.2.

Poughon, L. (2007). *Modelling of a Coupled Melissa Crew - Compartment C4a with Matlab/Simulink*. Technical Note TN 83.2.

Poughon, L., C.-G. Dussap, and J.-B. Gros (1997). "Preliminary study and simulation of the MELISSA loop including a higher plants compartment". Noordwijk, the Netherlands, pp. 879–886.

Poulet, L., J.-P. Fontaine, and C.-G. Dussap (2016). *Higher Plant Compartment model variables and requirements - ATSSE (ATmospheric SubSystems Engineering)*. Technical Note TN 117.1.

Prusinkiewicz, P. (2007). "Modelling architecture of crop plants using L-systems". *Functional-Structural Plant Modelling in Crop Production* 22.

Prusinkiewicz, P., M. Allen, A. Escobar-Gutiérrez, and T. M. DeJong (2007). "Numerical methods for transport-resistance sink-source allocation models". *Functional-Structural Plant Modelling in Crop Production* 22, pp. 123–137.

Prusinkiewicz, P. and A. Lindenmayer (1990). "Developmental models of herbaceous plants". *The Algorithmic Beauty of Plants*. The Virtual Laboratory. Springer, New York, NY, pp. 63–97.

Qiu, J. (2017). "China's quest to become a space science superpower". *Nature News* 547.7664, p. 394.

Quirino, B. F., Y. S. Noh, E. Himelblau, and R. M. Amasino (2000). "Molecular aspects of leaf senescence". *Trends in Plant Science* 5.7, pp. 278–282.

Raschke, K. (1960). "Heat Transfer Between the Plant and the Environment". *Annual Review of Plant Physiology* 11.1, pp. 111–126.

Rattner, A. and J. Bohren (2008). *Convection Correlations - MEAM333 - Heat and Mass Correlations*.

Ryan, M. G. and E. M. R. Robert (2017). "Zero-calorie sugar delivery to roots". *Nature Plants* 3.12, pp. 922–923.

Sadler, P. D., G. Giacomelli, R. L. Patterson, M. Kacira, R. Furfaro, C. Lobascio, G. Boscheri, M. Lamantea, L. Grizzaffi, S. Rossignoli, M. Pirolli, and S. DePascale (2011). "Bio-regenerative life support systems for space surface applications".

Sadler, P. D., G. Giacomelli, R. Furfaro, R. Patterson, and M. Kacira (2009). *Prototype BLSS Lunar Greenhouse*. SAE Technical Paper 2009-01-2484. Warrendale, PA: SAE Technical Paper.

Salisbury, F. B. and B. Bugbee (1988). "Space Farming in the 21st Century". *21st Century*.

Salisbury, F. B., I. I. Gitelson, and G. M. Lisovsky (1997). "BIOS-3: Siberian Experiments in Bioregenerative Life Support". *Bioscience* 47.9, pp. 575–585.

Sasidharan, S., P. Hezard, L. Poughon, and C.-G. Dussap (2010). "Higher Plant Modelling For Bio-regenerative Life Support Including Metabolic Pathways Description". *40th International Conference on Environmental Systems*. American Institute of Aeronautics and Astronautics.

Schlichting, H. (1955). "Boundary-layer theory". *The Journal of the Royal Aeronautical Society*. Pergamon Press, London 60.542, p. 143.

Schlichting, H. and K. Gersten (2017). "Fundamentals of Boundary–Layer Theory". *Boundary-Layer Theory*. Springer, Berlin, Heidelberg, pp. 29–49.

Schuepp, P. H. (1993). "Tansley Review No. 59 Leaf boundary layers". *New Phytologist* 125.3, pp. 477–507.

Schymanski, S. J., D. Or, and M. Zwieniecki (2013). "Stomatal Control and Leaf Thermal and Hydraulic Capacitances under Rapid Environmental Fluctuations". *PLOS ONE* 8.1, e54231.

Seleznyova, A. N. and J. Hanan (2017). "Carbon transport revisited: a novel approach for solving quasi-stationary carbon transport in a system with Michaelis-Menten sources and sinks". *Acta Horticulturae* 1160, pp. 269–276.

Seleznyova, A. N. and J. Hanan (2018). "Mechanistic modelling of coupled phloem/xylem transport for L-systems: combining analytical and computational methods". *Annals of Botany*.

Sherwood, T. K., R. Pigford, and C. Wilke (1975). *Mass Transfer*. New York: McGraw-Hill Inc.,US.

SpaceX (2016). *Mars*. Website: http://www.spacex.com/mars.

Stutte, G. W., O. Monje, G. D. Goins, and B. C. Tripathy (2005). "Microgravity effects on thylakoid, single leaf, and whole canopy photosynthesis of dwarf wheat". *Planta* 223.1, p. 46.

Tako, Y., S. Tsuga, T. Tani, R. Arai, O. Komatsubara, and M. Shinohara (2008). "One-week habitation of two humans in an airtight facility with two goats and 23 crops – Analysis of carbon, oxygen, and water circulation". *Advances in Space Research.* Space Life Sciences 41.5, pp. 714–724.

Tako, Y., R. Arai, S.-i. Tsuga, O. Komatsubara, T. Masuda, S. Nozoe, and K. Nitta (2010). "CEEF: Closed Ecology Experiment Facilities". *Gravitational and Space Research* 23.2.

Tako, Y., O. Komatsubara, S. Tsuga, R. Arai, K. Koyama, S. Fukuda, M. Akaishi, and M. Ogasawara (2007). "Circulation of Water in Addition to CO2, O2 and Plant Biomass in an Artificial Ecosystem Comprised of Humans, Goats and Crops During Three 2-Weeks Closed Habitation Experiments Using CEEF". *SAE Technical Paper* 2007-01-3091.

Thom, A. S. (1972). "Momentum, mass and heat exchange of vegetation". *Quarterly Journal of the Royal Meteorological Society* 98.415, pp. 124–134.

Thompson, M. V. and N. M. Holbrook (2003). "Scaling phloem transport: water potential equilibrium and osmoregulatory flow". *Plant, Cell & Environment* 26.9, pp. 1561–1577.

Thompson, M. V. and N. M. Holbrook (2004). "Scaling phloem transport: information transmission". *Plant, Cell & Environment* 27.4, pp. 509–519.

Thornley, J. H. M. and I. R. Johnson (1990). *Plant and crop modelling: a mathematical approach to plant and crop physiology.* Clarendon Press.

Tikhomirov, A. A. (1996). "Spectral composition of light and plant productivity". *Advances in Space Research.* Natural and Artificial 18.4, pp. 259–263.

Tikhomirov, A. A., Y. A. Kudenko, S. Trifonov, and S. A. Ushakova (2012). "Assessing the feasibility of involving gaseous products resulting from physicochemical oxidation of human liquid and solid wastes in the cycling of a bio-technical life support system". *Advances in Space Research* 49.2, pp. 249–253.

Tikhomirov, A. A., S. A. Ushakova, N. P. Kovaleva, B. Lamaze, M. Lobo, and C. Lasseur (2007). "Biological life support systems for a Mars mission planetary base: Problems and prospects". *Advances in Space Research* 40.11, pp. 1741–1745.

Tikhomirov, A. A., S. A. Ushakova, N. S. Manukovsky, G. M. Lisovsky, Y. A. Kudenko, V. S. Kovalev, I. V. Gribovskaya, L. S. Tirranen, I. G. Zolotukhin, J.-B. Gros, and C. Lasseur (2003a). "Synthesis of biomass and utilization of plants wastes in a physical model of biological life-support system". *Acta Astronautica*. The New Face of Space Selected Proceedings of the 53rd International Astronautical Federation Congress 53.4, pp. 249–257.

Tikhomirov, A. A., S. A. Ushakova, N. S. Manukovsky, G. M. Lisovsky, Y. A. Kudenko, V. S. Kovalev, V. G. Gubanov, Y. V. Barkhatov, I. V. Gribovskaya, I. G. Zolotukhin, J.-B. Gros, and C. Lasseur (2003b). "Mass exchange in an experimental new-generation life support system model based on biological regeneration of environment". *Advances in Space Research* 31.7, pp. 1711–1720.

Tong, L., D. Hu, H. Liu, M. Li, Y. Fu, B. Jia, F. Du, and E. Hu (2011). "Gas exchange between humans and multibiological life support system". *Ecological Engineering* 37.12, pp. 2025–2034.

Tyree, M. T. (1997). "The Cohesion-Tension theory of sap ascent: current controversies". *Journal of Experimental Botany* 48.10, pp. 1753–1765.

Tyree, M. T. (2003). "Plant hydraulics: the ascent of water". *Nature* 423.6943, p. 923.

UVED (2018). *Plant Growth Modelling - GreenLab model - Presentation*. Website.

Verseux, C., M. Baqué, K. Lehto, J.-P. P. d. Vera, L. J. Rothschild, and D. Billi (2016). "Sustainable life support on Mars – the potential roles of cyanobacteria". *International Journal of Astrobiology* 15.1, pp. 65–92.

Vesala, T. (1998). "On the Concept of Leaf Boundary Layer Resistance for Forced Convection". *Journal of Theoretical Biology* 194.1, pp. 91–100.

Vos, J., J. B. Evers, G. H. Buck-Sorlin, B. Andrieu, M. Chelle, D. Visser, and P. H. B (2010). "Functional–structural plant modelling: a new versatile tool in crop science". *Journal of Experimental Botany* 61.8, pp. 2101–2115.

Wang, G. H., G. B. Li, C. X. Hu, Y. D. Liu, L. R. Song, G. H. Tong, X. M. Liu, and E. T. Cheng (2004). "Performance of a simple closed aquatic ecosystem (CAES) in space". *Advances in Space Research*. Space Life Sciences: Radiation Risk Assessment and Radiation Measurements in Low Earth Orbit 34.6, pp. 1455–1460.

Wheeler, J. K., B. A. Huggett, A. N. Tofte, F. E. Rockwell, and N. M. Holbrook (2013). "Cutting xylem under tension or supersaturated with gas can generate PLC and

the appearance of rapid recovery from embolism". *Plant, Cell & Environment* 36.11, pp. 1938–1949.

Wheeler, R. M. (2017). "Agriculture for Space: People and Places Paving the Way : Open Agriculture".

Wheeler, R. M. (2011). "Plants for Human Life Support in Space: from Myers to Mars". *Gravitational and Space Research* 23.2.

Wieland, P. (1994). *Designing for human presence in space: An introduction to environmental control and life support systems*. Tech. rep.

Wiens, J., F. Bommarito, E. Blumenstein, M. Ellsworth, and T. Cisar (2001). *Water Extraction from Martian Soil*. Tech. rep. Colorado School of Mines.

Williams, M., B. J. Bond, and M. G. Ryan (2001). "Evaluating different soil and plant hydraulic constraints on tree function using a model and sap flow data from ponderosa pine". *Plant, Cell & Environment* 24.7, pp. 679–690.

Xie, B., G. Zhu, B. Liu, Q. Su, S. Deng, L. Yang, G. Liu, C. Dong, M. Wang, and H. Liu (2017). "The water treatment and recycling in 105-day bioregenerative life support experiment in the Lunar Palace 1". *Acta Astronautica* 140.Supplement C, pp. 420–426.

Zabel, P., M. Bamsey, C. Zeidler, V. Vrakking, D. Schubert, and O. Romberg (2017). "Future Exploration Greenhouse Design of the EDEN ISS". Charleston, South Carolina.

Zabel, P., M. Bamsey, C. Zeidler, V. Vrakking, D. Schubert, O. Romberg, G. Boscheri, and T. Dueck (2016). "The preliminary design of the EDEN ISS Mobile Test Facility - An Antarctic greenhouse". Vienna, Austria.

Zabel, P., D. Schubert, and M. Tajmar (2013). "Combination of Physico-Chemical Life Support Systems with Space Greenhouse Modules: A System Analysis". *43rd International Conference on Environmental Systems*. International Conference on Environmental Systems (ICES). American Institute of Aeronautics and Astronautics.

Zubrin, R. (2011). *Mars Regolith Water Extractor*. NASA SBIR NNX11CF93P.

Appendix A

Matlab Code

A.1 Main: Sensitivity Study

```
% This version of the model is specifically adapted to a
sensitivity study

clear all;
close all;

%% Variables declaration as global

global H g nu Tb R RH CO2PPM Pb P0Tb pO2b pH2Ob pCO2b pN2b
MN2 MO2 MH2O MCO2 rho_b K1 K2 K3 ds as ls alpha I0 Vforced
global Rvessel Wint Wext Wmu Dw Rhomol Cint Cext Dc molV Cpw
Do QY Tr DM Mmolw BCmol Na h c Sum_PDF_Lambda Epsilon Sigma
kt Lambda
global Biomass0 Mc0 Mw0 Tleaf0 pH2O_leaf0 pCO2_leaf0 pO2
_leaf0 pN2_leaf0 x0

%% Parameters
 % Changing parameters during sensitivity study
g=9.807; %gravity m/s2
alpha=0.79;%angle between the leaf and the vertical
direction in rad
I0=400e-6; %incident light intensity of the bulb
(mol.m^-2.s^-1)
Vforced=0.5; %Forced convection (m/s)
Tr=0.8; %ratio water transpiration/water uptake, g/g

   % Bulk Air
nu=1.8e-5;% Air kinematic viscosity (m2/s)
Tb=293; % Standard air temperature (K)
R=8.314; % Ideal gas constant (J.mol-1.K-1)
RH=0.5; % Standard Relative Humidity in bulk air
CO2PPM=1000; % CO2 content in bulk air (ppm)
Pb=101300; % Standard air total pressure(Pa)
P0Tb=100000*10^(5.4-1838.675/(Tb-31.737)); % Water vapor
saturating pressure at Tb (Antoine's equation) (Pa)
pO2b=0.2093*Pb; % partial pressure O2 in the bulk (Pa)
pH2Ob=RH*P0Tb; % partial pressure H2O in the bulk (Pa)
pCO2b=CO2PPM*1e-6*Pb; % partial pressure CO2 in the bulk
(Pa)
pN2b=Pb-pO2b-pH2Ob-pCO2b; % partial pressure N2 in the bulk
(Pa)
MN2=28e-3; %Molar mass N2 (kg/mol)
MO2=32e-3; %Molar mass O2 (kg/mol)
MH2O=18e-3; %Molar mass water (kg/mol)
MCO2=44e-3; %Molar mass CO2 (kg/mol)
rho_b=(pN2b*MN2+pO2b*MO2+pH2Ob*MH2O+pCO2b*MCO2)/(R*Tb);
Cext=pCO2b/(Tb*R); % Bulk air CO2 content (mol.m^-3)

    % Morphology
```

```
K1=0.0044; % Standard ratio canopy surface/biomass (m^
2.g^-1)
K2=4.9e-4; % Standard ratio stem length/biomass (m.g^-1')
K3=0.0979; % Standard ratio number of sap vessels/biomass
(g^-1)
ds=1.4e8; %stomatal density (m^-2)
as=170e-12; %stomatal cross-sectional area (m^2)
ls=11e-6;% depth of stomatal pore (m)

    % Physical
H=1;%Characteristic length of the plant chamber (m)
Rvessel=4.8e-5; %sap vessel radius, m
Wint=-5000; %lettuce water potential (Pa)
Wext=-120; %nutrient solution water potential (Pa)
Wmu=1.0e-3; %nutrient solution dynamic viscosity (Pa.s)
Dw=2.42104e-5; %diffusion coefficient of water vapour, m^
2.s^-1
Rhomol=41.58; %molar water vapour density, mol/m^5
Dc=1.7e-5; %CO2 diffusion coefficient in still atmosphere
(m^2.s^-1)
molV=1.8e-5; %molar volume of water in experimental
conditions (m^3/mol)
Cpw=75.327; %molar water heat capacity at constant pressure
(J/mol/K) - at 25Â°C
Do=1.76e-5; %O2 diffusion coefficient in still atmosphere
(m^2.s^-1)

    % Biochemical
QY=0.054; %Quantum Yield
DM=0.015; %Percentage of dry matter in the plant
Mmolw=18; %Molar mass water (g/mol)
BCmol=27; % (g/molC)

    % Energy
Na=6.02e23; %Avogadro Number (mol-1)
h=6.63e-34; %Planck constant (J.s)
c=3e8; %Light speed (m.s-1)
Sum_PDF_Lambda=5.54e6; % Sum alpha-i/lambda_i (m-1)
Epsilon=0.97; %Emissivity no unit
Sigma=5.670e-8; %Boltzmann constant (W.m-2.K-4)
kt=0.025; %Conduction coefficient (W.m-1.K-1)
Lambda=40788.3276; %latent heat of vaporization(J.mol-1)

%% Initialization of y=[Biomass Mw Tleaf]

Biomass0=5; %Initial Biomass (g)
Mc0=DM*Biomass0; %Carbon Mass(g)
Mw0=(1-DM)*Biomass0/Mmolw; %Initial water content (mol)
Tleaf0=293.0; %Initial leaf temperature (K)
```

```
pH2O_leaf0 = pH2Ob; % partial pressure H2O in the leaf (Pa)
pCO2_leaf0 = pCO2b; % partial pressure CO2 in the leaf (Pa)
pO2_leaf0 = pO2b; % partial pressure O2 in the leaf (Pa)
pN2_leaf0 = Pb-pH2O_leaf0-pCO2_leaf0-pO2_leaf0; % partial
pressure N2 in the leaf (Pa)
x0= 1; % initial BL thickness (m)
Cint=1.012e-2;%substomatal chamber CO2 content (300 ppm) at
1013 hPa (mol.m^-3)

y0=[Mc0 Mw0 Tleaf0]; % Initialization vector


%% First loop to compute initial BL thickness

% Time span
tf0=1;
tspan0=[0:tf0]; % in seconds

% Integration
[t1,y1]=ode45('fluxesBL8',tspan0,y0);

% Initialisation of BL and Mc, Mw, Tleaf after one
integration step
delta0=x0;
n=length(y1);
y02=[y1(n,1) y1(n,2) y1(n,3)];

%% Integration on whole timespan

% Time span
tf=120; % Steady=30days=3600s Transient=120s
tspan=[1:tf]; % in seconds

% Integration
[t,y]=ode45('fluxesBL8',tspan,y02);

Y=[y1(1,:);y];
%% Save the values

fileID=fopen('Physfluxes.txt', 'w');
fprintf(fileID,'%s \t', ' Imax ', ' UCO2max ', ' Phi_H2Omax
', ' UH2Omax ', ' I ', ' UCO2 ', ' Phi_H2O ');
fprintf(fileID,'%s \n',' UH2O ');
fileID2=fopen('Archi.txt', 'w');
fprintf(fileID2,'%s \t', 'Scanopy', 'L', 'Lstem');
fprintf(fileID2,'%s \n', 'Nvessel');
fileID3=fopen('Energy.txt', 'w');
fprintf(fileID3,'%s \t', 'E_photons', 'E_ray', 'E_conv');
fprintf(fileID3,'%s \n','E_transpi');
```

```
fileID4=fopen('Derivees.txt', 'w');
fprintf(fileID4,'%s \t', 'Jbiomass', 'JMw');
fprintf(fileID4,'%s \n','JTleaf');
fileID5=fopen('Partial Pressures.txt', 'w');
fprintf(fileID5,'%s \t', ' pCO2_leaf ', ' pH2O_leaf ');
fprintf(fileID5,'%s \t', ' pO2_leaf ');
fprintf(fileID5,'%s \n', ' pN2_leaf ');
fileID6=fopen('BL.txt', 'w');
fprintf(fileID6,'%s \t', ' delta ');
fprintf(fileID6,'%s \n', ' Vfree ');


%% Computation of intermediate fluxes

% initialization of vectors
delta=zeros(tf,1);
Scanopy=zeros(tf,1);
Lstem=zeros(tf,1);
Nvessel=zeros(tf,1);
L=zeros(tf,1);
Imax=zeros(tf,1);
UCO2max=zeros(tf,1);
UH2Omax=zeros(tf,1);
Phi_H2Omax=zeros(tf,1);
limit=zeros(tf,1);
I=zeros(tf,1);
UCO2=zeros(tf,1);
Phi_H2O=zeros(tf,1);
UH2O=zeros(tf,1);
Phi_O2=zeros(tf,1);
Vfree=zeros(tf,1);
pCO2_leaf=zeros(tf,1);
pH2O_leaf=zeros(tf,1);
pO2_leaf=zeros(tf,1);
pN2_leaf=zeros(tf,1);
rho_leaf=zeros(tf,1);
Delta_rho=zeros(tf,1);
E_conv=zeros(tf,1);
E_photons=zeros(tf,1);
E_ray=zeros(tf,1);
E_transpi=zeros(tf,1);
Bilan=zeros(tf,1);
JMc=zeros(tf,1);
JMw=zeros(tf,1);
JTleaf=zeros(tf,1);

for i=1:1:tf

% Initialization from computed ode45 values
```

```
Mc=y(:,1); % Carbon Mass computed on the timespan (g)
Mw=y(:,2); % Water content computed on the timespan (mol)
Tleaf=y(:,3); % Leaf surface temperature computed on the
timespan (K)
delta(1)=delta0;

%% Morphological characteristics

Scanopy(i)=K1/DM*Mc(i);    % Leaf Area m2
L(i)=2*sqrt(Scanopy(i)./pi); % Leaf Characteristic Length m
Lstem(i)=K2/DM*Mc(i); % Stem Length m
Nvessel(i)=K3/DM*Mc(i); % Number of vessels
gs=Dw*ds*as*Rhomol/ls; %stomatal conductance (mol/m2/s)

%% Physical fluxes

    % Mass transport fluxes
Imax(i) = I0 .*Scanopy(i);% Max Light absorption  mol/s
UCO2max(i) = Dc /delta(i) * Scanopy(i)* (Cext - Cint);  %
Max CO2 uptake  mol/s
Phi_H2Omax(i)=Dw*gs./(R*Tb*(Dw*Rhomol+delta(i).*gs)).*(1e5*
10.^(5.4-1838.675./(Tleaf(i)-31.737))-P0Tb*RH)*Scanopy(i);
% Max H2O transpiration  mol/s
UH2Omax(i) = Nvessel(i) .* ((Wext - Wint) * pi * Rvessel.^4
/ (molV * 8 * Wmu .* Lstem(i)));     % Max H2O absorption
mol/s

    % Stoechiometric tests: Determining the limiting flux
test1=Imax(i)*QY; %UCO2 expressed according to max light
absorption flux Imax
test2=UCO2max(i); %UCO2 expressed according to max carbon
uptake rate flux UCO2max
test3=(1-Tr)/Tr*DM/(1-DM)*Mmolw/BCmol*Phi_H2Omax(i); %UCO2
expressed according to max tranpsiration rate flux
Phi_H2Omax
test4=(1-Tr)*DM/(1-DM)*Mmolw/BCmol*UH2Omax(i); %UCO2
expressed according to max water absorption flux UH2Omax

Mintest(i)=min([test1, test2, test3, test4]); % The limiting
flux is the smallest UCO2 flux
    if Mintest<0
    limit(i)=0;
    else limit(i)=Mintest(i);
    end

    % Real physical fluxes: I, UCO2, Phi_H2O and UH2O
expressd according to the limiting flow rate
I(i)=limit(i)/QY;
UCO2(i)=limit(i); %UCO2 is equal to the lowest UCO2
```

```
calculated above
Phi_H2O(i)=Tr/(1-Tr)*(1-DM)/DM*BCmol/Mmolw*limit(i); %
Phi_H2O expressed according to the limiting flow rate
UH2O(i)=(1-DM)/(DM*(1-Tr))*BCmol/Mmolw*limit(i); %UH2O
expressed according to the limiting flow rate
Phi_O2(i)=limit(i); %Phi_O2 is equal to UCO2

%% Partial pressures at the leaf surface
pH2O_leaf(i)=pH2Ob+(Dw*Rhomol+delta(i).
*gs)/(Dw*gs*Rhomol)*Phi_H2O(i)*Rhomol/Scanopy(i)*R*Tb; %
Partial pressure leaf H2O (Pa)
pCO2_leaf(i)=pCO2b-delta(i).*R*Tb/(Dc*Scanopy(i))*UCO2(i); %
Partial pressure leaf CO2 (Pa)
pO2_leaf(i)=pO2b+delta(i).*R*Tb/(Do*Scanopy(i))*Phi_O2(i); %
Partial pressure leaf O2 (Pa)
pN2_leaf(i)=Pb-pO2_leaf(i)-pH2O_leaf(i)-pCO2_leaf(i); %
Partial pressure leaf N2 (Pa)

% Density gradient at the leaf surface
rho_leaf(i)=(pN2_leaf(i)*MN2+pO2_leaf(i)*MO2
+pH2O_leaf(i)*MH2O+pCO2_leaf(i)*MCO2)/(R*Tleaf(i)); % Air
density at the leaf surface (kg/m3)
Delta_rho(i)=abs(rho_b-rho_leaf(i))/rho_b; % Gradient of air
densities between bulk and leaf surface - equal to
beta*(Tleaf-Tb)

    % Free convection velocity
Vfree(i)=sqrt(2*g*H*Delta_rho(i)); % Vertical component of
the bulkl velocity generated by an air density gradient
(m/s)

    % Boundary Layer Thickness
delta(i+1)=2
*sqrt(L(i)*nu./(Vfree(i)*cos(alpha)+Vforced*sin(alpha))); %
BL thickness (m)

%% Energy fluxes

E_photons(i)= Imax(i)*Na*h*c*Sum_PDF_Lambda; % Photon Energy
E_photons (W)
E_ray(i)=Epsilon*Sigma*(Tleaf(i).^4-Tb.^4).*Scanopy(i); %
Radiation Energy E_ray (W)
E_conv(i)=kt./delta(i).*(Tleaf(i)-Tb).*Scanopy(i); %
Convection Energy E_conv (W)
E_transpi(i)=Lambda.* Phi_H2O(i); % Transpiration Energy
E_transpi (W)
Bilan(i)= E_photons(i) - E_ray(i) - E_conv(i) -
E_transpi(i); % Energy balance
```

```
%% Derivatives of Mc, Mw and Tleaf

JMc(i) = BCmol*UCO2(i); % Derivative of leaf carbon mass
(g/s)
JMw(i) = UH2O(i)-Phi_H2O(i); % Derivative of leaf water
content (mol/s)
JTleaf(i) = Bilan(i) ./ (Cpw * Mw(i)); % Derivative of leaf
surface temperature (K/s)

fprintf(fileID,'%12.11f\t',Imax(i));
fprintf(fileID,'%12.11f\t',UCO2max(i));
fprintf(fileID,'%12.11f\t',Phi_H2Omax(i));
fprintf(fileID,'%12.11f\t',UH2Omax(i));
fprintf(fileID,'%12.11f\t',I(i));
fprintf(fileID,'%12.11f\t',UCO2(i));
fprintf(fileID,'%12.11f\t',Phi_H2O(i));
fprintf(fileID,'%12.11f\n',UH2O(i));

fprintf(fileID2,'%12.11f\t',Scanopy(i));
fprintf(fileID2,'%12.11f\t',L(i));
fprintf(fileID2,'%12.11f\t',Lstem(i));
fprintf(fileID2,'%12.11f\n',Nvessel(i));

fprintf(fileID3,'%12.11f\t',E_photons(i));
fprintf(fileID3,'%12.11f\t',E_ray(i));
fprintf(fileID3,'%12.11f\t',E_conv(i));
fprintf(fileID3,'%12.11f\n',E_transpi(i));

fprintf(fileID4,'%12.11f\t',JMc(i));
fprintf(fileID4,'%12.11f\t',JMw(i));
fprintf(fileID4,'%12.11f\n',JTleaf(i));

fprintf(fileID5,'%12.11f\t',pCO2_leaf(i));
fprintf(fileID5,'%12.11f\t',pH2O_leaf(i));
fprintf(fileID5,'%12.11f\t',pO2_leaf(i));
fprintf(fileID5,'%12.11f\n',pN2_leaf(i));

fprintf(fileID6,'%12.11f\t',delta(i));
fprintf(fileID6,'%12.11f\n',Vfree(i));

end
```

A.2 Main: Parabolic Flight

```
% This version of the model is specifically adapted to the
parameters we had during the parabolic flight in October
2017.

clear all;
close all;

%% Variables declaration as global

global H g nu Tb R RH CO2PPM Pb P0Tb pO2b pH2Ob pCO2b pN2b
MN2 MO2 MH2O MCO2 rho_b K1 K2 K3 ds as ls alpha I0 Vforced
global Rvessel Wint Wext Wmu Dw Rhomol Cint Cext Dc molV Cpw
Do QY Tr DM Mmolw BCmol Na h c Sum_PDF_Lambda Epsilon Sigma
kt Lambda
global Biomass0 Mc0 Mw0 Tleaf0 pH2O_leaf0 pCO2_leaf0 pO2
_leaf0 pN2_leaf0 x0

%% Parameters
 % Changing parameters during sensitivity study
g=0.001;%9.807;%19.614; %gravity m/s2
alpha=1.57;%angle between the leaf and the vertical
direction in rad
I0=25e-6; %incident light intensity of the bulb
(mol.m^-2.s^-1)
Vforced=0; %Forced convection (m/s)
Tr=0.8; %ratio water transpiration/water uptake, g/g

   % Bulk Air
nu=1.8e-5;% Air kinematic viscosity (m2/s)
Tb=295.6; % Standard air temperature (K)
R=8.314; % Ideal gas constant (J.mol-1.K-1)
RH=0.70; % Standard Relative Humidity in bulk air
CO2PPM=700; % CO2 content in bulk air (ppm)
Pb=85000; % Standard air total pressure(Pa)
P0Tb=100000*10^(5.4-1838.675/(Tb-31.737)); % Water vapor
saturating pressure at Tb (Antoine's equation) (Pa)
pO2b=0.2093*Pb; % partial pressure O2 in the bulk (Pa)
pH2Ob=RH*P0Tb; % partial pressure H2O in the bulk (Pa)
pCO2b=CO2PPM*1e-6*Pb; % partial pressure CO2 in the bulk
(Pa)
pN2b=Pb-pO2b-pH2Ob-pCO2b; % partial pressure N2 in the bulk
(Pa)
MN2=28e-3; %Molar mass N2 (kg/mol)
MO2=32e-3; %Molar mass O2 (kg/mol)
MH2O=18e-3; %Molar mass water (kg/mol)
MCO2=44e-3; %Molar mass CO2 (kg/mol)
rho_b=(pN2b*MN2+pO2b*MO2+pH2Ob*MH2O+pCO2b*MCO2)/(R*Tb);
Cext=pCO2b/(Tb*R); % Bulk air CO2 content (mol.m^-3)
```

```
    % Morphology
K1=0.0044; % Standard ratio canopy surface/biomass (m^
2.g^-1)
K2=4.9e-4; % Standard ratio stem length/biomass (m.g^-1')
K3=0.0979; % Standard ratio number of sap vessels/biomass
(g^-1)
ds=2.51e8; %stomatal density (m^-2)
as=4.34e-10; %stomatal cross-sectional area (m^2)
ls=11e-6;% depth of stomatal pore (m)

    % Physical
H=0.3;%Characteristic length of the plant chamber (m)
Rvessel=4.8e-5; %sap vessel radius, m
Wint=-1800; %lettuce water potential (Pa)
Wext=-120; %nutrient solution water potential (Pa)
Wmu=1.0e-3; %nutrient solution dynamic viscosity (Pa.s)
Dw=0.242e-4/(Pb*10^(-5))*(Tb/293)^(3/2); %Dw=2.42104e-5; %
diffusion coefficient of water vapour, m^2.s^-1
Rhomol=41.58; %molar water vapour density, mol/m^5
Dc=0.177e-4/(Pb*10^(-5))*(Tb/317)^(3/2);%Dc=1.7e-5; %CO2
diffusion coefficient in still atmosphere (m^2.s^-1)
molV=1.8e-5; %molar volume of water in experimental
conditions (m^3/mol)
Cpw=75.327; %molar water heat capacity at constant pressure
(J/mol/K) - at 25Â°C
Do=0.176e-4/(Pb*10^(-5))*(Tb/298)^(3/2);%Do=1.76e-5; %O2
diffusion coefficient in still atmosphere (m^2.s^-1)

    % Biochemical
QY=0.054; %Quantum Yield
DM=0.015; %Percentage of dry matter in the plant
Mmolw=18; %Molar mass water (g/mol)
BCmol=27; % (g/molC)

    % Energy
Na=6.02e23; %Avogadro Number (mol-1)
h=6.63e-34; %Planck constant (J.s)
c=3e8; %Light speed (m.s-1)
Sum_PDF_Lambda=5.54e6; % Sum alpha-i/lambda_i (m-1)
Epsilon=0.97; %Emissivity no unit
Sigma=5.670e-8; %Boltzmann constant (W.m-2.K-4)
kt=0.025; %Conduction coefficient (W.m-1.K-1)
Lambda=40788.3276; %latent heat of vaporization(J.mol-1)

%% Initialization of y=[Biomass Mw Tleaf]

Biomass0=0.1; %Initial Biomass (g)
Mc0=0.001500038;
Mw0=0.005472363;
```

```
% Mc0=DM*Biomass0; %Carbon Mass(g)
% Mw0=(1-DM)*Biomass0/Mmolw; %Initial water content (mol)
Tleaf0=296.596278; %Initial leaf temperature (K)
pH2O_leaf0 = pH2Ob; % partial pressure H2O in the leaf (Pa)
pCO2_leaf0 = pCO2b; % partial pressure CO2 in the leaf (Pa)
pO2_leaf0 = pO2b; % partial pressure O2 in the leaf (Pa)
pN2_leaf0 = Pb-pH2O_leaf0-pCO2_leaf0-pO2_leaf0; % partial
pressure N2 in the leaf (Pa)
x0= 0.001; % initial BL thickness (m)
Cint=1.012e-2;%substomatal chamber CO2 content (300 ppm) at
1013 hPa (mol.m^-3)

y0=[Mc0 Mw0 Tleaf0]; % Initialization vector


%% First loop to compute initial BL thickness

% Time span
tf0=1;
tspan0=[0:tf0]; % in seconds

% Integration
[t1,y1]=ode45('fluxesBL8',tspan0,y0);

% Initialisation of BL and Mc, Mw, Tleaf after one
integration step
delta0=x0;
n=length(y1);
y02=[y1(n,1) y1(n,2) y1(n,3)];

%% Integration on whole timespan

% Time span
tf=22;
tspan=[1:tf]; % in seconds

% Integration
[t,y]=ode45('fluxesBL8',tspan,y02);

Y=[y1(1,:);y];
%% Save the values

fileID=fopen('Physfluxes.txt', 'w');
fprintf(fileID,'%s \t', ' Imax ', ' UCO2max ', ' Phi_H2Omax
', ' UH2Omax ', ' I ', ' UCO2 ', ' Phi_H2O ');
fprintf(fileID,'%s \n',' UH2O ');
fileID2=fopen('Archi.txt', 'w');
fprintf(fileID2,'%s \t', 'Scanopy', 'L', 'Lstem');
fprintf(fileID2,'%s \n', 'Nvessel');
```

```
fileID3=fopen('Energy.txt', 'w');
fprintf(fileID3,'%s \t', 'E_photons', 'E_ray', 'E_conv');
fprintf(fileID3,'%s \n','E_transpi');
fileID4=fopen('Derivees.txt', 'w');
fprintf(fileID4,'%s \t', 'Jbiomass', 'JMw');
fprintf(fileID4,'%s \n','JTleaf');
fileID5=fopen('Partial Pressures.txt', 'w');
fprintf(fileID5,'%s \t', ' pCO2_leaf ', ' pH2O_leaf ');
fprintf(fileID5,'%s \t', ' pO2_leaf ');
fprintf(fileID5,'%s \n', ' pN2_leaf ');
fileID6=fopen('BL.txt', 'w');
fprintf(fileID6,'%s \t', ' delta ');
fprintf(fileID6,'%s \n', ' Vfree ');


%% Computation of intermediate fluxes

% initialization of vectors
delta=zeros(tf,1);
Scanopy=zeros(tf,1);
Lstem=zeros(tf,1);
Nvessel=zeros(tf,1);
L=zeros(tf,1);
Imax=zeros(tf,1);
UCO2max=zeros(tf,1);
UH2Omax=zeros(tf,1);
Phi_H2Omax=zeros(tf,1);
limit=zeros(tf,1);
I=zeros(tf,1);
UCO2=zeros(tf,1);
Phi_H2O=zeros(tf,1);
UH2O=zeros(tf,1);
Phi_O2=zeros(tf,1);
Vfree=zeros(tf,1);
pCO2_leaf=zeros(tf,1);
pH2O_leaf=zeros(tf,1);
pO2_leaf=zeros(tf,1);
pN2_leaf=zeros(tf,1);
rho_leaf=zeros(tf,1);
Delta_rho=zeros(tf,1);
E_conv=zeros(tf,1);
E_photons=zeros(tf,1);
E_ray=zeros(tf,1);
E_transpi=zeros(tf,1);
Bilan=zeros(tf,1);
JMc=zeros(tf,1);
JMw=zeros(tf,1);
JTleaf=zeros(tf,1);
```

```
for i=1:1:tf

% Initialization from computed ode45 values
Mc=y(:,1); % Carbon Mass computed on the timespan (g)
Mw=y(:,2); % Water content computed on the timespan (mol)
Tleaf=y(:,3); % Leaf surface temperature computed on the
timespan (K)
delta(1)=delta0;

%% Morphological characteristics

Scanopy(i)=K1/DM*Mc(i);     % Leaf Area m2
L(i)=2*sqrt(Scanopy(i)./pi); % Leaf Characteristic Length m
Lstem(i)=K2/DM*Mc(i); % Stem Length m
Nvessel(i)=K3/DM*Mc(i); % Number of vessels
gs=Dw*ds*as*Rhomol/ls; %stomatal conductance (mol/m2/s)

%% Physical fluxes

    % Mass transport fluxes
Imax(i) = I0 .*Scanopy(i);% Max Light absorption  mol/s
UCO2max(i) = Dc /delta(i) * Scanopy(i)* (Cext - Cint);  %
Max CO2 uptake  mol/s
Phi_H2Omax(i)=Dw*gs./(R*Tb*(Dw*Rhomol+delta(i).*gs)).*(1e5*
10.^(5.4-1838.675./(Tleaf(i)-31.737))-P0Tb*RH)*Scanopy(i);
% Max H2O transpiration  mol/s
UH2Omax(i) = Nvessel(i) .* ((Wext - Wint) * pi * Rvessel.^4
/ (molV * 8 * Wmu .* Lstem(i)));     % Max H2O absorption
mol/s

    % Stoechiometric tests: Determining the limiting flux
test1=Imax(i)*QY; %UCO2 expressed according to max light
absorption flux Imax
test2=UCO2max(i); %UCO2 expressed according to max carbon
uptake rate flux UCO2max
test3=(1-Tr)/Tr*DM/(1-DM)*Mmolw/BCmol*Phi_H2Omax(i); %UCO2
expressed according to max tranpsiration rate flux
Phi_H2Omax
test4=(1-Tr)*DM/(1-DM)*Mmolw/BCmol*UH2Omax(i); %UCO2
expressed according to max water absorption flux UH2Omax

Mintest(i)=min([test1, test2, test3, test4]); % The limiting
flux is the smallest UCO2 flux
    if Mintest<0
    limit(i)=0;
    else limit(i)=Mintest(i);
    end

    % Real physical fluxes: I, UCO2, Phi_H2O and UH2O
```

```
expressd according to the limiting flow rate
I(i)=limit(i)/QY;
UCO2(i)=limit(i); %UCO2 is equal to the lowest UCO2
calculated above
Phi_H2O(i)=Tr/(1-Tr)*(1-DM)/DM*BCmol/Mmolw*limit(i); %
Phi_H2O expressed according to the limiting flow rate
UH2O(i)=(1-DM)/(DM*(1-Tr))*BCmol/Mmolw*limit(i); %UH2O
expressed according to the limiting flow rate
Phi_O2(i)=limit(i); %Phi_O2 is equal to UCO2

%% Partial pressures at the leaf surface
pH2O_leaf(i)=pH2Ob+(Dw*Rhomol+delta(i).
*gs)/(Dw*gs*Rhomol)*Phi_H2O(i)*Rhomol/Scanopy(i)*R*Tb; %
Partial pressure leaf H2O (Pa)
pCO2_leaf(i)=pCO2b-delta(i).*R*Tb/(Dc*Scanopy(i))*UCO2(i); %
Partial pressure leaf CO2 (Pa)
pO2_leaf(i)=pO2b+delta(i).*R*Tb/(Do*Scanopy(i))*Phi_O2(i); %
Partial pressure leaf O2 (Pa)
pN2_leaf(i)=Pb-pO2_leaf(i)-pH2O_leaf(i)-pCO2_leaf(i); %
Partial pressure leaf N2 (Pa)

% Density gradient at the leaf surface
rho_leaf(i)=(pN2_leaf(i)*MN2+pO2_leaf(i)*MO2
+pH2O_leaf(i)*MH2O+pCO2_leaf(i)*MCO2)/(R*Tleaf(i)); % Air
density at the leaf surface (kg/m3)
Delta_rho(i)=abs(rho_b-rho_leaf(i))/rho_b; % Gradient of air
densities between bulk and leaf surface - equal to
beta*(Tleaf-Tb)

    % Free convection velocity
Vfree(i)=sqrt(2*g*H*Delta_rho(i)); % Vertical component of
the bulkl velocity generated by an air density gradient
(m/s)

    % Boundary Layer Thickness
delta(i+1)=2
*sqrt(L(i)*nu./(Vfree(i)*cos(alpha)+Vforced*sin(alpha))); %
BL thickness (m)

%% Energy fluxes

E_photons(i)= Imax(i)*Na*h*c*Sum_PDF_Lambda; % Photon Energy
E_photons (W)
E_ray(i)=Epsilon*Sigma*(Tleaf(i).^4-Tb.^4).*Scanopy(i); %
Radiation Energy E_ray (W)
E_conv(i)=kt./delta(i).*(Tleaf(i)-Tb).*Scanopy(i); %
Convection Energy E_conv (W)
E_transpi(i)=Lambda.* Phi_H2O(i); % Transpiration Energy
E_transpi (W)
```

```
Bilan(i)= E_photons(i) - E_ray(i) - E_conv(i) -
E_transpi(i); % Energy balance


%% Derivatives of Mc, Mw and Tleaf

JMc(i) = BCmol*UCO2(i); % Derivative of leaf carbon mass
(g/s)
JMw(i) = UH2O(i)-Phi_H2O(i); % Derivative of leaf water
content (mol/s)
JTleaf(i) = Bilan(i) ./ (Cpw * Mw(i)); % Derivative of leaf
surface temperature (K/s)

fprintf(fileID,'%12.11f\t',Imax(i));
fprintf(fileID,'%12.11f\t',UCO2max(i));
fprintf(fileID,'%12.11f\t',Phi_H2Omax(i));
fprintf(fileID,'%12.11f\t',UH2Omax(i));
fprintf(fileID,'%12.11f\t',I(i));
fprintf(fileID,'%12.11f\t',UCO2(i));
fprintf(fileID,'%12.11f\t',Phi_H2O(i));
fprintf(fileID,'%12.11f\n',UH2O(i));

fprintf(fileID2,'%12.11f\t',Scanopy(i));
fprintf(fileID2,'%12.11f\t',L(i));
fprintf(fileID2,'%12.11f\t',Lstem(i));
fprintf(fileID2,'%12.11f\n',Nvessel(i));

fprintf(fileID3,'%12.11f\t',E_photons(i));
fprintf(fileID3,'%12.11f\t',E_ray(i));
fprintf(fileID3,'%12.11f\t',E_conv(i));
fprintf(fileID3,'%12.11f\n',E_transpi(i));

fprintf(fileID4,'%12.11f\t',JMc(i));
fprintf(fileID4,'%12.11f\t',JMw(i));
fprintf(fileID4,'%12.11f\n',JTleaf(i));

fprintf(fileID5,'%12.11f\t',pCO2_leaf(i));
fprintf(fileID5,'%12.11f\t',pH2O_leaf(i));
fprintf(fileID5,'%12.11f\t',pO2_leaf(i));
fprintf(fileID5,'%12.11f\n',pN2_leaf(i));

fprintf(fileID6,'%12.11f\t',delta(i));
fprintf(fileID6,'%12.11f\n',Vfree(i));

end
```

A.3 Function Fluxes

```
function [dy]=fluxesBL8(t,y)

global H g nu Tb R RH CO2PPM Pb P0Tb pO2b pH2Ob pCO2b pN2b
MN2 MO2 MH2O MCO2 rho_b K1 K2 K3 ds as ls alpha I0 Vforced
global Rvessel Wint Wext Wmu Dw Rhomol Cint Cext Dc molV Cpw
Do QY Tr DM Mmolw BCmol Na h c Sum_PDF_Lambda Epsilon Sigma
kt Lambda
global Biomass0 Mc0 Mw0 Tleaf0 pH2O_leaf0 pCO2_leaf0 pO2
_leaf0 pN2_leaf0 Tleaf Mw Mc x0

%% Initialisation de dy

Mc=y(1);
Mw=y(2);
Tleaf=y(3);

%% Morphological characteristics

Scanopy=K1/DM*Mc;     % Leaf Area m2
%L=2*sqrt(Scanopy/pi); % Leaf Characteristic Length m
Lstem=K2/DM*Mc; % Stem Length m
Nvessel=K3/DM*Mc; % Number of vessels
gs=Dw*ds*as*Rhomol/ls; %stomatal conductance (mol/m2/s)

%% Physical fluxes

    % Boundary Layer Thickness
delta=fzero('BL',x0); % The boundary layer thickness is the
zero of the function BL that computes the BL thickness
starting from an initialization x0
x0=delta; % New initialization of the BL thickness

    % Mass transport fluxes
Imax = I0 *Scanopy;% Max Light absorption  mol/s
UCO2max = Dc /delta * Scanopy* (Cext - Cint);   % Max CO2
uptake  mol/s
Phi_H2Omax=Dw*gs./(R*Tb*(Dw*Rhomol+delta*gs)).*(1e5*10.
^(5.4-1838.675./(Tleaf-31.737))-P0Tb*RH)*Scanopy;     % Max
H2O transpiration  mol/s
UH2Omax = Nvessel * ((Wext - Wint) * pi * Rvessel.^4 / (molV
* 8 * Wmu * Lstem));     % Max H2O absorption mol/s

    % Stoechiometric tests: Determining the limiting flux
test1=Imax*QY; %UCO2 expressed according to max light
absorption flux Imax
test2=UCO2max; %UCO2 expressed according to max carbon
uptake rate flux UCO2max
test3=(1-Tr)/Tr*DM/(1-DM)*Mmolw/BCmol*Phi_H2Omax; %UCO2
expressed according to max tranpsiration rate flux
```

```
Phi_H2Omax
test4=(1-Tr)*DM/(1-DM)*Mmolw/BCmol*UH2Omax; %UCO2 expressed
according to max water absorption flux UH2Omax

Mintest=min([test1, test2, test3, test4]); % The limiting
flux is the smallest UCO2 flux
    if Mintest<0
    limit=0;
    else limit=Mintest;
    end

    % Real physical fluxes: I, UCO2, Phi_H2O and UH2O
expressd according to the limiting flow rate
%I=limit/QY;
UCO2=limit; %UCO2 is equal to the lowest UCO2 calculated
above
Phi_H2O=Tr/(1-Tr)*(1-DM)/DM*BCmol/Mmolw*limit; %Phi_H2O
expressed according to the limiting flow rate
UH2O=(1-DM)/(DM*(1-Tr))*BCmol/Mmolw*limit; %UH2O expressed
according to the limiting flow rate
%Phi_O2=limit; %Phi_O2 is equal to UCO2

%% Energy fluxes

E_photons= Imax*Na*h*c*Sum_PDF_Lambda; % Photon Energy
E_photons (W)
E_ray=Epsilon*Sigma*(Tleaf.^4-Tb.^4)*Scanopy; % Radiation
Energy E_ray (W)
E_conv=kt./delta.*(Tleaf-Tb)*Scanopy; %Convection Energy
E_conv (W)
E_transpi=Lambda* Phi_H2O; % Transpiration Energy E_transpi
(W)
Bilan= E_photons - E_ray - E_conv - E_transpi; % Energy
balance

%% Derivatives of Mc, Mw and Tleaf

JMc = BCmol*UCO2; % Derivative of leaf carbon mass (g/s)
JMw = UH2O-Phi_H2O; % Derivative of leaf water content
(mol/s)
JTleaf = Bilan / (Cpw * Mw); % Derivative of leaf surface
temperature (K/s)

%% Output vector

dy=[JMc; JMw; JTleaf];

end
```

A.4 Function BL

```
function [z] = BL(x)

global H g nu Tb R RH CO2PPM Pb P0Tb pO2b pH2Ob pCO2b pN2b
MN2 MO2 MH2O MCO2 rho_b K1 K2 K3 ds as ls alpha I0 Vforced
global Rvessel Wint Wext Wmu Dw Rhomol Cint Cext Dc molV Cpw
Do QY Tr DM Mmolw BCmol Na h c Sum_PDF_Lambda Epsilon Sigma
kt Lambda
global Biomass0 Mc0 Mw0 Tleaf0 pH2O_leaf0 pCO2_leaf0 pO2
_leaf0 pN2_leaf0 Tleaf Mw Mc x0

%% Morphological characteristics
Scanopy=K1/DM*Mc;      % Leaf Area m2
L=2*sqrt(Scanopy/pi);     % Leaf Characteristic Length m
Lstem=K2/DM*Mc; % Stem Length m
Nvessel=K3/DM*Mc;    % Number of vessels
gs=Dw*ds*as*Rhomol/ls; %stomatal conductance (m-1)

%% Physical fluxes
    % Mass transport fluxes
Imax = I0 *Scanopy;% Max Light absorption  mol/s
UCO2max = Dc /x * Scanopy* (Cext - Cint);    % Max CO2 uptake
mol/s
Phi_H2Omax=Dw*gs./(R*Tb*(Dw*Rhomol+x*gs)).*(1e5*10.
^(5.4-1838.675./(Tleaf-31.737))-P0Tb*RH)*Scanopy;      % Max
H2O transpiration  mol/s
UH2Omax = Nvessel * ((Wext - Wint) * pi * Rvessel.^4 / (molV
* 8 * Wmu * Lstem));      % Max H2O absorption mol/s


    % Stoechiometric tests: Determining the limiting flux
test1=Imax*QY; %UCO2 expressed according to max light
absorption flux Imax
test2=UCO2max; %UCO2 expressed according to max carbon
uptake rate flux UCO2max
test3=(1-Tr)/Tr*DM/(1-DM)*Mmolw/BCmol*Phi_H2Omax; %UCO2
expressed according to max tranpsiration rate flux
Phi_H2Omax
test4=(1-Tr)*DM/(1-DM)*Mmolw/BCmol*UH2Omax; %UCO2 expressed
according to max water absorption flux UH2Omax

Mintest=min([test1, test2, test3, test4]);
    if Mintest<0
    limit=0;
    else limit=Mintest;
    end

    % Real physical fluxes: I, UCO2, Phi_H2O and UH2O
expressd according to the limiting flow rate
UCO2=limit; %UCO2 expressed according to the limiting flow
```

```
rate
Phi_H2O=Tr/(1-Tr)*(1-DM)/DM*BCmol/Mmolw*limit; %Phi_H2O
expressed according to the limiting flow rate
Phi_O2=limit; %Phi_O2 expressed according to the limiting
flow rate

    % Partial pressures at the leaf surface
pH2O_leaf=pH2Ob+(Dw*Rhomol+x.
*gs)/(Dw*gs*Rhomol)*Phi_H2O*Rhomol/Scanopy*R*Tb; % Partial
pressure leaf H2O (Pa)
pCO2_leaf=pCO2b-x.*R*Tb/(Dc*Scanopy)*UCO2; % Partial
pressure leaf CO2 (Pa)
pO2_leaf=pO2b+x.*R*Tb/(Do*Scanopy)*Phi_O2; % Partial
pressure leaf O2 (Pa)
pN2_leaf=Pb-pO2_leaf-pH2O_leaf-pCO2_leaf; % Partial pressure
leaf N2 (Pa)

    % New CO2 concentration at the leaf surface
Cint=pCO2_leaf/(Tleaf*R); % Leaf surface CO2 content
(mol.m^-3)

% Density gradient at the leaf surface
rho_leaf=(pN2_leaf*MN2+pO2_leaf*MO2+pH2O_leaf*MH2O+pCO2
_leaf*MCO2)/(R*Tleaf); % Air density at the leaf surface
(kg/m3)
Delta_rho=abs(rho_b-rho_leaf)/rho_b; % Gradient of air
densities between bulk and leaf surface - equal to
beta*(Tleaf-Tb)

    % Free convection velocity
Vfree=sqrt(2*g*H*Delta_rho); % Vertical component of the
bulkl velocity generated by an air density gradient (m/s)

    % Boundary Layer Thickness
z=2*sqrt(L*nu./(Vfree*cos(alpha)+Vforced*sin(alpha)))-x; %
BL thickness (m) when x equals the first term of this
equation

end
```

Appendix B

Murashige and Skoog Medium Recipe

Murashige & Skoog Medium Recipe

Macro-éléments MS (10X)	50 ml
Micro-éléments MS (1000X)	1 ml
Vitamines MS (200X)	5 ml
FeEDTA	10 ml
Myo-inositol (100X)	10 ml
Saccharose	20 g
H_2O	**1 L**
pH	5.7
Agar	10 g

Micro Elements	mg/l	µM
$CoCl_2.6H_2O$	0.025	0.11
$CuSO_4.5H_2O$	0.025	0.10
FeNaEDTA	36.70	100.00
H_3BO_3	6.20	100.27
KI	0.83	5.00
$MnSO_4.H_2O$	16.90	100.00
$Na_2MoO_4.2H_2O$	0.25	1.03

$ZnSO_4.7H_2O$	8.60	29.91
Macro Elements	**mg/l**	**mM**
$CaCl_2$	332.02	2.99
KH_2PO_4	170.00	1.25
KNO_3	1900.00	18.79
$MgSO_4$	180.54	1.50
NH_4NO_3	1650.00	20.61
Vitamins	**mg/l**	**µM**
Glycine	2.00	26.64
myo-Inositol	100.00	554.94
Nicotinic acid	0.50	4.06
Pyridoxine HCl	0.50	2.43
Thiamine HCl	0.10	0.30

Appendix C

Retour à l'Ecole: An outreach project for primary school children - Conference Article at the 68$^{\text{th}}$ IAC

68th International Astronautical Congress (IAC), Adelaide, Australia, 25-29 September 2017.

IAC-17-E1.1.7-37901

A Learning Method Based On A Mission To Mars For Primary School Children

Lucie Poulet[a]*, Antoine Vernay[a], Benjamin Dalmas[a], Mathilde Vernay[a], Pauline Delpeuch[a], Thomas Sinn[b]

[a] *Université Clermont Auvergne, Campus des Cézeaux, 63170 Aubière, France,* firstname.name@uca.fr
[b] *HPS GmbH, Hofmannstr. 25-27, 81379 München, Germany,* sinn@hps-gmbh.com
* Corresponding Author

Abstract

"Retour à l'Ecole" is a project initiated by four PhD students, alongside Bachelor and Master's students from Clermont-Auvergne University, willing to share their passion for science and research. Currently effective in two ground schools, this project involves children from 8 to 11 years old. On a weekly basis, the sessions take place during lunch break for about one hour. These sessions are organized in three-month periods, and are meant to cover a multidisciplinary project. Inspired and encouraged by current events in France (e.g. Thomas Pesquet flight to the ISS), this year's project couldn't be anything but a space-related project, and has naturally be entitled "Preparing for a trip to Mars". This paper is motivated by the initiative to undertake the strong but fascinating challenge of addressing technical topics with a young audience.
In contrast with traditional learning methods, this project focuses on the fact that the children must be actors of their learning process. Thus, the different sessions are built according to the questions they ask and in compliance with their expectations. In a relaxed and playful atmosphere, the children are introduced to diverse disciplines, from civil engineering to electronics, from botanics to space sciences. Around a quick but catchy lecture, the children are expected to work as a team, with an emphasis on interdisciplinarity, solidarity and critical thinking. For instance, children built small rockets using plastic bottles to discover notions of physics (rocket trajectory), chemistry (propulsion) and engineering (rocket assembly). This perspective is based on the fact that an open mind is forged mostly by actions. The objective of the sessions is not to shape astronauts out of the children, but to trigger their curiosity through a wide range of STEM topics, allowing them to imagine a future in which they have endless possibilities. After detailing the reasons that led to this project, describing the different sessions, this paper explores its contributions, which are threefold. First, the children proved to be able to learn and remember complex notions over the sessions. Secondly, the children have been introduced to disciplines they have never encountered before. Finally, the college students involved in the sessions improved their speaking and adaptation abilities in order to pass on technical knowledge to non specialists.

Keywords: STEM, popular education, multidisciplinary, Mars, primary education, outreach

Acronyms/Abbreviations

ADNA	Associations Des Naturalistes d'Auvergne
ASTEP	Accompagnement en Sciences et Technologie à l'Ecole Primaire
EVA	Extra Vehicular Activity
ISS	International Space Station
N.B.	Nota Bene
SCIC	Cooperative Society for Collective Interest
STEM	Science, Technology, Engineering & Maths

1. Introduction: context, motivation, and objectives

1.1 Context in France

The French educational system is organized in three big entities: "école primaire" (primary school in 5 years for children aged 6 to 11), "collège" (middle school in 4 years for children aged 11 to 15), and "lycée" (high school for children aged 15 to 18). In "école primaire", one teacher teaches all of the subjects, from mathematics to physical education, while in "collège" and "lycée", professors have dedicated subjects. This article focuses on a project called "Retour à l'Ecole", targeting children in primary school, referred to as "pupils" or "children" in the text; and "school" or "primary school" refers to "école primaire".
The school week in France comprises 24 hours, with pupils starting in the morning and finishing in the mid-

afternoon, eating lunch at school or at their home. Until 2013, the week was split into 4 days of 6 hours, with one free day (usually Wednesday). Since the decree of January 2013 [1], the French school system has reduced school hours per day, in order to increase extra-curriculum activities time. Now the 24 hours are spread over 4.5 days, thus shortening the time spent at school with the teacher, from 6 to a maximum of 5.5 hours per day (N.B.: on 28th June 2017, the law changed, letting each town decide whether or not to apply this restriction on school time). As a consequence, children finish school earlier everyday when most parents are not available at this time and the school team is not responsible for them anymore. Hence municipalities have proposed to set up after-school activities (cultural, athletic, manual, etc.) for which parents can register their children at the beginning of the school year for determined periods of time. These activities are also to be proposed on the lunch break. Indeed in France, unlike other countries in Europe and in the world, the lunch break can last for 2 hours, leaving the children eating at school unoccupied for roughly an hour every day.

Municipalities now have to ensure longer time frames with these activities, whose quality and diversity are prone to high expectation levels, but with often scarce and expensive offers. Despite these constraints, some teaching and municipal staffs wish to take advantage of this new system to offer and develop original and top-notch activities in accordance with popular education.

Although it is a relatively old concept which was born in the 19th century, popular education is developing more and more in France. Scandinavian countries have successfully developed an education system based on it [2] and Latin America thanks to Paulo Freire is also a pioneer in setting up this socially aware education [3]. It could be defined as a way to highlight "people's capacity for social change through a collective problem-solving approach emphasizing participation, reflection, and critical analysis of social problems" [4]. Popular education values like democracy, collective reflection, and experimentation lead to build intellectual capacity for social transformation thanks to the qualities and sensibility specific to each pupil.

1.2 Motivation: observations from new teaching assistants

All of the four PhD students at the root of the project "Retour à l'Ecole" gave classes to undergraduate students in civil and biological engineering, computer science, and biology. They all had the same observation: students did not learn to think by themselves, they aimed at getting the highest grade rather than aiming at thoroughly understanding the topic, they preferred to wait to get the answer rather than searching for it, and they were mostly not interested in the classes they were taking as their major subject.

Another observation was made at a higher level, about the French educational system itself: let it be in primary school, middle school, high school or university, it is always organized vertically. The knowledge transfer comes from the teacher to the pupils/students with very limited interactions. In addition learning methods in France are still very compartmentalized, with few interactions between disciplines, although this is slowly changing thanks to new decrees.

As a result, students may pass their exams without understanding the reasoning behind what they learned by heart and they often are not able to argue about their answers. Indeed we think that this educational system does not develop creativity and critical mind.

These two observations and the current context of extra free time for French school children led us, students from University Clermont-Auvergne, to set up the project "Retour à l'Ecole" with the ambition of tackling these learning issues and the following requirements:

- Start at an early age when children still have interest for a wide range of topics. Show them that projects always involve many different disciplines;
- Make school children become actors of their learning process instead of being passive listeners, so that they switch from knowledge consumers to knowledge builders;
- Use popular education principles.

1.3 Similar type of projects in France

In France many organizations already propose activities based on popular education principles. Some are directly targeting children; others are more directed towards educating their teachers.

At the national level, "Les petits débrouillards" is a French association organizing events to discover scientific phenomena thanks to funny and easy ways of carrying out experiments. The goal is to explain phenomena that people commonly observe in their everyday life. They also introduce people to scientific approaches, from questioning to experimental setup, in order to solve scientific problems. They punctually give talks in festivals or more regularly in schools.

More locally, "AstuScience" gathers several science associations in Auvergne (France) and allows its members to work with schools in order to promote scientific culture. This organization also organizes large events like ExpoScience where children from primary to high school can exhibit the scientific projects they have developed during a school year.

The foundation "La main à la pâte" and the "ASTEP" (Support for Science and Technology learning at primary school) are two organizations targeting teachers. The first one proposes pedagogic tools and courses in order to help teachers improve their scientific teaching approach and make more innovative and concrete classes. The second one enables teachers to build pedagogic sessions with a professional scientist.
These are examples of education outreach organizations out of many more in Clermont-Ferrand (France) and in France in general. Our project "Retour à l'Ecole" shares the same values as these organizations: promoting scientific knowledge and scientific approach, as well as encouraging the "do it yourself" spirit. However they also differ on many points and this is why we have created a project independently from these organizations.
First of all, we wanted to put an emphasis on a horizontal learning process, focusing on team work among children (Fig. 1), in terms of:

- Concept and organization: consider everyone's ideas, share different tasks, decide what to do;
- Hands-on: find one's role in the activities and bring their own contribution according to their own skills and ideas.

Fig. 1: team work and concentration during astronaut gloves making.

Secondly, our range of actions is not limited to scientific fields but can spread from literature to physics, economy, biology, arts, or history.
Finally, the whole project is led by a student team, which is an uncommon approach. It enables to create social interactions between primary school children, municipality agents, pedagogic staff and university students, which would be quasi-inexistent otherwise.

1.4 *Objectives*

Given all this, we have defined objectives for the project "Retour à l'Ecole":

1. Igniting children's curiosity and a real interest for learning, by transmitting the passion we have for our subjects.
2. Putting an emphasis on questioning everything, in order to improve their critical thinking.
3. Staying in a playful frame to allow new ways of learning to develop.
4. Making children strongly involved in the project so they can feel entitled to it. This is achieved by proposing a large diversity of topics and activities, allowing each child to find their role and strength.

We also had specific objectives for children joining the project:

1. Discovering new disciplines, which are not commonly taught in class (e.g. astronomy, civil engineering, gardening, and electronics).
2. Learning by doing concrete activities and understanding observed phenomena.
3. Taking initiatives and discussing with others to find solutions.

2. Description of the project and methodology

2.1 Genesis and organizational aspects of the project

The name "Retour à l'Ecole" means "Back to School", which is referring to PhD, Master's and undergraduate students from Clermont-Auvergne University going back to primary schools to share their passion with pupils. This project is supported by three student organizations: Doct'Auvergne, the PhD students' organization of Clermont-Ferrand and Auvergne, LieU'Topie, an organization aiming at improving students' lives, and ADNA, the organization of naturalists in Auvergne.
The students involved in the project all come from different backgrounds, leading to school activities covering a broad range of STEM disciplines such as space sciences, electronics, civil engineering, botanic or ecology. The topics covered depend on the students involved, since their availability from one year to another can vary a lot. This diversity has become the strength of our initiative.

In order to launch this project, we decided to choose an inspiring and popular topic: school children worked towards "Preparing a trip to Mars". Indeed in 2017 French people followed the awesome space adventure of ESA's (European Spatial Agency) French astronaut Thomas Pesquet and his mission Proxima in the International Space Station (ISS) from November 2016

to June 2017. Day after day during his mission, people and especially children (re)discovered the dream of a space mission, thanks to the great public outreach effort of Thomas Pesquet. Even though a mission to Mars would involve many different aspects compared to a mission on the ISS, the popularity of the Proxima mission enabled us to link our space topic to something they were seeing in the news and thus ignite their curiosity.

Preparing a trip to Mars implies having a good knowledge of the Solar System, building a rocket, thinking about the spacesuit, building a habitat to live on Mars, having good knowledge of electronics, and of course learning how to garden and having notions of ecology in order to grow food and recycle once on site. Hence it enabled us to give children a glimpse of different disciplines, while linking it to a general inspiring topic and pursuing a common goal (Fig. 2).

Fig. 2: Cardboard showing children the different sessions

The project involved four groups of children aged 8 to 11, in two different schools of Aubière (France). For a first try, we chose to address this specific audience because they have already become aware of science, but they are not yet into middle school; thus still eager to learn in a fun way.

Each activity was held once a week in each school and lasted for about one hour during lunch break. These activities were not part of the official school curriculum nor linked to a teacher's program but were part of the extra-time activities children can attend to. Depending on the school, between 8 and 14 children attended the activities, by signing up for a 3-month period, which equals to roughly 10 sessions. In 2017 we had two 3-month periods, with groups involving different children in each period. We interacted with a total of 45 children, almost half of them were in class CM1 (pupils aged 9-10), more than a third were in class CE2 (pupils aged 8-9), and less than a quarter were in class CM2, the last class before middle school (pupils aged 10-11 years old) (Fig. **3**). We had about the same number of boys and girls over the four groups: 56% girls and 44% boys.

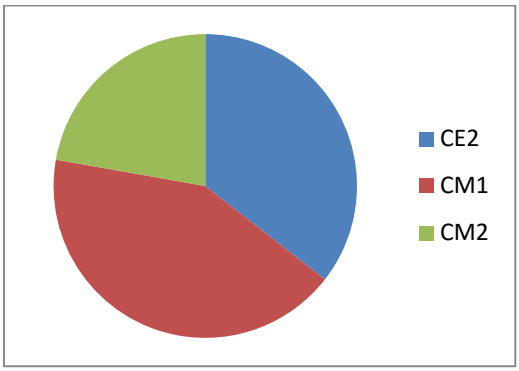

Fig. 3: Level distribution among children

2.2 Syllabus

All activities were proposed according to different vital needs for a long trip to Mars. Thanks to this approach, pupils participated in a large variety of activities and sometimes the link with a trip to Mars was a long stretch and indirect. It made them realize how many skills are needed for a big project such as a trip to Mars, as well as the significance and worth of team work.

Each session's topic followed the logic of preparing this journey to the red planet (Fig. **4**). Directly linked with space fields, school children first developed basic space "mandatory" knowledge before joining Mars. Hence they built a solar system mock-up; they made their own rocket with plastic bottles (the final session consisted in launching their rocket with vinegar and baking soda); and to be ready for potential Extra-Vehicular Activities (EVA), they made astronaut gloves. Finally, they tasted different dehydrated fruits to apprehend constraints of space food, concomitantly with natural cooking activity. They indeed learnt recipes using plants (pine syrup/mint cocktail). We wanted to sensitize them to ecology and food production, since being autonomous in terms of resources is essential to achieve a Mars mission. Consequently children started a garden with crop culture but also with "insect hotels" construction. Since on Mars it will be necessary to build habitats when the crew arrives on Mars, they built their own huts. We discussed with them about materials, the role of foundations, and the way to assemble walls. Finally, going to Mars requires the use of many sensors to control different systems functions, from the rocket itself to crop cultures. So this became an opportunity to work with electricity and to make humidity sensors they used to assess the garden's humidity and need for water.

Fig. 4: a collection of different activities we did with the children: (from top left to bottom right): solar system mock-up, astronaut gloves, rocket building, insects hotel, harvesting radishes, a Martian hut, and planting vegetables.

2.3 Example of one session: building plastic bottles rockets

In this paragraph we give the overview of one particular session, maybe the most representative of our year's topic "Preparing for a trip to Mars": the rocket building. Before starting the hands-on activity, we spent around fifteen minutes chatting with pupils about rockets and rocket launch, in order to gauge knowledge level about the topic and answer questions they might have. To illustrate this, they watched a video of Space Shuttle Discovery launch. Some of them had already seen a rocket launch but for many of them, it was the first time. Regardless of this, their emotion and wonder while watching the video was intense. Then we asked them to explain how a rocket was actually able to lift off the ground and listened to all proposals. We then carried out a small experiment consisting in mixing up white vinegar and baking soda in a bottle closed with a balloon: the chemical reaction produced CO_2 gas which inflated the balloon. After letting them find by themselves what was happening in the bottle we asked them how they could, at their level, launch plastic bottles rockets using this phenomena. With this small experiment they understood the propulsion phenomenon of a rocket (the reaction of gas on the ground) and were able to apply it to their own rockets.

The second part of the session consisted of building rockets made of plastic bottles that they would later on launch using vinegar and baking soda. They were randomly assigned to groups of two, which forced them to work with other children they did not know well. To build the rocket, two plastic bottles were necessary: one for the body of the rocket, with the bottleneck directed towards the bottom and the bottleneck of another one was taped on the bottom of the first one, representing the crew module, in which children were encouraged to add little astronauts. The children then decorated their rockets with colored paper (Fig. **5**).

Fig. 5: building rockets is a serious business!

On the day of the launch, the body of the rocket was filled up with vinegar and baking soda was added. Once closed with a cork, the children would run away from the bottle rocket, wait a few seconds for the released CO_2 to build up in the closed rocket body and then watch the launch resulting from the gas ejecting the cork.

3. Results

3.1 Children's satisfaction evaluation & observations

In order to evaluate the project, a questionnaire was given to the pupils and their parents.
The questions for the children were as follows:

1- Did you like the proposed activities? (all of them – most of them – some of them – none of them)
2- What were your most and least favorite activities?
3- Did you feel at ease to ask all of your questions?
4- Would you be ready to sign again for the next school year?

To the parents, we asked:

5- Did your child talk to you about the activities during the week?
6- Did your child show enthusiasm to the idea of meeting us?
7- Did your child learn new things?
8- Do you have any comments?

Out of the 45 children, two decided to give up on the project in the middle of a trimester and are thus not

counted for the results of this questionnaire. Out of the 43 remaining children, 15 of them answered to our questionnaire, so about 35% of the participants answered our questions. However about the same number of children from the four groups answered and the age proportions of the children are slightly similar to the 43-children population.
The answers for question #1 are summarized on the pie chart below (Fig. 6).

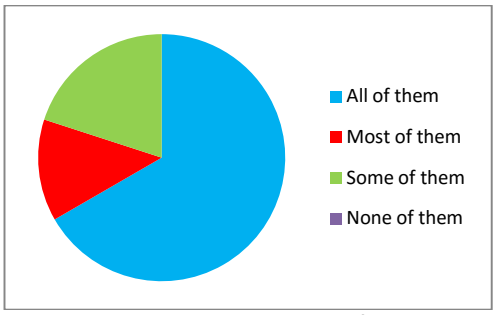

Fig. 6: Children's appreciation of the activities.

67% of the children who answered said they liked all of the proposed activities, while 13% of them liked most of the activities and 20% some of them. None of the children said they did not like any activity.
It is to be highlighted that 80% of the children who answered are very satisfied with the proposed activities, which might be a bias since only about a third of the children answered to our questionnaire and we can assume that almost only satisfied parents and children made the effort to answer.

But answers to question #1 are in accordance to the answers of question #2. Indeed there was no clear cut on their favorite activity (Fig. 7); one of them chose 3 favorite activities, while some were not able to choose one favorite because they liked them all equally, and some could not find one they did not like.

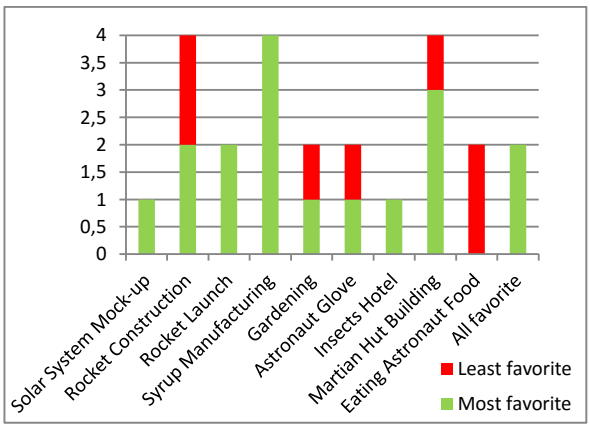

Fig. 7: Most and least favorite activities of children.

This shows that the project proposed broad enough topics so that each child could find something of interest for them.
Something to highlight however, is that this questionnaire was given during the summer holidays, after the school year, so it may happen that some children who participated during the first time period forgot some of the topics and activities we did together. Indeed the question was asked in an open format, rather than being a multiple choice question. Hence children were more inclined to list activities they had recently done with us and which were fresh in their memory. Not surprisingly, the rocket launch and the syrup manufacturing, which were among the last sessions we had, come in first. On the contrary, sessions like the Martian hut or the solar system mock-up during which children showed much enthusiasm, do not reflect this in the collected data.

Another interesting fact is that children listed the rocket building as a least favorite activity, while the launch is among their favorite. This can be explained by the fact that during the rocket building activity, we randomly assigned them to a two-people group, splitting up best friends. Indeed one aspect of the project was to promote team work and team work does not mean always working with your best friends. It was also an opportunity for them to get to know new pupils from their school. We noticed that groups of pupils who had never spoken to each other before were among the most effective and creative. So in the future we will continue proceeding this way, by randomly assigning groups.

Out of the 15 children who answered, only two said they were not at ease to ask all the questions they might have. This is one objective for us, which was reached and that we observed: most children knew they could ask us about any question in link with the topic. Although shy at the beginning, they quickly understood they could drive their own project by asking all the questions they needed to fully understand what we were doing.

A very rewarding data for us is the number of children who said they would sign up again for the following year (Fig. 8). Many had told us orally and the data confirms this: 73% of the children are sure they want to continue the adventure with us, without even knowing the new school year's theme.

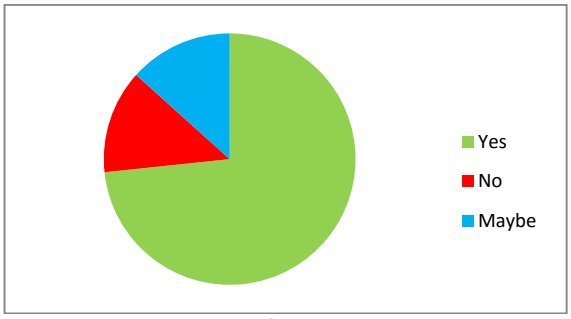

Fig. 8: Distribution of children who are willing to sign up for another year

From one session to another we noticed that children would remember an incredible amount of what they had done or what we had told them. This impression was corroborated by data from the parents' answers: 13 out of 15 who answered said their child was talking about what they were learning or doing with us at home during the week. Part of this came from the small objects they had built themselves and that they brought back at home with them. This highly contributed to their learning and memory process by obliging them to explain to their parents what it was and why it was this way. Also 100% of the parents said their child was showing enthusiasm when came the day of the session with us.

Above all, many parents thanked us for developing this project in their schools. They told us it made their children become more responsible and that is opened their mind to new perspectives. They liked the fact that the playful pedagogic approach differed from the one they have at school and that it generated in their children much enthusiasm towards learning.

In June 2017 we brought nine pupils from the different groups to an event called ExpoSciences, where they could showcase what they had done during the sessions with us on a booth dedicated to our project. They had to explain themselves the different phenomena and the objects they had built, to the public (adults and children) who was passing though our booth and to a jury (Fig. 9). They amazed us with the initiatives they took to explain the project and the fluency they had at explaining the different parts of the project.
This showed us that by giving more responsibilities to the children, they really felt entitled to the project and invest more themselves into it, thus learning and understanding more things.

Fig. 9: Children proud to showcase their work at Exposciences.

3.2 Benefits for undergraduate and graduate students

So far, we have showed that this project was mainly aiming at piquing the children's interest for STEM. However, even though we belong to major STEM disciplines, we were the targets of a learning process as well (Fig. 10). The benefits obtained by our involvement are threefold.

First, we don't *have to* teach science, we *want to*, and that makes all the difference compared to programs designed for university students, where they can "win" credits by going to primary schools. Through this project, we could seize the opportunity to share our knowledge, making the different sessions highly valuable for the children, due to this passion that drives us.

Then, beyond being a simple exchange with some children, each session was a real exercise for us. While we are used to address a scientific audience, making STEM accessible to a non aware audience is an art tough to master. And it gets even tougher when the audience is composed of children. They are able to struggle on the more obvious things as well as to question high-level knowledge. Far from being trivial, adjusting the speech for unpredictable reasoning and questions has improved our oral skills and made us work on our message clarity.

Finally, mastering our own disciplines does not mean that we are used to working with other disciplines. Alongside our colleagues, we had to understand the role we had to play "in the big picture". What is the place of our discipline in the overall project or how can other disciplines be used to improve ours and vice versa are questions we had to answer. The interdisciplinarity is a main asset in large projects, nowadays more than ever. Students must participate at building bridges between disciplines, and the best shot we had at achieving such a

goal was for us to get out of the comfort zone of our original research field.

We saw that beyond targeting solely school children, the project "Retour à l'Ecole" resulted in improving our oral skills and scientific critical thinking and made us think about STEM as a whole more than just the assembly of smaller pieces.

Fig. 10: : Part of the team of volunteer students.

3.4 Awards and prices

This first year was very rewarding, both literally and figuratively.
In addition to the satisfaction felt by the children, the project has been also very well received outside the schools. In March 2017, the project was awarded the Prix Etudiant Entrepreneur Auvergne (Auvergne Student & Entrepreneurship Prize) in the "Social and Solidarity Economy" category. The jury particularly liked the cohesion among the dozen of students that made them speak as one. Moreover, they highlighted our passion and the fact that we strongly believe in what we do, thus resulting in a high-quality education initiative. We were very pleased to see the values we stand for being shared by such a jury.
Two months later, in June 2017, we won the "Initiative Protect Contest", a social and environmental contest launched by the Atlantic Nature company. The results of the contest were based on votes made by internet users over the world on a two-month period, between May and June 2017. Both the Prix Etudiant Entrepreneur Auvergne and the Initiative Protect Contest were money prizes of a thousand Euros, enabling us to greatly improve our materials and pieces of equipment for the future activities.

As we spread the word of these rewards, the town of Aubière hosted a ceremony for our initiative towards children. Additionally many media echoed our initiative: La Montagne, a regional newspaper, as well as several radio shows.

3.5 Next year's topic

The acknowledgment of the different institutions towards our project and the satisfaction of the children made the town of Aubière extend their collaboration with us for a second school year.
Since this is a new year with new children, we chose a new overall theme for the school year: "The House of the Future", made of recyclable material and involving renewable energy and connected greenhouses.
The goal for children will be to investigate different energy production processes and how they can be integrated in our everyday life in the "house of the future". Especially different sources of energy will be studied such as the sun and mechanical sources (wind, human body,…) with an emphasis on the impacts for our planet and the solutions that exist.
This will involve physics, ecology, human physiology, and even electronics in order to understand the phenomena and then build an autonomous housing.

The novelty this year might be the collaboration with school teachers in order to propose activities that have a link with what they have been teaching in their class, so that both our project and their classes benefit from each other and are complementary.

4. Future / Next steps

This project has been very fulfilling for all parties involved – pupils, parents, students, and the municipality – during its first year. However keeping up with quality activities and content is very time-consuming, like any other associative activity. Moreover, a large amount of the students involved in the project are PhD students, who will either be too busy with their thesis at the end of their degree, either leave because they graduated. Therefore we made the choice to hire a part-time employee, who will do their civic service within our structure. This specific French contract allows associative structures to hire someone for 9 months with a maximum of 24 hours per week at a reduced cost, the main part of the salary being paid by the state. We would like to hire one of the undergraduate or Master's student who has already volunteered for the project in the previous year, so that 1) they know perfectly the project and all parties involved, and 2) we think it is a good way for students to earn money while working for an associative project. The hired student will benefit from a worthy and fulfilling practical experience, helped by all other volunteers and with an opportunity to take a lot of

initiatives. Their help will be really welcomed to manage the project with the support of all other volunteers.

A more ambitious objective is to take part in a social firm creation, following the French SCIC (Cooperative Society for Collective Interest) model. We would like to join our forces and energies with several other associative organizations to propose multiple services in different fields (e.g. environment, solidarity, social and solidarity project management, and education). “Retour à l’Ecole” would propose activities based on popular education principles with several schools and municipalities. We would like to extend our activities on the holiday time and we have imagined short holiday camps with wider range of activities. It is necessary to get helped from a full-time employee in order to support this project. “Retour à l’Ecole” would keep an associative status and would become one associate among plenty of other associative organizations, communities, and volunteers, taking part to a governance of society. “Retour à l’Ecole” volunteers would thus mainly focus on developing hands-on activities for children while the employee would manage all communication and administrative requirements.

5. Conclusions

The project “Retour à l’Ecole” has showed us that university students who are passionate about the different subjects they learn or do research on, with very limited teaching experience and almost no experience with young children, are still able to share this passion and pass on their knowledge to a young audience who is not familiar with the different topics.
It also demonstrated – in case this is still needed to be demonstrated – that innovative playful ways of learning work well, even for complex concepts, as long as children are actively learning, *i.e*. encouraged asking questions, building things by themselves (and bringing back “souvenirs” at home), resolving complex issues on their own, and taking up responsibilities, rather than just listening to a lecturer.
Finally it is an entirely student-led project, which is not common, but makes organizational things easier, since there is no bulky administration piloting it.
We hope this project will bring its little drop towards an entire remodeling of the French primary education system, which seems now obsolete and might need adjustments to face the challenges of the 21st century.

Acknowledgements

Authors and all “Retour à l’Ecole” volunteers warmly acknowledge all partner associations carrying the project, Doct’Auvergne, ADNA and LieU’topie for their communication, material, administrative helps. We thank a lot Aubière municipality (France) which has allowed us to work with pupils during lunch time in its two primary schools. Pedagogic and animation staffs of Vercingétorix and Beaudonnat primary schools have given us a warm welcome and help during our activities. We feel grateful for financial support and highlight that “Initiative project” and PEEA offered us thanks to project contest. Finally we thank AstuScience which invited us to participate to ExpoSciences with pupils and to local media (La Montagne, France Bleu Auvergne, RadioCampus), for different reports about the project, introducing it to more global audience.

References

[1] French Government, "LEGIFRANCE," [Online]. Available: www.legifrance.gouv.fr. [Accessed 15 08 2017].

[2] A.-M. Laginder, H. Nordvall and J. Crowther, "Popular education, power and democracy : Swedish experiences and contribution," in *NIACE - National Institute of Adult Continuing Education*, Leicester, 2013.

[3] S. Kerka, "Popular Education: Adult Education for Social Change," *ERIC Clearinghouse on Adult Career and Vocational Education Columbus OH*, vol. 4, 1997.

[4] R. Bates, "Popular theater: A useful process for adult educators," *Adult Education Quarterly*, vol. 46, pp. 224-236, 1996.

ABSTRACT: Challenges triggered by human space exploration of the solar system are different from those of the International Space Station because distances and time frames are of a different scale, preventing frequent resupplies. Bioregenerative life-support systems based on higher plants and microorganisms, such as the ESA Micro-Ecological Life-Support System Alternative (MELiSSA) project will enable crews to be autonomous in food production, air revitalization, and water recycling, while closing cycles for water, oxygen, nitrogen, and carbon, during long-duration missions and will thus become necessary. The growth and development of higher plants and other biological organisms are strongly influenced by environmental conditions (e.g. gravity, pressure, temperature, relative humidity, partial pressure of O_2 or CO_2). To predict plant growth in these non-standard conditions, it is crucial to develop mechanistic models of plant growth, enabling multi-scale study of different phenomena, as well as gaining thorough understanding on all processes involved in plant development in low gravity environment and identifying knowledge gaps. Especially gas exchanges at the leaf surface are altered in reduced gravity, which could reduce plant growth. Thus, we studied the intricate relationships between forced convection, gravity levels and biomass production and found that the inclusion of gravity as a parameter in plant gas exchanges models requires accurate mass and heat transfer descriptions in the boundary layer. We introduced an energy coupling to the already existing mass balance model of plant growth and this introduced time-dependent variations of the leaf surface temperature. This variable can be measured using infra-red cameras and we implemented a parabolic flight experiment, which enabled us to validate local gas transfer models in 0g and 2g without ventilation. Finally, sap transport needs to be studied in reduced gravity environments, along with root absorption and leaf senescence. This would enable to link our gas exchanges model to plant morphology and resources allocations, and achieve a complete mechanistic model of plant growth in low gravity environments.

RESUME: Les défis posés par les missions d'exploration du système solaire sont très différents de ceux de la Station Spatiale Internationale, car les distances sont plus importantes, limitant la possibilité de ravitaillements réguliers. Les systèmes support-vie basés sur des plantes et des micro-organismes, comme le projet de l'ESA MELiSSA (Micro Ecological Life-Support System Alternative) permettront aux équipages d'être autonomes en termes de production de nourriture, de revitalisation de l'air et de recyclage d'eau, tout en fermant les cycles de l'eau, de l'oxygène, de l'azote et du carbone, pendant les missions longue durée, et deviendront donc essentiels. La croissance et le développement des plantes et autres organismes biologiques sont fortement influencés par les conditions environnementales (comme la gravité, la pression, la température, l'humidité relative, les pressions partielles en O_2 et CO_2). Pour prédire la croissance des plantes dans ces conditions non-standard, il est crucial de développer des modèles de croissance mécanistiques, permettant une étude multi-échelle des différents phénomènes, ainsi que d'acquérir une compréhension approfondie de tous les processus impliqués dans le développement des plantes en environnement de gravité réduite et d'identifier les lacunes de connaissance. En particulier, les échanges gazeux à la surface de la feuille sont modifiés en gravité réduite, ce qui peut altérer la croissance des plantes. Ainsi, nous avons étudié les relations complexes entre convection forcée, niveau de gravité et production de biomasse et avons trouvé que l'inclusion de la gravité comme paramètre dans les modèles d'échanges gazeux des plantes nécessite une description précise des transferts de matière et d'énergie dans la couche limite gazeuse autour des feuilles. Nous avons ajouté un bilan d'énergie au bilan de masse du modèle de croissance de plante déjà existant et cela a ajouté des variations temporelles sur la température de surface des feuilles. Cette variable peut être mesurée à l'aide de caméras infra-rouges et nous avons réalisé une expérience en vol parabolique; cela a permis de valider des modèles de transferts gazeux locaux en 0g et 2g, sans ventilation. Enfin, le transport de sève, la croissance racinaire et la sénescence des feuilles doivent être étudiés en conditions de gravité réduite. Cela permettrait de lier notre modèle d'échanges gazeux à la morphologie des plantes et aux allocations de ressources dans une plante et ainsi arriver à un modèle mécanistique complet de la croissance des plantes en environnement de gravité réduite.